DISSERTATION

# EVALUATION OF SODIUM BISMUTHATE CHROMATOGRAPHIC SYSTEMS FOR THE SEPARATION OF AMERICIUM FROM CURIUM

Submitted by

Samantha A. Labb

Department of Environmental and Radiological Health Sciences

In partial fulfillment of the requirements

For the Degree of Doctor of Philosophy

Colorado State University

Fort Collins, Colorado

Summer 2023

Doctoral Committee:

Advisor: Ralf Sudowe

Alexander Brandl
Thomas Johnson
Charles Henry

ABSTRACT

EVALUATION OF SODIUM BISMUTHATE CHROMATOGRAPHIC SYSTEMS FOR THE SEPARATION OF AMERICIUM FROM CURIUM

The development of a successful and efficient americium (Am) and curium (Cm) separation method is necessary for stockpile stewardship science and for the simplification and improvement of currently proposed reprocessing schemes towards the closure of the nuclear fuel cycle. However, the similar chemical properties of these radionuclides (*e.g.,* similar ionic radii, ionic bonding, and predominant trivalent oxidation states in acidic media) makes this difficult to achieve. Differences in redox chemistry can be exploited based on the fact that Am can be oxidized to higher oxidation states in acidic media while Cm cannot. Recently, the ability of solid sodium bismuthate to oxidize Am and its ion exchange properties were demonstrated in solvent extraction and chromatographic systems, but were limited by oxidation stability, kinetics, and flow rates. This dissertation focuses on evaluating and characterizing new solid-liquid chromatographic systems that combine both the oxidation and ion exchange mechanisms into one material for a continuous separation process. In addition, the solution behavior of $NaBiO_3$ in nitric acid and the effect on acidity and dissolution kinetics is determined.

# ACKNOWLEDGMENTS

"The failures and partial failures of chromatography are as numerous as its successes."

-J. Calvin Giddings

It is with immeasurable gratitude that I acknowledge those that I have learned from, collaborated with, and celebrated with throughout the journey of this work. My passion for nuclear science was ignited through research conducted with Dr. Seth Friese as an undergraduate, and my ability to navigate through the stress and uncertainties of this journey would be much weaker without your constant support. My advisor, Dr. Ralf Sudowe, has been instrumental to my graduate experience. Thank you for sharing your knowledge of radiochemistry and life, for teaching me how to work through failures, for your continuous patience and support, and for being the mentor that all graduate students deserve. I would not be where I am now without you.

This journey was not voyaged without the support of many mentors, collaborators, and friends along the way. My work at Argonne with Dr. Derek McLain provided me with the fundamental tools needed for this project. Thank you for always making time to answer my numerous questions and for the advice given while I've navigated my journey so far. To Steffen Happel and Aude Bombard of TrisKem International who listened to and supported my idea for this work when first beginning my Ph.D. and for continually providing your expertise in the development of separations materials.

My committee members, Drs. Alexander Brandl, Thomas Johnson, and Chuck Henry showed incredible patience and support as I struggled to find the right stopping point in the final weeks leading up to my defense. Thank you for always believing in my project more than I would in times of uncertainty. My summers spent with Dr. Evelyn Bond have taught me lessons that I would have never encountered in the literature – the sharing of your expertise has taught me how to step away from overthinking and to approach problem solving in new and more practical ways.

To all of my lab mates and friends who never failed to remind me of my successes and lift me in times of stress. Maelle Coupannec, I am grateful for the late nights spent in the lab together (whether we were working hard or hardly working) and for the subsequent nights spent analyzing the data with a bottle of the finest wine. Michaella Swinhart, thank you for always providing me with new insights into research through the physical chemistry lens, for reminding me of my capabilities every day, and for always bringing me food when I've spent too much time in the lab.

And, finally, to my family who has shown unwavering confidence in me throughout the past nine years of school, for always supporting me when this journey has taken me further and further away from home, and for allowing me to go even further as I finally step out of the university and into my career.

TABLE OF CONTENTS

LIST OF TABLES

LIST OF FIGURES

# CHAPTER 1: INTRODUCTION

## 1.1 Motivation

Fast and efficient radiochemical separation methods are integral to the advancement of nuclear science and technology and its application to areas such as energy, medicine, forensics, and defense. Despite the large body of research geared towards the development of these methods that has been published over the last several decades, the separation of the two minor actinides (MAs), americium (Am) and curium (Cm), remains one of the most difficult separations to carry out on both process and analytical scales. The purification and/or quantification of these MAs has significant implications for used nuclear fuel (UNF) reprocessing, forensics, and stockpile stewardship purposes.

The similar size and charge of these radionuclides renders traditional size-based or ion-exchange methods insufficient, making achieving this separation a long-standing radiochemical challenge. Rather than approaching this separation based on slight differences in their trivalent chemistry, altering the speciation of Am through redox reactions can provide a greater difference in chemistry and, therefore, greater separation factors that can yield a more efficient method. While the redox approach has been explored, the instability of the higher oxidation states of Am limits its application. This dissertation aims to characterize both the solution and chromatographic behavior of a solid oxidizing agent, sodium bismuthate ($NaBiO_3$), in an effort to provide a better understanding of how this material may be incorporated into industrial and analytical scale Am/Cm separation processes.

## 1.2 Dissertation Goals

To address the efficiency, selectivity, and cost limitations associated with current Am/Cm separation techniques, this dissertation intends to contribute to the small body of research regarding the solid oxidizing agent, $NaBiO_3$. This material holds favorable redox and ion exchange properties conducive of achieving the selectivity necessary for a fast and efficient Am/Cm separation, but little is understood about its behavior in solution and even less is known about its behavior in chromatographic systems. Thus, this work aims to explore the solution behavior of $NaBiO_3$ in nitric acid systems that are prevalent in used nuclear fuel reprocessing to highlight the considerations that must be made when exploring the potential use of this material for such an application. In addition, its use in chromatographic systems is evaluated through its incorporation onto organic polymeric supports and its dispersion throughout inorganic filter aid materials. A successful chromatographic system should provide separation factors far greater than the currently available values that are below 10, have fast kinetics, and maintain the unstable higher oxidation states of Am.

## 1.3 Dissertation Overview

It is the hope of the author that the work presented in this dissertation provides a foundation for future studies exploring different approaches towards the incorporation of $NaBiO_3$ into chromatographic systems for actinide separations. Chapter one provides a brief introduction to highlight the role and importance that Am and Cm play within the nuclear fuel cycle and stockpile stewardship. Focusing on large-scale application, chapter two discusses the history and processes developed for actinide separations during the

Manhattan Project, the currently proposed reprocessing strategies, and the current reprocessing needs as they pertain to radiochemical separations. Chapter three provides background information regarding the fundamental chemistry of the lanthanide (Ln) and actinide (An) elements as well as a literature review covering the separation methods of trivalent Am and Cm and the separation of Am in higher oxidation states from Cm. The fundamental principles of precipitation, solvent extraction, and chromatographic radiochemical separation techniques and instrumental analysis methods are presented in chapters four and five, respectively. These chapters intend to provide a historical and theoretical overview of the concepts that are essential to radioanalytical chemistry and are far from exhaustive but provide relevant information for the rest of this work.

At the start of this work, only a small amount of literature, mostly focused on solid state chemistry, discussed the structural and solution behavior of $NaBiO_3$; however, a few articles have been published since. The dissolution kinetics, effects on acid concentration, potential for radionuclide hydrolysis, and sorption characteristics of $NaBiO_3$ in nitric acid are presented in chapter six. Chapter seven discusses the collaboration with TrisKem International which attempted to develop a polymer supported $NaBiO_3$ chromatographic material. The preparation, adsorption, kinetics, and chromatographic studies of Am and Cm were carried out but showed that the preparation procedure had degraded the favorable properties of $NaBiO_3$ deeming these materials unsuitable. The adsorption and chromatographic behavior of uranium, plutonium, and europium was also evaluated on these polymeric sorbents and is discussed in chapter eight. To investigate alternative chromatographic systems, chapter nine details how mixtures containing solid $NaBiO_3$ and

various inorganic filter aids affect adsorption, kinetics, capacity, and chromatographic behavior. The use of filter aids and the potential for the incorporation of $NaBiO_3$ onto solid inorganic supports is promising; however, there is much work to be done in the development, characterization, and optimization of this approach and is discussed in chapter ten.

## 1.4 Nuclear Fuel Cycle

### *1.4.1 Nuclear Energy Outlook*

As population growth and economic development continue to increase, the demand for primary energy is projected to grow by one quarter by 2040. There was a 2.3% increase in global energy demand in 2018 and subsequently the highest annual increase of carbon dioxide ($CO_2$) emissions of 1.9% was observed.[1] Currently, 194 parties are a part of The Paris Agreement which is a global initiative to limit the rise of global temperature to below 2°C relative to pre-industrial temperature as a means to limit the effects of climate change.[2] Limiting and reducing the amount of greenhouse gas (GHG) emissions is the primary pathway to meeting this long-term temperature goal, and the production and use of energy is the largest contributor to GHG emissions. The main strategy to limit fossil fuel energy dependence is through the introduction of alternate energy sources (*e.g.,* solar, wind, geothermal, nuclear) while also achieving energy security and GHG emission reduction.

When considering energy resources, their electricity production pathways and corresponding energy densities are important in identifying alternatives for meeting

energy demands. While it is important to introduce them into the infrastructure, the current fleet of renewable energy sources (wind, solar) are unable to meet baseload electrical demands (amount of power needed to power the electrical grid) due to their reliance on environmental factors. However, nuclear energy can play an important role in the transition to clean energy through its nearly carbon neutral footprint, while also meeting baseload needs. The uranium fuel used in nuclear energy has a high energy density, or energy per unit mass (MJ/kg). The physical process in which energy is produced from nuclear power is based on nuclear fission where a U-235 nucleus splits, or fissions, upon the absorption of a neutron. In this process, the nucleus overcomes the potential energy barrier of the strong nuclear force that holds it. When this occurs, a large amount of energy is released (~200 MeV per fission). In comparison, the burning of fossil fuels generates energy through the breaking and making of chemical bonds which has a lower potential, and therefore a lower energy output, than that of splitting the nucleus. To illustrate this, one pound of uranium approximately the size of a golf ball has an equivalent energy density to 3,000,000 tons of coal.[3]

Thus, the production of electricity through nuclear energy is integral in meeting the increasing demand for clean energy. As a result, there will be an increase in the hazardous UNF inventory and, with no long-term storage options, the development of improved recycling methods is necessary to address the concerns of long-term radiotoxicity and lifetime. As of 2019, the global UNF inventory was 265,000 tons of heavy metal (tHM) of which 84,000 tHM are in the U.S. inventory with the U.S. inventory expected to increase by about ~2,200 tHM per year.[4] Since the current inventory is kept

in either spent fuel pools at nuclear reactors or dry cask storage, alternatives to used nuclear fuel handling are necessary.

The United States currently operates on an open, or once-through, fuel cycle meaning that after the front-end processes of the nuclear fuel cycle (NFC) are complete, UNF that is generated is slated for decay in a deep geologic repository. While it is generally internationally agreed that permanent UNF disposal would be best achieved in deep geologic repositories, there are no approved repositories in the U.S. The fact that the storage lifetime of this material is on the order of hundreds of thousands of years makes the development of a disposal site with an equally as long performance lifetime the biggest engineering project attempted. The storage facility lifetime was initially set to 10,000 years; however, when considering Yucca Mountain as a repository site this time frame was increased to one million years which has hindered its approval.[5] Ultimately, the main priority of a long-term repository is to limit the exposure to the environment and public to acceptable levels in the event of the release of radionuclides. As a result of the engineering difficulties, regulatory requirements, and public/environmental safety concerns, it is difficult to come to a consensus about an appropriate geological repository site. While extensive research went into identifying Yucca Mountain as an appropriate final disposal site with these considerations in mind, funding for this project was eliminated during the Obama administration.

An alternative to the challenge of identifying a proper disposal pathway would be the implementation of a Partitioning and Transmutation (P&T) strategy. P&T is the process

of recovering or separating (partitioning) energy-dense radionuclides from UNF for fabrication into fuel for nuclear reactors. When used as fuel, these radionuclides will undergo fission (transmutation), generating shorter-lived or stable byproducts. In doing so, the resource utilization and energy efficiency of the nuclear option can be increased which can have a strong impact on the front end of the NFC by decreasing the amount of mining and energy-intensive fuel fabrication processes. Thus, the implementation of P&T within the NFC is a logical approach to reducing the volume and radiotoxicity of waste. When considering P&T, one of the greatest scientific challenges regarding the partitioning stage is the development of efficient actinide separations suitable for an industrial-scale process.

### *1.4.2 Nuclear Fuel Cycle: Back-End*

When removed from the reactor core, light water reactor (LWR) fuel has a composition of ~94% U, ~5% fission products (*e.g.,* Sr, Cs), and ~1.1% transuranic (TRU) elements (Figure 1.1).[6] However, the amount of the TRU elements continues to increase as a result of $^{241}$Pu and $^{241}$Am production during irradiation. The $\beta^-$decay of $^{241}$Pu ($t_{1/2}$ = 14.3 y) produces the longer-lived $^{241}$Am ($t_{1/2}$ = 432 y). In this scenario, $^{241}$Am production occurs faster than it decays resulting in its buildup in UNF over time. Similarly, the $\alpha$-decay of $^{241}$Am results in the generation of $^{237}$Np with a much longer half-life of 2.14 x $10^6$ y. As a result of the buildup of these long-lived radionuclides, the long-term radiotoxicity and storage time increases, making deep geologic disposal more difficult to achieve.

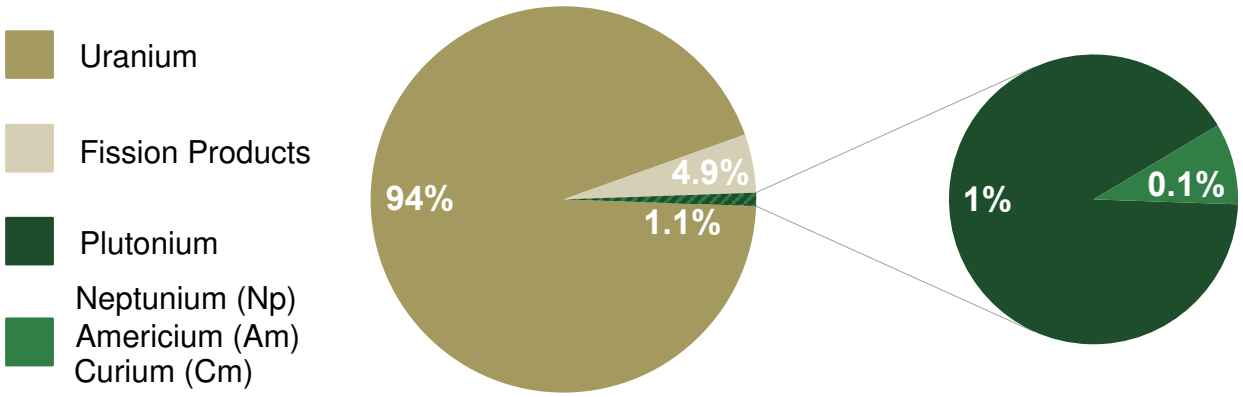


**Figure 1.1:** Composition of used nuclear fuel after irradiation in a light water reactor.

Although the MAs make up the smallest portion of UNF by mass, the longer half-lives of these radionuclides contribute the most to long-term radiotoxicity. Radiotoxicity provides a measure of the radiobiological hazard of UNF based on its radiation properties instead of its chemical toxicity and is therefore determined based on the type/energy of the radiation, biological half-life, and biokinetic behavior. Radiotoxicity values are typically reported in terms of ingestion radiotoxicity because the radiobiological risk is a concern after its migration into the biosphere where the possibility of ingestion arises. Thus, the ingestion radiotoxicity (Sv/tHM) for UNF is determined by the summation of the product of the individual radionuclide activities and their respective effective dose coefficients. The application of effective dose coefficients found in the International Commission on Radiological Protection (ICRP) Publication 119 accounts for both the radiation and tissue weighting factors allowing for the use of radiotoxicity as a measure of the adverse radiobiological effects on humans from the radioactive components in UNF.[7]

A reference level is implemented to illustrate the radiotoxic risk for UNF and is defined as the ingestion radiotoxicity of 7.83 tons of natural uranium in equilibrium with its daughter products (Figure 1.2). If UNF was to be placed directly into long-term storage post-irradiation, ~130,000 years of cooling time would be required to reach the radiotoxicity level of natural uranium found in the Earth.[8]

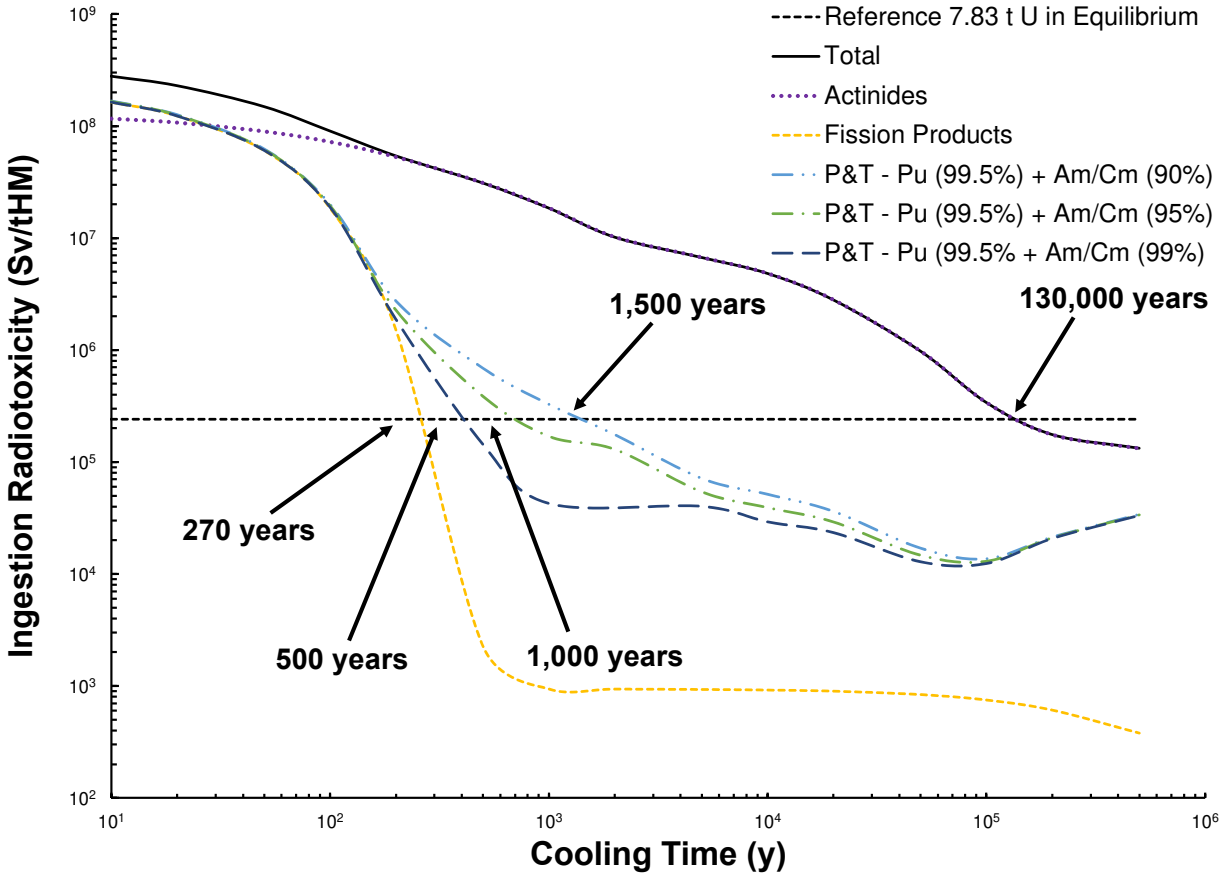


**Figure 1.2:** The effect of various modes of partitioning and transmutation on the ingestion radiotoxicity (Sv/tHM) of UNF as a function of time in year. Chart prepared using data from Magill, J. et. al.[10]

The magnitude of this time scale is the greatest obstacle in the implementation of an approved long-term storage plan since it is impossible to ensure that the UNF will remain contained over that period of time. The fission products (FPs) dominate the radiotoxicity

for the first several decades post-irradiation due to their greater abundance, but short half-lives result in a more rapid reduction in radiotoxicity. While there is a more favorable decrease in radiotoxicity for the FPs, they also emit a higher intensity of radiation and heat load over a shorter period making the handling of freshly irradiated fuel a major radiological hazard. This consequence of nuclear power generation cannot be avoided, and its effects are mitigated by cooling the irradiated fuel in spent fuel pools for several decades in both an open and closed fuel cycle scenario. However, the radiotoxicity curve for the FPs provides a theoretical limit for the total reduction in radiotoxicity assuming 100% elimination of the actinides in a closed fuel cycle.

### *1.4.3 Partitioning and Transmutation (P&T)*

The complete recovery and elimination of all actinides is limited by both the absence of an efficient partitioning method as well as the need for advanced fast reactors capable of burning up the entire actinide inventory. With these limitations in mind, there are several P&T strategies under consideration, and their effect on the long-term radiotoxicity has been thoroughly characterized.[6,8,9] If the P&T process implemented achieves a 99.5% Pu multi-recycling and a single Am/Cm recycling with a 90% efficiency, the radiotoxicity reduction time decreases to ~1,500 years; however, if Cm remains in the waste product, then ~3,000 years is necessary (Figure 1.2). If this is increased to a 95% Am/Cm recycling, the crossover point occurs after ~1,000 years. In the best-case scenario where full multi-recycling (99.5% Pu and 99% Am/Cm) is achieved, this time is further decreased to ~500 years. While there remains a long storage time for the resulting waste, the application of P&T strategies can reduce the radiotoxicity of the UNF by more than two

orders of magnitude which makes the development of high-confidence storage strategies more feasible. There are a number of additional considerations and scientific challenges regarding the transmutation process that can be found in the *IAEA Technical Reports Series No. 435*.[6]

### 1.5 Stockpile Stewardship

Following the first nuclear weapon test, Trinity, on July 16, 1945, and the end of World War 2, nuclear weapons testing by a number of countries marked the beginning of the atomic era. A large number of nuclear tests were conducted in atmospheric, underground, and underwater environments as a means to verify new weapons designs and evaluate yields. These experiments resulted in a total of 1,054 nuclear weapon detonations by the U.S. until the final test on September 23, 1992, at the Nevada Test Site (presently known as the Nevada Nuclear Security Site).[10]

A majority of nuclear tests were conducted in the atmosphere between 1945 and 1963; however, observed environmental effects led to the Limited Test Ban Treaty (LTBT) in 1963 which moved all nuclear tests underground in an effort to reduce radionuclide releases into the atmosphere.[11] In 1992, President George H. W. Bush declared a unilateral nuclear testing moratorium, halting the development of new weapon designs and testing. This was further reinforced in 1996 by President Clinton's signing of the Comprehensive Nuclear Test Ban Treaty (CTBT).[12] While the elimination of nuclear testing limits environmental damage, testing is a vital component for nuclear devices. Since plutonium produced for weapons during the Cold War was intended for eventual

replacement and the majority of tests were conducted with the focus of verifying design, there are concerns regarding the effects of material aging on weapon performance. Thus, the Stockpile Stewardship and Management Program (SSMP) was implemented with the aim of ensuring the safety and reliability of the current nuclear weapon stockpile through research geared towards better understanding nuclear weapons physics.[13] The SSMP depends on radioanalytical chemistry, which has played an important role throughout the history of stockpile science from pit purification and yield determination after weapons testing.

### *1.5.1 Nuclear Device Fundamentals*

Generally, the detonation of a nuclear device requires that a subcritical configuration of fissile material is assembled to generate a critical mass to initiate a self-sustained chain reaction. Upon detonation, a complex neutron reaction network is generated. “Prompt” fission neutrons that are immediately produced are mostly in the high energy (fast) region. However, due to numerous interactions within the system post-detonation, neutron energies will cover a wide range from fast to thermal. Neutron collisions with other nuclei present occurs, and consequently results in energy losses. In addition, the prompt neutrons can participate in inelastic and elastic scattering with heavy and light nuclei present in both the weapon debris and air, thermalizing the neutrons. As a result of these interactions, the resulting neutrons emitted encompass an energy spectrum, and the neutrons travel complex paths within the system making understanding the nuclear weapons physics difficult.[14]

A necessary component of a nuclear device is the core, or “pit”, that must contain a sufficient amount of a fissile isotope, typically $^{239}Pu$. A pit must be composed of “weapons-grade” material, meaning that the amount of the non-fissile isotopes of the primary isotope is minimal. This is because the neutrons required for the chain reaction are produced through (n, f) reactions with the fissile isotope. However, any non-fissile isotopes present will undergo (n, $\gamma$) reactions, thus reducing the neutron economy and decreasing the explosive yield of the weapon. Other pit characteristics such as shape, size, and density will affect the resulting yield. As the explosive yield is a measure of device performance, impurities within the assembly must be kept to a minimum.

Since there are numerous factors regarding the physical and chemical properties of the pit, understanding the effects of aging on the material is necessary for predicting how the overall performance is affected. However, this is a complex problem as it has been understood that properties such as thermal expansion, alloying, self-irradiation, and impurity ingrowth are characteristic of Pu materials.[15] One specific area of interest focuses on the radioactive decay of Pu that results in the ingrowth of non-fissile isotopes within the pit. The change in isotopic composition over time and its influence on the performance and reliability of the U.S.’s aging Pu inventory is a primary mission of the SSMP.

### *1.5.2 Radiochemical Diagnostics*

Ensuring the reliability of the stockpile depends on the fundamental understanding of the physics and chemistry that describes the performance of a weapon without underground

nuclear testing. One pathway towards achieving this is through the use of radiochemical diagnostics for yield determination. Past nuclear weapons tests employed radiochemical detectors as a means for yield evaluation. Stable isotopes such as yttrium-89 (Y-89) were loaded into known locations within a device and, following detonation, the isotopic ratio of the neutron activation products, $^{87}$Y and $^{88}$Y, were quantified. This data, along with neutron capture cross section data, was then used in theoretical yield and performance calculations. However, due to the complex neutron reaction network, radioactive nuclides produced also undergo nuclear reactions due to the high neutron fluence environment. Reliable cross section data sets for radioactive nuclides were not available or had large uncertainties.[16] Thus, the current computational simulation methods used for testing device reliability are limited by the accuracy and precision of this data, and obtaining more reliable data experimentally supports the SSMP mission.[17]

Since the composition of the Pu pits changes over time, computational simulations can be used to address and understand the effects of isotope ingrowth on weapons performance. Weapons-grade plutonium (WGPu) contains ~94% fissile $^{239}$Pu; however, there are also additional non-fissile Pu isotopes present. When newly produced, no impurities from other radionuclides are present and the pit is expected to perform as designed. However, the current U.S. stockpile of WGPu is old and, while there is no unclassified data regarding the age of Pu in the U.S. inventory, it is estimated to have an average age of ~50 years.[18,19] Due to the ingrowth of radionuclide impurities, understanding how this change in composition affects the physics and performance upon implosion is crucial and obtaining reliable nuclear data is needed to achieve this.

The half-lives of the Pu isotopes range from 14.4 years to 373,300 years for $^{241}$Pu and $^{242}$Pu, respectively. The change in isotopic composition as a result of the radioactive decay of Pu is shown in Table 1.1. Due to these half-lives, U ingrowth will occur throughout the lifetime of the material. Relevant to this dissertation is the presence of $^{241}$Pu which decays more quickly than the other Pu isotopes with its beta decay resulting in the buildup of $^{241}$Am.[20] After 50 years of aging, 89% of the $^{241}$Pu will have decayed and $^{241}$Am would contribute to ~0.17% of the WGPu. An increase in the amount of $^{241}$Am in Pu pits poses two significant concerns: radiation safety and device reliability. The handling of Pu pits in gloveboxes by workers is limited by dose received to the hands due to the intense gamma ray emissions from $^{241}$Am. Thus, this can hinder meeting the goal of producing 80 pits per year set by congress in 2019.[13]

**Table 1.1:** The change in composition of Pu isotopes weapons-grade plutonium and the resulting composition of ingrown radionuclides after 50 years of aging. Table prepared using data from CRS Report 7–5700.[21]

| Pu Isotopes in WGPu | Half-life (years) | Composition in Fresh WGPu (wt%) | Composition in 50 year-old WGPu (wt%) |
|---|---|---|---|
| $^{238}$Pu | 87.7 | 0.01 | 0.01 |
| $^{239}$Pu | 24,110 | 93.77 | 93.64 |
| $^{240}$Pu | 6,563 | 6 | 5.97 |
| $^{241}$Pu | 14.35 | 0.2 | 0.02 |
| $^{242}$Pu | 373,300 | 0.02 | 0.02 |
| **Decay Products** | | | |
| $^{241}$Pu → $^{241}$Am | 432.2 | 0 | 0.17 |
| $^{241}$Am → $^{237}$Np | 2,144,000 | 0 | 0.01 |
| $^{238}$Pu → $^{234}$U | 245,500 | 0 | 0 |
| $^{239}$Pu → $^{235}$U | 703,800,000 | 0 | 0.13 |
| $^{240}$Pu → $^{236}$U | 23,420,000 | 0 | 0.03 |
| $^{242}$Pu → $^{238}$U | 4,468,000,000 | 0 | 0 |
| **Total** | | 100 | 100 |

Obtaining the nuclear data relevant to the neutron activation of the $^{241}$Am reaction that occurs in the weapon's reaction network is one of particular interest. The (n,$\gamma$) reactions on $^{241}$Am produce $^{242}$Am isomers that subsequently $\beta^-$ decay to $^{242}$Cm (Figure 1.3).

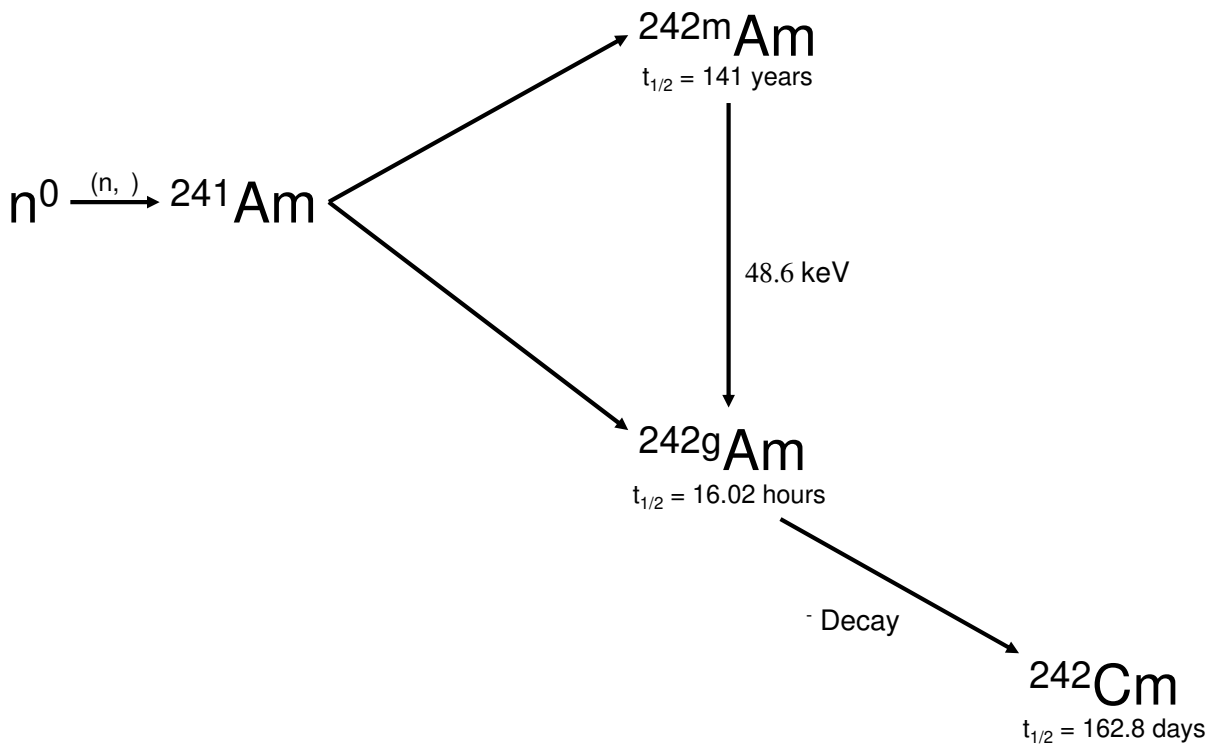


**Figure 1.3:** Neutron capture of $^{241}$Am results in the production of $^{242m}$Am and $^{242g}$Am which both decay to $^{242}$Cm.

While there is extensive data available regarding the $^{241}$Am(n,$\gamma$) cross section, these measurements were obtained over 30 years ago and background from scattered neutrons contributes to large uncertainties. Consequently, there is poor agreement between the neutron-capture cross section data sets available.[22–25] Thus, accurate measurements of these cross-section values across the neutron energy range are needed for meeting the goals of the SSMP.

Another important aspect of the $^{241}$Am(n,$\gamma$) nuclear reaction is the subsequent formation of the $^{242m}$Am and $^{242g}$Am isomers which can provide additional quantitative information regarding nuclear device physics. This reaction is interesting as the metastable state ($^{242m}$Am, $t_{1/2}$=141 y) is longer lived than the ground state ($^{242g}$Am, $t_{1/2}$=16.02 h). In addition to its long half-life, the thermal-fission cross section of $^{242m}$Am (~7,200 ± 300 barns) is nearly an order of magnitude greater than that of fissile $^{235}$U and $^{239}$Pu making it an isotope of interest for nuclear fuel.[26,27] However, the low availability and high neutron capture cross section of $^{242m}$Am limits its use. While the production of $^{242m}$Am can be achieved through neutron capture of $^{241}$Am, the $^{242m}$Am /$^{242g}$Am population ratio and its dependence on neutron energy is not well characterized. Therefore, determining both the (n,$\gamma$) cross sections and the isomeric population ratio as a function of neutron energy is essential to understanding potential production pathways and the neutron reaction network in nuclear device explosions.

Since $^{242m}$Am decays to $^{242g}$Am via isomeric transition and $^{242g}$Am $\beta^-$ decays to $^{242}$Cm, quantifying $^{242}$Cm at various times after irradiation provides a convenient way to obtain information about the $^{242m}$Am /$^{242g}$Am isomeric ratios as a function of neutron energy. This can be achieved through the neutron irradiation of $^{241}$Am targets at various neutron energies from the sub-eV to several hundred eV range. The amount of the shorter-lived $^{242g}$Am isomer produced can be determined by quantifying the $^{242}$Cm daughter immediately following the irradiation of $^{241}$Am. Additional $^{242}$Cm quantification at a later time post-irradiation will then allow for the determination of the amount of $^{242m}$Am produced. Since this approach relies on the accurate and precise quantification of $^{242}$Cm

produced from irradiated $^{241}$Am targets, the complete separation and recovery of $^{242}$Cm is required.[28–30]

# CHAPTER 2: USED NUCLEAR FUEL REPROCESSING METHODS

## 2.1 Large-Scale Reprocessing History

Precipitation techniques were among the first separation procedures used for TRU elements. At the beginning of the Manhattan Project, there were only trace quantities of Pu in the United States' inventory and, as a result, considerable resources were put into place to produce and purify Pu for its use in nuclear weapons.[31] Since small amounts of Pu was produced from the irradiation of several tons of U, the main problem was developing a method that would achieve a high yield and purity of the desired Pu product.[32] Direct precipitation of Pu is not possible because of the low concentration making coprecipitations with the use of a carrier necessary for Pu recovery. In addition, other FPs resulting from the irradiation of $^{235}U$ are present and must be separated to eliminate the high gamma radiation dose associated with them. While the lanthanum fluoride precipitation technique was pursued and was the preferred Pu recovery process at the Clinton Engineer Works facilities at the Hanford site, it was rejected as the main separation method due to resulting equipment corrosion. Based on the knowledge that heavy metal phosphates were insoluble in acid and that the key to achieving this separation was based on the exploitation of Pu's oxidation states, S. G. Thompson pursued the early development of the bismuth phosphate process.[32]

The bismuth phosphate process was verified at the X-10 pilot plant in Oak Ridge, Tennessee in 1944 and resulted in the first Pu shipment to Los Alamos. A 90% recovery of Pu was achieved and by 1945, X-10 had produced 326.4 grams of Pu.[33] The bismuth

phosphate method was then utilized on a large-scale at the T-Plant, the world's first large-scale separation facility for Pu, with the goal of recovering ~250 grams of Pu metal from one ton of irradiated U every day.[34]

The bismuth phosphate process required numerous decontamination stages and is based on the oxidation-reduction cycle of Pu that carries Pu(IV) and Pu(VI) from an acidic aqueous solution using Bi(III) phosphate. The irradiated uranium is dissolved in nitric acid followed by the addition of sulfuric acid to prevent U precipitation. Bismuth phosphate is then used to precipitate Pu(IV) which is then re-dissolved in nitric acid and oxidized to Pu(VI). Bismuth phosphate byproducts are then precipitated leaving Pu(VI) in solution which undergoes another reduction reaction to Pu(IV) and precipitation with bismuth phosphate. To further decontaminate and concentrate the recovered Pu so that is it suitable for weapons use, a similar oxidation-reduction cycle is then carried out with lanthanum fluoride.[32] However, this process is limited by the large amounts of chemicals used in the batch process and its inability to recover U.

When it was found that tributylphosphate (TBP) could oxidize and extract cerium nitrate from the trivalent lanthanides in a solvent extraction separation system, this separation concept was applied to U and Pu systems.[35] Thus, the Plutonium, Uranium, Reduction, EXtraction (PUREX) process was developed at Oak Ridge National Laboratory and, with over 70 years of research and operation, is the most mature large-scale reprocessing method.[36] Since PUREX utilizes solvent extraction, it provides continuous operation with a more complete extraction while generating less waste relative to the bismuth phosphate

process. Thus, it was implemented as a replacement for the bismuth phosphate process at Hanford but has also been modified in more recent years to be more suitable for commercial use. The PUREX Process uses the accessible higher oxidation states of U and Pu to isolate them from other chemically similar elements (*e.g.,* Lns, MAs, and fission products). Adjustment of the U and Pu oxidation states allows for their transition between the aqueous and organic phases which allows for their separation.

The three main steps in the PUREX process are: 1) Co-extraction of U and Pu from other fission products, 2) Partitioning of Pu from U, and 3) Stripping (Figure 2.1).

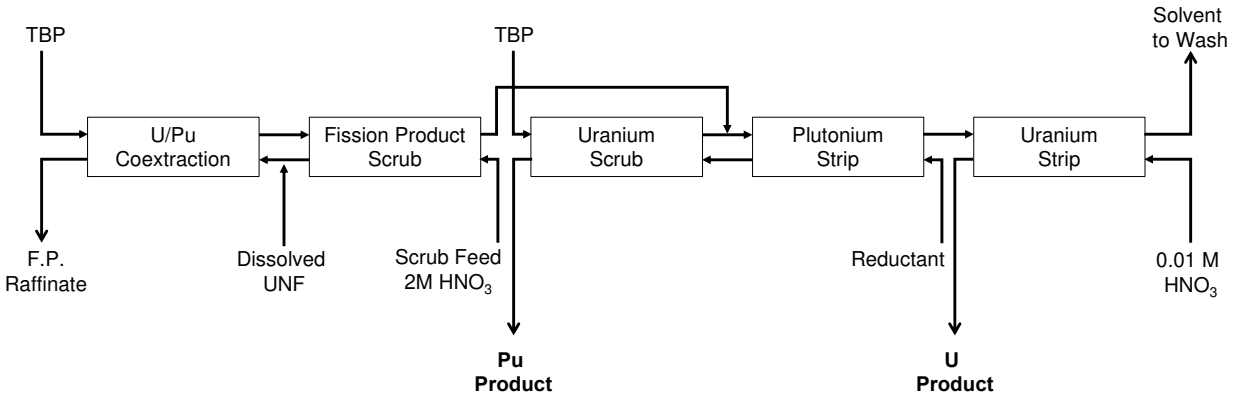


**Figure 2.1:** General Plutonium, Uranium, Reduction, EXtraction (PUREX) process flowsheet for a counter-current solvent extraction system. This process utilizes the tributyl phosphate (TBP) extractant in n-dodecane as the organic phase for the U/Pu and fission product (FP) separation from the used nuclear fuel (UNF) dissolved in the acidic aqueous phase and produces pure U and Pu product streams for their conversion into nuclear fuel.

After cladding removal, the irradiated fuel is dissolved in highly concentrated nitric acid producing the feed solution. U and Pu are extracted from other fission products by contacting the feed solution with the organic phase consisting of 30% TBP in kerosene or n-dodecane. Both U and Pu can be back extracted into a dilute acidic aqueous phase,

and, after the addition of a Pu reductant, U is back extracted into the organic phase leaving Pu in the aqueous phase. The radionuclides are then stripped from their solvent streams for conversion to their oxide forms that can be used for mixed oxide fuel (MOX) fabrication.

### 2.2 Advanced Reprocessing Methods

While PUREX has been successfully applied to large scale separations, the lanthanides are not eliminated from the waste stream and the resulting pure Pu stream poses proliferation concerns. To address this, in 1999 the U.S. developed the URanium EXtraction (UREX) process that modifies the PUREX process through the addition of acetohydroxamic acid (AHA).[37–39] The addition of AHA prior to the initial extraction step suppresses the extraction of the TRU elements and FPs into the organic phase and therefore eliminates the generation of a pure Pu waste stream (Figure 2.2).

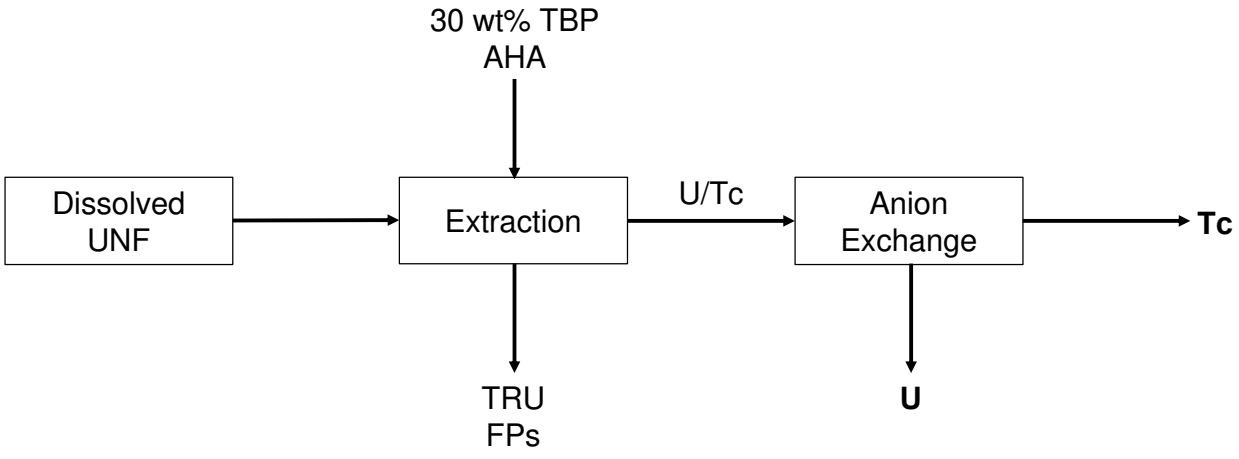


**Figure 2.2:** Simplified general block diagram of the URanium EXtraction (UREX) process the uses the tributyl phosphate extractant and acetohydroxamic acid reductant to generate two separate U and Tc product streams and a mixed transuranic/fission product raffinate.

In addition, the fission product, technetium (Tc), is coextracted in the U stream from which it can be stripped and vitrified for disposal. Other variations of the UREX process have been proposed including UREX+, UREX+1, and UREX+2 which introduce additional separation stages to recover other fission products and actinides.[40]

Similarly, the COmbined EXtraction (COEX) process developed in France is another alternate PUREX process that results in three streams: U, U/Pu, and MAs + Ln. By adjusting oxidation states to produce a combined U-Pu stream, proliferation risks are reduced, and the recovered U and Pu are used as MOX fuel in LWRs. The U stream undergoes purification, conversion, and enrichment for use as recycled fuel.[41,42]

For a post-uranium separation scheme, the raffinate containing the TRU, rare earth elements (REEs)/Ln(III), and FPs would move towards the Fission Product EXtraction (FPEX) process (Figure 2.3).

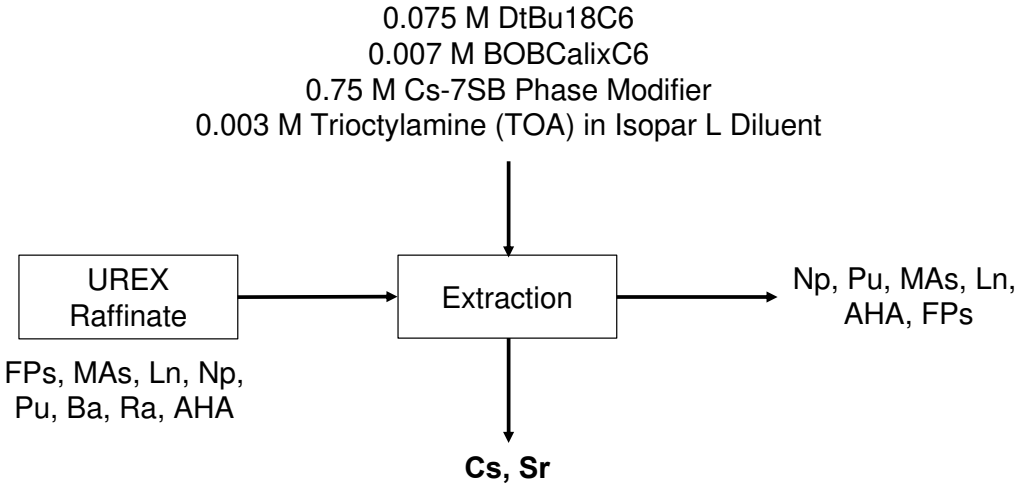


**Figure 2.3:** Simplified general block diagram of the Fission Product EXtraction (FPEX) process that uses crown ether extractants to recover the Cs and Sr fission products resulting in a mixed TRU/FP/Ln raffinate.

Using crown ether extractants (Figure 2.4), the bulk of the heat-generating FPs (Cs, Sr, Ba, and Rb) can be removed.[43,44] FPEX has been demonstrated on dissolved UNF in centrifugal contactor and mixer-settler systems and the sound understanding of the physical and chemical processes involved makes its presence into reprocessing schemes standard.

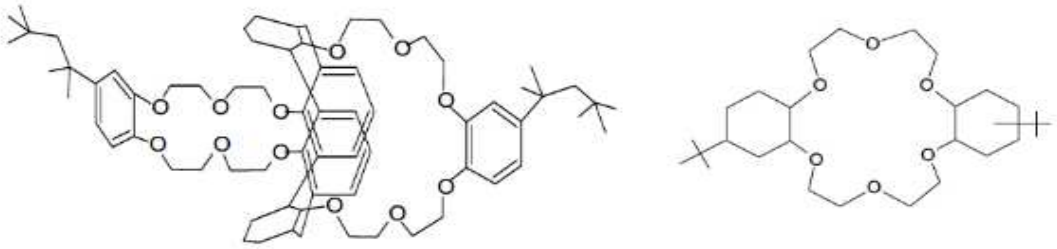

BOBCalixC6 DtBu18C6

**Figure 2.4:** Structures of the BOBCalixC6 and DtBuCH18C6 crown ether extractants used in the Fission Product EXtraction (FPEX) separation.

Following the FPEX separation, a TBP-based separation called the Neptunium Plutonium EXtraction (NPEX) process co-recovers Np and Pu (Figure 2.5). This is achieved by increasing the $HNO_3$ concentration of the aqueous phase to remove the FPs, MAs, and Ln and to ensure that Np and Pu are present in the extractable IV and VI oxidation states. They would be recovered in a TBP/dodecane organic phase and stripped using AHA to produce the Np/Pu product stream.[45,46] Thus, the incorporation of NPEX into a proposed reprocessing scheme would also eliminate the concerns regarding a pure Pu product stream.

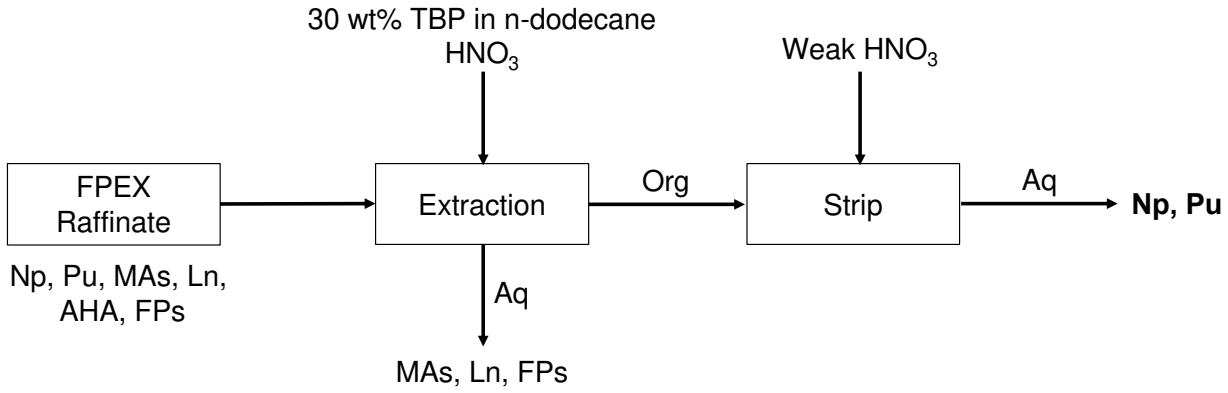


**Figure 2.5:** Simplified general block diagram of the Neptunium Plutonium EXtraction (NPEX) process that co-extracts Np and Pu into a product stream and generates a TRU/FP/Ln raffinate.

The TRansUranium EXtraction (TRUEX) process shown in Figure 2.6 was developed at Argonne National Laboratory and is another modified PUREX process based on TBP extraction and introduces the addition of carbamoylmethylphosphine oxide (CMPO).

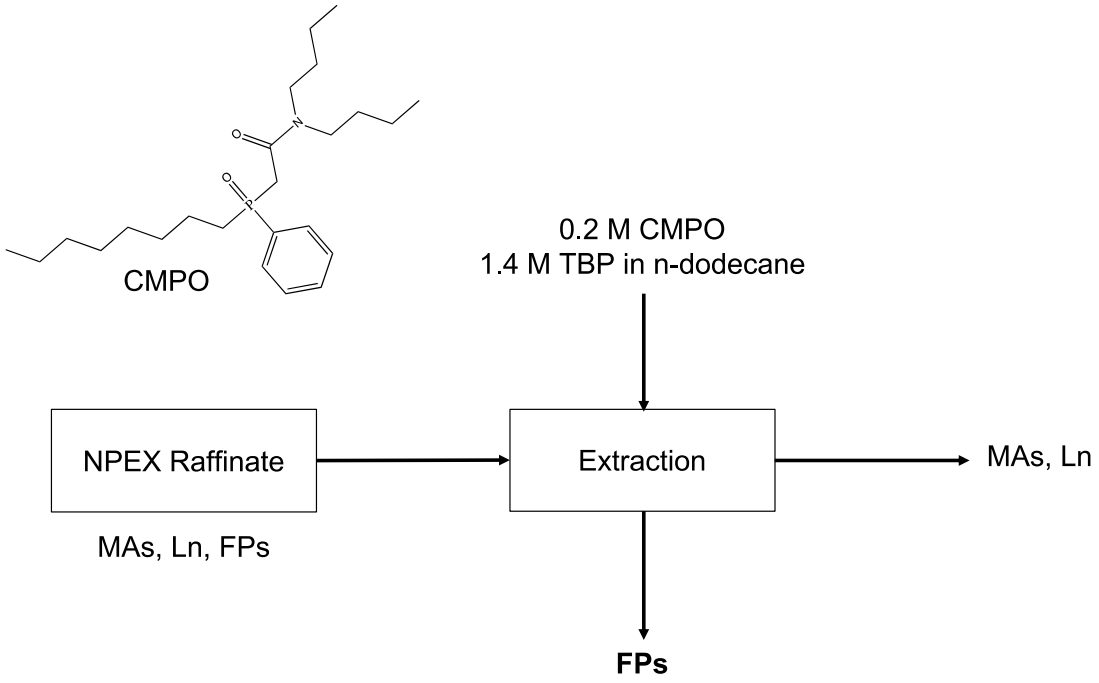


**Figure 2.6:** Simplified general block diagram of the TRansUranium EXtraction (TRUEX) process that removes the remaining fissions products from the resulting raffinate containing the MAs and Ln.

The introduction of CMPO has two benefits: 1) reduction in third phase formation minimizing criticality hazard through the concentration of Pu and 2) facilitating the extraction of tri-, tetra-, and hexavalent actinides.[47–50] In theory, the TRUEX process could be introduced at the beginning of reprocessing to co-recover the TRU and REEs from the fission products but it has been preferred as a post-FPEX process to separate the MAs and Lns from the remaining FPs in solution. Since CMPO is the key to this separation, the need for oxidation state adjustment is eliminated and the resulting waste streams are easier to handle. Because this process is nearly identical to PUREX, the physical and chemical behavior is well understood. TRUEX has been demonstrated in commercial systems using a continuous countercurrent extraction and has also been used in the U.S. and other countries to decontaminate actinide-containing waste.[51–53]

Similarly, the Group ActiNide EXtraction (GANEX) process developed proposes to simplify the scheme using two post-dissolution extraction cycles. First, U(VI) extraction would occur using an N,N-dialkylamine (DEHiBA) instead of TBP. A group separation of the TRU elements along with the REEs and FPs would then follow. The GANEX process has been performed in both mixed-settler and counter-current systems which achieved ~99.99% U recovery. In addition, there is favorable agreement between calculated and experimental data.[54–56]

The DIAMide EXtraction (DIAMEX) process is another iteration of the TRUEX process towards the recovery of the MA and Lns from UNF that replaces the phosphorus-based TBP reagent with oxygen-donor ligands. Malonamide or diglycolamide (DGA) extractants

have been chosen as suitable reagents for this process based on their high affinity for MAs. The extractant, *N,N,N',N'*-tetraoctyl diglycolamide (TODGA), is the most common DGA used in the DIAMEX process for its superior selectivity and solubility in the organic phase. However, the necessary third phase modifiers complicate the chemistry in the system, making it less favorable for large-scale separations. DIAMEX has been demonstrated using UNF on industrial technology and validated the system's behavior.[57–61]

Regardless of which of the above processes described above are implemented, they all leave a MA/Ln bearing raffinate which must be further processed if the desired outcomes of P&T are to be achieved. The presence of the Ln elements in MA waste streams hinders the P&T goal since the Lns are considered "neutron scavengers". Their high neutron capture cross section makes them a poison in nuclear fuel as they decrease the efficiency of the transmutation process by absorbing neutrons and generating heavier isotope byproducts. The predominant trivalent oxidation state for the Lns and MAs results in similar size to charge ratios and therefore similar electrostatic interactions that would typically be exploited in separation methods. Thus, the Ln and MAs have similar hard acid/base interactions with the typically employed oxygen and phosphorus based extractants. However, it has been found that using ligands containing donor atoms softer than oxygen (*e.g.,* nitrogen, sulfur) preferentially complex with the MAs over the Lns. While the underlying chemistry to explain this behavior is still an area of uncertainty, it is believed that the answer lies within minor differences in the radial extension of the lanthanide's 4f and actinide's 5f/6d orbitals.[62]

Extensive research has been conducted that explores the use of soft donor extractants for selective complexation with the MAs over the Lns. The observed increase in covalent interactions between the MAs and soft nitrogen donor ligands have been promising as the shielding effects of 4f orbitals by the 5d and 6s orbitals eliminate these interactions for lanthanides. Although there is a large body of research demonstrating the successful use of soft donor atoms for An(III)/Ln(III) separations, a separation suitable for industrial application has yet to be achieved.

The most well-characterized option An(III)/Ln(III) separation option is the Trivalent Actinide Separations by Phosphorous Reagent Extraction from Aqueous Komplexes (TALSPEAK) process developed at Oak Ridge National Laboratory in the 1960s (Figure 2.7).[63]

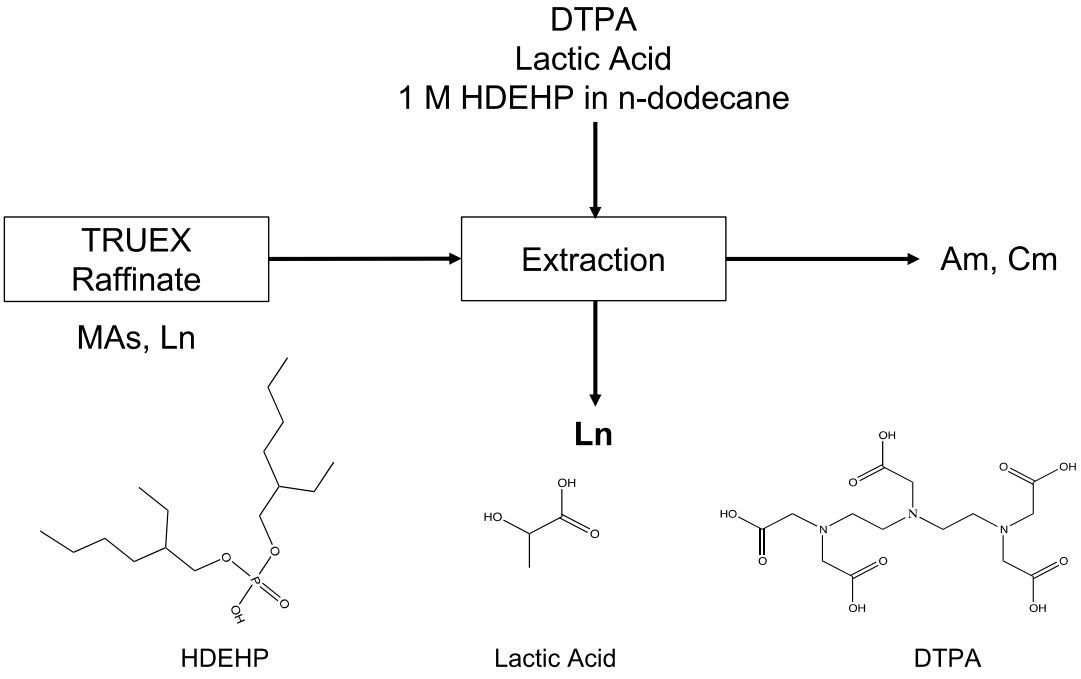


**Figure 2.7:** Simplified general block diagram of the Trivalent Actinide Separations by Phosphorous Reagent Extraction from Aqueous Komplexes (TALSPEAK) process for the lanthanide/actinide separation.

TALSPEAK uses the organophosphate (HDEHP) and soft N-donor (DTPA) ligand pair and lactic acid as a pH buffer. In this system, the Ln(III) are selectively extracted into the organic phase by HDEHP while the An(III) are retained by DTPA in the aqueous phase. Separation factors >100 have been achieved for a group Ln(III) separation from Am(III) which is desirable for large-scale reprocessing; however, the lack of understanding of the underlying chemistry that occurs in the aqueous and organic phases coupled with the disagreement between experimental and theoretical data impedes its application.[64,65]

Recently, in 2014 the Actinide Lanthanide SEParation (ALSEP) method was introduced which combines a neutral diglycolamide extractant (TODGA or T2EHDGA) and an acidic extractant (HEH[EHP] or HDEHP) to achieve an An(III)/Ln(III) separation. ALSEP has afforded high Eu(III)/Am(III) separations and its application has been demonstrated using a commercial centrifugal contactor system.[66–68]

Based on the methods discussed above, a proposed reprocessing scheme (Figure 2.8**)** can be developed by incorporating the separations processes that have the largest body of research on both the laboratory and process scales. After dissolution of the UNF, the UREX process can be applied to generate a U/Tc stream and a Pu/MA/FP stream. This process is more beneficial than the established PUREX process due to the elimination of a pure Pu stream. The U/Tc stream will undergo stripping using anion exchange to recycle U as reactor fuel and dispose of Tc. The Pu/MA/FP raffinate will then follow the FPEX process to eliminate the short-lived, heat producing FPs (Cs, Sr). Subsequently, the NPEX process will co-extract Pu and Np to eliminate proliferation concerns.

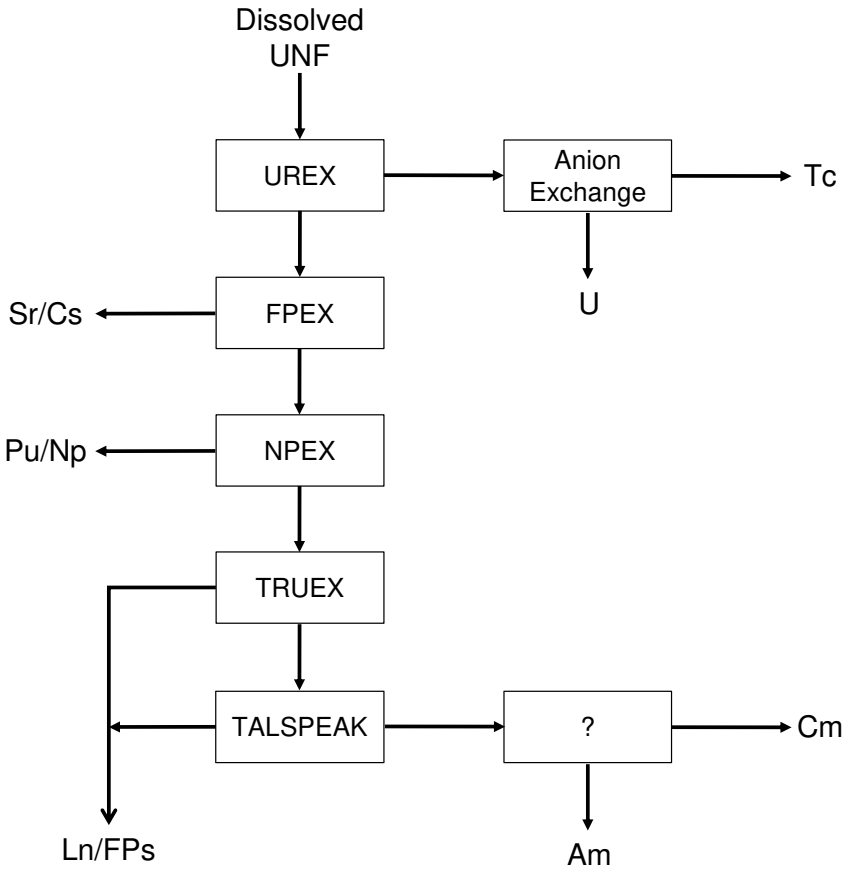


**Figure 2.8:** Potential flowsheet for the reprocessing of used nuclear fuel based on well-characterized separation methods.

The TRUEX process will facilitate the co-extraction of MAs from the remaining FPs and the subsequent TALSPEAK process will achieve the An(III)/Ln(III) separation. In view of full recycling, the MA waste stream could undergo an additional Am/Cm separation for the recycling of Am in a nuclear reactor; however, a suitable method has yet to be identified.

### 2.3 Current Reprocessing Needs

As can be seen, the large number of elements present in UNF has resulted in numerous solvent extraction processes and reprocessing scheme variation proposals. Each

addresses the major proliferation, engineering, and radiation safety concerns that come with the P&T option. However, to achieve the complete P&T strategy, a large-scale separation method for americium from curium needs to be identified and fully characterized. As these are the primary radionuclides that inhibit the development of a long-term storage plan for the resulting waste, this separation must be included in P&T schemes.

The separation of Am and Cm has been historically understood as one of the greatest challenges in radioanalytical chemistry since their nearly identical chemical behavior makes even small analytical scale separations difficult to achieve. While this separation has been demonstrated successfully by taking advantage of americium's access to higher oxidation states using strong oxidants, the instability of oxidized americium and the use of strong oxidants limits their application to industrial scale processes. A literature review of the current literature regarding the separation of both trivalent and oxidized Am from Cm is provided in chapter three. This dissertation aims to add to this body of research through the exploration of chromatographic systems that exploit redox principles. In addition, the application of this system to a hexavalent group actinide separation from lanthanides has been investigated to simplify the currently proposed reprocessing schemes.

# CHAPTER 3: CHEMISTRY OF THE LANTHANIDE AND ACTINIDE ELEMENTS

## 3.1 Introduction

The lanthanide (Ln) and actinide (An) elements feature electrons that progressively fill the *4f* and *5f* orbitals, respectively, and are therefore considered *f*-block elements. Thus, the An elements are analogous to the Ln elements based on their similar electron occupancy.[69] As a result, the separation of these elements has been a long-standing challenge due to similar chemical properties (*e.g.,* decreasing ionic radii with increasing atomic number, charge density, oxidation states).

Both the Ln and An elements are present in UNF and are important considerations in the development of UNF reprocessing schemes. Efficient transmutation of the long-lived An elements requires the elimination of the neutron scavenging Ln elements as the unfavorably large neutron capture cross sections of the Lns decreases the neutron economy. Current reprocessing schemes have been proposed to implement an An/Ln separation followed by an Am/Cm separation to achieve the closure of the NFC.[70,71] However, there is an increasing interest in the development of a group hexavalent An/Ln separation since the An/Ln and Am/Cm separations would be carried out simultaneously, decreasing the number of reprocessing steps.[72–74]

The management of Cm in MA recycling is a necessary component for both fuel/target preparation and/or post-transmutation handling in a closed NFC. While Cm could be incorporated into MOX fuels for MA transmutation in theory, a high spontaneous fission

probability results in high neutron and heat emissions from Cm that requires advanced engineering and facility controls. In addition, the neutron irradiation of Cm-bearing targets results in the production of higher actinides (*e.g.,* californium) that increase neutron dose rates and poison the back end of the NFC. With this in mind, Cm transmutation is considered impractical and the generally accepted approach is through the recycling of Am in fast reactors and the vitrification of Cm with other FPs for geologic disposal.[70,75] An Am/Cm separation is necessary for this to be realized; however, the predominant trivalent oxidation states in acidic aqueous solutions, bonding characteristics, and ionic radii have made this separation a technological challenge.

### 3.2 Lanthanides

Elements with atomic numbers 57 – 71 are a part of the lanthanide series and are also known as “rare earth elements” (REEs). However, the lanthanides are stable, primordial elements with abundances comparable to that of nickel and were discovered prior to 1907. An exception to this is promethium which has no stable isotopes and was not identified until its isolation from irradiated uranium.[76] While the MAs are generated from the neutron activation of uranium fuel, the radioactive lanthanides are produced as fission products. The fission-produced lanthanides exist in UNF in a much higher concentration than the MAs; however, a majority of them will decay during cooling due to their shorter half-lives.

The lanthanides have electron configurations that consist of a xenon core with *4f*, *5d*, and *6s* subshells accessible for electron filling. Since the *5d* subshell of lanthanum is lower in

energy than the *4f* subshell, the addition of the *f*-electrons begins with the second member of the series and ends with the 15$^{th}$ member giving a total of 14 *f*-electrons. This is explained by the lanthanide contraction which describes the rapid contraction of the *4f* orbitals as protons are added across the series. The *4f* orbitals are then more stable than the *5d* orbitals, and electrons sequentially fill the *4f* orbitals with the exception of gadolinium and lutetium which favor the stability of the half-filled and fully filled *4f* subshells, respectively.[69,77]

The lanthanide contraction causes the *4f* orbitals to penetrate into the xenon core and therefore the *5s* and *5p* orbitals. As a result, the *4f* orbitals are shielded within the *5s* and *5p* orbitals which are not as effectively shielded from the nuclear charge resulting in contraction.[69,77] This gives rise to the characteristic lanthanide trend of a decrease in both the atomic and ionic radii as the series is traversed. With the *4f* orbitals being more core-like in behavior, they are unable to form bonds with ligands and ionization occurs through the removal of electrons from the *6s* and *5d* orbitals limiting the oxidation states available for the lanthanides and yielding ionic bonding characteristics. The lanthanide contraction is responsible for the predominant trivalent oxidation states that exist in solution; therefore, separations must exploit the size and charge differences of these ions.

### 3.3 Actinides

The actinides are elements with atomic numbers 89 – 103 and are heavy, unstable nuclei that undergo radioactive decay through alpha or beta emission followed by the release of excess energy through gamma emission, as well as spontaneous fission. The earlier

actinides, Ac, Th, Pa, and U are the naturally occurring daughters of the primordial decay chains, but the transuranic (TRU) elements are synthetically produced through successive neutron capture of the parent radionuclide followed by subsequent beta emission.[69,78,79] Similar to the lanthanides, the actinides are a part of the *5f* block of the periodic table with progressive electron filling of the *5f* subshell. However, the early actinides (Ac – Pu) feature less pronounced contraction and therefore more complex chemistry than the early lanthanides due to an energetic overlap between the *6d* and *5f* orbitals.[69,77]

For heavier actinides beyond Pu, relativistic effects are more pronounced as the velocities of the electrons increase toward the speed of light resulting in an increase in relativistic momentum. This results in the contraction and stabilization of the *s* and *p* orbitals and the expansion and destabilization of the *5f* orbitals.[80,81] The *5f* orbitals being unshielded by the *6s* and *6p* orbitals and the near degeneracy of the *5f*, *6d*, and *7s* orbitals allows for the delocalization of *5f* electrons and more outer-shell electrons available for bonding. As a result, a wider range of oxidation states are available and it is widely believed that an increased tendency for covalent bonding character is at play; however, a lack of experimental data does not fully support this hypothesis (Table 3.1).[82] Since the *5f* electrons are not as effectively shielded from the nucleus, as the atomic number increases so too does the effective nuclear charge causing the energy of the *5f* orbitals to decrease.

**Table 3.1:** The observed oxidation states of the actinide elements and the electronic configurations of the most stable species.

| | Ac | Th | Pa | U | Np | Pu | Am | Cm | Bk | Cf | Es | Fm | Md | No | Lr |
|---|---|---|---|---|---|---|---|---|---|---|---|---|---|---|---|
| +2 | | | | | | | | | | | | | | $5f^{13}$ | |
| +3 | $5f^0$ | | | | | | $5f^6$ | $5f^7$ | $5f^8$ | $5f^9$ | $5f^{10}$ | $5f^{11}$ | $5f^{12}$ | | $5f^{14}$ |
| +4 | | $5f^0$ | | $5f^2$ | | $5f^4$ | | | | | | | | | |
| +5 | | | $5f^0$ | | $5f^2$ | | | | | | | | | | |
| +6 | | | | $5f^0$ | | | | | | | | | Known | | |
| +7 | | | | | | | | | | | | | Most Stable | | |

As the *5f* orbitals continue to contract and become more core-like, there is a greater energy difference between the *5f* and valance orbitals making electrons more localized and unavailable for bonding. Due to this contraction, the trivalent oxidation state dominates the heavier actinides beyond Am (with the exception of No). Thus, the main difference between the oxidation states exhibited by the actinides depends on the energy required for the *5f* → *6d* transition.

### 3.4 Solution Chemistry of Americium and Curium

Americium (Z=95) and curium (Z=96) were first produced by Seaborg, James, Morgan, and Ghiorso in 1945 and 1944, respectively. Using the 60" cyclotron at the Radiation Laboratory of the University of California, Berkeley, irradiation of $^{238}U$ and $^{239}Pu$ targets by 40 MeV helium ions resulted in the synthesis of $^{241}Am$ and $^{242}Cm$ by the following reactions:[83–85]

$$^{238}U(\alpha,n)^{241}Pu \rightarrow {}^{241}Am$$

$$^{239}Pu(\alpha,n)^{242}Cm$$

The development of a fast and efficient separation method for these two radionuclides was necessary for the elucidation of their nuclear and chemical properties; however, initial separation routes were pursued based on the chemistry of the earlier actinides. As discussed previously, the early actinides exhibit a wide range of chemical behavior comparable to that of the *d*-block elements and attempts to isolate Am and Cm based on similar chemical properties to that of U, Np, and Pu were unsuccessful.[86]

Thus, Seaborg's actinide concept proposed the rearrangement of the periodic table and predicted that Am and Cm would be chemically similar to the lanthanide homologues, europium and gadolinium.[86,87] The predicted electronic configurations suggested that the transplutonium elements would instead exhibit trivalent oxidation states which ultimately resulted in the successful isolation of Am and Cm. However, the nearly identical properties made achieving the separation of Am from Cm and other lanthanides a time and resource consuming challenge. To date, the separation of these elements remains regarded as one of the most difficult chemical separations in the periodic table.

Seaborg's prediction that actinide chemistry would shift towards more lanthanide-like behavior around Am or Cm proved to be correct in that Am displays chemical characteristics similar to both the early and late actinides. While the ground state electron configuration of [Rn]$5f^7 7s^2$ with a favorable half-filled *5f* subshell would indicate divalent speciation, Am readily exists in the trivalent oxidation state in acidic aqueous solutions as a hydrated ion. This deviation from Eu-like behavior has been attributed to the near degeneracy of the *5f* and *6d* orbitals allowing for accessible electronic transitions from the

*5f* orbitals. In contrast, the half-filled *5f* subshell that results from the removal of the *7s* and *6d* electrons from the [Rn]$5f^7 6d^1 7s^2$ ground state electron configuration of Cm makes the trivalent oxidation state the most stable in acidic aqueous solutions.

Along with common trivalent speciation, $Am^{3+}$ and $Cm^{3+}$ exhibit nearly identical cationic radii (0.975 and 0.97 Å, respectively), solubilities, and complexation in aqueous acidic solutions.[88] These trivalent species form insoluble precipitates as fluoride, hydroxide, phosphate, oxalate, and iodate compounds. In addition, $Am^{3+}$ and $Cm^{3+}$ are sensitive to hydrolysis as a function of pH with insoluble hydrolysis product formation occurring at pH 5 and are also prone to hydrolysis at elevated temperatures.[89] Thus separations are typically carried out in acidic aqueous solutions to prevent loss of activity to container walls.

Since Am is located in the middle of the actinide series, the ability to adopt chemical properties of both the light and heavy actinide elements provides a route towards achieving the separation of Am from Cm and lanthanides. When determining the chemical properties of Am after its discovery, the pentavalent ($AmO_2^+$) and hexavalent ($AmO_2^{2+}$) oxidation states were observed spectroscopically and were found to be analogous in behavior to U, Np, and Pu.[90,91] While the trivalent oxidation state is most prevalent in acidic aqueous solutions, Am can also exist in the penta- and hexavalent states as the trans-dioxo actinyl species. In alkaline or carbonate media, Am can also exist in four valance states simultaneously through the oxidation of Am(III) by Am(VI).[92]

However, the instability of Am(V) and Am(VI) and the fast disproportionation of Am(V) to Am(III) and Am(VI) in acidic solutions was also observed.[93] The instability of the higher oxidation states are a result of both chemical and radiolytic processes. Although there are significant stability issues with Am(V) and Am(VI), several methods have been developed for the chemical separation of these oxidized species.

### 3.5 Separation of Trivalent Americium and Curium

While the solution chemistries of Am and Cm are nearly identical, the slight decrease in cationic radii observed with increasing atomic number resulting from actinide contraction has been exploited to achieve the separation of trivalent Am and Cm. The first separations carried out for the isolation and identification of Am and Cm achieved sequential chromatographic elution of the trivalent actinides on the Dowex-50 cation exchange resin with eluent solutions consisting of HCl and ammonium citrate. At lower HCl concentrations (3 – 9 M), elution order followed Cm>Am>Pu; however, at higher HCl concentrations (12 M) the reverse elution order of Pu>Am>Cm was observed which provided insight into the effects of the actinide contraction of *5f* element chemistry.[94,95] While the separation was satisfactory for the discovery of Am and Cm, small fractionation of these radionuclides is insufficient for its application.

The observed elution behavior in the HCl cation exchange system showed that at lower HCl concentrations, the effect of decreasing ionic radii dominates the chemistry. The greater charge density of Cm(III) yields a larger effective hydrated ionic radius that results in weaker ionic interactions between the metal ion and anionic functional group of the

resin. Thus, a stronger interaction between solvent molecules is observed for the heavier actinides relative to the lighter actinides giving a resulting elution profile that is in order of highest to lowest atomic number. In contrast, at higher chloride concentrations the An(III) cations with *5f* orbitals that have a greater radial extension form stronger chloride complexes resulting in their preferential elution.[94,95]

Expanding on the work done by Thompson, Street, and Seaborg, a gram scale separation using the Dowex-1 anion exchange resin containing quaternary amine functional groups and an NTA chelator in the eluent achieved >99% purity, but only ~60% recovery making it unsuitable for large-scale reprocessing application.[96] The adjustment of the eluent composition, interfering cations, and holdback reagents was determined to be beneficial in the tailoring of trivalent actinide separation protocols.[97–100] In addition, anion exchange methods using Dowex 1 x 8 have been successful for Am/Cm separations using mixed $HNO_3$/alcohol and strong electrolyte eluents; however, separations factors remain below 2.5 for these methods.[101,102]

Horwitz et. al. carried out numerous studies using tertiary and quaternary amines for trivalent actinide separations from nitrate salt solutions.[103,104] This work led to the development of an extraction chromatographic resin prepared through the adsorption of the quaternary ammonium nitrate Aliquat-336 onto diatomaceous earth.[105,106] More recent advancements in trivalent actinide separations using extraction chromatography include the successful use of malonamide extractants in countercurrent chromatography,

lipophilic extractant/hydrophilic complexant systems, tertiary pyridine extractants in mixed $HNO_3$/methanol eluents, and organophosphorus extractants.

Over the past two decades, a large body of literature has focused on trivalent actinide separations utilizing solvent extraction based on Pearson's Hard-Soft Acid-Base theory.[107] While it is generally understood that soft-donor ligands relative to oxygen (*e.g.,* S, N) show preferential complexation with the An(III) over the Ln(III), complexation behavior for the intragroup separation of trivalent An ions is not well understood; however, a wide array of new extractants have been proposed in view of Am(III)/Cm(III) separations. Crown ether extractants have also been used in liquid-liquid extraction systems for a size-based Am/Cm separation; but fission products must be eliminated prior to extraction.[108] Despite favorable separation factors, the large-scale implementation of these liquid-liquid processes is unfavorable due to the large number of contact stages and sensitive process flowsheets required. A thorough review of the liquid-liquid processes for Am(III)/Ln(III) separation can be found in Zsabka et. al.[109]

### 3.6 Separation of Oxidized Americium from Curium

The adjustment of oxidation states as a means to facilitate chemical separations has been used for both analytical and industrial scale processes via precipitation, solvent extraction, and chromatographic techniques. The chemical behavior of metal ions deviates greatly for different oxidation states offering a path towards the development of more efficient partitioning techniques. Thus, the separation of higher valent Am from

various metal ions (mainly $Cm^{3+}$ and $Ln^{3+}$) can be carried out by exploiting similar oxidation-reduction cycles utilized for the separation of the earlier actinides.

However, the Am(VI)/Am(III) reduction potential of ~1.7 V makes finding a suitable oxidizing agent capable achieve Am(III) oxidation difficult (Figure 3.1).[110] In addition, the penta- and hexavalent oxidation states of Am are difficult to maintain as they are strong oxidizers themselves. Redox reactions between the higher oxidation states of Am with nitric acid, radiolysis products, and any impurities present in the system undergo rapid kinetics limiting the application of redox-based separations on an industrial scale.

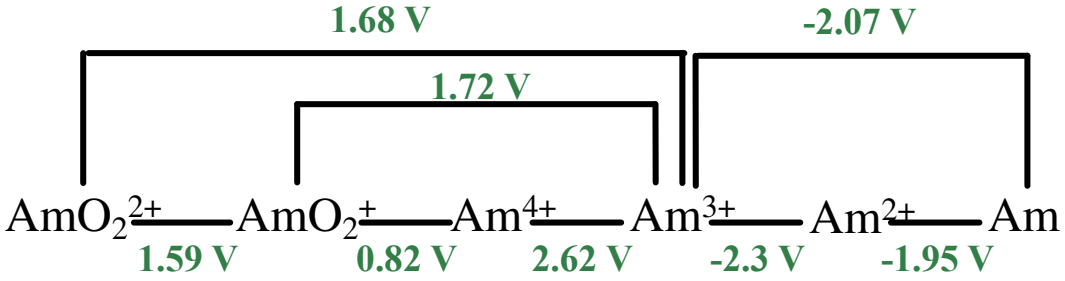


**Figure 3.1:** Standard reduction potentials for Am in acidic aqueous media

Initial redox based Am separations took advantage of the different solubility behavior through precipitation techniques. As trivalent elements are insoluble as fluoride, carbonate, and oxalate salts, they are able to be separated from hexavalent Am.[111–113] Am(III) oxidation to Am(VI) with potassium peroxydisulfate led to the separation of soluble Am(VI) from the $CmF_3$ precipitate.[114] Combining precipitation and column chromatography, silver-catalyzed peroxydisulfate was used to oxidize Am in solution prior to its introduction into a calcium fluoride column resulting in the elution of Am(VI) and retention of the trivalent metal ions.[115]

Redox reactions have also been coupled with ion exchange and extraction chromatography to yield better separations factors. A phosphorus-based extractant selective for hexavalent actinides at low acidities was successful in separating $K_2S_2O_8$-oxidized Am(VI) from Cm(III); however, this method would not perform well in large-scale environments that require greater acidity.[116] Recently, metal (IV) pillared phosphate phosphonate unconventional metal organic frameworks (UMOFs) were used as ion exchangers that retained Am(V) giving $SF_{Am(V)/Cm(III)}$ as high as 20.[117]

The separation of Am in higher oxidation states has been carried out in solvent extraction systems; however, the instability of these higher oxidation states has resulted in rapid reduction and separation factors undesirable for large-scale application. A group hexavalent actinide separation was demonstrated using copper(III) periodate as an oxidant and resulted in the quantitative oxidation of Am under molar $HNO_3$ concentrations, but requires short (~10 s) contact times to prevent Am(VI) reduction.[118]

*3.6.1 Am(VI)/Cm(III) Separations Using Sodium Bismuthate*

Increased interested in sodium bismuthate ($NaBiO_3$) as a promising solid oxidizing agent for Am/Cm separations has emerged due to the large Bi(III)/Bi(V) reduction potential of ~2.03 V). The first use of $NaBiO_3$ for the oxidation of $Am^{3+}$ to $AmO_2^{+}$ and $AmO_2^{2+}$ was demonstrated by Hara and Suzuki through the recovery of Am(V) and Am(VI) using fluoride precipitations.[119]

In solvent extraction systems, solid $NaBiO_3$ was used to oxidize Am(III) prior to tributylphosphate, diamylamylphosphonate, or dibutylbutylphosphonate extraction.[120–122] Since these extractants require higher acidities, the compatibility of $NaBiO_3$ at $HNO_3$ concentrations up to 6 M makes this a suitable candidate for Am(III) oxidation. While immediate Am(VI) reduction upon contact with the organic phase occurred, it was found that the addition of $HClO_4$ prevents this by promoting the dissolution of Bi(V) that acts as a holding oxidant for Am(VI). The separation factors achieved in these solvent extraction systems were low, however, and the interference of the Ce(III)/Ce(IV) redox couple interfered with Am(VI) extraction. Am(VI) solvent extraction was also demonstrated with three *N,N*-dialkyl amide extractants on both bench-scale and centrifugal contactor systems, but the presence of the fine $NaBiO_3$ powders proved incompatible with the mechanical systems thus limiting its use on an industrial scale.[123,124] Am(III) oxidation with perxenate ions and $NaBiO_3$ allowed for the 90% recovery of Am(VI) using 30% tributylphosphate, but the addition of solid sodium bismuthate would retain Am(III) preventing its oxidation and separation.[125]

While the presence of solid $NaBiO_3$ in solvent extraction systems is unfavorable for large-scale application, it was found that $NaBiO_3$ has a layered ilmenite structure similar to aluminum oxide that offers ion exchange behavior.[126] Thus, solid $NaBiO_3$ was used in a column chromatographic system taking advantage of the fact that both oxidation and ion exchange mechanisms are combined into one material. Due to the poor flow properties of $NaBiO_3$, the oxidant was dispersed into a Celite 535 filter aid and the chromatographic method afforded 97% and 98% recovery of Am and Cm, respectively. This method was

limited by the gas evolution resulting from reactions between $NaBiO_3$ and $HNO_3$, showed some Am contamination in the Cm fraction, and faces column bed inhomogeneity due to the density differences between $NaBiO_3$ and Celite.[127]

To date, $NaBiO_3$ is the most promising candidate for the chromatographic separation of Am/Cm and would allow a shift from large-scale solvent extraction separations to reduce costs, hazardous waste volumes, and simplify reprocessing flow schemes. However, a more thorough understanding of the structural changes throughout the separation procedure, behavior of $NaBiO_3$ in acidic aqueous solutions, and the interferences of other metal ions present in reprocessing raffinate is necessary.

# CHAPTER 4: RADIOCHEMICAL SEPARATION TECHNIQUES

## 4.1 Introduction

Chemical separations have played an integral role in the discovery, purification, and application of elements throughout history and are the foundation of current separation technologies. The basis of all separation techniques lies in the exploitation of differences in chemical behavior, such as size and bonding characteristics, between the analyte of interest from other contaminants present in a sample. Classical separation methods that were developed for stable nuclides have been successfully applied to the separation of radioactive nuclides due to the fact that the chemical behavior of an element (and its isotopes) is driven by electronic structure. Since the isotopes of a given element differ in their number of neutrons, not electrons, the use of these classical methods led to some of the first identifications of primordial radionuclides and, subsequently, the creation of the field of radioanalytical chemistry.

While these techniques are commonly used for conventional separations, modification is often necessary for their use in radiochemical separations to account for low radionuclide concentrations, short half-lives, and high activities requiring rapid and complex procedures. Common radiochemical separation techniques used for the preconcentration and/or purification of radionuclides includes precipitation and co-precipitation, solvent extraction, ion exchange, and extraction chromatography. The selection of an appropriate separation technique and corresponding process parameters depends on a number of

factors including sample type and composition, availability of reagents, resulting waste streams, and economics.

### 4.2 Precipitation and Co-precipitation

The emergence of radiochemical separations occurred when the naturally occurring radioactive elements polonium (Po) and radium (Ra) were isolated through the co-precipitation of the sulfide and chloride forms, respectively, by Marie and Pierre Curie.[128,129] As a result, precipitation and co-precipitation were key methods for the discovery of additional radionuclides and radioisotopes, nuclear fission, and for the understanding of radioactive growth and decay.[130–138] Precipitation techniques continued to play an important role in the advancement of nuclear science when it was applied to the discovery of the transuranium elements (Np, Pu, Am, and Cm) and to the large-scale bismuth phosphate purification during the Manhattan Project.[139–142]

Precipitation achieves the isolation of a radionuclide from other undesired ions in solution through the formation of an insoluble ionic solid, or precipitate, when cations and anions combine in solution.[143,144] The isolation of the target analyte can be approached by precipitating the analyte of interest or by precipitating unwanted ions. Successful precipitations require the quantitative recovery of the analyte, a resulting product suitable for source preparation or subsequent handling, and be free of impurities.

Precipitation is governed by the solubility equilibria that describe a solid dissolving in or forming from a solution. The solubility product, $K_{sp}$, is the equilibrium constant that

describes this process. The dissolution and dissociation of an ionic compound, $A_xM_y$, can be described according to Equation 4.1:

$$A_xM_{y(s)} \leftrightarrow xA^{n+}{}_{(aq)} + yM^{n-}{}_{(aq)} \qquad \textbf{Equation 4.1}$$

where A and M represent the cation with charge $^{n+}$ and anion with charge $^{n-}$, respectively. The activity coefficient, $\gamma$, is a thermodynamic measure of the extent of an ion's deviation from ideal behavior in solution. The product of the component ions' concentrations and activity coefficients yields $K_{sp}$ which is useful in determining its precipitation behavior. However, for the dilute solutions typically used in radiochemical separations, $\gamma$ is approximately one. Thus, $K_{sp}$ can then be expressed in terms of the molar concentrations of the ions in solution at equilibrium (Equation 4.2).

$$K_{sp} = [A^{n+}]^x \cdot [M^{n-}]^y \qquad \textbf{Equation 4.2}$$

$K_{sp}$ is used as a comparative measure to the ion product, Q, that can determine if a precipitate will form when two solutions are mixed. The ion product is calculated in the same manner as $K_{sp}$; however, while $K_{sp}$ reflects equilibrium concentrations, Q is determined at concentrations that are not at equilibrium. The behavior of an ionic solid in an aqueous solution can then be determined by the following parameters:[144]

$Q < K_{sp}$: Unsaturated solution, the ionic solid will dissolve and no precipitation will occur

$Q = K_{sp}$: Saturated solution, no precipitation

$Q > K_{sp}$: Supersaturated solution, the ionic solid will precipitate

Thus, the selection of an appropriate counter ion that yields a compound with a Q value that exceeds the $K_{sp}$ value is necessary. The relationship between Q, $K_{sp}$, and solution conditions can be further described by the processes involved that induce precipitation. The general steps of precipitation are supersaturation, nucleation, and growth. Supersaturated solutions ($Q > K_{sp}$) conducive of rapid nucleation and solid growth are necessary to initiate precipitation. It is not possible for the precipitation processes to begin in saturated solutions and does not necessarily begin once supersaturation is reached depending on the Gibbs free energy and interfacial tension in the system. This is because a crystal of a "critical" size, determined by its ratio of concentration to solubility, is required to begin the nucleation process.[145,146]

Nucleation can occur through heterogeneous or homogeneous pathways. Solutions containing dust, colloids, or other foreign particles act as heteronuclei that provide a surface for solute adsorption. This will form layers larger than the face of a particle to reach critical size and initiate nucleation and growth. Homogeneous nucleation occurs when a small fraction of subcritical particles (embryos), reach critical size through thermal fluctuation; however, this process is more difficult to achieve due to the likelihood of heteronuclei present in solution.[145,146]

Since the nuclei formed during nucleation are small, the precipitate nuclei are not observed during nucleation but rather when they have been developed through growth. Growth occurs through the addition of layers of molecular units by diffusion through the crystal-solution interface which forms the crystal lattice. The growth process can follow different patterns such as mononuclear or polynuclear layer formation, rough surface, or spiral step growth and is dependent on kinetic processes.[145] Subsequently, the precipitate can be collected through centrifugation or through a filtration apparatus.

However, when radionuclides in solution are at trace levels, insufficient concentration prevents direct precipitation. Since this was the case for the first experiments designed to recover Pu, a coprecipitation technique using carriers was implemented to isolate and study Pu.[147] Carriers are added in large (mg) amounts and are typically stable isotopes of the same chemical form as the radionuclide of interest due to their similar chemical behavior. If the actinide metal ion forms an insoluble salt with the anion of the bulk precipitate, it will also be carried on the precipitate.[148]

The addition of a carrier increases the concentration of the analyte to achieve the desired separation; however, both the carrier and radionuclide must be in the same oxidation state and chemical form. The addition of the carrier must occur early in the process so that it is treated in the same manner as the radionuclide. Since radionuclide concentrations are low, any losses are significant and the addition of a carrier aids in preventing losses during any preceding precipitations of other analytes in the solution. However, in cases where there is no suitable or readily available isotopic carrier, non-

isotopic carriers are used. Non-isotopic carriers are still chosen based on their chemical similarity to the radionuclide of interest but are instead selected based on other similarities such as the position in the periodic table, ionic charge, or crystalline morphology.

For actinide precipitations, especially those for Pu and other fissile actinides, control over nucleation, growth, and product properties is necessary. Thus, parameters such as temperature, time, acid concentration, precipitant type/concentration, and matrix constituents can influence the reaction behavior and resulting precipitate characteristics. Rapid batch processes used for Pu isolation are beneficial for their simplification of criticality safety operations and extensive research has been conducted to identify optimal conditions to achieve the desired product. Adjusting the system is necessary to achieve larger particle sizes while limiting the formation of the undesired soluble anionic complexes that reduce the product yield.

The bismuth phosphate process was a coprecipitation method implemented for industrial scale Pu production for the Manhattan Project that has now been replaced with solvent extraction processes.[32] However, precipitations remain an invaluable tool for actinide preconcentration and purification. Actinide precipitations using oxalates, peroxides, hydroxides, and fluorides remain valuable for both analytical and industrial scale applications due to their good recoveries, suitable product form and purity, and convenience. A summary of the precipitation reactions for actinide metal ions of various oxidation states in aqueous media is shown in Table 4.1.

**Table 4.1:** Precipitation behavior of actinide metal ions of various oxidation states in acidic aqueous media. I = Insoluble, S = Soluble

| Anion | $M^{3+}$ | $M^{4+}$ | $MO_2^{+}$ | $MO_2^{2+}$ |
|---|---|---|---|---|
| $OH^-$ | I | I | I | I |
| $F^-$ | I | I | I[2] | S |
| $IO_3^-$ | I | I | S | S |
| $O_2^{2-}$ | - | I | - | I[6] |
| $C_2O_4^{2-}$ | I | I | I | I |
| $CO_3^{2-}$ | I[3] | I[3] | I[4] | S |
| $CH_3CO_2^-$ | S | S | S | I |
| $PO_4^{3-}$ | I | I | I[5] | I[6] |
| $Fe(CN)_6^{4-}$ | I | I | S | I |

[1] $OH^-$ and $CO_3^{2-}$ precipitations occur in alkaline solutions

[2] $RbPuO_2F_2$ and $NH_4PuO_2F_2$ precipitate by addition of RbF or $NH_4F$ at pH 6

[3] Complex carbonates are formed

[4] $NaPuO_2(CH_3CO_2)_3$ precipitates from a solution of Pu(VI) in $CH_3CO_2H$ after $Na^+$ addition

[5] $NH_4HPuO_2PO_4$ precipitates from Pu(V) solutions after addition of $(NH_4)HPO_4$

[6] $HPuO_2PO_4{*}xH_2O$ precipitates on addition of $H_3PO_4$

[6] $UO_4{*}2H_2O$ precipitates at pH 2-4, Np(V), Pu(V), Np(VI), and Pu(VI) reduced by $H_2O_2$

### 4.3 Solvent Extraction

Precipitation was the preferred separation technique for radioanalytical separations prior to and during the Manhattan Project. However, solvent extraction was found to be a favorable alternative to the bismuth phosphate precipitation process as it was able to recover valuable U present in the irradiated feed in addition to Pu.[149] The ability for solvent extraction to achieve kilogram scale separations through continuous and remote operations resulted in the development of the REDOX and PUREX processes.

Solvent extraction is based on the differences in solute solubility properties for a given solution in two liquid phases. Accordingly, this method is also commonly referred to as liquid-liquid extraction. The partitioning of solutes occurs when they are distributed between immiscible acidic aqueous and organic solvent phases. Fundamentally, all

solvent extraction processes begin with the dissolution of the solute in an acidic aqueous phase where equilibrium is established between the ionic ($M^{2+}_{(aq)}$) and neutral complex ($M(NO_3)_{2(aq)}$) of the metal ion (Equation 4.3).[150,151]

$$M^{2+}_{(aq)} + 2NO^{-}_{3\,(aq)} \leftrightarrow M(NO_3)_{2\,(aq)} \qquad \textbf{Equation 4.3}$$

Complexation of the metal ion with an organic extractant ($\overline{E}$) increases the hydrophobicity and therefore partitioning of the complex (Equation 4.4).

$$M(NO_3)_{2\,(aq)} + \overline{E}_{(org)} \leftrightarrow \overline{M(NO_3)_2E}_{(org)} \qquad \textbf{Equation 4.4}$$

In solvent extraction, the aqueous phase containing the dissolved metal ions is called the "pregnant feed" and the organic phase is the solvent. The organic phase is typically made up of a diluent (nonpolar hydrocarbon) and one or several extractants and phase modifiers. An extractant is a complexing component that aids in the transfer of a metal ion between phases by introducing more favorable solubility characteristics. The solubility-based distribution of the solutes occurs when each phase is dispersed into one another through mixing. After settling, the solutes remain in their preferential phase (Figure 4.1). After this process, the loaded organic phase is called the "extract" and the depleted aqueous phase is the "raffinate". Stripping or back-extraction refers to the transfer of species back to the aqueous phase from the extract.

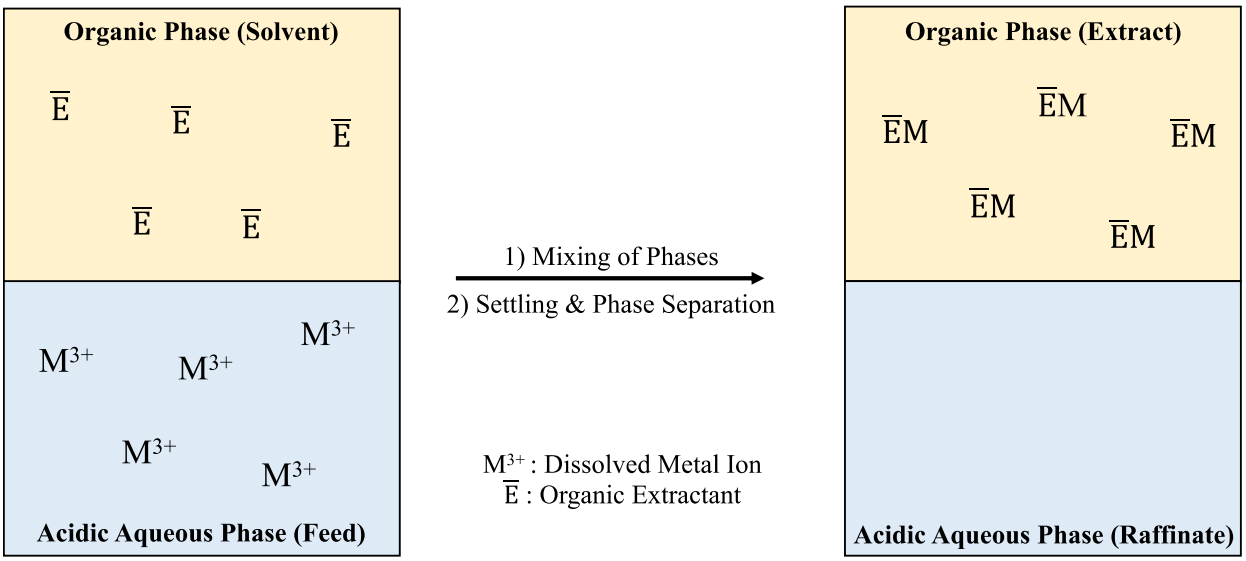


**Figure 4.1:** Simplified schematic of a solvent extraction process that recovers a trivalent metal ion from the aqueous phase into the organic phase using an organic extractant ligand.

The quality of a separation can be quantified by the distribution ratio, D, which is a dimensionless measure of the concentration of a metal ion in the aqueous and organic phases (Equation 4.5). Therefore, the distribution ratio describes the solubility behavior of a metal ion in one phase relative to the other at equilibrium (when the net change of the metal ion concentration between phases remains constant).

$$D = \frac{[M]_{org}}{[M]_{aq}} \qquad \textbf{Equation 4.5}$$

Measurement of the distribution ratio as a function of various parameters (*e.g.,* acid/ligand concentration, temperature, time) allows for a comparison of the efficiency and optimization of various solvent extraction systems. The distribution ratios of two different solutes in the same solvent extraction system is determined by the separation factor (SF) shown in Equation 4.6:

$$SF_{M1/M2} = \frac{D_{M1}}{D_{M2}}$$ **Equation 4.6**

, where $D_{M1}>D_{M2}$ gives an SF > 1. The distribution ratio of the target solute to be extracted must be >1 and the distribution ratio for the undesired solute(s) to be separated must be <1 to be considered a successful solvent extraction system. Large D values are difficult to achieve and, due to the complex chemistry in these systems, large-scale application requires numerous solvent extraction stages.

Generally, metal ions and charged complexes are more soluble in the aqueous phase as a result of their hydration from coordinating water molecules. To achieve extraction, the coordinated water ligands must be replaced to dehydrate the metal ion and form a neutral species that is soluble in the organic phase. There are a number of different chemical processes that form an extractable metal species which are divided into numerous classes. Four major extraction classes that play a predominant role in radiochemical separations include chelate, solvate, ion pair formation, and synergistic extractions.[150,151]

Extraction of a neutral metal species can be achieved through chelate complexation with the metal ion that forms a stable, neutral, and hydrophobic complex. Typically, bidentate or polydentate chelating agents are used to replace the water molecules in the metal ion's coordination sphere. In doing so, the chelates form a stable hydrophobic ring around the metal ion to be extracted. The metal ion is then located within the cavity of the chelate and the resulting neutral complex readily dissolves into the organic phase.[150,151] As shown in Equation 4.7, the distribution of the neutral complex is a function of the hydronium ion

concentration and is therefore favored by low acidity. The extraction of U into chloroform using 8-hydroxyquinoline in a chelate extraction process has been demonstrated.[152]

$$\mathrm{M}^{3+}_{(\mathrm{aq})} + \mathrm{nHL}_{\mathrm{org}} \leftrightarrow \mathrm{ML}_{\mathrm{n,org}} + 3\mathrm{H}^{+}_{(\mathrm{aq})} \qquad \textbf{Equation 4.7}$$

Phase transfer can also be accomplished for electroneutral metal ions that are complexed with an anion in the aqueous phase (*e.g.,* mineral acid) through solvation extraction (Equation 4.8). A solvating reagent in the organic phase replaces the remaining coordinated water ligands to increase hydrophobicity and form the extractable complex. Oxygenated solvents are used for this process as the lone electron pair on the oxygen atoms gives rise to the basicity that enables its incorporation into the coordination sphere of the metal ion.[153] As a result, the solute is contained within the cavity of the solvent and is an extractable solvated complex. Solvating extraction systems have been important for radioanalytical separations as it is the principal extraction pathway for the recovery of hexavalent U and Pu in the PUREX process using TBP as a solvating extractant.

$$\mathrm{M}^{3+}_{(\mathrm{aq})} + 3\mathrm{X}^{-}_{\mathrm{aq}} + \mathrm{nS}_{\mathrm{org}} \leftrightarrow \mathrm{MX}_3\mathrm{S}_{\mathrm{n,org}} \qquad \textbf{Equation 4.8}$$

A neutral extractable species can also be produced by ion pair formation via electrostatic forces (Equation 4.9).[154]

$$\mathrm{M}^{3+}_{(\mathrm{aq})} + 3\mathrm{X}^{-}_{\mathrm{aq}} + \mathrm{A}^{+}\mathrm{X}^{-}_{\mathrm{org}} \leftrightarrow \mathrm{MX}_4\mathrm{A}_{\mathrm{org}} \qquad \textbf{Equation 4.9}$$

Ion pair formation is also referred to as liquid anion exchange because it follows a similar process to that of ion exchange. For example, metal ions in the aqueous phase can complex with the inorganic anions (*e.g.,* $NO_3^-$, $Cl^-$) in the aqueous phase forming an anionic complex. Cationic organic molecules present in the organic phase can extract the mineral acid from the aqueous phase to form an ion pair salt that is insoluble in the aqueous phase. The anionic metal complex can then be extracted via ion exchange and ion pair formation with the organic cation. Historically, tertiary and quaternary alkyl amines such as trioctylamine and Aliquat 336 have been used as liquid anion exchangers for actinide and lanthanide separations in solvent extraction systems.[155]

To afford a greater extraction efficiency, a synergistic solvent extraction system uses a combination of two extractants (Equation 4.10). Synergistic systems feature chelates and solvating extractants that will both neutralize and dehydrate the metal ion in the aqueous phase to form the extractable species.[150,151] However, the higher distribution ratios obtained are often at the expense of lower selectivity.[156]

$$\mathrm{M^{3+}_{(aq)} + 3HL_{org} + nS_{org} \leftrightarrow ML_3S_{n,org} + 3H^+_{aq}} \qquad \textbf{Equation 4.10}$$

These extraction classes and their associated equilibria above are simplified and it is common for several of these mechanisms to occur in one system simultaneously. As a result, the equilibria that describe any given solvent extraction system are extensive and their elucidation remains a research priority. Given the differences in solute characteristics such as charge, size, and electronic structure, a large deviation in the

extraction behavior for different metal ions in the same extraction system can be observed.

The phase distribution behavior of a solute is altered by solute-solute and solute-solvent interactions that are dependent on a number of parameters. When considering solute-solute interactions, the charge density and electronic structure of metal ions influence complex formation and correlates to the extraction efficiency of the system.[150,151] Similarly, the organic phase diluent has an effect on solute-solvent interactions and influences the distribution of the extractant and resulting neutral metal complex in the system. The concentration and type of salts in the aqueous phase can affect the metal complex distribution through a “salting-out” effect that reduces the hydration of the metal ion. Other considerations such as reagent solute concentrations, temperature, donor ligand behavior, sterics, and coordination type have a significant impact on extraction behavior.

These parameters can influence the kinetics of the system that describes the rate at which the metal ion is transferred between phases. Since solvent extraction systems are biphasic, chemical reactions can occur in either of the bulk phases as well as at the phase boundary where current mechanistic understanding is limited. In addition, these chemical reactions contribute to the rates of diffusion describing how the various species move from higher concentration to lower concentration. Thus, the chemical reaction and diffusion rates associated with a given solvent extraction system govern the kinetics. While complex, the kinetic data and the influence of the above parameters can be

evaluated using available experimental information. However, due to the complex nature of these systems, it is common for several mechanisms to be proposed.[150,151]

In practice, solvent extraction can be performed in batch small-scale studies using accessible laboratory equipment. These analytical-scale studies are useful for the preliminary determination of extraction efficiencies and for preconcentration and separation methods necessary in typical laboratory operations. However, more advanced equipment is required when applying these systems to large-scale industrial processes like UNF reprocessing. As mentioned previously, the distribution ratios obtained with the most developed solvent extraction processes are low and multiple stages of contact are required to accomplish the desired separation. To achieve this, continuous extraction processes that consist of mixer (phase contact/mass transfer) and separator (phase separation) components are applied on an industrial scale. These processes feature consecutive single-stage contacts between the aqueous and organic streams in a counter-current (opposite flow) directionality.

Mixer-settler systems are commonly used for large-scale processes due to their ease of operation, construction, and low cost. A single mixer-settler consists of a mixing chamber for phase contact and a gravity-settling chamber for phase separation (Figure 4.2) and provides a single extraction stage. Adding numerous mixer-settlers in tandem is relatively simple and provides the number of extractions stages necessary for a given process; however, the time to reach steady-state conditions and large volume of organic solvent required can limit the use of this equipment. Extraction processes that are easily

separated by gravity and require longer mixing times are suitable for mixer-settler extractions.[157]

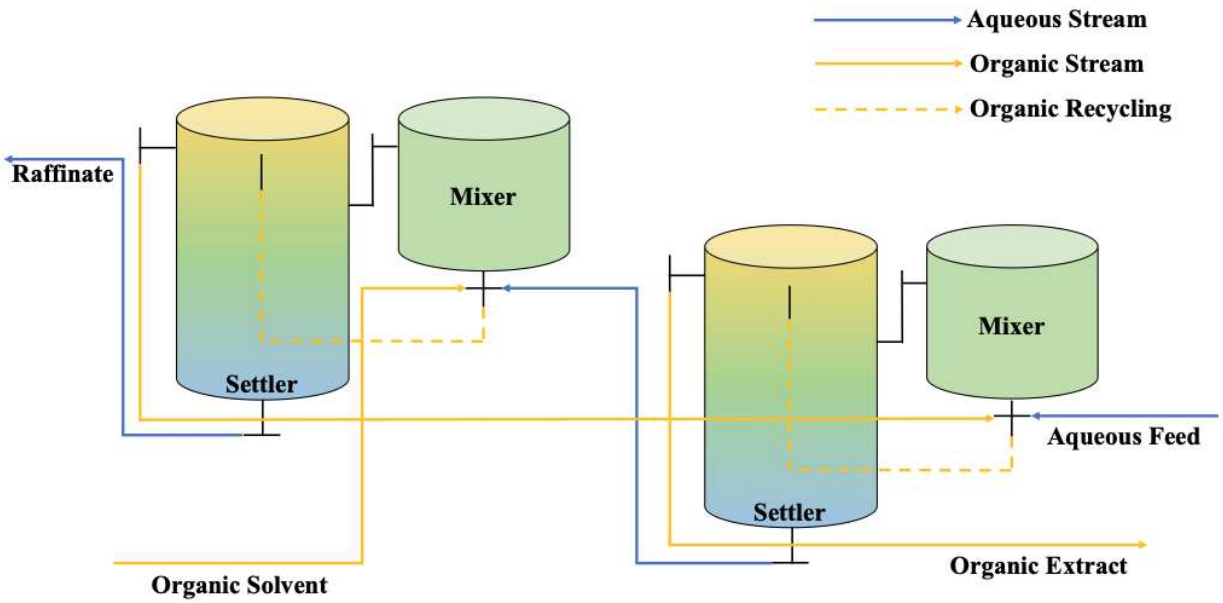


**Figure 4.2:** Block diagram of a mixer-settler system operating under a continuous, counter-current flow.

Similar to mixer-settlers, centrifugal contactors provide a single extraction stage and can be connected to yield numerous stages of contact. However, they have high extraction efficiencies in a single stage, rapid phase separation, and fast kinetics. Each contactor has a spinning rotor that rapidly mixes the aqueous and organic phases that are then separated inside the rotor where the two phases are separated. This system also has the benefit of higher capacity with a smaller volume but are more mechanically complex and sensitive to solids present in the system.[157] Operations that follow a counter-current, continuous multistage process improve the mass transfer of solutes and afford higher separation factors and flow rates (Figure 4.3).[158]

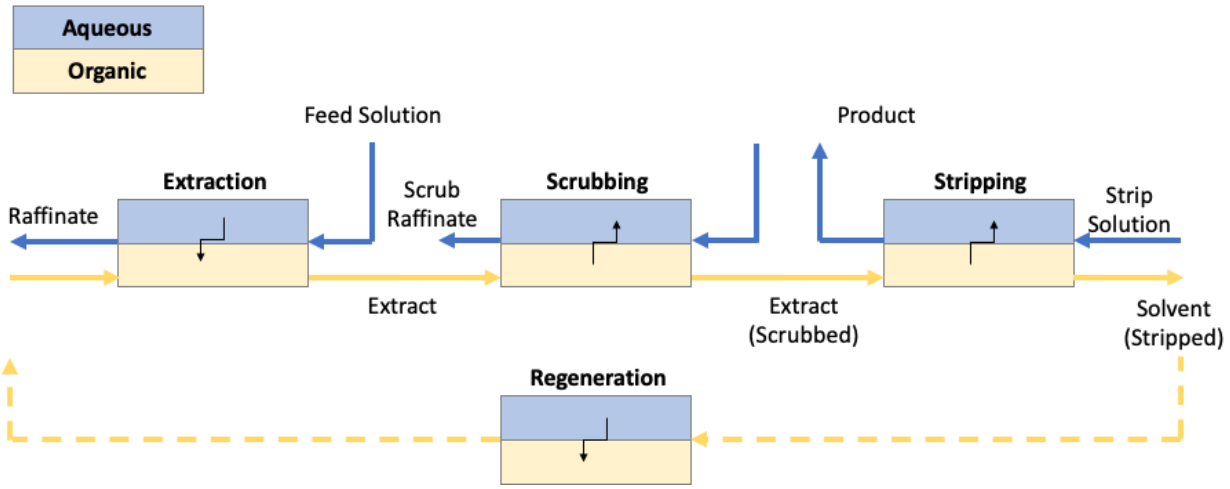


**Figure 4.3:** Block diagram of a counter-current, continuous multistage extraction process.

To date, these techniques remain the most established on both small and large scales for radiochemical separations. Since advanced solvent extraction infrastructure is already in place, the improvement and development of solvent extraction systems remains at the forefront of radioanalytical chemistry research. Furthermore, the ability to apply this technique to both atom-scale and large-scale separation processes makes this a powerful technique for both analytical and industrial application.

### 4.4 Solid-Liquid Extraction

Solid-liquid extraction techniques also feature the distribution of solutes between two phases similar to of solvent extraction. However, they differ in the fact that solutes are partitioned through their distribution between a solid (stationary) phase and a liquid (mobile) phase. Solutes are dissolved in the mobile phase and are passed through solid particles that certain solutes have a greater affinity for resulting in their retention onto the stationary phase.

Stationary phase materials include adsorbents (*e.g.,* silica, alumina), natural or synthetic ion exchangers, and extractants. Recently, there have been advancements in solid phase extraction (SPE) that are performed using equipment such as cartridges, disks, pipette-tips, and permeable membranes that incorporate sorbents. Solid liquid extraction has emerged as a favorable alternative to solvent extraction systems because of the ease of operation, elimination of organic solvents, faster operations, and low costs.[159,160]

Separations are achieved when there is a difference in the strength of interaction between various ions of interest with the stationary phase. This can be quantified through batch methods by calculating the weight distribution ratio ($D_w$) shown in Equation 4.11.

$$D_w = \frac{A_s/m}{A_{aq}/V}, \text{where } A_s = A_o - A_{aq} \qquad \textbf{Equation 4.11}$$

$D_w$ is determined by measuring the activity concentration of the analyte on the solid ($A_s$) per unit mass (m) relative to the activity concentration in the aqueous phase ($A_{aq}$) per unit volume (V). The greater the $D_w$, the greater the affinity of the ion for the stationary phase and the lower activity of the ion in the aqueous phase. The greater the difference in $D_w$ between two solutes, the greater the separation factor, SF (Equation 4.12).

$$SF = \frac{[D_w]_{M1}}{[D_w]_{M2}} \qquad \textbf{Equation 4.12}$$

The $D_w$ of a given solute depends on the same parameters that influence solvent extraction systems such as solvent type, pH, ionic strength, and temperature. The dependency on these parameters can be determined through the measurement of a $D_w$ value at specific sample conditions. In addition, the solute affinities for the solid sorbent can be enhanced based on the chemical nature, surface chemistry, and the incorporation of ion exchange groups or extractants within the stationary phase. Quantitative adsorption behavior can be elucidated through batch studies and is useful in estimating how different solutes will migrate throughout a chromatographic system. However, distribution ratios determined during batch studies cannot often be translated directly to chromatographic behavior due to the different operating parameters and phenomena that occur in a chromatographic system.

### 4.5 Chromatography

Chromatography was first used over 100 years ago to separate pigments using a column packed with calcium carbonate. Bands of color appeared that were associated with different species as they migrated throughout the column at various rates.[161] Since then, the field of chromatography has expanded significantly and the mechanistic theories of operation have grown more complex. The ease of operation and ability to develop and tailor new materials to achieve specific separations has resulted in its use across a wide range of applications. However, the detailed processes that take place in a chromatographic system are so numerous and complex that the development of mathematical models that accurately describe experimental data remains incomplete.

Fundamentally, chromatographic methods rely on the differential migration of various components in a mixture influenced by flow, diffusion, and kinetic phenomena. The influence of these parameters on zone migration was first introduced by J. N. Wilson.[162] Soon after, Martin and Synge published a Nobel Prize winning paper describing the plate theory of chromatography.[163] Plate theory was an adaptation of a model developed to describe fractional distillation and treats chromatographic systems as if made up of "plates" or zones where individual equilibrations occur. However, the assumption of equilibrium conditions in these zones is not valid in dynamic chromatographic systems and does not accurately represent these systems. Nonetheless, plate theory has introduced concepts that have been built upon in subsequent models and is deeply embedded within the chromatographic literature.

Solutes are dissolved in a mobile phase and are introduced at the top of a column packed with a solid, stationary phase where distribution between the two phases begins. As fresh mobile phase is continuously added to the column, the solutes move through the column as a series of transfers between the two phases. Since solutes are only able to travel down the column in the mobile phase, their migration is dependent on the distribution ratios. Solutes that spend less time in the mobile phase when more strongly retained on the stationary phase migrate at a slower rate resulting in zone formation.

However, the downward migration of a solute is variable due to the interplay of various random processes. Thus, the random walk theory of chromatography was introduced by J. C. Giddings where the individual paths a solute follows within a column occurs

unpredictably. This is due to molecular diffusion, sorption-desorption kinetics, and flow phenomena that result in zone spreading or brand broadening.[164] Band broadening describes the distance between the solutes in a column as they travel down a column and is an important consideration in evaluating the performance of a given chromatographic system. A successful chromatographic separation results in the elution of solutes in narrow, resolved elution peaks and can be quantified through the efficiency (N) and resolution (R). Band broadening can result in a deviation from the ideal, Gaussian profile of elution peaks and decreases column efficiency by decreasing the separation between elution curves.

The efficiency of the system relates to the relative retention times of the solutes and the peak width of their associated elution peaks. Efficiency can be quantified by determining the number of theoretical plates (N) expressed as:

$$\mathrm{N} = \left(16\frac{\mathrm{t_R}}{\mathrm{W}}\right)^2 \qquad \textbf{Equation 4.13}$$

, where $t_R$ is the solute retention time and $W$ is the peak width. When considering the number of theoretical plates, a greater separation efficiency is achieved with a greater number of theoretical plates as more stages of equilibration are introduced to exploit differences in a solute's distribution coefficients.[165]

The height equivalent to a theoretical plate (HETP) can then be determined using Equation 4.14, where L is the column bed length.

$$H = \frac{L}{N}$$ **Equation 4.14**

Measuring the peak-to-peak separation of the eluted solutes gives the resolution, R, which can be calculated with Equation 4.15:

$$R = \frac{2\Delta t_R}{W_1 + W_2}$$ **Equation 4.15**

, where $\Delta t_R$ is the resolution at peak maxima and $W_1$ and $W_2$ are the peak widths. The resolution provides an adequate way to describe the peak separation between two solutes where the baseline separation requires an R ~1.5.[165]

Band broadening influences the efficiency and resolution of the column due to longitudinal diffusion, eddy diffusion, and resistance to mass transfer phenomena. Longitudinal diffusion is a result of solute diffusion away from high concentration to low concentration regions. Inequalities in the radial flow through a packed bed introduces eddy diffusion effects causing the solutes to follow different channels with different path lengths as they travel through solid particles. Mass transfer describes the mechanism of which solutes move through the boundary between phases and is determined by the diffusion in and out of the mobile and stationary phases. These three main contributions to band broadening and plate height have been combined to generate the van Deemter equation (Equation 4.16).[166–168]

$$H = A + \frac{B}{u} + (C_S + C_M)u \qquad \textbf{Equation 4.16}$$

Eddy diffusion is represented by the A term and can be minimized by using small particle diameters with a narrow size range. Longitudinal diffusion is represented by the B/u term and is inversely proportional with the mobile phase velocity, u. Thus, longitudinal diffusion can be mitigated with higher flow rates; however, smaller particle sizes used to reduce the contribution of eddy diffusion limits the use of higher flow rates. The C terms are the contributions of mass transfer in the stationary and mobile phases and are proportional to the flow rate. Since it is beneficial for solutes to undergo distribution quickly, faster flow rates result in fewer interactions between the solute and stationary phase. In addition, the use of smaller particles decreases the void volume between particles decreasing diffusion time and broadening.[167]

While the manipulation of parameters offers a means to improving column performance, the selection of parameters to optimize the system is complicated due to the complex relationships between them. When considering the other requirements of radiochemical separations, such as the need for rapid methods, the use of small particle size and low flow rates leads to a longer operation time. Thus, the adjustment of parameters must be chosen based on both theoretical principles and experimental demands and a balance must be found between the two. Generally, long and narrow columns with uniform resin bed packing yields better separations. The selection of a flow rate that avoids the introduction of channels or air pockets in the resin bed while providing faster separations is favorable.

*4.5.1 Ion Exchange Chromatography*

Ion exchange was first introduced over a century ago when Thompson and Way observed that some soils had the ability to retain molecules to a greater extent than others.[169,170] This led to the identification of natural ion exchange materials that feature fixed ionic sites within their framework. The first synthetic organic ion exchangers were prepared in 1935 by Adams and Holmes. During the Manhattan Project, a large body of work explored the use of ion exchangers for the separation of rare earth elements and actinides and was published several years later in a series of papers by G. E. Boyd et. al.[171–173] Ion exchange features selectivity and reaction mechanisms similar to that of solvent extraction but offers a more convenient and rapid setup resulting in its widespread use for laboratory separations.

Radiochemical separations using ion exchange chromatography rely on the reversible exchange of ions between the mobile phase and a solid, porous, inert material having ion exchange sites. Typically, ionic functional groups are covalently bound onto inert polymeric supports where oppositely charged ions (counter ions) can be displaced by charged polar solutes present in solution (Figure 4.4).[174–176] Cation and anion exchangers are materials that feature negatively and positively charged fixed functional groups, respectively. This process is governed by the relative affinities between the solutes dissolved in solution and the exchange sites on the solid. The choice of the type of ion exchanger and functional group is determined by the charge of the analytes of interest in solution. These resins are available in various ionic forms (defined by the counter ion)

that can also be converted and the ionic form should be such that the functional group has a more favorable selectivity for the analyte relative to the counter ion.[177]

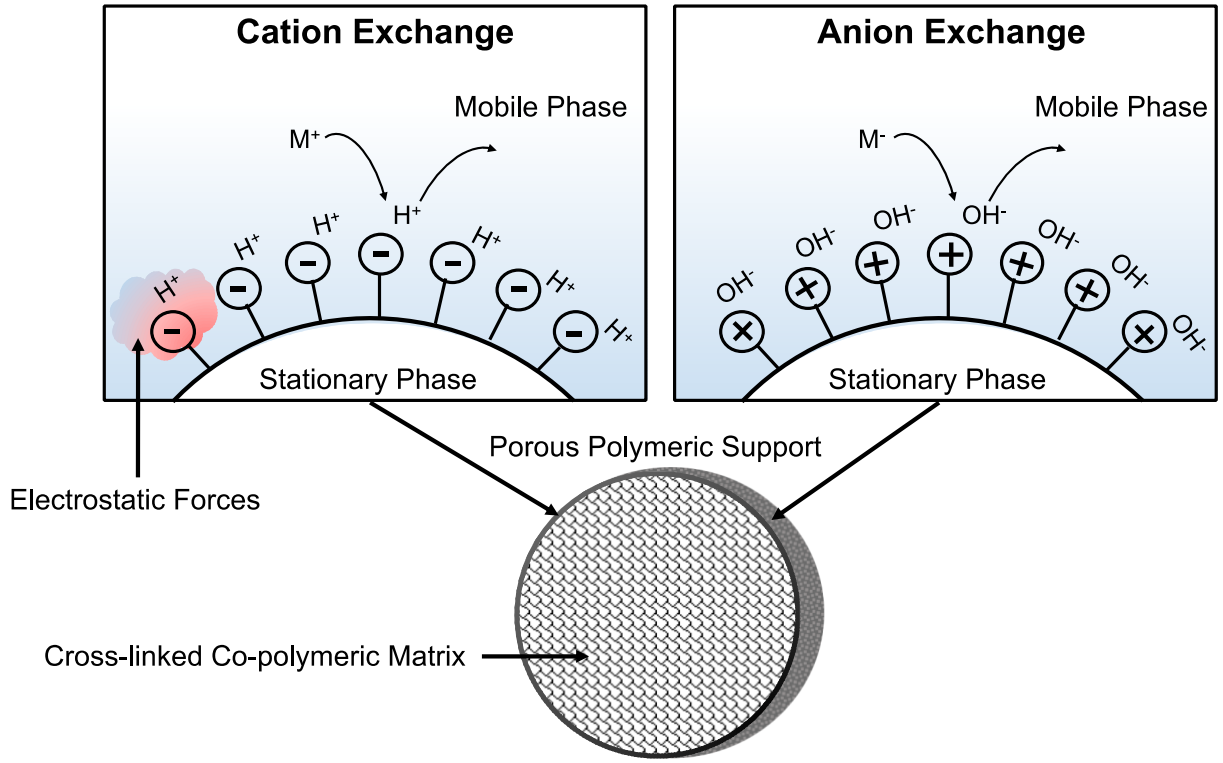


**Figure 4.4:** Illustration of the ion exchange concept where cation exchangers (left) feature the exchange of positively charged ions and anion exchangers (right) of negatively charged ions. Ion exchange resins are comprised of insoluble permeable polymeric beads with charged functional groups covalently bound to the surface.

Mineral ion exchangers are cation exchangers and undergo surface reactions through two mechanisms. Cations in solution can displace those already present on the surface and are held there through electrostatic forces in a cation exchange process. Alternatively, solutes can undergo sorption processes where they are able to adsorb onto the solid surface as surface ions are not coordinated and have an electrostatic charge. These processes can happen individually or together and are enhanced by the nature of the solid surface (*e.g.,* amorphous solids feature high electropotential surface charges).

Other ion exchangers can feature interstitial ions within the structure that can exchange with those present in the sample solution. However, mineral ion exchangers are limited due to their lower ion exchange capacities and narrow operational pH ranges.[178]

Synthetic ion exchange materials have found widespread use since they can be prepared with cationic or anionic functional groups (or a mixture of the two). Cation and anion exchangers have a similar behavior to that of acids and bases and are therefore further classified as strong or weak acid or base ion exchangers.[179] Strong acid cation exchangers are typically useful across a wide pH range while weak acid cation exchangers are not useful below a pH of 4-6. Similarly, anion exchange resins featuring strongly basic function groups function well over the entire pH range and those of weak basicity cannot be used in alkaline solutions. A summary of common functional groups can be found below (Table 4.2).

**Table 4.2:** List of common functional groups for cation and anion exchangers

| | Resin Type | Functional Group | Chemical Formula |
|---|---|---|---|
| **Cation Exchange Resins** | Strongly Acidic | Sulfonic | $RSO_3^-H^+$ |
| | Moderately acidic | Phosphoric | $PO(OH)_2$ |
| | Weakly Acidic | Carboxylic Acid | RCOOH |
| **Anion Exchange Resins** | Strongly Basic | Tetraalkylammonium | $[RN(CH_3)_3]^+Cl^-$ |
| | Weakly Basic | Ternary Amine | $[RN(CH_3)_3]^+Cl^-$ |
| | Weakly Basic | Secondary Amine | $[RNH(CH_3)_2]^+Cl^-$ |

Synthetic ion exchange resins are prepared using polymeric supports which can feature either minimal pores (microporous gel resins) or multichannel structures (microporous resins). The internal structure influences the surface area, stability, functionalization, and overall ion exchange behavior of the material. Cross-linking of the polymeric structure

occurs during synthesis and contributes to the chemical and physical properties of the material such as pore and particle size, moisture content (hydration of functional groups), and overall strength of the resin. Important characteristics of ion exchange resins that must be taken into consideration include resin matrix, ion exchange capacity, and the functional group type and concentration. Generally, a suitable material should feature chemical/radiolytic stability, uniform particle size, high surface area, fast kinetics, and high capacity. The exchange capacity is a measure of the number of counter ion equivalents that can be adsorbed in some mass of the solid ion exchange material (in meq/g) and indicates the number of sites available for exchange. The capacity depends on the chemical and physical properties of the reaction and the ionization of the exchanger groups.

Just as the nature of the functional group plays an important role in selectivity, so too does the nature of the counter ion in solution. The electrostatic interactions between the two depend on the valance and size of the counter ion as well as on other interactions between the counter ion and its environment. Equation 4.17 shows how a cation exchange reaction can be expressed as a reversible and stoichiometric reaction:

$$\mathrm{R-SO_3^-H^+ + M^+ \leftrightarrow R-SO_3^-M^+ + H^+} \qquad \textbf{Equation 4.17}$$

, where $R\text{-}SO_3^-$ represents the resin matrix with an anionic function group, $H^+$ represents the counter ion, and $M^+$ represents the metal ion in solution. Characteristics of a metal ion such as hydration/ionic radius, valance, polarizability, and complexation drive the

selectivity behavior, and therefore, distribution coefficients of a given ion exchange process.

The equilibria kinetics have been explored for various ion exchange systems using various theories and models.[180–183] In theoretical models, ion exchange occurs by an adsorption mechanism and is a diffusion-controlled process. In these systems, a liquid film with differing properties forms around the resin beads resulting in an additional interface for diffusion to occur. During any given ion exchange reaction, the counter ions must diffuse through the bulk solution, hydrated film, and within the resin matrix. Once the ion exchange reaction occurs, the exchanged species must then diffuse outside of the resin bed and into the bulk solution.

Adsorption isotherms are commonly used to describe the phenomena that govern the retention or mobility of a solute in these systems based on the adsorption equilibria. These models are often applied to experimental data obtained from batch systems where the concentration of solute adsorbed per unit mass is plotted as a function of equilibrium concentration. The Langmuir and Freundlich isotherms are among the numerous proposed models and are based on kinetic considerations. The Langmuir isotherm assumes reversible, monolayer adsorption, that no lateral movement occurs, and that the adsorption energy is the same for all sites. In contrast, the Freundlich isotherm is not restricted by monolayer adsorption or uniform distribution of adsorption heat. The resulting behavior of these models is indicative of the adsorption behavior of the adsorbent.[184–187]

Ion exchange processes are used in a diverse number of applications in radiochemistry and are principally applied for lanthanide and actinide separations. Based on electrostatic interactions, diffusion processes typically represent the rate limiting step yielding fast kinetics that are favorable for rapid separations. In addition, their customizable selectivity, lower waste generation, and lower costs make ion exchange-based techniques a more favorable alternative to solvent extraction.

### *4.5.2 Extraction Chromatography*

Extraction chromatography (EXC), also known as reverse phase chromatography, has been used for a wide range of chemical separations for over 70 years. In radiochemistry, it has played a role in element discovery and rare earth and actinide separations.[188,189] Currently, there is a large research focus on the development of new extractants, polymeric supports, and integration of these materials into complex radiochemical separation systems.

In EXC, a liquid extractant is adsorbed onto an inert polymeric support resin bead (Figure 4.5). The incorporation of organic ligands on the resin offers the selectivity of solvent extraction methods while providing the benefit of the multistage separation process found in chromatography. The extraction of the analyte(s) of interest occurs when the resin beads contact with the aqueous mobile phase that contains the metal ions. The addition of complexants or redox agents in the mobile phase can enhance selectivity or facilitate the stripping of strongly retained metal ions from the resin bed.

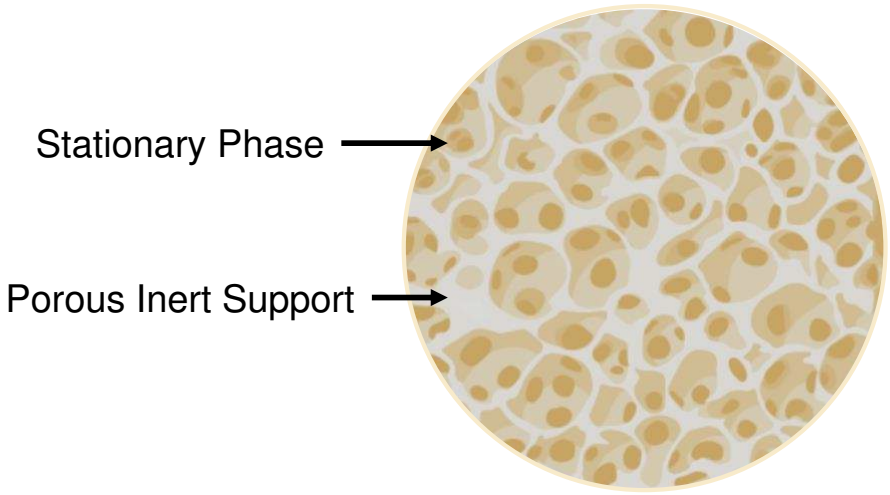


**Figure 4.5:** Structure of an extraction chromatographic resin bead impregnated with an extractant located within the pores of the inert support.

The favorable extraction behavior of solvent extraction system was translated to extraction chromatographic materials prepared through the physiosorption of liquid organic extractants onto a chromatographic support. To maintain the extraction behavior, the nature of the stationary phase is an important consideration in EXC. Early material development looked at diatomaceous earth and silica microspheres as support materials, but required pretreatment to prepare a hydrophobic surface.[190] Soon after, polyacrylic ester supports were the primary backbone of these materials and are the basis of most commercially available EXC resins.[191,192]

Suitable supports must be inert with uniform particles, have the ability to retain the stationary phase, be mechanically and radiolytically stable, affordable, and provide sufficient surface area/porosity. The porous character of the support is important as they retain the stationary phase but must be kept in a narrow size range as the effects of pore size on kinetics are similar to that of particle diameter. Like ion exchange, the resin

properties (*e.g.,* size distribution, capacity) have significant effects on column performance.

The extractants present in the stationary phase drive the selectivity in EXC and are designed based on the chemical behavior of the ions of interest. Polar groups are attached to nonpolar substituents that interact with the metal ions to enhance phase transfer. The polar and nonpolar donor groups are selected to limit loss of the extractant from the support, alter electron donating/withdrawing and steric effects, and influence kinetics. The loading amount of the extractant depends on the pore volume of the support. When approaching the loading capacity, lower column resolutions are observed due to slower kinetics and band broadening.[190] A selection of commercially available extractants is shown in Table 4.3.

**Table 4.3:** Commercially available Eichrom, LLC EXC resins, their associated extractants, and applied separations.

| Resin | Extractant | Separations |
|---|---|---|
| TEVA | Aliquat-336 | An(IV)/An(III,V,VI) |
| LN | HDEHP | Trivalent f-elements |
| LN2 | HEH[EHP] | Ln/Ln', An/Ln, An/An' |
| LN3 | H[DTMPP] | |
| Actinide | Dipex | An(III,VI,IV)/matrix |
| UTEVA | DAAP | An(IV,VI)/An(III,V) |
| TRU | CMPO in TBP | An(IV,VI)/An(III) |
| DGA | TODGA/TEHDGA | An(III)/An(IV)/An(VI) |

When considering the extraction mechanisms at play, EXC provides a better alternative to separating metal ions with nearly identical chemical behavior than IEX. While IEX relies solely on the charge and ionic radii of the ions involved in the reaction, the reaction

mechanisms present in EXC mainly rely on complexation.[193] Similar mechanisms observed in solvent extraction such as chelate formation, solvation, ion pair formation, and complex formation are also present in EXC.

Thus, successful separations still rely on the difference in the strength of interaction between ions of interest with the extractant. Separations can therefore be characterized using the distribution ratio and separation factor from Equations 4.11 and 4.12. This ratio can be converted to the retention factor, k', by determining the volume distribution ratio, $D_V$ (Equation 18).

$$D_v = D_w \left(\frac{\rho_{ext}}{m_{load}}\right) \qquad \textbf{Equation 4.18}$$

$D_w$ is the weight distribution ratio, $\rho_{ext}$ is the density of the extractant, and $m_{load}$ is the amount of the extractant loaded onto the support in grams of extractant per gram of resin. The retention factor can then be calculated by Equation 4.19:

$$k' = D_v \left(\frac{v_s}{v_m}\right) \qquad \textbf{Equation 4.19}$$

, where $v_s$ and $v_m$ are the stationary and mobile phase volumes, respectively. For a well characterized EXC resin, k' can be converted from $D_w$ directly by Equation 4.20:

$$k' = D_w F_c \qquad \textbf{Equation 4.20}$$

, where $F_c$ is a conversion factor that represents the number of free column volumes to peak maximum. $F_c$ is determined by measuring the interstitial space of a column packed with a specific resin. For commercially available EXC resins, $F_c$ is known and adsorption data is typically reported as k' as it provides information about the efficiency of the system.[190]

EXC has been a powerful technique for radioanalytical applications and continues to expand as an alternative to solvent extraction or ion exchange methods. While EXC provides a rapid separation alternative with less waste generation and increased purification, the resins are much more expensive than the ion exchange alternative, have flow rate limitations, lower capacities, and face radiolytic degradation issues.

# CHAPTER 5: INSTRUMENTAL ANALYSIS TECHNIQUES

## 5.1 Liquid Scintillation Counting (LSC)

### *5.1.1 Theory*

For single nuclide analysis, liquid scintillation counting (LSC) is the preferred method to quantify the activities of the alpha and beta emitting radionuclides as it offers nearly 100% counting efficiency. Following a decay event, the kinetic energy of the emitted ionizing radiation dissipates its energy through collisions with the components in the sample's medium and is converted into light that can be detected (Figure 5.1).

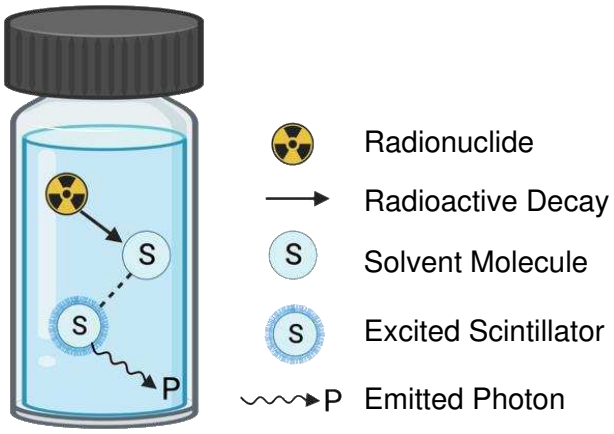


**Figure 5.1:** Illustration of the collision process between the particles emitted by a radionuclide with a solvent molecule that leads to the excitation and subsequent photon emission of the scintillator.

To achieve this, the radionuclide of interest is dissolved in a liquid scintillation cocktail that consists of a solvent, surfactant, organic scintillator, and a waveshifter. The solvent ensures the efficient energy transfer between the decay particle and the solution. The surfactant is included to allow for analysis of radionuclides in both polar and nonpolar solvents. The liquid organic scintillator converts the ionizing radiation into light through

fluorescence that results from the electronic transitions occurring within the molecule. Since not all photons emitted by the scintillator may be compatible with the photomultiplier tubes (PMTs), the waveshifter absorbs photons that are emitted by the scintillator and re-emits them at longer wavelengths that can be detected by the photomultipliers tubes and reduces self-absorption by the cocktail.

Following a decay event, a portion of the released energy is imparted on the solvent molecules that transfers the energy to other solvent and scintillator molecules (Figure 5.1). When this energy transfer occurs, the electrons in the scintillators are promoted to an excited state. When the electrons return to the ground state, the energy is emitted as a light photon in the low-energy ultraviolet region. The photon's energy is measured when. it collides with two PMTs that convert the radiant energy to electrical energy.

The PMTs are coated with a photosensitive material that produces photoelectrons following photon collision. Applying an electric field to the PMTs accelerates the negatively charged photoelectrons that then collide with a surface called a "dynode". This collision produces secondary electrons that are accelerated into another dynode. This process results in electron multiplication at each electrode and produces an electron cascade. This electron cascade generates an electrical pulse and, due to the linear conversion of energy to photons, the intensity of light detected by the PMTs is proportional to the initial energy of the emitted particle.

However, the high sensitivity of PMTs generates noise which is a fundamental limitation with this technology. Thus, a coincidence technique is applied to modern LSC techniques that uses two photomultiplier tubes that prevent the counting of single-photon events that influences analysis (Figure 5.2). Single-photon events can arise from chemical reactions in the sample, static electricity from the sample vial, and electrical noise from the PMTs.

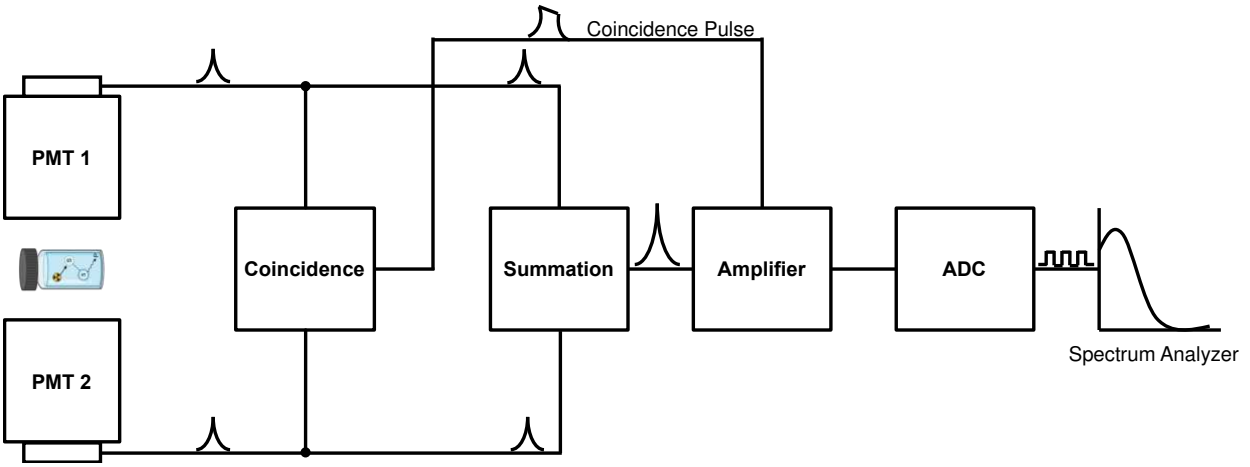


**Figure 5.2:** Block diagram of a general liquid scintillation counter set up.

A nuclear decay event produces 10 photons per keV of energy and, when these photons produce the first photoelectron in one of the PMTs, the signal opens an electronic gate in the coincidence circuit that remains open for ~6 – 20 ns. The signal from each PMT is fed into the circuit and is only considered a decay event if both signals occur during that period. Therefore, the counter only recognizes coincident events for processing to eliminate false positives. To address the effect of the geometrical location of the emitted photon from the scintillation vial relative to each PMT, a summation circuit is also employed. Through the summation of the pulse amplitudes from each PMT, the output is proportional to the total scintillator intensity (Figure 5.2). This design reduces the instrumental background and increases counting efficiency.

The amplitude of the electrical pulse is converted into a digital value by the analog to digital converter (ADC). This value represents the energy of the particle that is stored as a count in a 4000-channel multichannel analyzer (MCA). The energy spectrum ranges from 0 – 2000 keV thus equating each channel to one-half keV. The number of pulses in each channel is recorded and displayed as a spectrum. From this spectrum, information about the energy and activity of the radionuclide in the sample can be acquired. Region limits can be defined to determine the activity for a radionuclide specific to that energy region.

The system efficiency can be reduced as a result of energy loss through a process called quenching. Quenching can occur through physical, chemical, or optical mechanisms. The loss of energy during transfer from solvent to solute or when another chemical in the sample competes with the scintillator is referred to as chemical quenching. Optical quenching is relevant for colored samples that absorb the light emitted by the scintillators and attenuate the photons. These processes reduce the number of photons produced and, therefore, reduce the detected counts per minute (CPM) and counting efficiency. In addition, the energy spectrum experiences a shift to lower energies. To mitigate the effects of quenching on sample analysis, the level of quench must be quantified. This is achieved through quench indicating parameters (QIPs) that relate to counting efficiency.

To determine the shift in the energy spectrum caused by quench, the Special Index of the Sample (SIS) method uses the sample isotope spectrum to monitor the quench of the solution. The SIS value decreases inversely with quench and is only accurate for single-

nuclide analysis with activity great enough to give a clear distribution. The transformed Spectral Index of the External Standard (t-SIE) QIP uses an external Ba-133 gamma source under the sample vial to produce the Compton spectrum induced in the scintillation cocktail. The t-SIE value also decreases with increasing quench. Unlike the SIS QIP, t-SIE is independent of the radionuclide and sample identity and its large dynamic range provides a reproducible quench-tracking method.

Both QIPs can generate quench curves and a standard quench curve can be generated using standards with a constant activity (in disintegrations per minute, DPM) and varying quantities of quenching agents. The measured CPM as it relates to the known DPM value are used to determine counting efficiency by Equation 5.1.

$$\frac{\text{CPM}}{\text{DPM}} \cdot 100\% = \text{Counting Efficiency (\%)} \qquad \textbf{Equation 5.1}$$

When plotting % Counting Efficiency vs. QIP, direct DPM calculations can be determined automatically through Equation 5.2.

$$\text{DPM} = \frac{\text{CPM}}{\text{Efficiency (expressed as a decimal)}} \qquad \textbf{Equation 5.2}$$

*5.1.2 Operation*

Perkin Elmer Tri-Carb 2800TR and Tri-Carb 5110TR LSCs were used for analysis of all alpha or beta samples. Prior to sample analysis, the LSC was calibrated, normalized, and the performance was assessed. A C-14 standard source with a known activity is used for

calibration that adjusts the voltage applied to both PMTs to obtain synchronized responses. During normalization, the C-14 standard, H-3 standard, and blank are measured and a t-SIE value of 1,000 is assigned to each sample. Any value below 1,000 indicating quenching. Instrument Performance Assessment's (IPA) were performed daily to record the background counts, counting efficiencies, sensitivities, and reproducibility of these standards.

Samples contained 1.0 mL aliquots of the solution to be analyzed and 15 mL of Ultima Gold AB cocktail (Perkin Elmer) in 20 mL high-density polypropylene (HDPE) LSC vials. The plastic vials provide a lower background and higher counting efficiency than glass vials and are more suitable for sample transportation and waste disposal. In addition, matrix blanks for background correction and standards containing total sample spike activity were prepared for each acid concentration and analyzed. Each sample was counted for one hour or until 40,000 counts were obtained (0.5% relative uncertainty). Data acquisition and analysis was performed using the QuantaSmart 5.01 software.

## 5.2 UV-Vis-NIR Spectroscopy

### *5.2.1 Theory*

UV-Vis-NIR spectroscopy is an analytical method used to identify both the identity and concentration of a molecule through the interaction of electromagnetic radiation with a sample. Samples can be exposed to ultraviolet (UV) to visible (Vis) wavelengths in the range of 190 – 900 nm as well as the extended near-infrared (NIR) region of 800 – 3,200 nm.

The energy of the electromagnetic radiation is defined by Equation 5.6 as:

$$E = h\nu \qquad \textbf{Equation 5.6}$$

, where E is the energy in joules (J), h is Planck's constant ($6.62 \times 10^{-34}$ Js), and $\nu$ is frequency ($s^{-1}$). Due to the wave-like nature of electromagnetic radiation, it can be classified in terms of frequency or wavelength related by Equation 5.7:

$$\nu = \frac{c}{\lambda} \qquad \textbf{Equation 5.7}$$

, where *c* is the speed of light ($3 \times 10^8$ m $s^{-1}$), and $\lambda$ is wavelength (m). Through these relations, electromagnetic radiation with a higher energy (and frequency) has a shorter wavelength. UV light has the highest energy in this system.

The general components of a spectrophotometer include a light source that generates a continuous spectrum of electromagnetic radiation across the UV-Vis-NIR regions, a monochromator that separates the broadband radiation into individual wavelengths, a sample cell, and a detector that measures the intensity of the transmitted or reflected light.

The light source should provide constant intensity over all wavelengths with long-term output stability and a high signal-to-noise ratio. Deuterium arc lamps operate using an arc discharge from deuterium gas and provide good intensity in the UV spectrum and part of

the visible region (185 – 400 nm). The steady deterioration of these lamps over time (operation time ~ 1,000 hours) and the generated noise are limiting factors. Tungsten-halogen lamps provide good intensity over the entire visible region and part of the UV region (350 – 3,000 nm). When a current is passed through the lamp filament, light is emitted as it is heated. Tungsten-halogen lamps provide low noise, low drift, and have a lifespan of ~10,000 hours. Typically, UV-Vis spectrophotometers utilize both lamps to either generate specific energies in their operable regions or simultaneously to provide a broadband source. A Xenon flash lamp operates in the 185 – 2500 nm wavelength range requiring no secondary sources and the life span is extended due to light emission in brief flashes only during sample irradiation.

The broad spectrum of white light produced is passed through a monochromator prior to sample irradiation to obtain the wavelengths of interest. The monochromator consists of an entrance slit, a dispersion device to separate wavelengths, and an exit slit. The main types of monochromators include prisms and diffraction gratings. Diffraction gratings are the most common and are composed of glass with narrow grooves etched onto the surface. The dimensions of the grooves correspond to the wavelengths to be dispersed. The interference and diffraction of the light hitting the grating reflects off an aluminum coating at different angles depending on the wavelength of interest. Filters can be added to the system to further tailor the wavelengths that will interact with the sample.

Spectrophotometers can operate with either a single or double monochromator system. Single monochromator spectrophotometers do not provide as narrow wavelength

selectivity and are therefore only useful for general spectroscopy with samples that have broad absorption peaks. In contrast, a double monochromator system arranged two monochromators in series yielding better spectral accuracy.

Samples are positioned so that the resulting beam from the monochromator interacts with the sample. These compartments are matte black to absorb and mitigate stray light from the surroundings. Liquid samples are typically contained in a glass, quartz, or plastic cuvette with a fixed pathlength. Plastic cuvettes are unable to transmit UV light, so are only used for measurements in the visible region. To ensure good transmittance of UV light, quartz cuvettes with a 10 mm pathlength are standard.

UV-Vis-NIR spectrophotometer systems can have single or double beam setups. In a simple single beam system, light passes through the sample to the detector requiring fewer optical components. A baseline measurement of a blank sample must be performed prior to sample measurement to account for any absorbance of the sample holder or solvent. However, the measurement may be less accurate due to variations within the system between baseline and sample measurements. In a double beam system, the light that exits the monochromator is split into two beams. The two identical beams interact with a reference sample and the sample of interest simultaneously to correct for instrument fluctuations.

The detector should provide a linear response over the wide range of wavelengths, have low noise, and high sensitivity. Detectors are typically PMTs or photodiodes, which have

different sensitivities and wavelengths. The PMT detectors provide high sensitivity and a high signal-to-noise ratio at low light levels making them an attractive option for dilute samples. When light hits the semiconductor material of a photodiode, electrons flow and deplete the charge in the capacitor. The light intensity is proportional to the charge required to recharge the capacitor. Photodiodes offer a wider dynamic range when compared to PMTs, good linear response, and high sensitivity. In NIR systems, lead sulfide (PbS) detectors are used in conjunction with PMTs for coverage across all wavelengths.

When light interacts with a sample, different processes like absorbance, reflection, scattering, and fluorescence/phosphorescence can occur. Spectra are obtained through the measurement of transmittance or absorbance and are plotted as %T or A as a function of wavelength (nm). The transmittance is typically defined in terms as a fraction of one and calculated using Equation 5.8.

$$\mathrm{T} = \frac{\mathrm{I}}{\mathrm{I_o}} \text{ or } \%\mathrm{T} = \frac{\mathrm{I}}{\mathrm{I_o}} * 100 \qquad \textbf{Equation 5.8}$$

$I_o$ is the incident radiation, and I is the transmitted radiation. From the transmittance, the absorbance can be determined with Equation 5.9.

$$\mathrm{A} = -\log \mathrm{T} \qquad \textbf{Equation 5.9}$$

Absorption of light results in the increase of the total energy in an atomic or molecular system and is represented as a sum of the discrete energy levels (Equation 5.10).

$$E_{total} = E_{electronic} + E_{vibrational} + E_{rotational} \qquad \textbf{Equation 5.10}$$

When the absorbed energy is equal to the energy required to promote an electron from a lower energy level to an excited energy level, narrow absorbance bands are observed. The bands in the resulting spectrum are characteristic of the electronic energy levels for a specific species. In atoms, spectra would appear as monoenergetic lines (Figure 5.3).

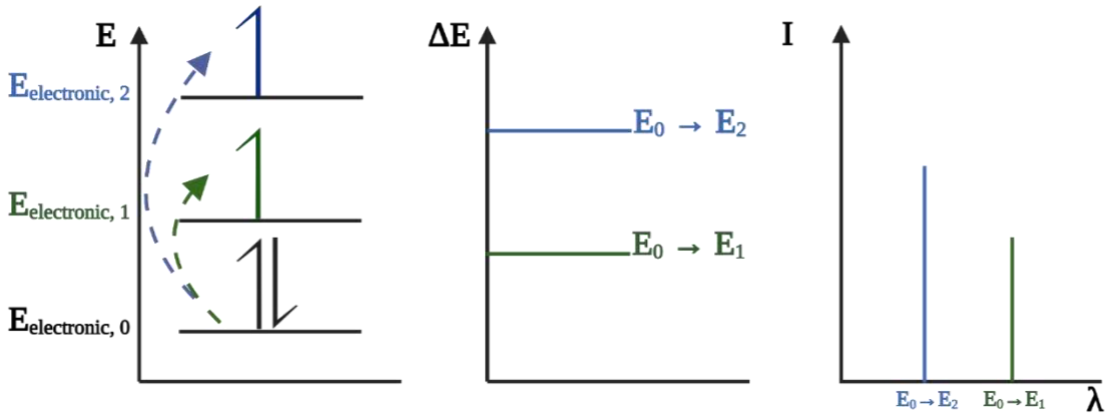


**Figure 5.3:** Spectrum of monoenergetic absorbance lines with wavelengths proportional to the energy difference between two discrete energy levels.

However, in molecular species the vibrational and rotational energy levels are superimposed on the electronic energy levels. As a result of the many transitions of different energies, the spectral bands are broadened (Figure 5.4). The energies of these transitions are discrete, or quantized, and aid in the elucidation of structure information

for species identification. In addition, observation of the shifts in wavelength or changes in intensity provides insight into chemical reactions, equilibria, and kinetics.

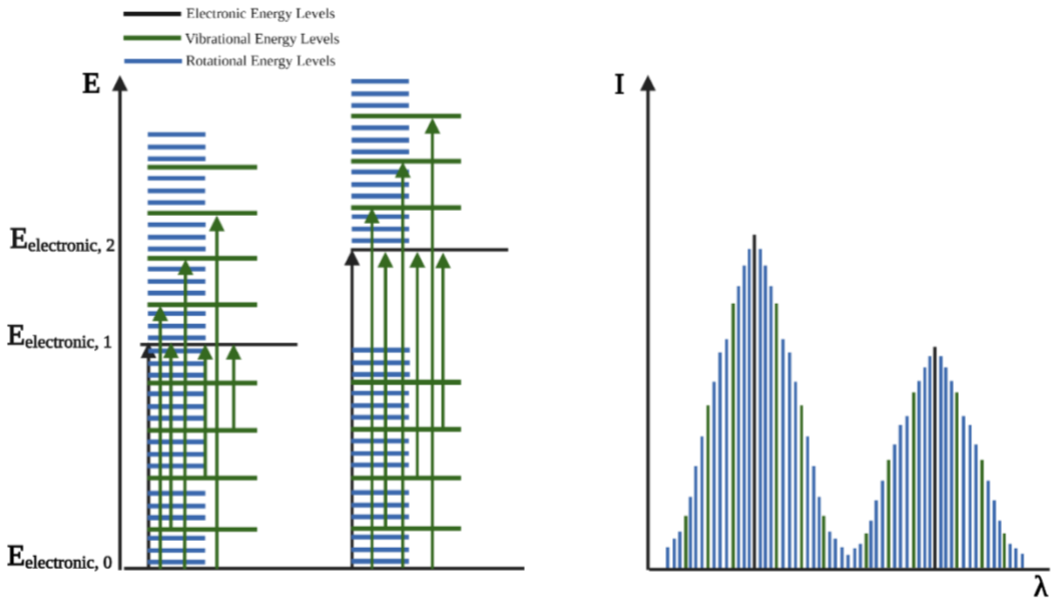


**Figure 5.4:** Absorbance spectrum of the different photons produced from transitions within the electronic, vibrational, and rotational energy levels of a molecular species.

The linear relationship between absorbance, concentration, and pathlength as described by the Beer-Lambert Law (Equation 5.11) provides a route for the quantification of the concentration of the analyte of interest.

$$A = \varepsilon bc \qquad \textbf{Equation 5.11}$$

A is the absorbance, ε is the extinction coefficient (L $mol^{-1}$ $cm^{-1}$), b is the sample path length (cm), and c is the sample concentration (mol $L^{-1}$). The extinction coefficient is defined for a specific substance under a defined set of conditions (e.g., solvent,

wavelength, temperature, instrument) and a calibration curve should be used for the measurement of ε.

*5.2.2 Operation*

An Agilent Cary 6000i UV-Vis-NIR spectrophotometer with deuterium and tungsten-halogen lamps with an operating range of 175 – 1,800 nm was used for all sample measurements. This instrument employs a double out-of-plane Littrow monochromator and beam chopper system that divides the light beam into three. An R928 PMT detector is used for UV-Vis measurements and an InGaAs photodiode detector is used for NIR measurements. Instrument parameters were selected based on Agilent's standard operation parameters and are shown in Table 5.1.

**Table 5.1:** Operation parameters of the Cary 6000i UV-Vis-NIR spectrophotometer.

| Operation Parameters | Setting |
|---|---|
| **Y Mode** | Absorbance |
| **X Mode** | nm |
| **Scan Rate** | 600.00 nm/min |
| **Data Interval** | 1 nm |
| **SBW** | 1 nm |
| **Source Changeover** | 350.00 nm |
| **Detector Changeover** | 800.00 nm |
| **Grating Changeover** | 800.00 nm |

**5.3 ICP-OES**

*5.3.1 Theory*

Inductively Coupled Plasma-Optical Emission Spectroscopy (ICP-OES) is an elemental analysis method that measures characteristic atomic emissions from elements of interest. Since specific atoms and ions have different electronic structures, characteristic

wavelengths are emitted when excited electrons return to lower energy levels. These characteristic emissions generate spectra useful for both quantitative and qualitative analysis of elements. Thus, ICP-OES analysis requires the atomization and/or ionization of the sample.

The ICP energy source is generated when inert argon gas is introduced to the torch containing coils with a high radio frequency field. Ionization of the gas is initiated by a discharge spark and an electromagnetic field accelerates the electrons that generate the plasma torch that can reach temperatures between 8,000 and 10,000 K. Sample solutions are taken up into a nebulizer via a peristaltic pump and are aerosolized with a stream of argon carrier gas and are introduced into the plasma torch for ionization.

As the analytes of interest de-excite, the emitted photons are directed through the instrument with mirrors and other optical components. The light is separated into specific wavelengths with a monochromator and are converted to an electrical signal by the detector. PMTs have been historically used as detectors in ICP-OES systems but are limited due to the fact that a single PMT is required for each emission line of interest. Charged coupled devices (CCD) are solid state detectors divided into pixels allowing for detection over a wide range of wavelengths and are featured in modern ICP-OES instruments.

The output provides the light intensity as a function of wavelength and the intensity is proportional to the analyte concentration in the sample. Using the Beer-Lambert Law, the

preparation of a calibration curve using solutions with known analyte concentrations will allow for the determination of the analyte concentration in an unknown sample. However, the components in the sample matrix will also produce characteristic emissions which may be of the same wavelength as the analyte resulting in detector interferences. Thus, it is important to select a wavelength of interest that is unique to the analyte.

*5.3.2 Operation*

A Thermo Jerrel-Ash iCAP 61E ICP-OES coupled with an AS300 autosampler was used for all measurements. Five-point calibration curves with concentrations ranging from 0.1 to 100 ppm in solution matrices that matched the samples to be analyzed to prevent differences is nebulizing efficiency. Reagent blanks and sample spike solutions were prepared in the appropriate solution matrix and used during the analysis. Calibration verification was performed after every 10 samples using a continuous calibration verification solution. The ICPManager2 software reported the output for each sample in terms of intensity and ppm was used for data analysis.

**Table 5.2:** Operation parameters for the Thermo Jerrel-Ash iCAP 61E ICP-OES.

| Parameter | Setting |
|---|---|
| **RF Power** | 1200 W |
| **Auxiliary Flow** | 1 L $min^{-1}$ |
| **Nebulizer Flow** | 0.6 L $min^{-1}$ |
| **Torch Flow** | 13 L $min^{-1}$ |
| **Torch Position** | Axial |
| **Measurements per Sample** | 6 |
| **Flush Time** | 30 s |

# CHAPTER 6: BEHAVIOR OF SODIUM BISMUTHATE IN NITRIC ACID SYSTEMS

## 6.1 Introduction

Sodium bismuthate ($NaBiO_3$) is a strong oxidant ($E_0$ = 2.03 V) that has historically been used for the determination of manganese and cerium oxidation and, despite slow kinetics, the near quantitative oxidation of $Am^{3+}$ to $AmO_2^{2+}$ has been reported.[119,194–201] However, the application of a $NaBiO_3$-based separation within UNF reprocessing is severely limited by the lack of data regarding the behavior of $NaBiO_3$ outside of solid-state research for photocatalysis.

Specifically, the solution behavior of $NaBiO_3$ remains underexplored, especially in nitric acid systems relevant to UNF reprocessing. Initial use of $NaBiO_3$ for selective separations focused on the pre-oxidation of Am for solvent extraction studies. The solid $NaBiO_3$ was filtered prior to SX experiments due to the reports that $NaBiO_3$ forms an insoluble suspension in solution that is easily removed via filtration.[202] However, other studies have claimed that solid $NaBiO_3$ decomposes in acid or warm water and is not insoluble.[203,204] Although numerous papers demonstrate the oxidation of Am in $HNO_3$, a recent paper by Rice et. al. surprisingly reported that not Am oxidation was observed in $HNO_3$.[205]

Iodometric titrations and chelatometry showed that the solubility of $NaBiO_3$ increases with increasing acid concentration and temperature, but was independent of the amount of $NaBiO_3$ in the system that ranged from 2 – 20 mg/mL.[128] When determining the reductive dissolution kinetics of $NaBiO_3$ by $Mn^{2+}$ and $Ce^{3+}$ ions, Mills and Li determined that the

rate-limiting step involved reactions between the adsorbed cation and the surface site of $NaBiO_3$; however, they concluded that the optimal conditions for the oxidation of Mn and Ce are high temperatures and pressures with high-purity (low Bi(III) amount) $NaBiO_3$ which would not be the ideal conditions for this system.[206]

Kumada et. al. reported the first observation of the partial ion exchange of $Sr^{2+}$ and $Ba^{2+}$ with the interstitial $Na^+$ cations located within the ilmenite structure of $NaBiO_3$ (Figure 6.1).[130] The hydrated structure of $NaBiO_3$ was found to be a layered material with six $BiO_6$ octahedra that form sheets of hexagonal rings with $Na^+$ cations located between the layers and are octahedrally coordinated by three $BiO_6$ oxygen atoms and three oxygen atoms from interlayer water molecules.[213]

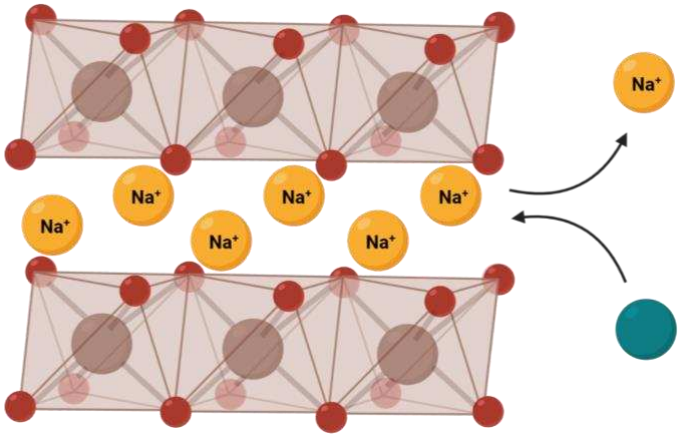


**Figure 6.1:** Ilmenite structure of solid sodium bismuthate featuring parallel sheets of octahedrally bound Bi atoms with interstitial sodium cations capable of undergoing ion exchange with other metal cations.

An increase in solution pH upon contact with $NaBiO_3$ led to the suggestion that ion exchange between $Na^+$ and $H^+$ in solution was occurring. A distortion in the $Bi^{5+}$ environment was observed at high acid concentrations and was assumed to be a result

of the reduction of $Bi^{5+}$ to $Bi^{3+}$ that distort the hexagonal rings and releases $O_2$.[207] A similar distortion in the solid structure was observed by Ding et. al. where higher acid concentrations suggested the reduction of $Bi^{5+}$ and the self-doping of the solid with $Bi^{3+}$. Thus, the presence of $Bi^{3+}$ would act as an unfavorable competing agent for $Cm^{3+}$. The same team suggested the ion exchange between $H^+$ and $Na^+$ at higher acid concentrations (11.4 M $HNO_3$) with a color change from light to dark brown occurring as a result of $Bi^{5+}$ to $Bi^{3+}$ reduction within the solid structure.[208,209]

More recently, Einkauf and Burns published several studies aimed towards elucidating the solution behavior of $NaBiO_3$ and its interactions with various metal ions.[210,211] This work reports the first absorbance spectra showing the ingrowth of the $BiO_3^-$ ion in nitric acid solutions. Studies of the solution behavior in the presence of $U^{6+}$ showed shifts in the $UO_2^{2+}$ IR spectra that indicated potential 1:1 displacement of $NO_3^-$ ligands with $BiO_3^-$ based on their identical geometry and symmetry. The presence of $Cs^+$ in solution with $NaBiO_3$ and the ion exchange of this metal ion with Na increased the dissolution of $NaBiO_3$. It was hypothesized that the increased size of the $Cs^+$ ion relative to $Na^+$ (1.74 and 1.02 Å, respectively) results in the distortion or destruction of the hexagonal ring structure. Due to decreased steric hindrance, easier diffusion of smaller metal ions increased the $BiO_3^-$ ingrowth in solution. In addition, the dissolution behavior of $NaBiO_3$ in the presence of alkaline earth metals and lanthanides showed a linear reduction in dissolution with increasing charge from $Cs^+$ to $Sr^{2+}$ to $Nd^{3+}$ indicating an increased stability of $BiO_3^-$.[210,211]

To add to the body of literature highlighting the adsorption and solution behavior of $NaBiO_3$ and to address some of the discrepancies in results, this chapter aims to characterize the adsorption behavior of Am and Cm on $NaBiO_3$ solid, the extent of the sorption of aqueous solutions, and the effect on solution pH and its influence on actinide hydrolysis. Based on this data, the overall implications on the use of $NaBiO_3$ in an Am/Cm separation procedure will be discussed.

### 6.2 Adsorption Behavior of Americium and Curium on Sodium Bismuthate

The adsorption behavior of radionuclides in a solid-liquid separation system and the separation capability of the solid was determined through batch contact studies. These studies provide a quick pathway towards obtaining information about the behavior of analytes in the system under numerous conditions and with many replicates. The weight distribution ratio, $D_w$, can be determined by measuring the tracer activity before and after contact with the resin, the mass of the resin, and the volume of the aqueous phase (Equation 4.11). Comparison of the activity in the aqueous solution before and after contact gives an indication of the activity retained on the resin.

Trivalent Am and Cm exhibit nearly identical $D_w$ values and adsorption trends on commercially available ion exchange and extraction chromatographic resins. While attempts have been made to achieve a separation on these materials through Am, reduction and incomplete separation would result from interactions with the separation material. The benefit of using $NaBiO_3$ as a solid oxidant and chromatographic material is due to the fact that the oxidizing agent is always present would prevent $AmO_2^{2+}$ reduction

as it travels down the column. Given the ion exchange and redox properties, $AmO_2^{2+}$ and $Cm^{3+}$ would be expected to exhibit different adsorption behavior on $NaBiO_3$ in the batch contact studies. Ion exchange of the trivalent $Cm^{3+}$ ion with the interstitial $Na^+$ ions would result in greater $D_w$ values whereas the oxidation of $Am^{3+}$ would generate the hexavalent $AmO_2^{2+}$ species that would not participate in ion exchange and therefore exhibit lower $D_w$ values.

### *6.2.1 Materials and Method*

Peroxide-free sodium bismuthate was obtained from Idaho National Laboratory (>93% purity) and used as received. Calibrated radiotracer stock solutions were obtained from Eckert & Ziegler in the chloride form and all working solutions were converted to the nitrate form for these studies. The working solutions were prepared by transferring aliquots of the desired activity from the stock solutions and evaporating to dryness. The residue was then reconstituted in concentrated $HNO_3$ and evaporated three times before reconstitution in the desired 0.1 M $HNO_3$ solution to give a working solution of 1000 Bq $mL^{-1}$ in 0.1 M $HNO_3$ that was verified via liquid scintillation counting. All $HNO_3$ solutions were prepared volumetrically in a calibrated volumetric flask using ACS Reagent Grade $HNO_3$ and 18 Ω deionized water from a Millipore water purification system. While the desired acid concentrations for this study were in the range of 0.01 – 2 M $HNO_3$, the working solutions were adjusted to account for the 50 μL of the 0.1 M $HNO_3$ tracer solution added to the samples.

All batch contact studies in this work follow this general procedure with any modifications discussed when applicable (Figure 6.2). 50 mg (± 0.5 mg) of $NaBiO_3$ was weighed into 2.0 mL polypropylene microcentrifuge tubes and 1.45 mL of the desired $HNO_3$ solution was added to the samples. The samples were placed on a LabQuake shaker table for one hour which was sufficient for equilibration. Following preconditioning, the samples were spiked with 50 μL (50 Bq) of the radionuclide tracer solution giving a total volume of 1.5 mL. The tracer was contacted with the resin for one hour under constant mixing on a shaker table. The sample was then filtered through a syringe equipped with a 0.45 μm PTFE syringe filter into microcentrifuge tubes and a 1.0 mL aliquot was transferred into a 20 mL scintillation vial with 15 mL of Ultima Gold AB liquid scintillation cocktail for analysis by LSC. Samples were counted for one hour or until 40,000 counts were reached.

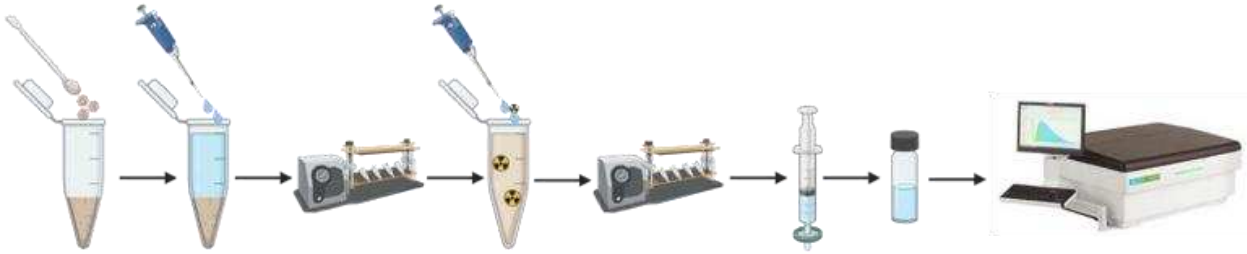

**Figure 6.2:** General batch contact study procedure.

All data points are the average of four replicates and the error bars show the statistical uncertainty of the $D_w$ to two standard deviations ($2\sigma$). Activities in the aqueous phase were considered negligible for samples with high $D_w$ values indicating full retention of the radionuclide; thus, the limit of detection (LOD) was determined using the Currie method determined from the following equation:

$$N_D = 4.65\sigma_{N_B} + 2.71 \qquad \textbf{Equation 6.1}$$

, where $N_B$ is the background counting error and $N_D$ represents the minimum counts in a sample where the false negative rate is no greater than 5%. The uncertainty was not plotted for data points at the limit of detection.

### *6.2.2 Results*

Figure 6.3 illustrates the measured $D_w$ values for $^{241}Am$ and $^{244}Cm$ on solid $NaBiO_3$ as a function of nitric acid concentration.

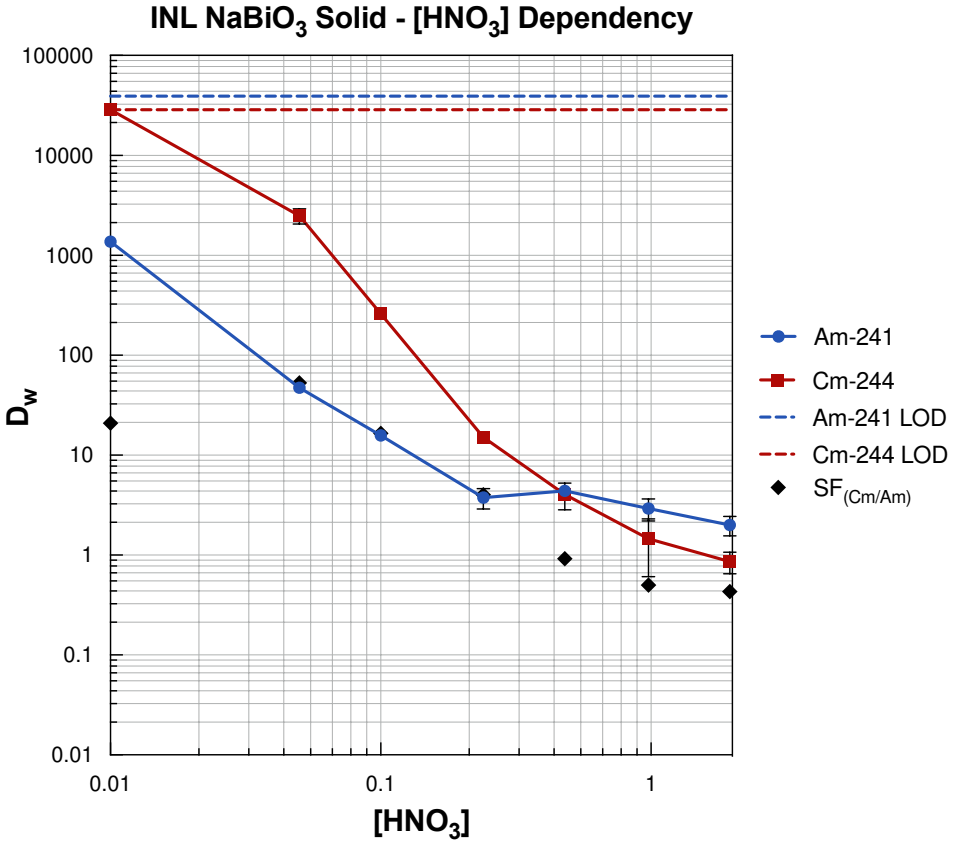


**Figure 6.3:** Adsorption of $^{241}Am$ and $^{244}Cm$ on solid sodium bismuthate as a function of nitric acid concentration. All data points are an average of four replicates and error bars represent the uncertainty to 2σ.

Both radionuclides show high adsorption at low acid concentrations with a decrease in $D_w$ as acid concentration increases. The difference in adsorption behavior of the two radionuclides implies a difference in speciation of the radionuclides and that the oxidation of $Am^{3+}$ to $AmO_2^{2+}$ has occurred. In addition, the greater adsorption of $^{244}Cm$ is indicative of the ion exchange between the $Cm^{3+}$ and interstitial $Na^+$ metal ions. At low acid concentrations, SFs greater than 10 are obtained at $HNO_3$ concentrations of 0.1 M and below with a maximum $SF_{Cm/Am}$ of 53 at 0.05 M $HNO_3$.

At 0.01 M $HNO_3$ $^{244}Cm$ is at the limit of detection indicating either complete adsorption onto the solid or potential loss of activity due to hydrolysis and subsequent adsorption to the sample container. If $^{244}Cm$ is at the LOD as a result of adsorption onto $NaBiO_3$, a chromatographic separation could be achieved through the elution of $^{241}Am$ at 0.01 M $HNO_3$ where $^{244}Cm$ co-elution is not likely to occur. However, the $D_w$ of $^{241}Am$ at 0.01 M $HNO_3$ is quite high which may require large volumes of eluent for complete recovery. Similarly, a separation at 0.05 M $HNO_3$ would also be favorable as indicated by the large $SF_{(Cm/Am)}$ and the lower $^{241}Am$ $D_w$ value would, in theory, result in a more rapid elution. As a result of the decrease in adsorption with increasing acid concentration, recovery of $^{244}Cm$ would be possible at an acid concentration of 0.25 M or higher.

### 6.3 Sorption of Aqueous Solutions

A decrease in the solution volume due to sorption by the solid adsorbent was observed for the batch study samples. This decrease in the total sample volume increases the specific activity of the radionuclide in solution which would influence the $D_w$ calculations.

To correct for the change in volume and mitigate the effect on the resulting $D_w$ determination, batch studies were carried out to determine the amount of solution lost to the resin.

### *6.3.1 Method*

Nitric acid solutions with concentrations equal to the concentration of the final samples (1.45 mL $HNO_3$ + 50 μL 0.1 M tracer) were prepared volumetrically in a calibrated volumetric flask. This ensured that the samples most closely reflected the conditions of the batch adsorption studies. The densities of the $HNO_3$ solutions were determined gravimetrically by delivering 1 mL of solution from a calibrated pipette into a scintillation vial and weighed ten times. Prior to contact with $NaBiO_3$, aliquots of these solutions were titrated with standardized NaOH solutions in triplicate to determine the actual concentration.

Microcentrifuge tubes containing 50 mg (± 0.5 mg) of $NaBiO_3$ and 1.5 mL of the $HNO_3$ solutions were placed on a shaker table for 1 hour. The samples were then filtered into a pre-weighed scintillation vial. The mass of the collected solution and previously determined densities were used to determine the volume of solution lost to sorption on the solid. Blank measurements were also completed in triplicate for each acid concentration without the presence of $NaBiO_3$ to correct for any solution that was absorbed by the PTFE syringe filter. The collected solutions after contact were then used for the following acid concentration studies in Section 6.4.

*6.3.2 Results*

Across all $HNO_3$ concentrations, ~65 – 96 μL of solution is lost with a potential trend of increasing sorption with increasing acid concentration (Figure 6.4).

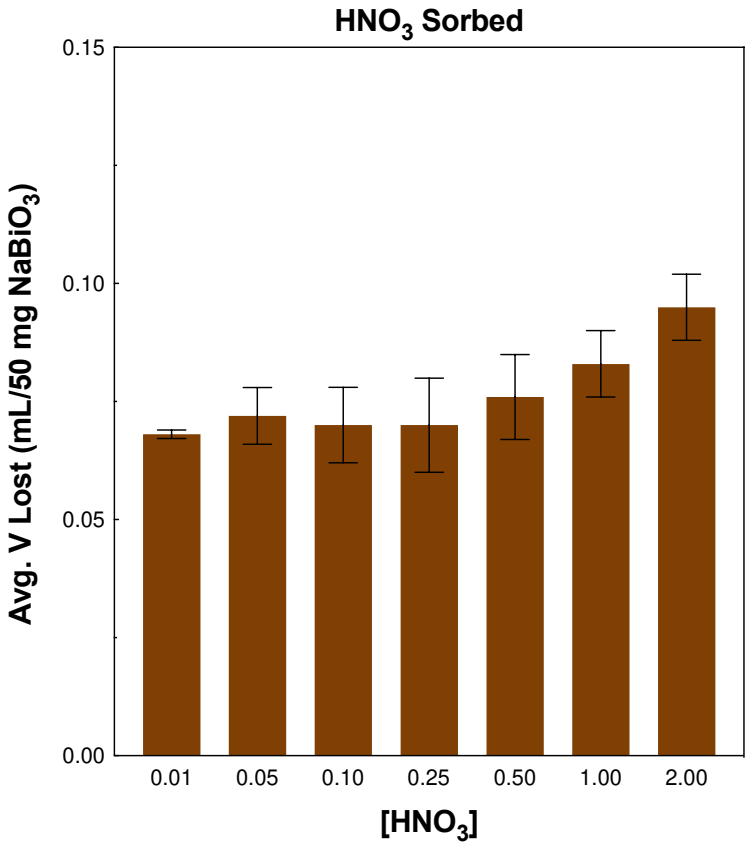


**Figure 6.4:** Average volume of solution lost after one hour of contact with 50 mg $NaBiO_3$ solid. Each data point is an average of three replicates and the error bars represent the statistical uncertainty to 2σ.

Prior to batch contact studies, the solid $NaBiO_3$ is assumed to have a dehydrated, ilmenite structure. However, due to the ion exchange behavior of $NaBiO_3$ it has been suggested that contact with aqueous solutions hydrates the solid $NaBiO_3$ and results in the incorporation of water molecules within the crystal lattice. Both the absorption and potential adsorption of the nitric acid solution in batch samples not only affects sample

volumes but may also potentially interfere with Cm adsorption. The volumes lost due to preconditioning were used to correct for volume in all following $D_w$ calculations.

### 6.4 Effect on Nitric Acid Concentration

A potential mechanistic pathway describing the oxidation of $Am^{3+}$ by $NaBiO_3$ in nitric acid could be described by the following reaction and corresponding half-reactions:

$$2Am^{3+} + 3BiO_3{}^{-} + 10H^{+} \rightarrow 2AmO_2{}^{2+} + 3Bi^{3+} + 5H_2O$$

$$2Am^{3+} + 4H_2O \leftrightarrow 2AmO_2{}^{2+} + 6e^{-} + 8H^{+}$$

$$3BiO_3{}^{-} + 6e^{-} + 18H^{+} \leftrightarrow 3Bi^{3+} + 9H_2O$$

Based on these reactions and Le Chatelier's Principle, it would be logical to assume that increasing the acid concentration would increase the amount of $Am^{6+}$ formed resulting in a greater separation factor between $Am^{6+}$ and $Cm^{3+}$. However, the batch adsorption studies showed a decrease in both the separation factor and $Cm^{3+}$ retention as the $HNO_3$ concentration increased. In addition, upon contact with $HNO_3$ concentrations of 0.5 M and greater, the solid was observed to change from a red-brown color to black and was also accompanied by visible gas production. Thus, it is possible that $NaBiO_3$ is participating in additional reactions in solution that depletes $Bi^{5+}$ through reduction to $Bi^{3+}$ affecting both the oxidation and adsorption mechanisms for the radionuclides. The half-reaction describing $Bi^{5+}$ reduction shows the consumption of $H^{+}$ ions potentially influencing the acid concentration of the samples and would have implications for the adsorption behavior of the radionuclides, especially at lower acid concentrations.

### *6.4.1 Method*

To determine the change in acidity, the post-contact solutions collected from the volume correction study were titrated. Three drops of a 0.1% phenolphthalein indicator solution were added to each sample and samples were titrated using standardized 0.1 N or 1.0 N NaOH solutions. However, the acid concentration of the 0.01 and 0.05 M $HNO_3$ samples was significantly decreased after contact. As a result, the available standardized 0.1 N NaOH solution was too concentrated to be used as a titrant. In this case, a 0.01 M NaOH titrant solution was prepared and standardized with a 0.1 M potassium hydrogen phthalate (KHP) solution. The KHP solution was prepared after drying the reagent in an oven for 24 hours and standardizing with 0.1 N NaOH. The titrant was delivered to the samples from a 25 mL burette during constant mixing of the sample until the solution turned pink for several seconds before returning to a clear solution indicating that the endpoint was reached.

### *6.4.2 Results*

A significant decrease in the $HNO_3$ concentration was observed for all $HNO_3$ solutions (Figures 6.5 and 6.6). Due to the strong oxidizing nature of $NaBiO_3$, the potential for redox reactions occurring with water and excess acid must be considered as the reduction of Bi(V) through these reactions limits the amount available for Am(III) oxidation.

$$2BiO_3^- + 4H_2O \rightarrow 2Bi^{3+} + 8OH^- + O_{2(g)}$$

$$2BiO_3^- + 8H^+ \rightarrow 2Bi^{3+} + 4H_2O + O_{2(g)}$$

In these proposed reactions, the oxidation of water by $BiO_3^-$ results in the formation of hydroxyl ions while the oxidation of acid consumes acidic $H^+$ ions to generate water. Both of these reactions support the decrease in acid concentration that was observed. In addition, both reaction pathways result in the generation of oxygen gas which was observed in both batch and chromatographic systems. The production of gas is unfavorable for a column chromatographic setup due to the influence and decrease in operational flow rate.

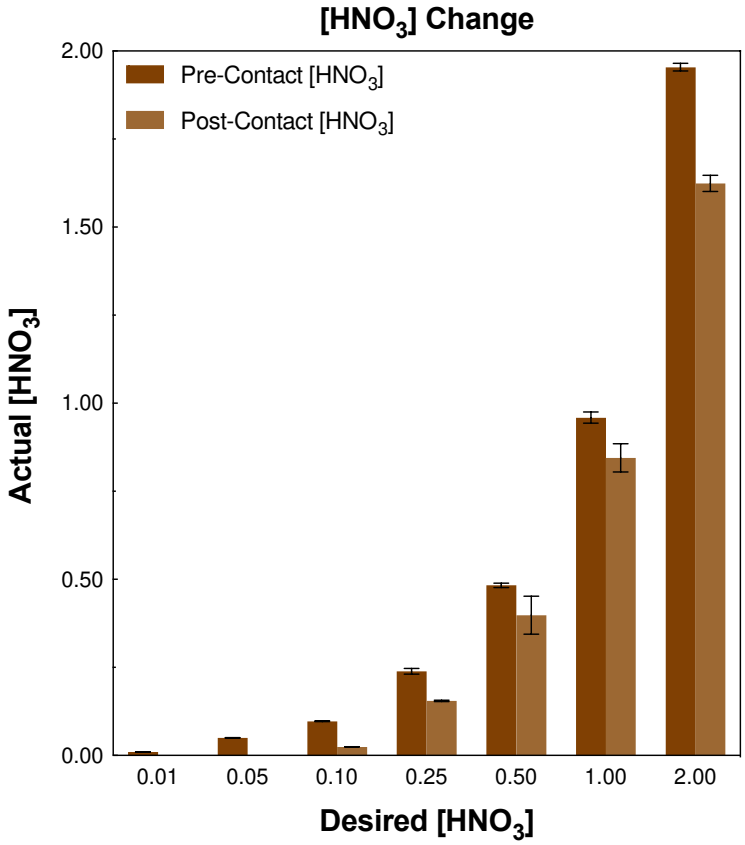


**Figure 6.5:** The concentration of the nitric acid solutions before and after contact with 50 mg of $NaBiO_3$. Each data point is the average of three replicates and the error bars represent the standard deviation to $2\sigma$.

A much larger % change was observed for the lower (0.01 – 0.1 M $HNO_3$) samples and a trend of decreasing % change with increasing initial $HNO_3$ concentration might be followed (Figure 6.6).

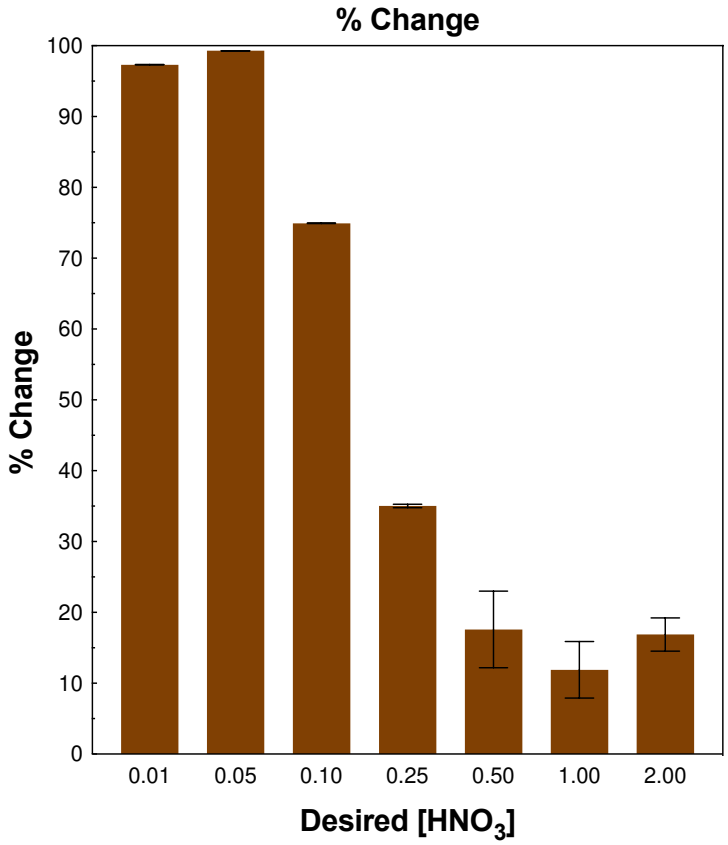


**Figure 6.6:** The percent change of the nitric acid concentration after a one-hour contact time for 1.5 mL of acid with 50 mg of $NaBiO_3$. Each data point is the average of three replicates and the error bars represent the standard deviation to $2\sigma$.

### 6.5 Hydrolysis

For aqueous solutions containing very low concentrations of actinides, especially at higher pH values and temperatures hydrolysis is possible. Thus, the potential of their precipitation must be considered. Under these conditions, loss of activity due to sorption onto the surface of the vials or other materials used during experimental studies will

significantly increase the calculated $D_w$ values determined during the batch contact studies. Accounting for the potential for loss of activity to sample containers at $HNO_3$ concentrations of 0.05 M and lower is necessary due to the results obtained in the acidity study. To determine if hydrolysis is occurring at these acid concentrations, batch studies using $NaBiO_3$-treated $HNO_3$ solutions that align with the batch adsorption samples were carried out in a similar manner as the previous batches.

### *6.5.1 Method*

To first ensure that the acid concentration of the samples was representative of the $NaBiO_3$-containing samples, 1.5 mL of 0.01 and 0.05 M $HNO_3$ was contacted with 50 mg of $NaBiO_3$ in 2 mL microcentrifuge tubes for 1 hour on a shaker table. The samples were then centrifuged at 850 rpm for 30 minutes and 1.45 mL of the supernatant was transferred to a new 2 mL microcentrifuge tube containing no $NaBiO_3$. The samples were then spiked with 50 μL of the radiotracer solution to give a total volume of 1.5 mL and were placed on a shaker table for 1 hour. After shaking, a 1 mL aliquot was transferred to a scintillation vial with 15 mL of scintillation cocktail and was analyzed using liquid scintillation counting to determine the amount of activity lost.

### *6.5.2 Results*

The percentage of activity of $^{241}Am$, $^{244}Cm$, $^{233}U$, and $^{239}Pu$ lost after contact with the $NaBiO_3$-treated 0.01 M and 0.05 M $HNO_3$ solutions is shown in Figure 6.7. These results are interesting because if hydrolysis were occurring, based on the batch study data 100%

of the $^{244}Cm$ activity would be lost at 0.01 M $HNO_3$; however, only ~34% of the activity is unaccounted for at 0.01 M $HNO_3$.

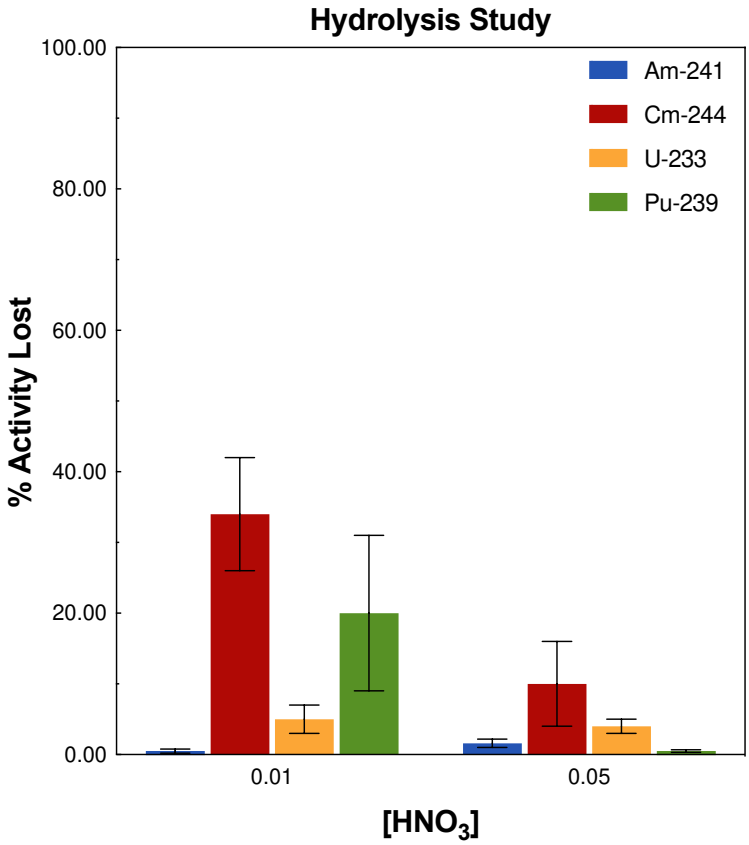


**Figure 6.7:** Amount of $^{241}Am$, $^{244}Cm$, $^{233}U$, and $^{239}Pu$ activity lost (%) to the container after one hour of contact with sodium bismuthate-treated 0.01 M and 0.05 M $HNO_3$. All data points are the average of three replicates and error bars represent the standard deviation to $2\sigma$.

This could mean that either the high $D_w$ value is truly a result of adsorption by $NaBiO_3$ or that the hydrolysis study is not an accurate reflection of the chemistry occurring during adsorption studies. A ~0.5% activity loss for $^{241}Am$ is observed at 0.01 M which might be supported by the batch study data as, while the retention is an order of magnitude lower than $^{244}Cm$, the $D_w$ is still quite high at 0.01 M $HNO_3$. It is puzzling, however, that there is a greater (1.6%) loss of $^{241}Am$ activity at 0.05 M considering the immediate drop in

retention of $^{241}Am$ seen in the batch studies. This is likely due to experimental error as indicated by the uncertainty of these values. Even more puzzling is the fact that only 5% and 20% of $^{233}U$ and $^{239}Pu$ activity, respectively, is lost at 0.01 M $HNO_3$ as both radionuclides also had $D_w$ values at the LOD at 0.01 M $HNO_3$ (Figure 8.1). While a decrease in the % activity lost is expected and observed for 0.05 M $HNO_3$, this decrease is nowhere near as substantial as would be expected for $^{233}U$ based on the batch adsorption data discussed in chapter eight.

There are two possible reasons for the unusual results which may also explain the large standard deviations of these values. The first is that, while the acid concentration was decreased prior to the study through pre-treatment with $NaBiO_3$, there was no $NaBiO_3$ present when the samples were spiked with the tracer solutions. The tracer solutions have a significantly higher acid concentration of 0.1 M $HNO_3$ relative to the pre-treated solutions and can therefore alter the sample conditions to a lower pH. However, a small (50 μL) volume of the 0.1 M tracer solution is added which is likely not large enough to significantly influence the total sample acid concentration. This could be proven by repeating both batch adsorption and hydrolysis and titrating all solutions before and after to determine the differences between the samples.

Although the solutions that were pre-treated with $NaBiO_3$ were centrifuged extensively and complete separation of the two phases seemed to be achieved, the fine $NaBiO_3$ particles were dispersed throughout the supernatant and not detected until sample settling after the experiment was completed. As a result, when transferring the

supernatant to the microcentrifuge tubes to be spiked with the radionuclides, solid $NaBiO_3$ was still present. Since solid $NaBiO_3$ was observed to be settled at the bottom of the sample tubes that the LSC aliquots were taken from, the unaccounted-for activity may have been adsorbed onto the solids in the sample. Instead of loss due to adsorption onto the microcentrifuge tube walls, the missing activity may be located on the solids based on the high adsorption of $^{244}Cm$. On the other hand, if any suspended $NaBiO_3$ solids with $^{244}Cm$ retained were transferred to the LSC vial, that would account for the lower-than-expected activity loss. To further determine whether or not hydrolysis is responsible, this study should be repeated as a function of temperature where the production of the hydrolysis products would increase. Thus, an increase in the amount of activity lost would indicate hydrolysis.

### 6.6 Dissolution in Nitric Acid

Since the ion exchange and oxidation mechanisms provided by solid $NaBiO_3$ makes this material favorable for its implementation in a chromatographic system for Am/Cm separations, the loss of the solid due to dissolution limits the longevity and efficiency of the column. The dissolution behavior needs to be further understood due to the lack of consensus in the literature. Determination of the dissolution kinetics and identifying the system conditions that minimize dissolution are necessary when designing a chromatographic system.

To further explore the solution behavior of $NaBiO_3$ and the potential redox reactions occurring with water and excess acid, the dissolution of $NaBiO_3$ was determined through the quantification of the $Bi^{3+}$ and $Bi^{5+}$ species in 2 M $HNO_3$. Favorable system parameters

for an Am/Cm separation can be identified through $NaBiO_3$ dissolution and redox studies so that the amount of $Bi^{3+}$ produced would be limited. Due to its trivalent speciation, the increased concentration of $Bi^{3+}$ in solution could act as a competing ion for $Cm^{3+}$ and determining the conditions where this is minimized is necessary. In addition, larger $Bi^{3+}$ concentrations would indicate the reduction of $Bi^{5+}$ that would decrease $Am^{3+}$ oxidation efficiency.

The dissolution of this material can be determined by measuring the total Bi concentration in solution and the degradation of $NaBiO_3$, defined here as the ingrowth of both Bi(III) and Bi(V) in solution, can also be determined by quantifying Bi(V) and obtaining the Bi(V):Bi(III) ratio.

### *6.6.1 Bi(V) Dissolution in 2 M Nitric Acid as a Function of Mixing Time*

#### *6.6.1.1 Method*

The dissolution of $NaBiO_3$ was determined by first carrying out batch contact studies as a function of mixing time. 0.5 g of $NaBiO_3$ and 2 mL of 2.0 M $HNO_3$ were added to a 15 mL centrifuge tube followed by mixing at times ranging from 15 to 180 minutes. The samples were filtered through a 0.45 μm syringe filter and collected in a 2 mL microcentrifuge tube. The resulting solution was pink indicating the presence of the $BiO_3^-$ ion in solution and a 0.5 mL aliquot was transferred to a 1 cm quartz cuvette and diluted to 2.1 mL with 2 M $HNO_3$ for UV-Vis determination of the $BiO_3^-$ concentration. Baselines with 2.0 M $HNO_3$ blank solutions were obtained prior to each measurement for the background correction of the spectra. Spectra were collected from 400 – 750 nm with the

$BiO_3^-$ weak absorption band occurring in the range of 450 – 600 nm. The absorbance values measured at 527 nm and an extinction coefficient, ε, of 11.1 L $mol^{-1}$ $cm^{-1}$ was used for the calculation of the Bi(V) concentration.

*6.6.1.2 Results*

The weak absorbance bands from 450 – 600 nm characteristic of the $BiO_3^-$ anionic species are shown in Figure 6.8 and provide clear qualitative data representative of the ingrowth of the Bi(V) anion in solution.

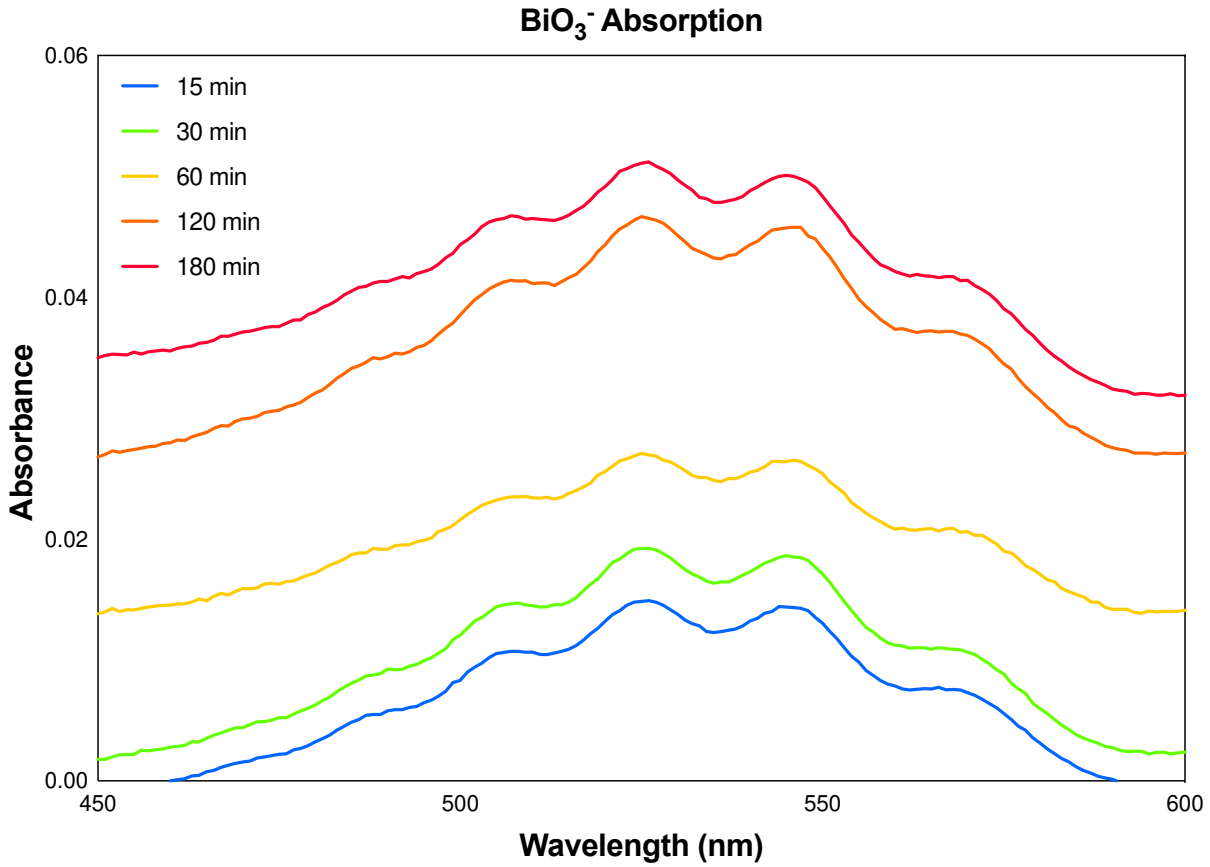


**Figure 6.8:** $BiO_3^-$ absorbance bands in the 450 – 600 nm region at shaking times of a) 180 min, b.) 120 min, c.) 60 min, d.) 30 min, e.) 15 min.

Interestingly, the absorbance of not only the $BiO_3^-$ absorbance band, but the entire spectrum, increased indicating that the 2.0 M $HNO_3$ blank was not appropriate. This is potentially due to the presence of other species dissolving in solution that introduces both absorbance and scattering interferences. It is possible that any $Bi^{3+}$ present in solution may form a hydrolysis product that precipitates and causes scattering; however, no solids were observed in the UV-Vis samples.

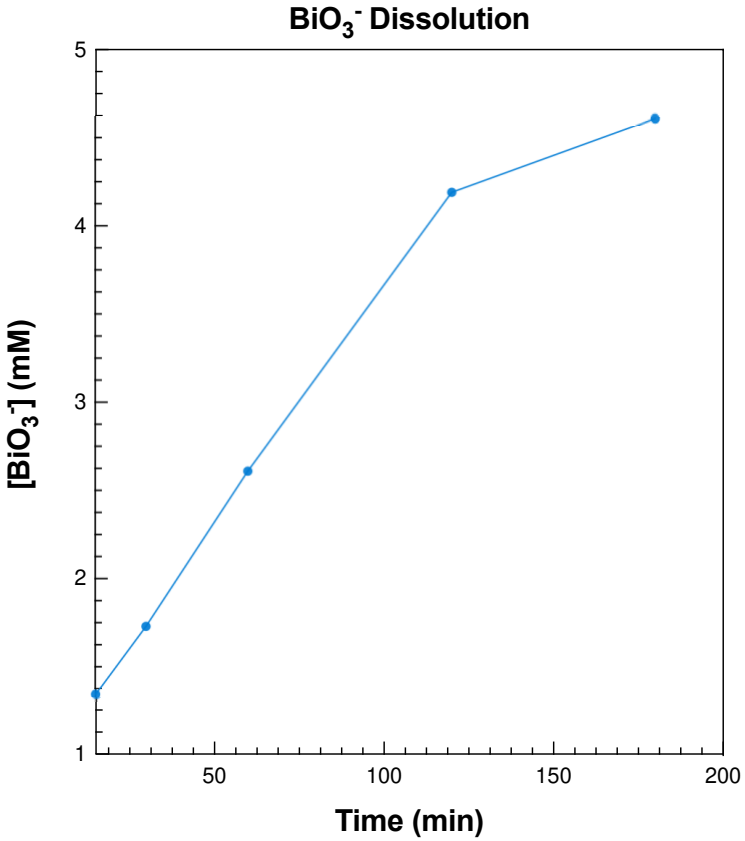


**Figure 6.9:** The dissolution of Bi(V) from $NaBiO_3$ solid in 2 M nitric acid as a function of shaking time. The Bi(V) concentrations were determined from the absorbance value measured at 527 nm for the $BiO_3^-$ absorbance band with a molar extinction coefficient of 11.1 L $mol^{-1}$ $cm^{-1}$ for a 1 cm pathlength.

The concentration of $BiO_3^-$ in mM was determined using the measured absorbance values at 527 nm in the Beer-Lambert equation and plotted as a function of shaking time (Figure

6.9). It was found that just after 15 minutes of contact 1.34 mM of the Bi(V) species was present in solution with a relatively linear increase with increased shaking time. The $BiO_3^-$ concentration appears to begin to plateau after 180 minutes of mixing and was assumed to have reached equilibrium.

The kinetics of $NaBiO_3$ dissolution could be described using an inverse-cubic rate law assuming that the $NaBiO_3$ particles are spherical, homogeneous, and monodispersed (Equations 6.2 and 6.3).

$$\left(1 - \frac{[BiO_3^-]_t}{[BiO_3^-]_{Eq}}\right)^{1/3} = 1 - tk_{Obs} \qquad \textbf{Equation 6.2}$$

$$k = \rho r_0 k_{Obs} \qquad \textbf{Equation 6.3}$$

, where $[BiO_3^-]_t$ and $[BiO_3^-]_{Eq}$ are the $BiO_3^-$ concentrations at time *t* and at equilibrium in mM, *t* is the mixing time in minutes, $r_0$ is the initial particle radius in cm, $\rho$ is the density in mg $cm^{-3}$, *k* is the rate constant in mg $cm^{-2}$ $min^{-1}$, and $k_{obs}$ is the analytical rate constant in $min^{-1}$.

A linear plot of $\left(1 - \frac{[BiO_3^-]_t}{[BiO_3^-]_{Eq}}\right)^{1/3}$ as a function of shaking time is shown in Figure 6.10, where $k_{Obs}$ is the negative of the slope of the line. To determine the dissolution rate, *k*, density, and average particle radius, $\rho$ and $r_0$, respectively, must be known. The density of $NaBiO_3$ is 6.5 g/$cm^3$ and the $r_0$ was estimated to be ~1.5 microns (0.015 cm) by

Richards et. al.[212] From Figure 6.10, $-k_{Obs}$ is 0.0045 $min^{-1}$ and from Equation 6.3, the dissolution rate constant for 2 M $HNO_3$ was determined to be 0.44 mg $cm^{-2}$ $min^{-1}$. However, this determination is limited due to uncertainties regarding the $BiO_3^-$ equilibrium concentration, model assumptions, $\rho$ and $r_0$ estimations, and small number of data points.

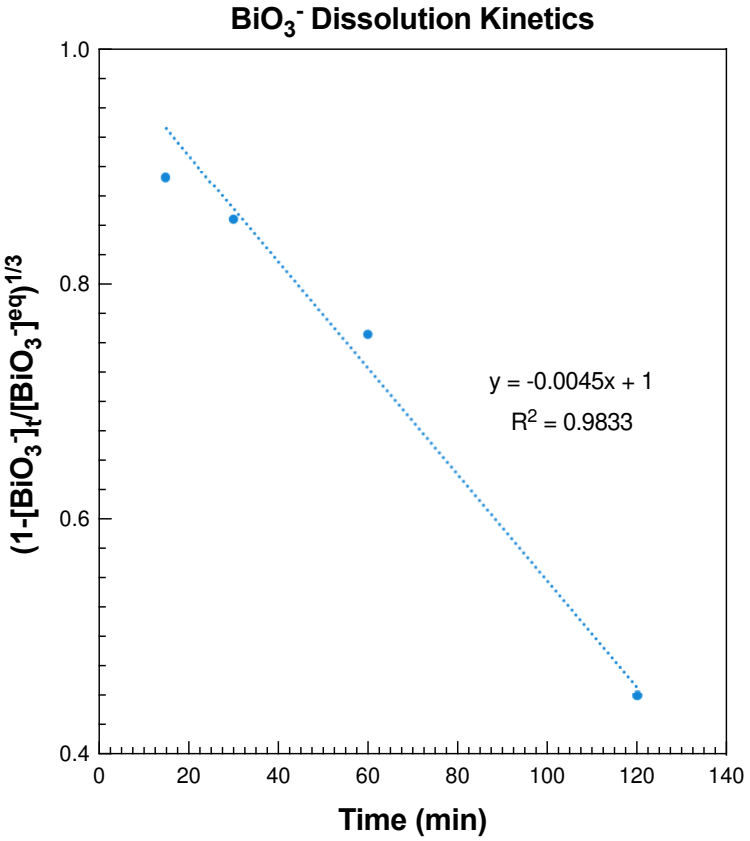


**Figure 6.10:** Linear plot describing the dissolution kinetics of 0.5 g of $NaBiO_3$ in 2 M $HNO_3$ as a function of shaking time where the negative of the slope is equal to $k_{Obs}$.

Characteristics such as purity, particle size, and surface area of the $NaBiO_3$ reagent may also influence the dissolution behavior. Understanding the dissolution of the $BiO_3^-$ oxidant is crucial in understanding the redox mechanisms for an Am separation system because, while the solid $NaBiO_3$ material is responsible for oxidizing $Am^{3+}$ to $AmO_2^{2+}$, $BiO_3^-$ present

in solution could act as a holding reagent that increases the stability of hexavalent Am in solution and improve the separation efficiency.

### *6.6.2 Total Bi Dissolution in 2 M Nitric Acid as a Function of Mixing Time*

#### *6.6.2.1 Method*

After the initial UV-Vis measurements were taken, a 0.5 mL aliquot of the UV-Vis sample was diluted to 3 mL and analyzed via ICP-OES to determine the total Bi concentration. A 10,000 ppm Bi ICP-OES standard solution in 2 wt% $HNO_3$ was used to prepare 100 ppm Bi standard working solutions for each of the desired acid concentrations. These solutions were then used to prepare seven sets of calibration solutions containing Bi concentrations of 0.1, 1, 2, 5, 10, and 25 ppm to provide a six-point calibration curve at each of the seven desired acid concentrations to be analyzed.

#### *6.6.2.2 Results*

The total $Bi^{3+}$ + $Bi^{5+}$ concentration also increased with increasing shaking time as expected (Figure 6.11). At shorter contact times, the $[Bi^{5+}]$ and $[Bi]_{Tot}$ concentrations are nearly identical indicating that a majority of the Bi is dissolving as the $BiO_3^-$ species. However, with increased contact time, the $[Bi^{5+}]$:$[Bi]_{Tot}$ ratio decreases which would suggest that the $Bi^{3+}$ species begins to dominate in the solution. This increase in $Bi^{3+}$ may be detrimental to ensuring the stability of $AmO_2^{2+}$; therefore, limiting contact times between the solution and solid is necessary . The reduction of $Bi^{5+}$ through redox reactions with water and excess acid leading to production of $Bi^{3+}$ may increase with mixing time, but the presence of the $Bi^{3+}$ species in solution may also a result of $NaBiO_3$

solid dissolution. Depending on the purity of the $NaBiO_3$ reagent, the $Bi^{3+}$ content in the solid can vary and would result in an increase in the $Bi^{3+}$:$Bi^{5+}$ ratio in solution.

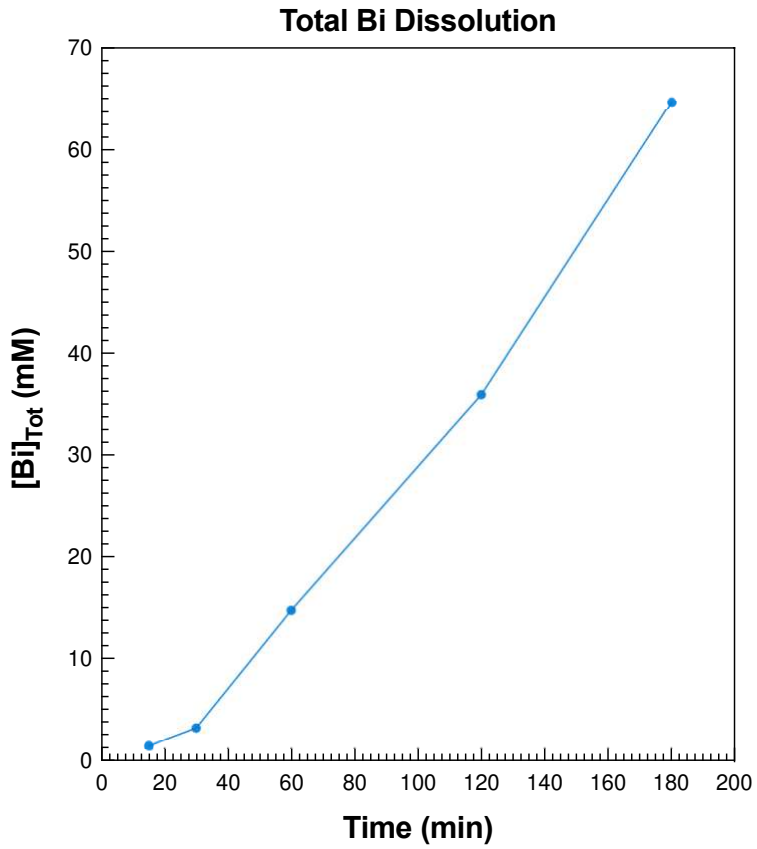


**Figure 6.11:** Total Bi (Bi(III) + Bi(V)) concentration in solution as a result of ingrowth during sample shaking in 2 M nitric acid.

While the dissolution of $NaBiO_3$ and the increased concentration of $Bi^{3+}$ is unfavorable, these studies were performed using 2 M $HNO_3$. Based on the batch adsorption data, $^{241}Am$ recovery would occur at low $HNO_3$ concentrations where dissolution may not be as significant. Thus, the dissolution and increased $Bi^{3+}$ concentration observed in this study would occur during $^{244}Cm$ elution which is less detrimental to the separation as it relates to Am oxidation. To better understand the implications of Bi dissolution, it is necessary to

repeat these studies at the lower nitric acid concentrations where $^{241}Am$ would elute and to also quantify the $Bi^{5+} \rightarrow Bi^{3+}$ decay rate in solution after $NaBiO_3$ is removed.

### 6.7 Conclusions and Future Work

Understanding the solution behavior of $NaBiO_3$ in nitric acid systems is important for understanding the ion exchange mechanisms, redox reactions, and system conditions conducive of a successful and efficient Am/Cm separation. Based on the $^{241}Am$ and $^{244}Cm$ batch adsorption study, the difference in the adsorption between the two radionuclides is a clear indication of $Am^{3+}$ oxidation to the hexavalent $AmO_2^{2+}$ species that has a decreased retention on the solid. In addition, the high adsorption of $Cm^{3+}$ supports the occurrence of an ion exchange reaction with the $Na^+$ cations within the solid. A decrease in $D_w$ and $SF_{(Cm/Am)}$ values with increasing $HNO_3$ concentration for both radionuclides was observed; thus, a chromatographic separation could be achieved through the elution of $^{241}Am$ at a low $HNO_3$ concentration (<0.25 M) followed by $^{244}Cm$ elution at a higher $HNO_3$ concentration. However, this system is simplified relative to the matrices that would be encountered in both laboratory and reprocessing separations. The influence of other system parameters on the adsorption behavior of these radionuclides must be determined and batch studies exploring the effect of ionic strength, pH, and interfering ions should be carried out.

Several changes in the samples were observed during the batch adsorption studies including a decrease in solution volume. Volume correction studies were performed across $HNO_3$ concentrations which showed volume losses ranging from ~65-95 μL and

were used to correct the sample volume for $D_w$ calculations. While absorption of the solution may be occurring, it is also possible that adsorption is occurring through ion exchange reactions between $H^+$ and $Na^+$ cations which should be explored further through x-ray spectroscopic studies of $NaBiO_3$ solid before and after acid treatment.

Degradation of $NaBiO_3$ was also observed based on the change in color of the solid from red-brown to black at $HNO_3$ concentrations of 0.5 M and above and was suspected to be a result of $Bi^{5+}$ reduction to $Bi^{3+}$. Since $BiO_3^-$ is a strong oxidizing agent, the potential for redox reactions occurring with water and excess acid is likely and would be accompanied by a decrease in the acid concentration of the solution. A large decrease in the acid concentration of the 0.01 and 0.05 M samples was observed and would have significant implications on actinide hydrolysis. However, the hydrolysis studies performed for $^{241}Am$, $^{244}Cm$, $^{233}U$, and $^{239}Pu$ were inconclusive and should be extended to include higher temperatures to further understand whether or not hydrolysis is occurring. In addition, due to the highly oxidizing nature of $NaBiO_3$ in acidic media, studying the adsorption and solution behavior in other acid systems would be beneficial. Since $HNO_3$ also has a strong reducing/oxidizing behavior, exploring alternative systems such as $H_3PO_4$ and $H_2SO_4$ may reduce the effects observed in solution and aid in maintaining the longevity and oxidizing capability of $NaBiO_3$ chromatographic systems.

These redox reactions occurring in solution also influence the dissolution and degradation of $NaBiO_3$. The loss of solid $NaBiO_3$ and the $BiO_3^-$ oxidant is necessary to understand in order to provide insight into the ion exchange and redox capabilities as well as the

longevity of the material in a chromatographic system. The dissolution kinetics were determined through the ingrowth of the $BiO_3^-$ and $Bi^{3+}$ ions in solution as a function of mixing time. Significant ingrowth of both Bi species occurs in 2 M $HNO_3$ with the $BiO_3^-$ species comprising a majority of the dissolved species at shorter mixing times and a greater ingrowth of $Bi^{3+}$ at longer mixing times. This indicates the reduction of $Bi^{5+}$ to $Bi^{3+}$ in solution with increasing mixing time, but the decay kinetics of $Bi^{5+}$ should be determined through the measurement of the decrease in the $BiO_3^-$ absorbance band over time. Since the presence of $Bi^{3+}$ indicates loss of the oxidant and poses as an interference for $Cm^{3+}$ ion exchange, identifying the system conditions that minimize $Bi^{3+}$ ingrowth is imperative.

The dissolution study should be improved through the measurement of the dissolved Bi species at longer contact times to ensure equilibrium has been reached and the physical properties of the solid such as particle size, radius, surface area, and purity should be determined to ensure the application of the inverse rate law is accurate. In addition, the dissolution should be further characterized across all $HNO_3$ concentrations as well as in different acid systems. Since most sample matrices encountered in the application of this system will contain other nuclides, the effect of ionic radii and charge density on the rate of dissolution should be studied.

# CHAPTER 7: BEHAVIOR OF AMERICIUM AND CURIUM ON POLYMER SUPPORTED SODIUM BISMUTHATE SORBENTS

## 7.1 Introduction

The Bi(V) – Bi(III) redox couple has a 2.03 V reduction potential which makes $NaBiO_3$ a candidate for Am(III) oxidation in view of radiochemical separations.[203] While it has been successfully utilized in solvent extraction systems, its low solubility in water and nitric acid limits its utilization in large-scale centrifugal contactor systems.[200,201] The structure of $NaBiO_3$ is similar to aluminum oxide in that it features parallel sheets of octahedrally bound $Bi^{5+}$ atoms with interstitial $Na^+$ cations giving the solid oxidant favorable ion exchange behavior.[126,213,214] Thus, the favorable redox and ion exchange properties of $NaBiO_3$ makes it an attractive option for column chromatographic systems; however, since $NaBiO_3$ is a fine particulate, the mechanical properties of the solid in a chromatographic system are poor.

The ability to use $NaBiO_3$ for the chromatographic separation of $^{241}Am$ from $^{244}Cm$ was demonstrated using 5 wt% $NaBiO_3$ dispersed in 95 wt% celite 535 and resulted in recoveries and purities >95%. The high separation factors, short contact times, and ease of operation of this separation system provide a promising alternative to solvent extraction systems for the separation of oxidized $^{241}Am$ from $^{244}Cm$. This method, however, suffers from poor adsorption capacity and flow rate properties, gradual dissolution of the material during the separation, and gas production in nitric acid.[127] It is clear that $NaBiO_3$ has the advantage of combining both ion exchange and oxidation mechanisms into one material,

but in order to be used in a column chromatographic system, the granular properties of the solid must be modified to improve column dynamics.

Composite inorganic-organic ion exchange sorbents were first prepared to employ fine microcrystalline or powdered ion exchangers in packed bed chromatographic systems through their incorporation into larger particles that improve flow dynamics. These composite materials are formed through the coagulation of a binding polymer in solution with the active component (solid ion exchanger) suspended in the mixture. This results in the incorporation of the fine ion exchange powder into the binding polymer to generate a sorbent with improved ion exchange kinetics and capacity relative to the original ion exchange material.[215]

These composite sorbents have been prepared and utilized for successful radioanalytical separations over the past several decades with the first use of a polyacrylonitrile (PAN) organic binder demonstrated in 1980 for radium separations.[215] Since then, dozens of PAN-based derivatives containing a multitude of inorganic ion exchangers have been prepared with several available commercially. The evaluation of 16 PAN-based sorbents for the treatment of U.S. Department of Energy radioactive wastes was carried out by Marsh et. al. yielding favorable results.[216] Today, manganese dioxide ($MnO_2$)-, ammonium molybdophosphate (AMP)-, and potassium-nickel hexacyanoferrate (KNiFC)-PAN resins are commercially available from TrisKem Int. for radium and cesium separations.

PAN-based composite resins have found their widespread use due to ease of production and tailoring of physical properties (*e.g.,* porosity, stability). No degradation of the PAN binder has been observed in aqueous solutions with a pH range from 0 to 13 making it favorable for use in radiochemical separations. Dissolution occurs in aqueous solutions with concentrations greater than 8 M $HNO_3$ and hydrolysis has been observed in alkaline solutions with a pH>13; however, these operating parameters are not typically used as the inorganic ion exchangers also exhibit poor stability under these conditions. PAN was found to be radiolytically stable up to doses as high as $10^6$ Gy with higher doses affecting cross-linking resulting in polymer hardening. Thus, the radiolytic stability of a composite ion exchange material would be limited by the radiolytic stability of the active ion exchanger itself.[217] In addition, polyethersulfone (PES) is also widely used as a polymeric material due to its favorable mechanical strength and chemical, radiolytic, hydrolytic, and thermal stabilities.

While $NaBiO_3$ has been shown to exhibit favorable oxidation and adsorption properties, its granular form limits its efficacy in column chromatographic systems due to poor mechanical properties that ultimately leads to bed clogging and poor flow rates. Thus, the incorporation of $NaBiO_3$ within an organic polymer binding matrix such as PAN or PES is a logical approach toward improving the chromatographic performance of this inorganic ion exchange material. In addition, since the solid ion exchanger is finely divided and embedded throughout the polymeric matrix, sorption kinetics are expected to be faster than that of the pure granular solid which is favorable for large-scale separations of used nuclear fuel.

## 7.2 Preparation of $NaBiO_3$ Polymer-Supported Resins

The $NaBiO_3$-PAN and $NaBiO_3$-PES resins were prepared by TrisKem International and used as received. The binding polymer solution was prepared by dissolving PAN or PES in the polar aprotic dimethylsulfoxide (DMSO) solvent and solid $NaBiO_3$ (~80% purity) was suspended in the binding polymer solution and mixed. This mixture was delivered to a DI-$H_2O$ coagulation bath through a syringe at a constant flow rate using a peristaltic pump where the $NaBiO_3$-PAN/PES resin beads were formed upon coagulation of the binding polymer. The resulting sorbent beads were separated from the bath and washed with water before shipment. It was recommended that these wet sorbents (~40% hydration) are stored swollen to prevent bead shrinkage; thus, care was taken to ensure that no drying of the resins occurred.

To explore the effect of $NaBiO_3$ weight loading, TrisKem prepared several PAN-based composite sorbents that varied the $NaBiO_3$ dry weight content from 10, 25, 50, and 75 wt% $NaBiO_3$. The PES-based resin was prepared with a 10 wt% $NaBiO_3$ content. Upon receipt, the resins were wet-sieved as a means of particle size analysis which showed that the resin beads had a particle size range from 125 – 500 microns.

## 7.3 Adsorption of Americium and Curium on 75 wt% $NaBiO_3$-PAN

### *7.3.1 Nitric Acid Concentration Dependency*

The dependency of $D_w$ for $^{241}Am$ and $^{244}Cm$ as a function of nitric acid concentration is shown in Figure 7.1. Similar to the adsorption behavior on solid $NaBiO_3$, there is high

$^{241}$Am and $^{244}$Cm adsorption ($D_w$ ~1,400 and 16,000, respectively) observed at 0.01 M $HNO_3$ giving a separation factor of ~11.

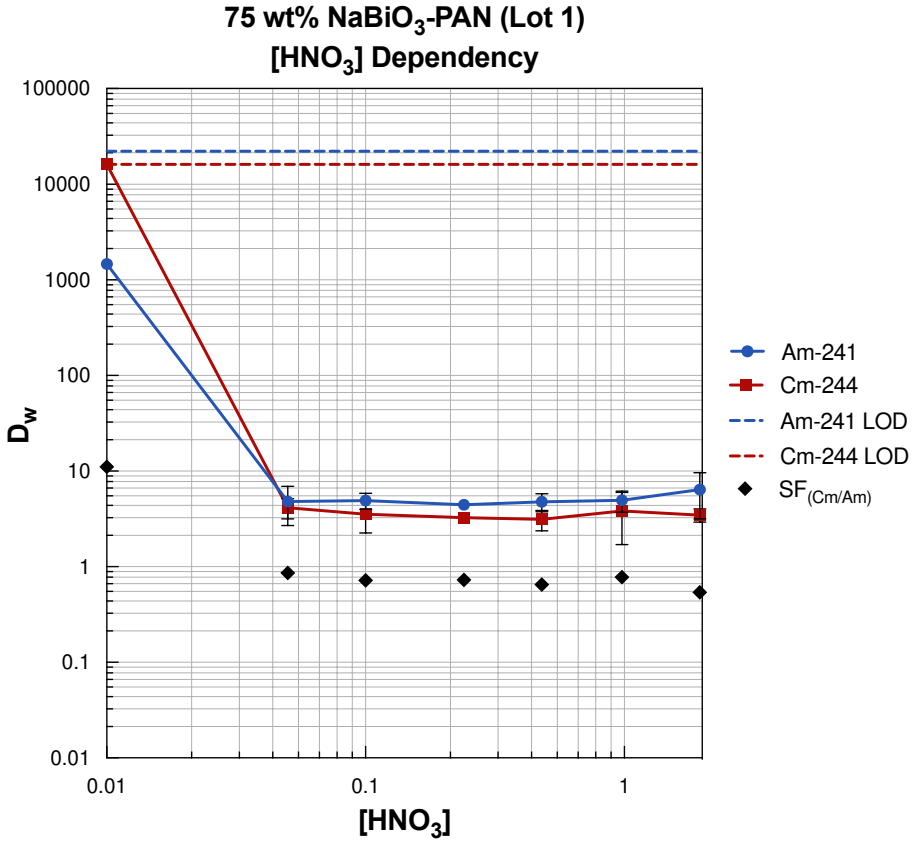


**Figure 7.1:** Adsorption of $^{241}$Am and $^{244}$Cm on 75 wt% $NaBiO_3$-PAN resin as a function of nitric acid concentration. All data points are an average of four replicates and error bars represent the uncertainty to 2σ.

The difference in behavior of the two radionuclides at 0.01 M $HNO_3$ suggests that the expected redox and ion exchange reactions are occurring. However, there is an instantaneous decrease in adsorption at acid concentrations above 0.01 M $HNO_3$ for both radionuclides and $D_w$ values remain constant as acid concentration increases. This behavior deviates significantly from the favorable differences observed in the adsorption behavior across nitric acid concentrations for solid $NaBiO_3$. While this lack of adsorption and identical behavior of $^{241}$Am and $^{244}$Cm suggest that neither redox nor ion exchange

reactions are at play, the significant change in adsorption behavior suggests that the PAN support has altered the properties of $NaBiO_3$.

Polymer-based ion exchange resins are typically prepared through the covalent attachment of ionic functional groups onto the support material where ion exchange is accessible for the analytes in solution; however, the solid is merely coated onto the support for this resin. It is also well-understood that the performance of polymeric ion exchange resins heavily depends on factors such as degree of crosslinking, porosity, and surface area. Since the $NaBiO_3$-PAN is prepared through the impregnation of $NaBiO_3$ within the polymer beads, the $NaBiO_3$ distribution throughout the sample relative to the $NaBiO_3$ solid studies is an important consideration.

Depending on how the active $NaBiO_3$ ion exchange material has been embedded within the PAN matrix, the kinetics, mass transfer, and ion exchange capacity may have been unfavorably affected. Thus, it is possible that $^{244}Cm$ access to the ion exchange sites and $^{241}Am$ access to $Bi^{5+}$ for oxidation has been hindered. In addition, it is possible that the $NaBiO_3$ itself was severely altered or degraded during the resin preparation process thus diminishing the favorable $^{241}Am$ and $^{244}Cm$ adsorption behavior previously observed.

Although the $NaBiO_3$-PAN material is not conducive of a successful separation across a range of nitric acid concentrations, the favorable $SF_{Cm/Am}$ of ~11 at 0.01 M $HNO_3$ may produce a successful separation through the recovery of Am using 0.01 M $HNO_3$ followed by $^{244}Cm$ stripping with an eluent of a greater nitric acid concentration. However, the $D_w$

of Am is still high at 0.01 M $HNO_3$ which may require large volumes of eluent to achieve full recovery. Since the difference in behavior for Am and Cm at 0.01 M $HNO_3$ could indicate the occurrence of favorable redox and ion exchange reactions, kinetics studies performed at this acid concentration were carried out to further understand the adsorption behavior of the minor actinides on this material.

### *7.3.2 Acid Preconditioning Time Dependency*

Due to the observed decrease in sample solution volume and nitric acid concentration after contact with solid $NaBiO_3$ as well as the potential for the increased dissolution of $NaBiO_3$, batch studies were conducted to determine the effect of the length of resin preconditioning time. A decrease in preconditioning time could limit the extent to which the pH of the solution is altered which may decrease $^{244}Cm$ retention in the event that hydrolysis is occurring. In addition, since $NaBiO_3$ undergoes redox reactions with water and excess acid, the reduction of Bi(V) during preconditioning and result in a decrease in trivalent Am oxidation as well as potentially introduce $Bi^{3+}$ into ion exchange sites preventing $Cm^{3+}$ adsorption. Thus, limiting the time for resin preconditioning may preserve the solid oxidant necessary for ion exchange and oxidation as well as limit the effects on the sample matrix.

#### *7.3.2.1 Method*

Precondition dependency batch studies were carried out identically to the concentration dependency study; however, the acid concentration for all samples was 0.01 M $HNO_3$ due to the favorable $SF_{Cm/Am}$ obtained during the batch contact study. The initial resin

preconditioning time was varied from 1 to 120 minutes prior to spiking with the radionuclide tracer for the standard one-hour contact time.

*7.3.2.2 Results*

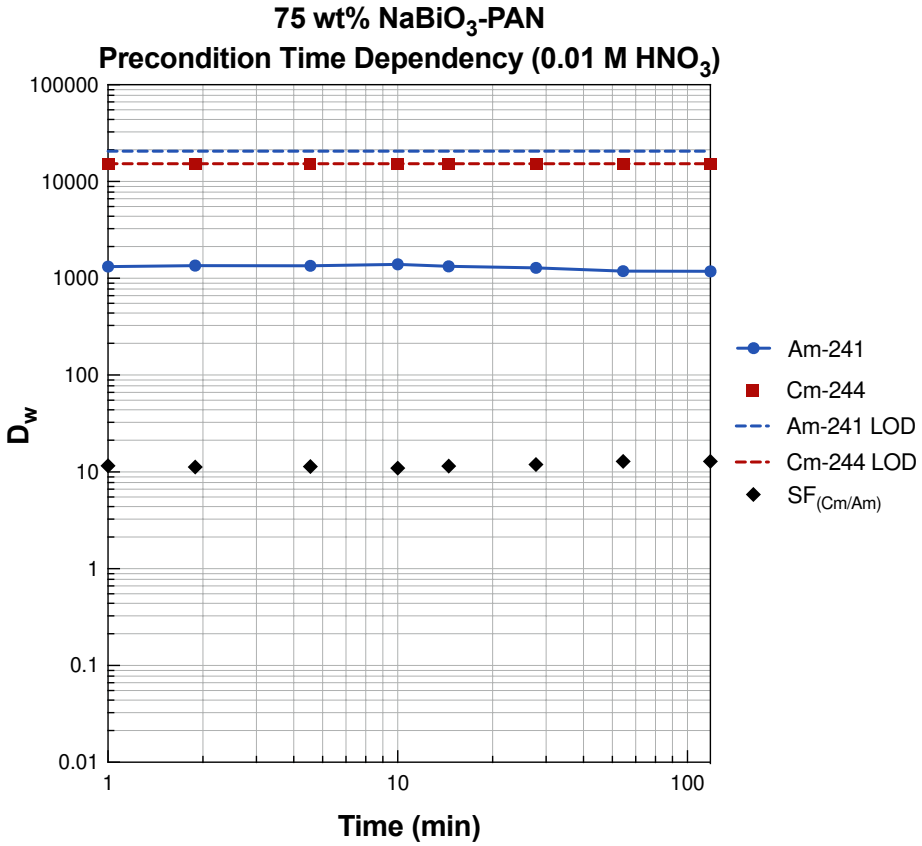


**Figure 7.2:** Adsorption of $^{241}$Am and $^{244}$Cm on 75 wt% $NaBiO_3$-PAN resin as a function of preconditioning time in 0.01 M $HNO_3$. All data points are an average of four replicates and error bars represent the uncertainty to 2σ.

As shown in Figure 7.2, the acid preconditioning time has no effect on the adsorption of $^{241}$Am or $^{244}$Cm. The $D_w$ for $^{241}$Am remained constant across all preconditioning times and agreed with the $D_w$ value obtained at 0.01 M $HNO_3$ for the concentration dependency study which indicates that any effects due to the reactions between the $NaBiO_3$ oxidant and $HNO_3$ do not affect $^{241}$Am adsorption. In addition, $^{244}$Cm remained at the limit of

detection across all time points suggesting that the contact time between the $NaBiO_3$-PAN resin and $HNO_3$ solution does not decrease the extent to which the pH change influences complete $^{244}Cm$ adsorption.

### *7.3.3 Contact Time Dependency*

The kinetics of both the redox and ion exchange mechanisms were further explored in a contact time study that varied the radionuclide contact time with the $NaBiO_3$-PAN resin at 0.01 M $HNO_3$ from 1 – 300 minutes after the standard one-hour preconditioning step (Figure 7.3).

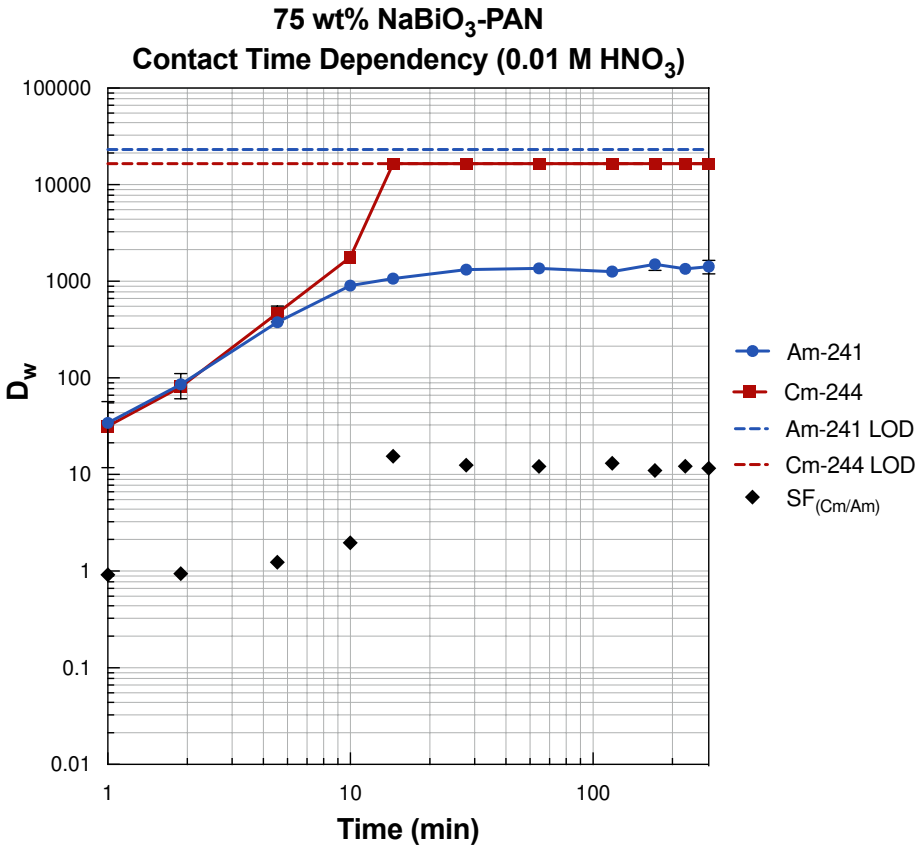


**Figure 7.3:** Adsorption of $^{241}Am$ and $^{244}Cm$ on 75 wt% $NaBiO_3$-PAN resin as a function of radionuclide contact time in 0.01 M $HNO_3$. All data points are an average of four replicates and error bars represent the uncertainty to $2\sigma$.

For both radionuclides, the $D_w$ value increases with increasing contact time and the nearly identical behavior of $^{241}Am$ and $^{244}Cm$ indicates that both have trivalent speciation and Am oxidation has not yet occurred. This identical behavior begins to deviate after 10 minutes of contact with $^{244}Cm$ being more strongly retained and implies $^{241}Am$ oxidation by $NaBiO_3$. Cm reaches the limit of detection, or complete adsorption, after 15 minutes of contact and $^{241}Am$ reaches and maintains its maximum $D_w$ after 30 minutes of contact.

Since the pH of the $HNO_3$ solution changes immediately upon contact with $NaBiO_3$ solid, it would be expected that immediate hydrolysis would occur, and all $^{244}Cm$ activity would be lost to the sample container. As this is not observed throughout the first 10 minutes of contact, $^{244}Cm$ retention may not a result of hydrolysis, but due to its predicted ion exchange with $NaBiO_3$. In any event, rapid kinetics were expected to be observed in the $NaBiO_3$-PAN batch system relative to the solid $NaBiO_3$ batch data reported by Richards that showed a favorable separation factor achieved within the first minute of contact.[127] Since $^{241}Am$ and $^{244}Cm$ did not reach the respective $D_w$ values observed after one hour of contact in the $HNO_3$ dependency study until 10 minutes of contact time, it is likely that the PAN matrix has unfavorably affected the kinetics of the reactions by inhibiting interactions between the analytes and $NaBiO_3$.

### *7.3.4 Temperature Dependency*

The effect of temperature on the $D_w$ for $^{241}Am$ and $^{244}Cm$ on the $NaBiO_3$-PAN resin at 0.01 M $HNO_3$ was determined for a one-hour preconditioning and one-hour contact time at 20, 30, 40, 50, and 60 °C (Figure 7.4).

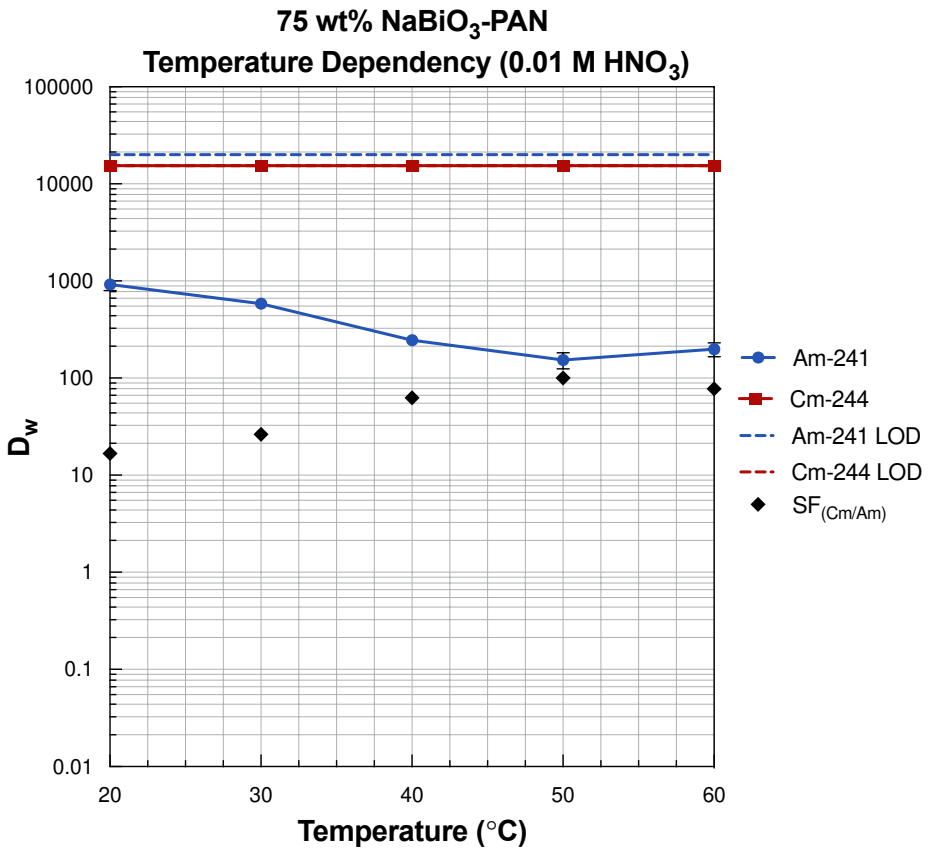


**Figure 7.4:** Adsorption of $^{241}$Am and $^{244}$Cm on 75 wt% $NaBiO_3$-PAN resin as a function of shaking temperature in 0.01 M $HNO_3$. All data points are an average of four replicates and error bars represent the uncertainty to 2σ.

Cm-244 remains at the limit of detection regardless of system temperature. However, while $^{241}$Am $D_w$ values for all previous batches agree, the $D_w$ of Am at room temperature is lower than that of the previously determined value. This is likely due to the fact that the temperature-controlled shaker table has a different shaking speed and angle than the LabQuake shaker used during the previous studies.

It has been reported that $NaBiO_3$ is unstable and degrades in aqueous solutions at temperatures greater than 20 °C.[119] Based on the higher temperature instability of $NaBiO_3$, the observed decrease in $^{241}$Am adsorption with increasing temperature is

expected and could be attributed to the degradation and/or dissolution of $NaBiO_3$. However, if the high $^{244}Cm$ $D_w$ values are a direct result of ion exchange and adsorption onto $NaBiO_3$ solid, a decrease in $D_w$ values for $^{244}Cm$ would also be expected. Since this is not observed, the hypothesis that hydrolysis is occurring resulting in the formation of the $CmOH^{2+}$ hydrolysis product may be correct.

However, Hara et. al. found that at lower acidities and higher temperatures the oxidation of Am(III) to Am(VI) with $NaBiO_3$ proceeds more rapidly.[119] In addition, preliminary UV-Vis studies for $NaBiO_3$ dissolution showed no Bi in solution using UV-Vis or ICP-OES analysis at 0.01 M $HNO_3$. Thus, it is possible that the rate at which $NaBiO_3$ degradation/dissolution occurs at 0.01 M $HNO_3$ is negligible relative to the extent to which Am(III) oxidation occurs in 0.01 M $HNO_3$ at elevated temperatures. While it is unclear what exact mechanism is responsible for the reduction of $^{241}Am$ adsorption at higher temperatures, the $^{241}Am$ $D_w$ decreased by an order of magnitude at 50 °C yielding a favorable $SF_{Cm/Am}$ of ~100. Conducting a chromatographic separation at elevated temperatures is feasible and would offer a more efficient separation method as a smaller volume of eluent would be required to achieve complete $^{241}Am$ recovery.

### 7.4 Chromatographic Behavior of Americium and Curium on 75 wt% $NaBiO_3$-PAN

Although the batch adsorption data for the 75 wt% $NaBiO_3$-PAN resin showed an unfavorable deviation in adsorption behavior relative to that of $NaBiO_3$ solid, the $SF_{Cm/Am}$ of ~11 achieved at 0.01 M $HNO_3$ is much greater than what is currently available. Therefore, attempts at a chromatographic separation under these conditions were made

in view of $^{241}Am$ elution at 0.01 M $HNO_3$ and $^{244}Cm$ stripping at 2 M $HNO_3$. However, if the observed complete $^{244}Cm$ adsorption is actually a result of the precipitation of the $CmOH^{2+}$ hydrolysis product, no $^{244}Cm$ elution from the chromatographic system would be expected to occur.

### *7.4.1 Method*

The elution profiles for $^{241}Am$ and $^{244}Cm$ were performed on individual columns and elution fractions were analyzed using gross alpha beta counting with a Ludlum Model 3030 and LSC for total activity (Figure 7.5). Both columns were performed such that the packing, radionuclide loading, and elution profiles were identical. A slurry of the 75 wt% $NaBiO_3$-PAN resin in 0.01 M $HNO_3$ was prepared and the resin was washed three times to remove fine, column-clogging particulates and to monitor the solution pH.

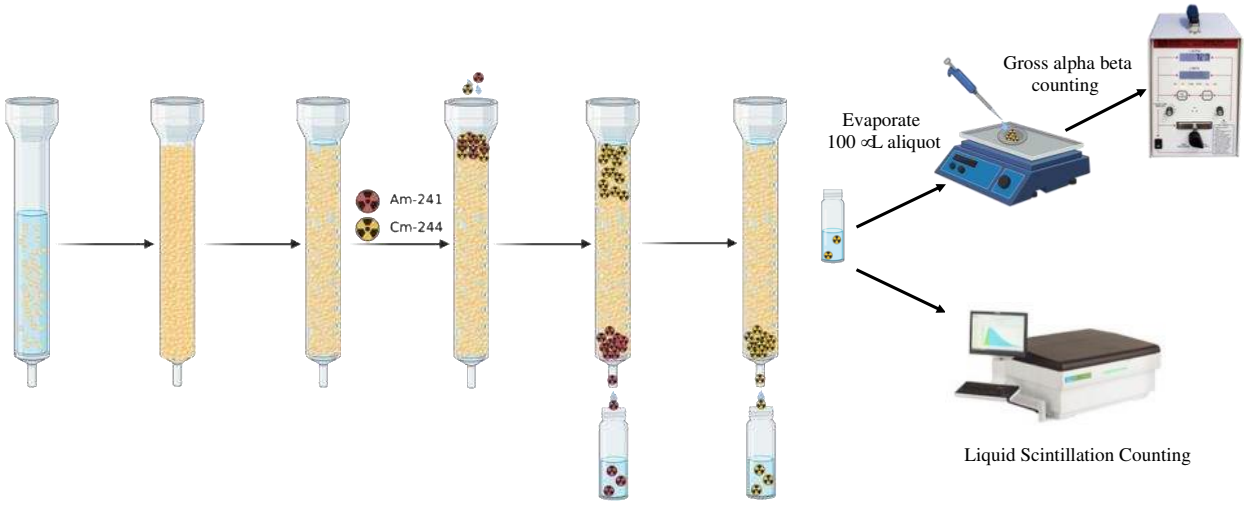


**Figure 7.5:** General column chromatographic procedure.

The $NaBiO_3$-PAN was then slurry packed into 2 mL Eichrom columns with a 5 mL reservoir and a glass wool plug or filter was placed on top of the resin bed. However,

slurry packing was time consuming as the large range of particle sizes resulted in frequent pocket formation in the resin bed during packing requiring the use of a glass Pasteur pipette to gently create a uniform bed. Dry packing was also attempted; however, upon the addition of acid, pockets would form in the bed. Attempts to pack the bed tighter when dry packing would release a large volume of solution from the resin beads.

The column was conditioned with 15 mL of 0.01 M $HNO_3$ and the eluate pH was monitored to ensure the acidification of the resin surface. A 1 mL aliquot of the $^{241}Am$ or $^{244}Cm$ stock solution (1,000 Bq/mL) was loaded onto the column and eluted with the $HNO_3$ solutions of appropriate concentration under gravity flow. The eluate was collected in 10 mL fractions and 0.1 mL aliquots of each fraction were evaporated to dryness at 80 °C on a counting planchet. The planchets were counted five times on a Ludlum Model 3030 gross alpha beta counter to determine the recovery in real time and the recovery was verified by counting 1 mL aliquots of each fraction using LSC.

### *7.4.2 Results*

Figure 7.6 shows the elution profiles for $^{241}Am$ and $^{244}Cm$ in a 75 wt% $NaBiO_3$-PAN column. While the elution behavior does align with the batch adsorption study, co-elution of both radionuclides occurred. As expected, based on the complete retention of $^{244}Cm$ at 0.01 M $HNO_3$, there was no $^{244}Cm$ recovery observed in the 0.01 M $HNO_3$ elution fractions.

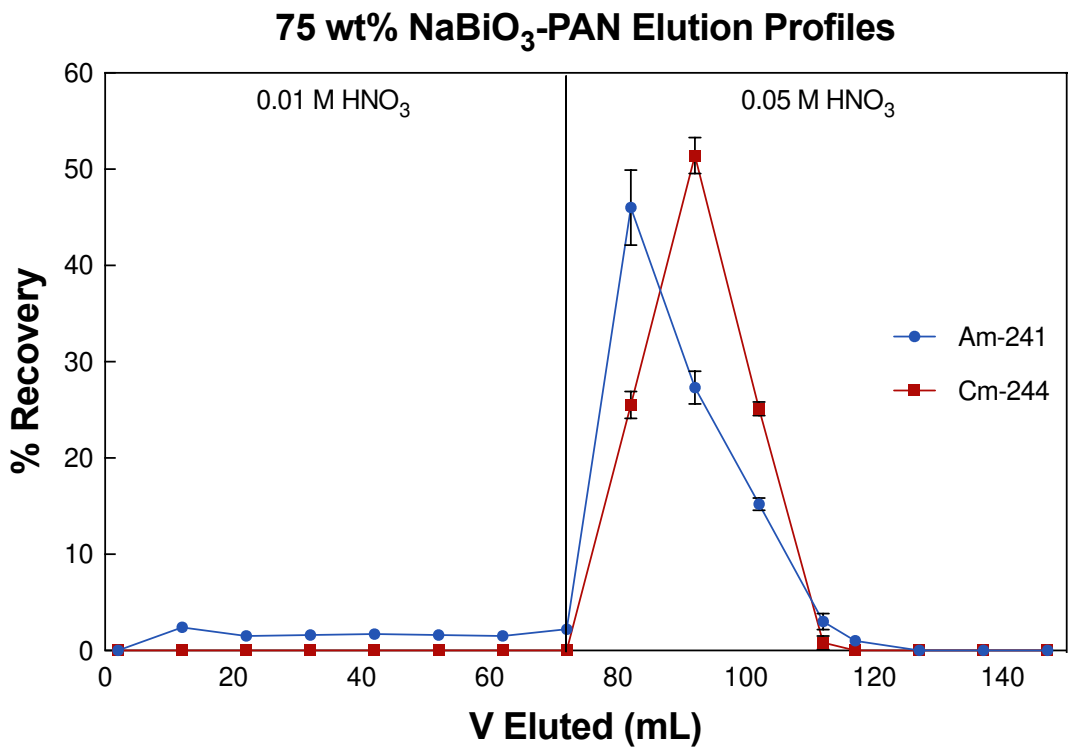


**Figure 7.6:** Elution profiles of $^{241}$Am and $^{244}$Cm on 75 wt% $NaBiO_3$-PAN using a 2 mL slurry-packed column. All data points represent an average of five replicate fraction counts and error bars represent the uncertainty to 2σ.

However, the high $^{241}$Am $D_w$ value at 0.01 M $HNO_3$ is apparent as there was only ~2% $^{241}$Am recovery for every 10 mL of 0.01 M $HNO_3$ eluant collected and only ~14% of $^{241}$Am activity was recovered after the addition of 70 mL of 0.01 M $HNO_3$. In an effort to increase the rate of $^{241}$Am recovery, the elution matrix was increased to 0.05 M $HNO_3$ and, while the remaining $^{241}$Am activity was recovered, 100% of the loaded $^{244}$Cm activity was also eluted.

While the elution profiles are in line with the batch adsorption data, the elution behavior is not practical for an Am/Cm chromatographic separation on either analytical or industrial scales. However, the elution profiles show favorable symmetry while peak tailing is common with ion exchangers. The complete recovery of $^{244}$Cm indicates that the

complete retention as implied by the $D_w$ value at 0.01 M $HNO_3$ is not a result of $Cm^{3+}$ hydrolysis as the $CmOH^{2+}$ hydrolysis product would have precipitated out of solution and adsorbed to the column walls preventing any recovery of activity. Thus, if the $NaBiO_3$-PAN resin could be prepared in such a way that maintained the high $^{244}Cm$ adsorption at 0.01 M $HNO_3$ while decreasing the $^{241}Am$ retention, a chromatographic separation would be possible.

## 7.5 Chromatographic Behavior of Americium and Curium for Mixed $NaBiO_3$-PAN/PAN Bead Resin Beds

The elution profiles of the minor actinides on the 75 wt% $NaBiO_3$-PAN resin did not achieve the desired separation but did show good alignment with batch adsorption data and indicated that Cm(III) hydrolysis was not occurring. To explore the potential of a PAN-based system further, chromatographic studies were carried out using resin beds that contained 75 wt% $NaBiO_3$-PAN resin mixed with unmodified PAN beads in varying ratios. Since the $^{241}Am$ $D_w$ on $NaBiO_3$ solid alone is comparable to that of the 75 wt% $NaBiO_3$-PAN resin, reducing the amount of the active $NaBiO_3$ ion exchanger may aid in increasing $^{241}Am$ recovery at lower acid concentrations.

### *7.5.1 Method*

Columns were prepared by mixing 50 mg and 0.95 g for the 5 wt% mixture or 100 mg and 0.9 g for the 10 wt% mixture of the 75 wt% $NaBiO_3$-PAN resin with PAN beads, respectively. Slurry packing of these mixtures resulted in the concentration of the $NaBiO_3$-PAN beads at the bottom of the column due to density differences between the two

materials. Attempting to homogenize the bed by stirring resulted in the formation of air pockets within the bed; however, dry packing provided a more uniform bed. Fractions were collected in 15 mL elutions rather than 10 mL based on the large volumes required during the initial chromatographic setup.

### *7.5.2 5 wt% $NaBiO_3$-PAN/PAN Bead Mixture*

Diluting the amount of $NaBiO_3$ in the PAN-based composite system significantly decreased the retention of both $^{241}Am$ and $^{244}Cm$ as expected. However, the $NaBiO_3$ content was decreased so much in the 5 wt% system that co-elution of both radionuclides occurred during the first wash with 0.01 M $HNO_3$ (Figure 7.7).

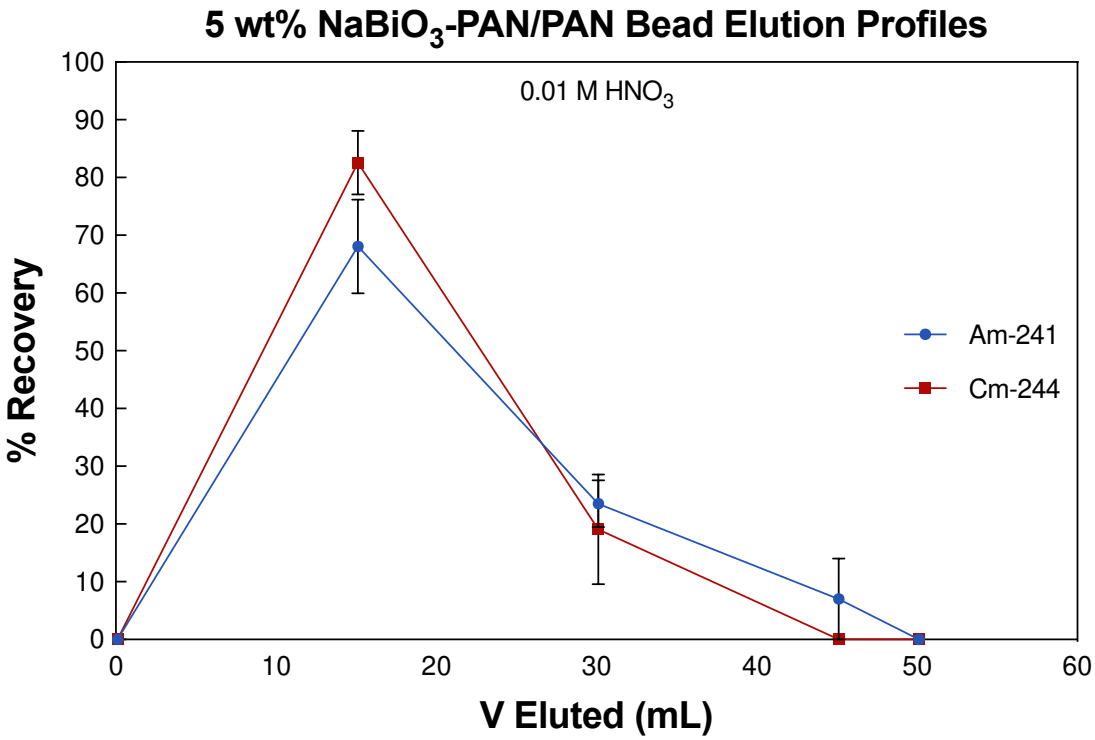


**Figure 7.7:** Elution profiles of $^{241}Am$ and $^{244}Cm$ on a 5 wt% mixture of 75 wt% $NaBiO_3$-PAN and PAN beads using a 2 mL dry-packed column. All data points represent an average of five replicate fraction counts and error bars represent the uncertainty to $2\sigma$.

Complete recovery of both radionuclides was achieved with more significant tailing observed for both elution profiles. This is likely due to the inhomogeneity of the packed bed resulting in various analyte interactions with the sorbent at different band zones within the chromatographic system.

### *7.5.3 10 wt% $NaBiO_3$-PAN/PAN Bead Mixture*

Since the 5 wt% mixed bed reduced the adsorption for both analytes so much that co-elution occurred, the amount of the 75 wt% $NaBiO_3$-PAN was increased to 10 wt% (Figure 7.8).

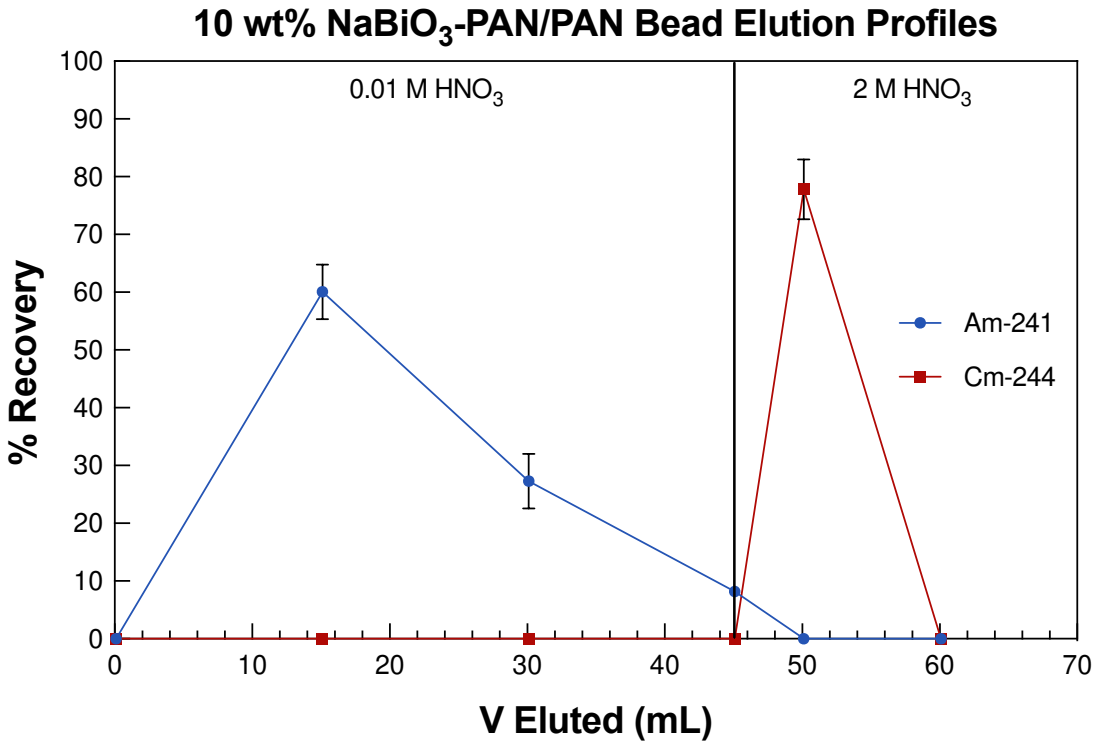


**Figure 7.8:** Elution profiles of $^{241}Am$ and $^{244}Cm$ on a 10 wt% mixture of 75 wt% $NaBiO_3$-PAN and PAN beads using a 2 mL dry-packed column. All data points represent an average of five replicate fraction counts and error bars represent the uncertainty to 2σ.

Elution with 0.01 M $HNO_3$ recovered ~88% of the $^{241}Am$ activity from the column, with an additional 8% co-eluting with $^{244}Cm$ in the 2 M $HNO_3$ fraction. No $^{244}Cm$ elution occurred using 0.01 M $HNO_3$ which yielded high purity $^{241}Am$ fractions and ~78% of the $^{244}Cm$ was recovered in the 2 M $HNO_3$ fractions. Peak tailing was significant for $^{241}Am$, but less prevalent for the $^{244}Cm$ elution curve.

The degradation/dissolution of $NaBiO_3$ was observed to increase with increasing $HNO_3$ concentration and, upon introduction of 2 M $HNO_3$, the column bed was observed to turn black with a significant amount of gas bubbles forming. If $^{244}Cm$ elution is a result of the degradation of the solid itself instead of the reversible ion exchange mechanism, then the effects of band broadening due to zone migration would be less apparent. While this elution system is not practical for application, it showed the effect of $NaBiO_3$ amount on the adsorption and elution behavior of $^{241}Am$ and $^{244}Cm$.

### 7.6 Effect of $NaBiO_3$ Loading on Polymer Composites

Based on the batch adsorption and chromatographic data obtained for the 75 wt% $NaBiO_3$-PAN resin, TrisKem prepared additional variations of the resin the adjusted the $NaBiO_3$ content and polymeric support. $NaBiO_3$-PAN resins with 10, 25, 50 and 75 wt% dry weight $NaBiO_3$ content were prepared. In addition, a 10 wt% $NaBiO_3$-PES resin was prepared based on the favorable chemical and radiolytic stability of PES-based polymeric supports. Since these resin batches were being prepared from a new lot of $NaBiO_3$, a new lot of the 75 wt% $NaBiO_3$-PAN resin was prepared to verify adsorption behavior across lots.

*7.6.1 Adsorption Behavior of Americium and Curium*

For all other versions of the $NaBiO_3$-PAN resin, the same trend of higher adsorption at 0.01 M $HNO_3$ followed by decrease in adsorption with increasing nitric acid concentration occurs (Figure 7.9).

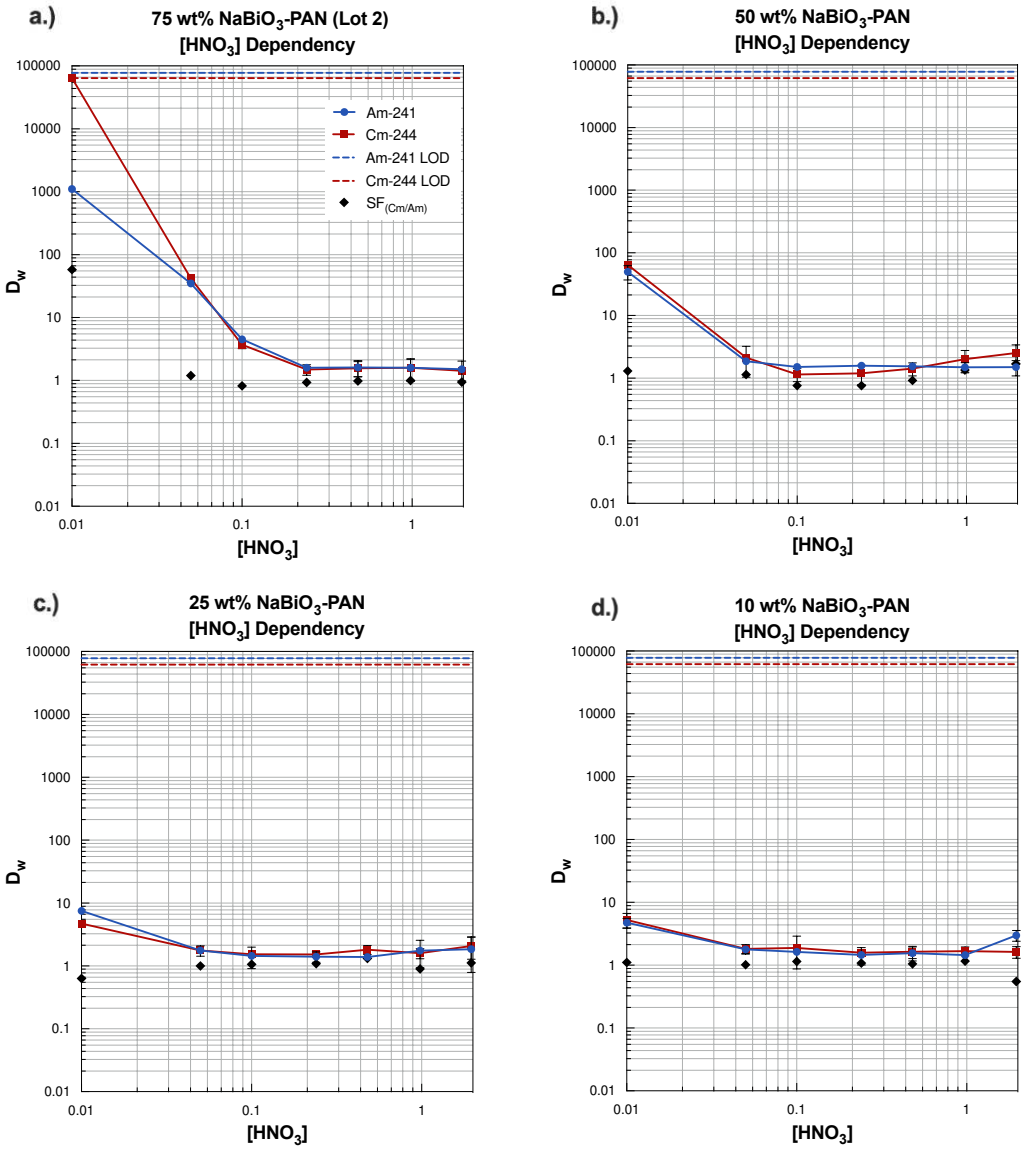


**Figure 7.9:** Weight distribution data for $^{241}Am$ and $^{244}Cm$ on a) 75 wt% $NaBiO_3$-PAN (Lot 2), b) 50 wt% $NaBiO_3$-PAN, c) 25 wt% $NaBiO_3$-PAN, and d) 10 wt% $NaBiO_3$-PAN. All data points represent an average of four replicates and error bars represent the uncertainty to $2\sigma$.

As expected, decreasing the amount of $NaBiO_3$ in the PAN composite material decreases the $D_w$ values for both $^{241}Am$ and $^{244}Cm$; however, no favorable $SF_{Cm/Am}$ is obtained at any $HNO_3$ concentration. The adsorption behavior of $^{241}Am$ and $^{244}Cm$ on the second lot of the 75 wt% $NaBiO_3$-PAN resin showed nearly identical trends relative to the first lot received by TrisKem; however, a more gradual decrease in $D_w$ is observed at 0.05 and 0.1 M $HNO_3$ (Figure 7.9a). In addition, a greater $SF_{Cm/Am}$ of ~58 was obtained at 0.01 M $HNO_3$ relative to the $SF_{Cm/Am}$ of ~11 for the first resin lot. This may be due to a difference in $NaBiO_3$ purity as a new lot of $NaBiO_3$ was purchased by TrisKem in the preparation of these resins.

The data shows a decrease in $D_w$ values for both radionuclides as the $NaBiO_3$ loading decreases, which was anticipated. While $^{241}Am$ and $^{244}Cm$ do have a greater retention at 0.01 M $HNO_3$ for all resins with $D_w$ values ranging from ~100 to 10, the $D_w$ values for both are nearly identical at this concentration (Figure 7.9b, c, d). Thus, these resins are not conducive of a successful separation.

The identical adsorption behavior on these lower-loaded resins indicates that the adsorption observed is likely due to the PAN beads rather than $NaBiO_3$. While it is logical that the decreased loading would decrease adsorption, favorable SFs at 0.01 M $HNO_3$ were expected based on the promising chromatographic behavior of the 10 wt% $NaBiO_3$-PAN/PAN bead mixture. This may suggest that the incorporation of the $NaBiO_3$ within the pores of polymeric matrix plays a role where a greater amount of $NaBiO_3$ would fill a larger volume of the pores leaving some of the solid accessible for oxidation and ion exchange.

In contrast, the resins with a reduced loading would yield beads with a majority of the $NaBiO_3$ located within the polymeric matrix. As the separation was carried out using a 10 wt% mixture of the 75 wt% $NaBiO_3$-PAN resin with unmodified PAN beads, the faster elution is expected due to the smaller amount of $NaBiO_3$ present throughout the system. However, since the resin contained 75 wt% of the solid, it would be more accessible to the analytes and yield more favorable elution behavior than the 10 wt% $NaBiO_3$-PAN resin with the solid located primarily within the pores of the beads.

*7.6.2 Adsorption of Americium and Curium on Polyacrylonitrile Beads*

The matrix properties of any chromatographic resin have a large influence on adsorption behavior; therefore, the $D_w$ values for $^{241}Am$ and $^{244}Cm$ on unmodified PAN beads were determined as a function of $HNO_3$ concentration (Figure 7.10). Across all acid concentrations, both radionuclides exhibit identical adsorption behavior which is expected due to the lack of an Am(III) oxidizing agent present. It is clear that, while low, the adsorption of $^{241}Am$ and $^{244}Cm$ onto the PAN polymer beads is not negligible and has likely contributed to the $D_w$ values determined in the prior $NaBiO_3$-PAN batch adsorption studies.

At 0.01 M $HNO_3$ the $D_w$ value of ~10 for both radionuclides aligns with that observed in the 10 and 25 wt% $NaBiO_3$-PAN studies indicating that any adsorption behavior in those systems is not due to the presence of $NaBiO_3$. Greater adsorption for both radionuclides occurs in the 50 and 75 wt% $NaBiO_3$-PAN systems and supports the hypothesis that the higher $NaBiO_3$ content increases the potential for analyte interaction with the material.

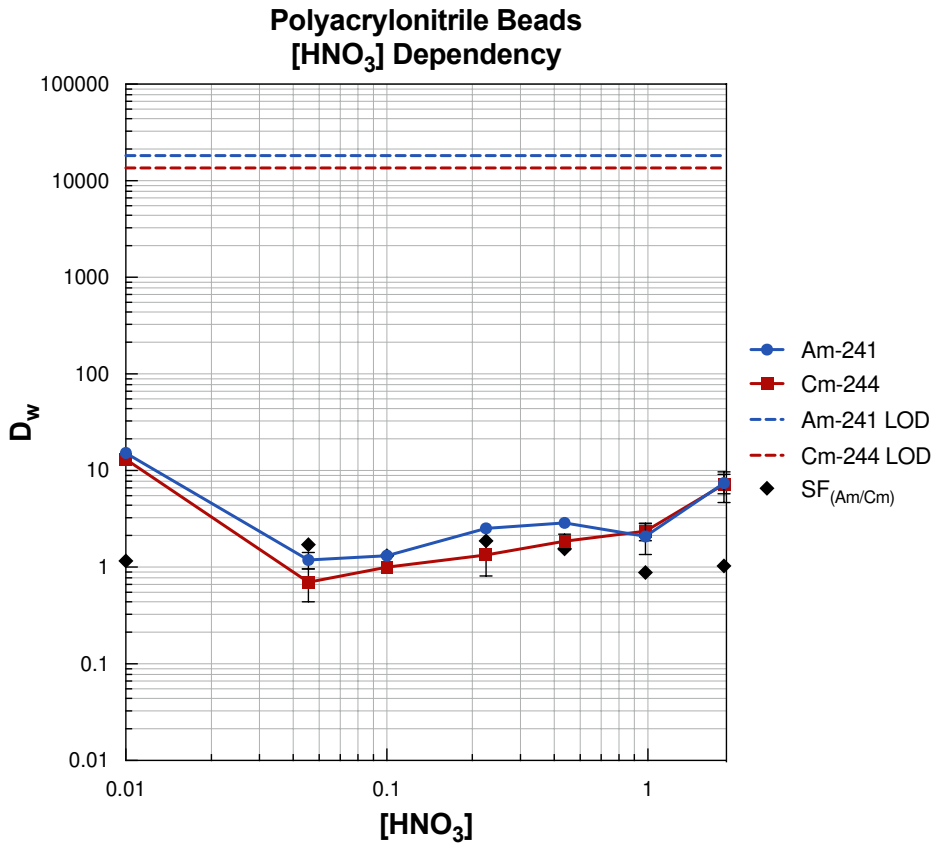


**Figure 7.10:** Adsorption behavior of $^{241}$Am and $^{244}$Cm on unmodified polyacrylonitrile (PAN) beads as a function of nitric acid concentration. All data points represent an average of four replicates and error bars represent the uncertainty to 2$\sigma$.

While it is possible that the PAN beads may have encapsulated the $NaBiO_3$ in such a way that the analytes are unable to interact with the solid, the synthesis may have affected the $NaBiO_3$ structure based on the number of PAN-based sorbents that incorporate inorganic ion exchange materials. The behavior of $NaBiO_3$ in aqueous acidic solutions is still not fully understood and, similarly, the reactions that occur between $NaBiO_3$ and the binding matrix solution are unknown. Fortunately, the preparation of the PAN-based resin is rather straight forward in that there are two components that may play a role in the degradation of $NaBiO_3$: the PAN polymeric matrix and the DMSO solvent. Although the incorporation of the ion exchanger likely plays a role in the observed behavior, the potential for the

degradation of $NaBiO_3$ by DMSO should also be considered. The influence of both can be explored by modifying the preparation conditions and characterizing the resulting material to understand the structural changes in the $NaBiO_3$ ion exchanger.

### *7.6.3 Adsorption of Americium and Curium on $NaBiO_3$-PES Resin*

Since polyethersulfone (PES) polymeric supports have demonstrated high chemical and radiolytic stability relative to PAN supports, a 10 wt% $NaBiO_3$-PES resin was also prepared and the adsorption behavior of $^{241}Am$ and $^{244}Cm$ characterized (Figure 7.11).

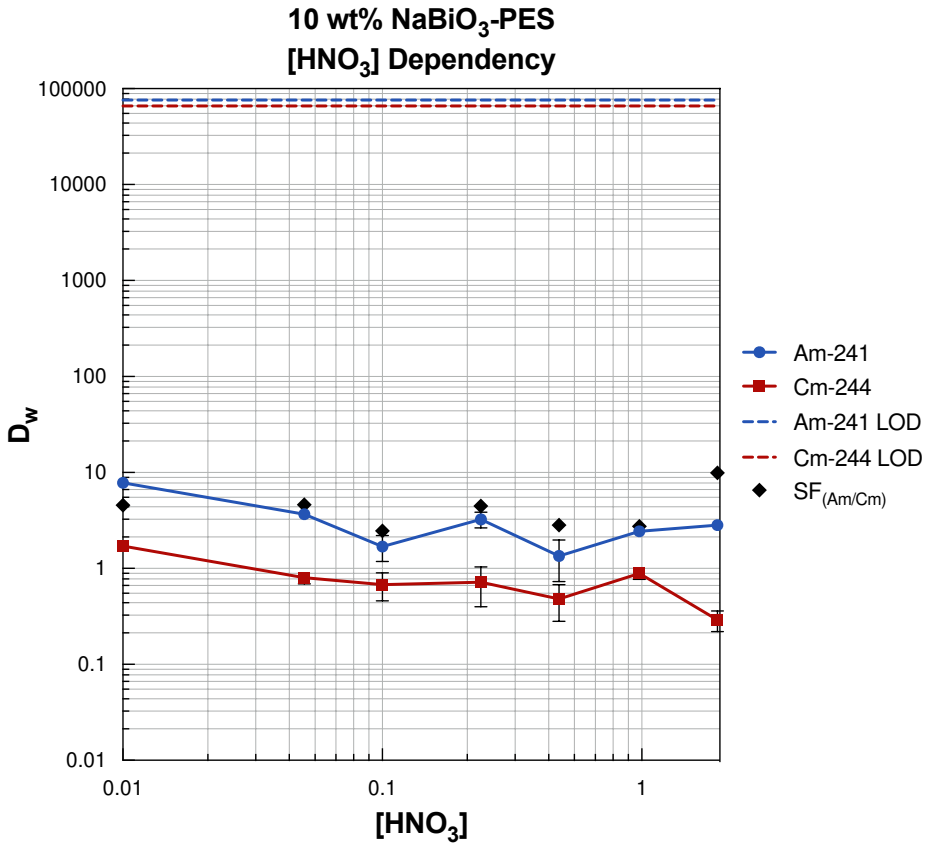


**Figure 7.11:** Adsorption behavior of $^{241}Am$ and $^{244}Cm$ on 10 wt% $NaBiO_3$-PES resin as a function of nitric acid concentration. All data points represent an average of four replicates and error bars represent the uncertainty to $2\sigma$.

PES was also selected due to the potential benefit of additional electrostatic interactions from the sulfonyl and ether groups present in the polymeric structure. Both $^{241}Am$ and $^{244}Cm$ exhibit similar adsorption behavior on the PES-based resin; however, $^{244}Cm$ may be more strongly retained. The $^{244}Cm$ $D_w$ values are similar to that of the 10 wt% $NaBiO_3$-PAN resin while $^{241}Am$ has slightly lower retention yielding $SF_{Cm/Am}$ values ranging from ~2 – 10 across all $HNO_3$ concentrations and may be a result of a decreased affinity of Am for the PES beads.

It is important to note that the PES-based resin had a much lower water content than that of the PAN-based resins when received and was inconsistent in moisture content across batch samples which likely introduced larger uncertainties into the batch adsorption studies. As $NaBiO_3$ is an ion exchanger, this decrease in moisture content may play a more significant role in that there may be fewer water molecules located within the layers of $NaBiO_3$ allowing for increased $^{244}Cm$ adsorption. While these greater SFs may be a result of the large uncertainties introduced as a result of the inhomogeneity of the resin, these subtle differences could be due to the change in the resin matrix and may make PES a favorable polymeric support alternative.

Unfortunately, since the only PES-based sorbent received was prepared with a 10 wt% $NaBiO_3$ loading, its efficacy cannot be determined.

### 7.7 Conclusions and Future Work

An attempt was made to mitigate the flow rate issues that resulted from the effervescence of gas production by incorporating solid $NaBiO_3$ within organic polymeric matrices. Since

there are a number of commercially available PAN-based resins available and even more with reported success in the literature, this was a logical approach. However, its incorporation onto the surface resulted in batch adsorption data that showed no retention for either radionuclide above 0.01 M $HNO_3$. While $^{241}Am$ retention is low above 0.01 M $HNO_3$ for $NaBiO_3$ solid and a decrease in $D_w$ values is expected, the lack of $^{244}Cm$ adsorption indicated that the ion exchange reaction was not occurring. This may be a result of the way in which the $NaBiO_3$ was incorporated within the pores of the polymer bead that may have obstructed access to the ion exchange sites.

Due to an $SF_{Cm/Am}$ greater than 10 at 0.01 M $HNO_3$, kinetics studies performed at 0.01 M $HNO_3$ showed that resin preconditioning time in acid had no influence on the resulting $D_w$ values. However, adsorption kinetics were slow with $^{241}Am$ and $^{244}Cm$ exhibiting identical behavior until deviating after 10 minutes of contact. Elevated temperatures decreased the $^{241}Am$ retention yielding a $SF_{Cm/Am}$ of ~100 at 50 °C. While a chromatographic separation was attempted at 0.01 M $HNO_3$ due to the complete adsorption of $^{244}Cm$, the large $D_w$ of $^{241}Am$ required a large amount of eluent for its recovery making a separation under those conditions inefficient. Interestingly, a partial separation was achieved by diluting the 75 wt% $NaBiO_3$-PAN resin with un-modified PAN beads; however, the reason for this is unclear as the preparation of the resin with lower $NaBiO_3$ loadings resulted in lower retentions and SFs. It is likely that the resins with lower $NaBiO_3$ loading results in the solid being deeply incorporated within the pores while the 75 wt% resin has filled pores with additional $NaBiO_3$ available closer to the surface.

Structural characterization of the $NaBiO_3$ starting material, un-modified PAN beads, and $NaBiO_3$-PAN beads should be completed to better understand how $NaBiO_3$ is incorporated and distributed throughout the support and what structural and chemical alterations were made. Scanning electron microscopy with energy dispersive x-ray spectroscopy (SEM/EDS) and x-ray diffraction (XRD) can be used to characterize the surfaces, structures, and elemental composition of the materials. Using these techniques post-$HNO_3$ or radionuclide contact will also provide information regarding the changes in the structure and composition of $NaBiO_3$. The degradation or distortion of the octahedral structures and the potential retention of $H^+$ or $Bi^{3+}$ ions that may degrade the favorable separation behavior can also be characterized.

While this work was unsuccessful, the incorporation of $NaBiO_3$ onto an inert support remains an area of exploration. This can be pursued through either modifying the procedure for polymeric supports or evaluating other support materials. While these resins were prepared using DMSO, the PAN binding polymer is also soluble in concentrated sulfuric acid and concentrated aqueous solutions containing inorganic salts (*e.g.,* lithium bromide, zinc chloride). Thus, different preparation methods and subsequent material characterization may be a reasonable area to explore. However, these materials also displayed poor chromatographic performance due to their physical characteristics such as large particle size with a wide range of sizes that resulted in difficulty during column packing due to pocket formation. To improve the column dynamics of such material, modifying the preparation process through the use of a multi-channel microfluidic setup would allow for the production of uniformly shaped resin beads with a

narrower range in particle size that would improve the flow and mass transfer behavior in the chromatographic system.

The adsorption of Am and Cm on the un-modified PAN beads was not negligible and featured $D_w$ values as high as 10, but the $D_w$ values for the $NaBiO_3$-PAN resins were below even that. Therefore, even adsorption onto the polymeric backbone was hindered. Since not all resin preparation steps are known, it is uncertain whether the resin was washed with water after preparation. If the organic DMSO solvent is present on the surface of the resin bead, it may have inhibited radionuclide adsorption. If the DMSO is not the cause of reduced retention, its presence in any capacity would certainly result in the rapid reduction of $AmO_2^{2+}$. $NaBiO_3$ is a common reagent in organic synthesis reactions for oxidative cleavage and for $Bi^{3+}$ catalysis but has been shown to have slow kinetics in aprotic solvents like DMSO which was observed in the kinetics study at 0.01 M $HNO_3$. While there is no literature available regarding the reaction between $NaBiO_3$ and DMSO, complexation of DMSO with $Bi(NO_3)_3$ has been observed. It is possible that the preparation of the resin in DMSO resulted in either the complexation of DMSO with the Bi octahedral or its incorporation within the structure's layers which would prevent adsorption of the metal ions.

Since the preparation method is a well-established procedure, it is not unreasonable to assume that the DMSO solvent in which the polymer was dissolved and the $NaBiO_3$ was suspended has disturbed the layered ion exchange structure of $NaBiO_3$. The PAN binding polymer is also soluble in concentrated sulfuric and nitric acid as well as concentrated

aqueous solutions containing inorganic salts (*e.g.,* lithium bromide, zinc chloride) which could be explored as an alternate synthetic route in the future. However, it is important to note that the instability of $NaBiO_3$ in concentrated mineral acids would make the use of $H_2SO_4$ or $HNO_3$ for resin preparation unfavorable. However, the use of inorganic salt solutions may prove successful, but the interaction between $NaBiO_3$ and the ions in solution should be characterized beforehand.

In addition, even if the prepared resins provided the desired adsorption characteristics necessary to achieve a column chromatographic separation, the physical characteristics of the PAN and PES-based resins lacked the uniformity that is desired for ideal chromatographic dynamics. The syringe-based preparation that is currently employed for the synthesis of the resin beads limits both the production throughput and particle size/shape uniformity. Translating this preparation to a multi-channel microfluidic setup would allow for the production of uniformly shaped resin beads with a narrower range in particle size that would improve the flow and mass transfer behavior in the chromatographic system.

# CHAPTER 8: BEHAVIOR OF THE EARLY ACTINIDES AND EUROPIUM IN SODIUM BISMUTHATE SYSTEMS

## 8.1 Introduction

When considering radiochemical separations for advanced NFC reprocessing schemes, the behavior of other radionuclides present in the waste streams must be considered. Building off the currently proposed flowsheets, a $NaBiO_3$-based separation would be useful in facilitating the separation of Am from Cm following either 1) actinide/lanthanide separation, 2) post-TRUEX process, or 3) post-PUREX process. Following an actinide/lanthanide separation method (*e.g.,* TALSPEAK, ALSEP, GANEX), the Am/Cm separation could be carried out with little modification as most interfering ions would have been eliminated from the raffinate. Placing a $NaBiO_3$-based separation process after the TRUEX process would be advantageous due to its tolerance of the low nitric acid concentration of the TRUEX raffinate and the fact that trivalent Cm is identical in adsorption behavior to that of the trivalent lanthanides. Thus, the resulting raffinate containing Cm and the lanthanides could proceed directly to disposal. In a post-PUREX scenario, the interference of non-lanthanide fission products and rare earth elements must be understood.

An alternate route that would simplify the number of stages necessary for UNF reprocessing strategies would be through the use of a hexavalent group actinide separation from the lanthanides. The PUREX process takes advantage of the access to the hexavalent oxidation states of U and Np to separate the linear dioxo-cation species, $UO_2^{2+}$ and $NpO_2^{2+}$ from the $Ln^{3+}$, $Am^{3+}$, and $Cm^{3+}$. The accessibility of the hexavalent

oxidation states of these actinides provides a relatively straightforward way to achieve their separation from the FPs and Lns though Am recovery has been limited by the high stability of the trivalent species. As new reagents capable of oxidizing $Am^{3+}$ to $AmO_2^{2+}$ emerge, the similarities between the chemistries of $AmO_2^{2+}$, $UO_2^{2+}$, $NpO_2^{2+}$, and $PuO_2^{2+}$ can be exploited. The strong $Bi^{5+}$ to $Bi^{3+}$ reduction potential is capable of not only oxidizing $Am^{3+}$ to the hexavalent oxidation state, but also U, Np, and Pu. This chapter aims to characterize the adsorption and chromatographic behavior of these earlier actinides and the trivalent lanthanide, Eu, on the $NaBiO_3$-PAN resin.

## 8.2 Adsorption of Uranium, Plutonium, and Europium on Solid $NaBiO_3$

### *8.2.1 Nitric Acid Concentration Dependency*

The adsorption behavior of $^{233}U$, $^{239}Pu$, and $^{152}Eu$ as a function of nitric acid concentration is shown in Figure 8.1. Trivalent $^{152}Eu$ closely follows the adsorption curve of $^{244}Cm$ as expected, with complete retention at 0.01 M $HNO_3$ followed by a gradual decrease in $D_w$ with increasing acid concentration. Since both $^{233}U$ and $^{239}Pu$ are able to be oxidized to the hexavalent state by $NaBiO_3$, lower $D_w$ values and adsorption behavior similar to that of $^{241}Am$ were expected and similar $D_w$ values to $^{241}Am$ are observed at 0.1 M and below. At acid concentrations below 0.25 SFs for $^{152}Eu$ and $^{233}U/^{239}Pu$ as high as ~45 were achieved. Interestingly, above 0.1 M $HNO_3$ $^{233}U$ adsorption increases with increasing acid concentration yielding an $SF_{U/Pu}$ and $SF_{U/Eu}$ of ~214 and 1144, respectively. This deviation in behavior may be due to the rich redox chemistry of U and may indicate the presence of multiple species. In addition, $UO_2^{2+}$ cations can form nitrato complexes in nitric acid solutions and due to the identical geometry and symmetry of the $BiO_3^-$ and $NO_3^-$ anions,

displacement of $NO_3^-$ ligands with $BiO_3^-$ has been suggested based on spectroscopic studies.[210] If this were the case, inner sphere complexation of U to the surface of $NaBiO_3$ at greater nitric acid concentration could contribute to the increased adsorption observed.

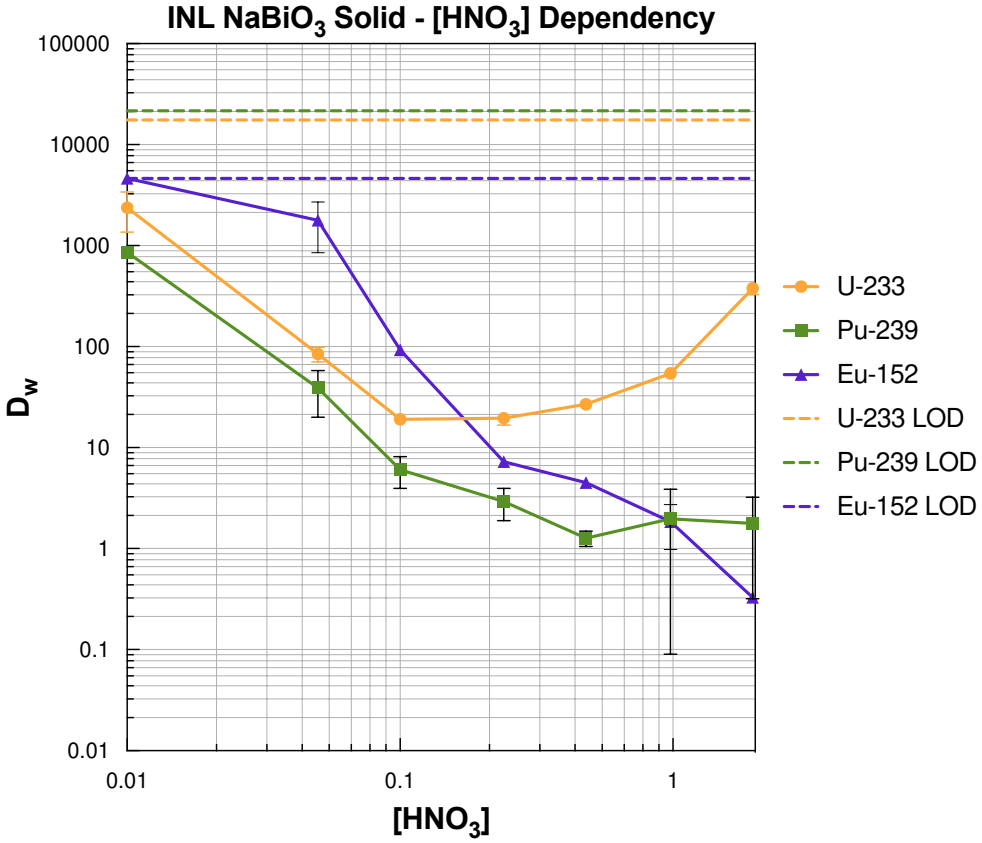


**Figure 8.1:** Adsorption of $^{233}U$, $^{239}Pu$, and $^{152}Eu$ on solid $NaBiO_3$ (>90% purity) as a function of nitric acid concentration. All data points are an average of four replicates and error bars represent the uncertainty to 2σ.

Although both $^{239}Pu$ and $^{152}Eu$ exhibit nearly identical adsorption behavior to $^{241}Am$ and $^{244}Cm$, respectively, they both exhibit slightly lower $D_w$ values than their analogues. This may be a result of differences in charge density that could influence the diffusion of the cations throughout the solid $NaBiO_3$. Overall, there remains a clear difference in the adsorption behavior for the hexa- and trivalent species indicating the potential for a group

hexavalent actinide lanthanide separation; however, understanding the speciation and interactions of these radionuclides in a $NaBiO_3$ system is necessary. Additionally, the increased adsorption and resulting SFs of $^{233}U$ at higher acid concentrations provides a potential route for a U/Pu or U/Eu separation.

### *8.2.2 Chromatographic Separation of Uranium, Plutonium, and Europium*

To further explore the possibility of a group hexavalent actinide separation from lanthanides, a chromatographic separation was performed for $^{233}U$, $^{239}Pu$, and $^{152}Eu$ by replicating the Am/Cm separation procedure reported by Richards and Sudowe (Figure 8.2).[127]

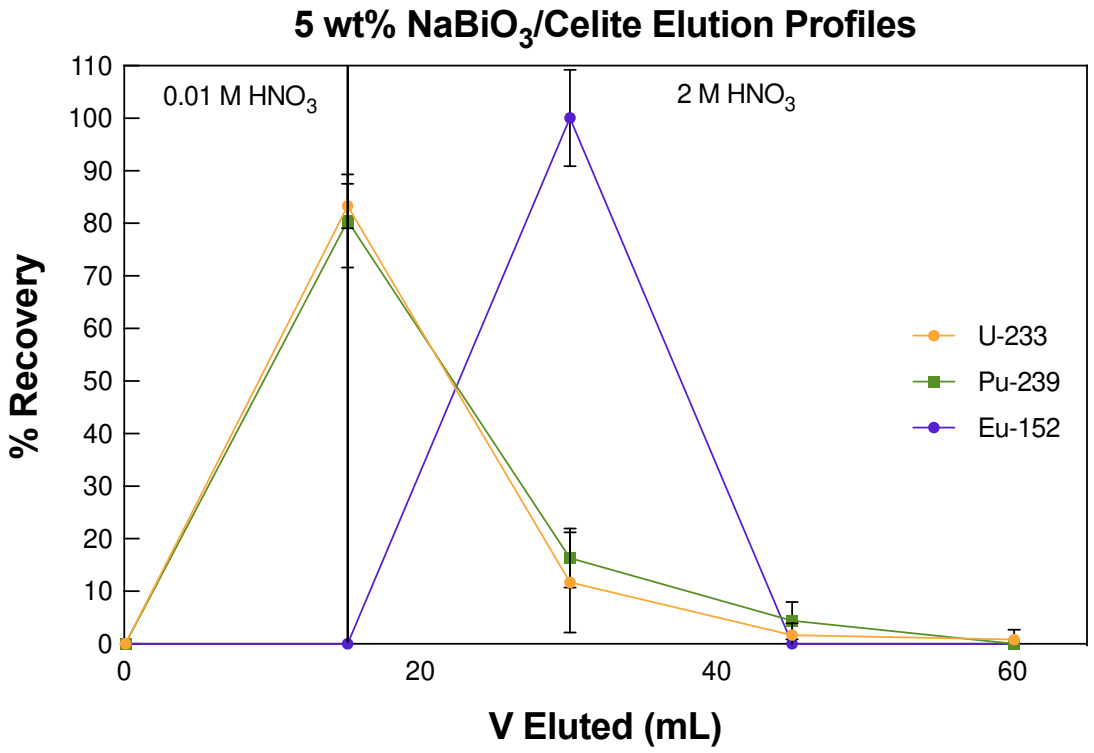


**Figure 8.2:** Elution profiles of $^{233}U$, $^{239}Pu$, and $^{152}Eu$ using a 2 mL column slurry packed with a 5 wt% $NaBiO_3$ mixture with Celite 535. All data points represent an average of five replicate fraction counts and error bars represent the uncertainty to $2\sigma$.

However, the procedure was modified to attempt $^{233}U$ and $^{239}Pu$ recovery at 0.01 M $HNO_3$ as the SFs relative to $^{152}Eu$ were greater than at 0.1 M. Thus, the incomplete separation observed may be due to the fact that the large $D_w$ values for the actinides required additional eluate to achieve full recovery in that eluate matrix. Since the eluate was collected in two separate 15 mL fractions (0.01 M and 2.0 M $HNO_3$), the elution behavior of $^{233}U$ and $^{239}Pu$ cannot be thoroughly characterized. Still, the obtained elution profiles follow the batch data as 85% and 80% of the $^{233}U$ and $^{239}Pu$ activity was recovered in the 0.01 M fraction with no $^{152}Eu$ co-elution. The eluate collected using the 2 M $HNO_3$ wash recovered 100% of the $^{152}Eu$ activity as expected and the remaining $^{233}U$ and $^{239}Pu$ activity was also co-eluted.

This scoping study shows the potential for a An(VI)/Ln(III) separation, but further characterization is necessary to determine the optimal parameters that would yield a complete separation. Determination of the adsorption kinetics, relative to that of Am and Cm, would provide valuable insight regarding the deviations between the batch and chromatographic behavior for the different radionuclides. It is also necessary to determine the oxidation states of U and Pu as their redox chemistry is more extensive than that of Am making the existence of multiple species that may affect elution behavior a possibility. Based on the determined oxidation states, the stock solutions could be pre-treated prior to experimental studies to ensure complete control over speciation. Beyond this, changing the amount of $NaBiO_3$ and column parameters (height, flow rate) could prove advantageous for this separation.

## 8.3 Behavior of Uranium and Plutonium on 75 wt% $NaBiO_3$-PAN

### *8.3.1 Nitric Acid Concentration Dependency – $NaBiO_3$-PAN ($2^{nd}$ Lot)*

The concentration dependency of $^{233}U$ and $^{239}Pu$ on $D_w$ for the second lot of the 75 wt% $NaBiO_3$-PAN resin was determined to further understand the differences between the behavior of the actinides and is shown in Figure 8.3.

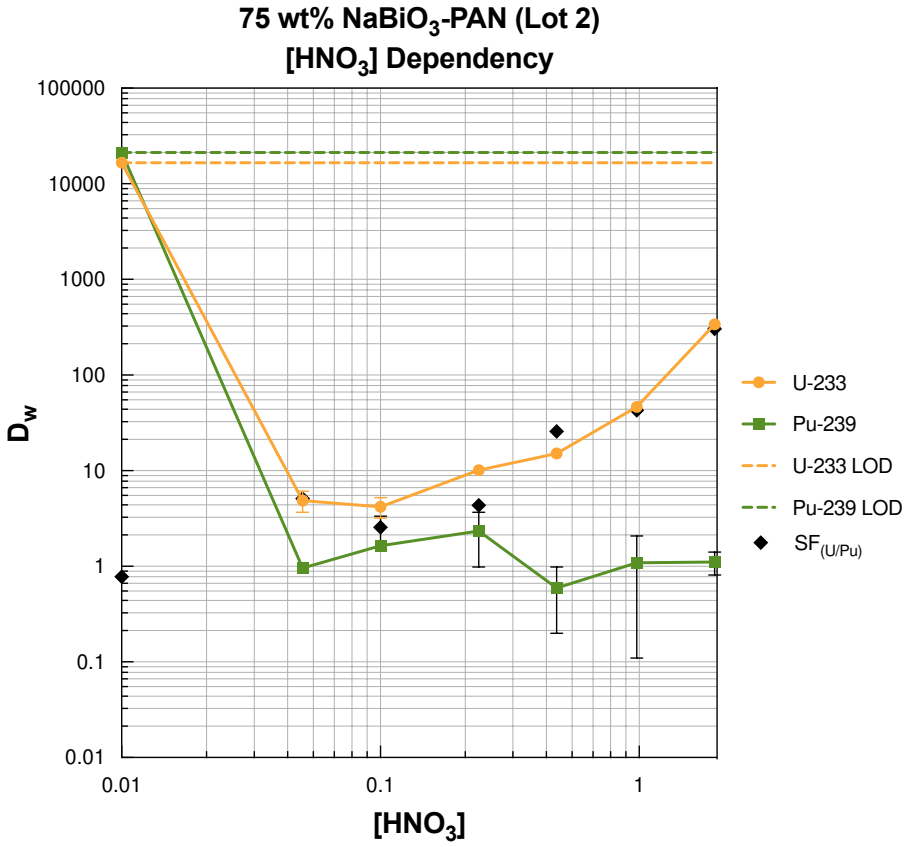


**Figure 8.3:** Adsorption of $^{233}U$ and $^{239}Pu$ on the second lot of 75 wt% $NaBiO_3$-PAN resin as a function of nitric acid concentration. All data points are an average of four replicates and error bars represent the uncertainty to $2\sigma$.

Both radionuclides follow the expected adsorption behavior that was observed for $^{241}Am$ and $^{244}Cm$ where high retention at 0.01 M $HNO_3$ immediately decreases at higher concentrations. Surprisingly, both radionuclides are at the limit of detection at 0.01 M $HNO_3$ which is characteristic of trivalent $^{244}Cm$, not hexavalent $^{241}Am$ and was also not

observed in the adsorption studies using solid $NaBiO_3$. In comparison to the data presented in Figure 8.1, the $D_w$ values for $^{233}U$ and $^{239}Pu$ at 0.01 M $HNO_3$ are an order of magnitude lower for $NaBiO_3$ solid which may be a result of differences in $NaBiO_3$ purity or influences from the PAN support.

While trace impurities within the system may influence the redox and adsorption behavior, this effect would have also been expected for $^{241}Am$. It is important to note, however, that the 75 wt% $NaBiO_3$-PAN resin used for this study was the second lot received from TrisKem and differences in the materials or preparation methods used could influence the sensitive chemistry occurring.

Similar to $NaBiO_3$ solid, $^{233}U$ exhibits a decrease in $D_w$ at lower acid concentrations followed by increasing $D_w$ with increasing [$HNO_3$] above 0.1 M. The increasing retention of $^{233}U$ and decreasing retention of $^{239}Pu$ yields an $SF_{U/Pu}$ as high as ~300 at 2 M $HNO_3$. This large difference in behavior at 2 M $HNO_3$, combined with the slight differences in $D_w$ for $^{233}U$, $^{239}Pu$, and $^{241}Am$ at lower acid concentrations, may provide the possibility of an intragroup actinide separation.

### *8.3.2 Nitric Acid Concentration Dependency – Polyacrylonitrile Beads*

The adsorption of $^{241}Am$ and $^{244}Cm$ on the PAN matrix was non-negligible and was therefore characterized for $^{233}U$ and $^{239}Pu$ as well (Figure 8.4). Both radionuclides had large $D_w$ values that increased with increasing acid concentration. The $D_w$ values for $^{233}U$ are nearly identical to those for the 75 wt% $NaBiO_3$-PAN resin at 0.1 M and greater.

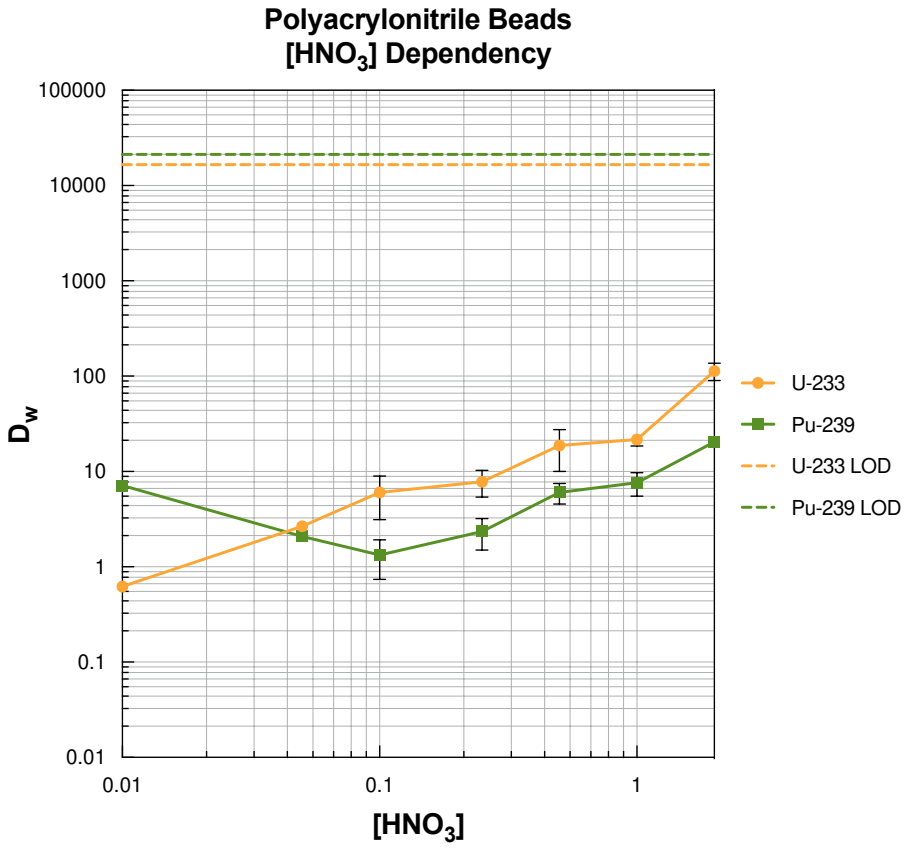


**Figure 8.4:** Adsorption behavior of $^{233}U$ and $^{239}Pu$ on unmodified polyacrylonitrile (PAN) beads as a function of nitric acid concentration. All data points represent an average of four replicates and error bars represent the uncertainty to $2\sigma$.

In theory, this would indicate that the resin matrix is the surface at which the interactions related to retention are occurring; however, this trend also occurring in solid $NaBiO_3$ would indicate a loss of activity elsewhere in the method. Pu-239 adsorption also follows the same upward trend on the PAN beads and the associated $D_w$ values are an order of magnitude greater than that observed on the $NaBiO_3$-PAN resin. Thus, the $NaBiO_3$ coating may have inhibited the adsorption of $^{239}Pu$ onto the PAN support; however, this would imply that $^{233}U$ adsorption on the $NaBiO_3$-PAN resin is due to adsorption onto the ion exchanger and is supported by the trend observed on the solid alone.

*8.3.3 Contact Time Dependency*

The kinetics of $^{233}U$ and $^{239}Pu$ adsorption onto the 75 wt% $NaBiO_3$-PAN resin was determined for comparison to that of the $^{241}Am$ and $^{244}Cm$ kinetics. An identical contact time study was carried out at 0.01 M $HNO_3$ and is shown in Figure 8.5.

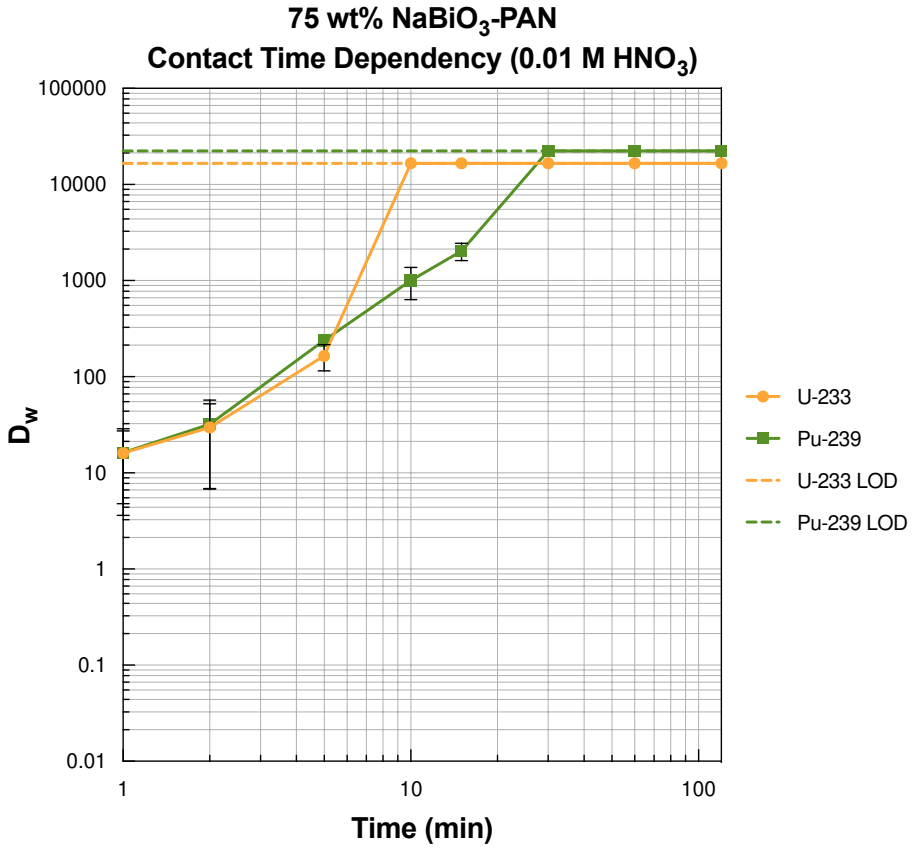


**Figure 8.5:** Adsorption of $^{233}U$ and $^{239}Pu$ on 75 wt% $NaBiO_3$-PAN resin as a function of radionuclide contact time at 0.01 M $HNO_3$. All data points are an average of four replicates and error bars represent the uncertainty to $2\sigma$.

Similar to the kinetics study for $^{241}Am$ and $^{244}Cm$, both radionuclides exhibit identical behavior during the first several minutes of contact which begins to deviate after 5 minutes of contact, but kinetics remain slow in this system. Slightly faster kinetics are observed for $^{233}U$ relative as full retention occurs after 10 minutes of contact while $^{239}Pu$ reaches

the LOD after 30 minutes of contact and may be attributed to potential differences in speciation or charge density since nearly identical behavior is to be expected if both radionuclides were present in the same oxidation state.

*8.3.4 Uranium and Plutonium Elution Profiles on 75 wt% $NaBiO_3$-PAN*

Based on the large $SF_{U/Pu}$ for both $NaBiO_3$ solid and 75 wt% $NaBiO_3$-PAN, it would be expected that a U/Pu separation could be carried out through the elution of the lesser retained $^{239}Pu$ at 2 M $HNO_3$ followed by the stripping of $^{233}U$ at 0.1 M $HNO_3$. The elution profiles for both radionuclides at 2 M $HNO_3$ are shown below in Figure 8.6.

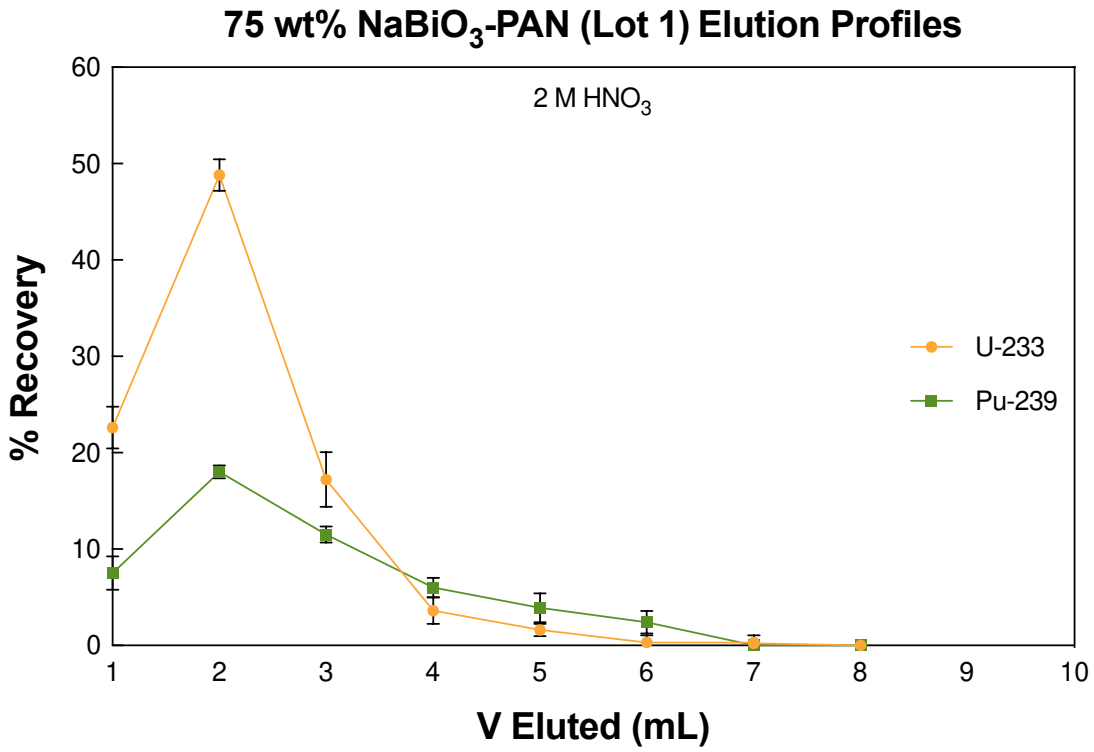


**Figure 8.6:** Elution profiles of $^{233}U$ and $^{239}Pu$ on 75 wt% $NaBiO_3$-PAN using a 2 mL slurry-packed column. All data points represent an average of five replicate fraction counts and error bars represent the uncertainty to 2$\sigma$.

Interestingly, the elution behavior of both radionuclides did not favor a separation and did not align well with the batch adsorption studies. While $^{233}U$ was expected to be strongly retained at 2 M $HNO_3$, ~20% eluted in the load fraction and ~95% of the $^{233}U$ activity was recovered with an additional 7 mL of 2 M $HNO_3$ indicating that there is very low adsorption at this acid concentration. Conversely, only ~50% of the $^{239}Pu$ activity was recovered using 2 M $HNO_3$ with significant tailing indicating greater retention.

While this elution behavior does not align with what would be anticipated based on the $D_w$ data, it is more in line with the expected behavior of the hexavalent trans dioxo-cationic actinides. The deviation between the adsorption and chromatographic behavior of these radionuclides may be explained by the fact that the batch adsorption studies were carried out on the second lot of resin received from TrisKem, while the first lot received from TrisKem was used for the chromatographic study. A difference in the $NaBiO_3$ used for these resins (*e.g.,* purity, source) may influence the behavior of $^{233}U$ and $^{239}Pu$.

*8.3.5 Nitric Acid Concentration Dependency – $NaBiO_3$-PAN (1st Lot)*

The batch adsorption study was repeated for $^{233}U$ and $^{239}Pu$ on the first lot of 75 wt% $NaBiO_3$-PAN received from TrisKem (Figure 8.7) to address the discrepancies throughout the various experiments. The trends for both radionuclides indeed follow that of all other radionuclides studied on this resin indicating that differences in the reagents or resin preparation methods may have had a strong influence on the resulting adsorption behaviors. However, the interesting $^{233}U$ adsorption behavior observed in the second $NaBiO_3$-PAN lot does agree with that of the >90% pure $NaBiO_3$ solid which contradicts

the theory that the PAN support is responsible for the deviation in $^{233}U$ adsorption. In addition, neither radionuclide is at the limit of detection at 0.01 M $HNO_3$ as observed for the second resin lot and the $D_w$ values at 0.01 M $HNO_3$ more closely align with those measured for $NaBiO_3$ solid.

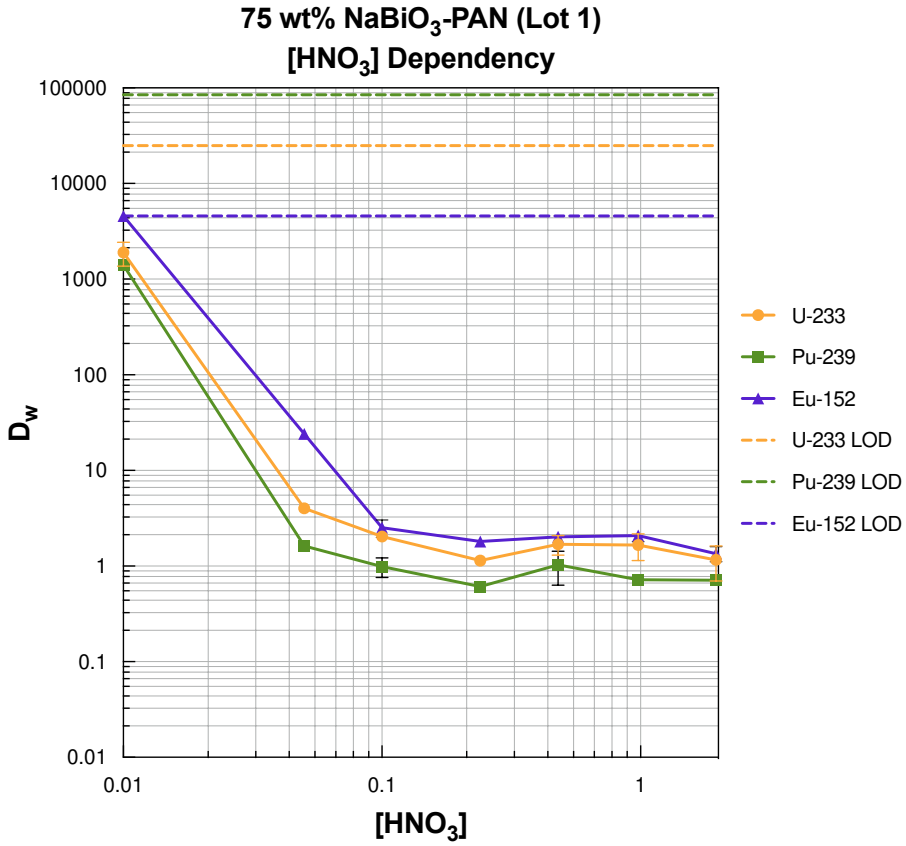


**Figure 8.7:** Adsorption of $^{233}U$ and $^{239}Pu$ on the first lot of 75 wt% $NaBiO_3$-PAN resin as a function of nitric acid concentration. All data points are an average of four replicates and error bars represent the uncertainty to $2\sigma$.

### 8.4 Conclusions and Future Work

Since a main goal of separations as it relates to the NFC is to develop methods that will allow for the simplification of the current reprocessing flowchart, achieving a hexavalent actinide separation from lanthanides is a useful approach. To assess the ability of a

$NaBiO_3$ system to accomplish this, the adsorption of the early actinides, $^{233}U$ and $^{239}Pu$, as well as a trivalent lanthanide, $^{152}Eu$, on $NaBiO_3$ solid and $NaBiO_3$-PAN was characterized. Because trivalent $^{152}Eu$ is nearly identical in chemistry to trivalent $^{244}Cm$, the adsorption behavior on $NaBiO_3$ was also nearly identical to $^{244}Cm$ as expected. While the majority of the lanthanide series is most stable in the trivalent oxidation state, cerium is a lanthanide of concern as $NaBiO_3$ is a common reagent used for the oxidation of Ce(III) to Ce(IV). The presence of Ce(IV) would likely result in the interference with the recovery of the hexavalent actinides and its presence as an impurity in the resulting product is undesirable; thus, adsorption studies of Ce in the $NaBiO_3$ systems are necessary. The interference of other fission products is also necessary to understand potential interferences and to identify points within the currently proposed reprocessing schemes suitable for a $NaBiO_3$-based separation.

The oxidation of the early actinides to the hexavalent state and their identical behavior to $^{241}Am$ was expected, but $^{233}U$ adsorption varied throughout batches. The adsorption curve for $^{239}Pu$ followed the same trend as $^{241}Am$ with slightly lower $D_w$ values which is favorable. U-233 also exhibited similar adsorption behavior at lower $HNO_3$ concentrations with slightly smaller $D_w$ values relative to $^{241}Am$; however, a steady increase in retention occurred at acid concentrations greater than 0.1 M. This likely indicates the presence of U in different oxidation states which should be monitored through UV-Vis-NIR spectroscopy in the future. In addition, the speciation of all radionuclide stock solutions should be characterized and their oxidation states adjusted and controlled prior to future batch adsorption studies.

The behavior of $^{239}Pu$ on the 75 wt% $NaBiO_3$-PAN resin followed the same trend as both $^{241}Am$ and $^{244}Cm$ with $D_w$ values <1 above 0.05 M $HNO_3$. However, unlike $^{241}Am$, $^{239}Pu$ was at the limit of detection at 0.01 M $HNO_3$ which was not expected due to the lower $D_w$ value observed on $NaBiO_3$ solid. The hydrolysis study showed ~20% loss of $^{239}Pu$ activity at 0.01 M $HNO_3$ but the large standard deviation and presence of fine $NaBiO_3$ particles do not allow for a confident determination that hydrolysis is occurring. U-233 also had a $D_w$ at the limit of detection at 0.01 M $HNO_3$ and exhibited the same trend of increasing $D_w$ above 0.1 M $HNO_3$. Kinetics studies at 0.01 M $HNO_3$ were also unfavorably slow similar to those observed for $^{241}Am$ and $^{244}Cm$ with $^{239}Pu$ exhibiting slightly slower adsorption rates than $^{233}U$.

While $^{233}U$ did not behave as the expected hexavalent ion, its high $D_w$ at higher acid concentrations resulted in $SF_{U/Pu}$ as high as 300 suggesting the possibility of a U/Pu separation. It was expected that at 2 M $HNO_3$ $^{239}Pu$ elution would occur followed by $^{233}U$ elution at a lower acid concentration; however, both radionuclides co-eluted with the 2 M $HNO_3$ eluent and, surprisingly, there was a greater recovery for $^{233}U$. The chromatographic study was, however, performed on a second lot of the PAN resin provided by TrisKem relative to the first lot used for the batch contact studies. When repeating the batch study for the second lot of resin, $^{233}U$ exhibited the expected behavior identical to all other radionuclides on the PAN resin. Thus, further studies into the sources and purities of $NaBiO_3$ reagents should be conducted.

The speciation of these radionuclides in the stock solution should be characterized and controlled prior to the batch adsorption studies. UV-Vis-NIR studies should be completed to determine $NaBiO_3$'s ability to oxidize $NpO_2^+$ and $Pu^{4+}$ as a function of acid concentration and its kinetics and stability should be characterized to assess the applicability of this oxidant. The redox kinetics of $UO_2^{2+}$ in $NaBiO_3$ systems should also be further studied through spectroscopic characterization as well as through adsorption isotherms that may aide in the elucidation of the adsorption mechanism at play at higher acid concentrations and whether or not inner or outer sphere complexation is occurring.

# CHAPTER 9: BEHAVIOR OF AMERICIUM AND CURIUM IN MIXED SODIUM BISMUTHATE SYSTEMS

## 9.1 Introduction

Separations through sorption methods have provided a low cost, low waste, easy, efficient, and readily available alternative to large-scale solvent extraction processes. As a result, numerous materials have been explored for the selective sorption of metals such as clays, chelating resins, activated carbon, and functionalized silica. However, the use of the PAN and PES polymeric supports diminished the favorable redox and ion exchange characteristics that $NaBiO_3$ solid exhibits and it is known that reduction of Am(VI) occurs upon contact with organic materials. Thus, exploring inorganic supports may be a better approach towards a successful chromatographic system.

Recently, Richards and Sudowe used the Celite 545 diatomaceous earth as a filter aid to improve the poor flow properties of $NaBiO_3$ in a column chromatographic system by dispersing 5 wt% $NaBiO_3$ solid in Celite. The high separation factors, short contact times, and ease of operation of this separation system provide a promising alternative to solvent extraction systems for the separation of oxidized $^{241}Am$ from $^{244}Cm$. This method, however, suffers from poor adsorption capacity and flow rate properties, gradual dissolution of the material during the separation, and gas production in nitric acid. This method, however, suffers from poor adsorption capacity and flow rate properties, gradual dissolution of the material during the separation, and gas production in nitric acid.[127] This method was successful as it resulted in a near complete Am/Cm separation; however, in-depth characterization of this system was not carried out. This chapter will characterize

the adsorption behavior of $^{241}Am$ and $^{244}Cm$ in the $NaBiO_3$/celite system as well as compare that behavior to that of other inorganic filter aids and supports.

## 9.2 Experimental Methods

### *9.2.1 Batch Adsorption Studies*

Batch studies followed the same general method as described in section 6.2.1; however, samples were prepared by mixing both the solid $NaBiO_3$ and filter aid material in different ratios. Celite 545 and silica gel (70 – 230 mesh, 60 Å) from MilliporeSigma as well as microgrit alumina from Agilent were used as inorganic filter aids. Briefly, 2.5 mg (± 0.25 mg) of $NaBiO_3$ and 47.5 mg (± 4.75 mg) of the appropriate filter aid were weighed into 2 mL polypropylene microcentrifuge tubes for the 5 wt% mixtures. The 10 wt% mixtures had a composition of 5 mg (± 0.5 mg) of $NaBiO_3$ and 45 mg (± 4.5 mg) of the filter aid in each sample. Samples were prepared in triplicate and were shaken until a homogeneous mixture was obtained prior to the addition of the aqueous phase.

### *9.2.2 Adsorption Capacity Determination*

Batch studies using La were conducted to determine the adsorption capacity of $NaBiO_3$ in the 10 wt% systems and was quantified using ICP-OES. The Ultra Scientific La standard solution had a concentration of 10,000 ppm in 2 wt% $HNO_3$ and was used to prepare calibration solutions with a concentration range of 0 to 100 ppm. The ICP-OES system did not have a La detector; however, the complete spectral overlap of the As emission at 189 nm allowed for the use of the As detector for the quantification of the La concentration. The As detector was first calibrated using a single point calibration using

a blank and 5 ppm As standard calibration solution (Ultra Scientific). A calibration curve for the As detector response to La was prepared to accurately determine the La concentration and showed good linearity with a $R^2$ value of 0.9999 (Figure 9.1). The limit of detection (LOD) and limit of quantification (LOQ) for the As detector were defined as three and 10 times the standard deviation of 10 blank analyses and were determined to be 0.04 and 0.13 ppm, respectively.

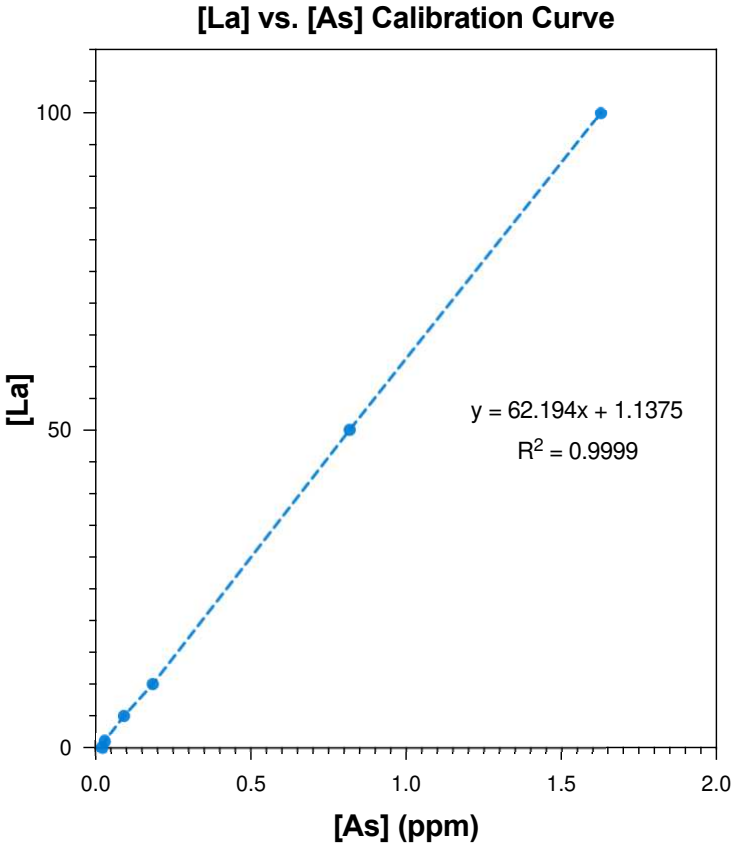


**Figure 9.1:** Calibration curve for [La] quantification using the As detector at 189 nm.

The adsorption capacities for the 10 wt% $NaBiO_3$/filter aid systems were determined by following the general batch study method at 0.01 M $HNO_3$. Samples were spiked with La concentrations ranging from 1 to 100 ppm and performed in triplicate. After contact, 1 mL

aliquots of the aqueous phase were transferred to test tubes and diluted to 2 mL with 0.01 M $HNO_3$ prior to ICP-OES analysis. The best-fit equation obtained from the calibration curve was used to determine the La concentration from the intensity of the As signal. Reagent blanks and La sample spike solutions were prepared and used during the analysis. Calibration verification was performed after every 10 samples using a continuous calibration verification solution with an As concentration of 5 ppm.

*9.2.3 Chromatographic Separations*

Individual 2-mL Eichrom polypropylene columns were slurry packed with the 5 wt% and 10% $NaBiO_3$ Celite 535 and silica mixtures in 0.01 M $HNO_3$. Column packing was carried out by adding portions of the slurry into the column and pulling the solution through the column with a peristaltic pump until the mobile phase was just above the bed and repeated until a bed height of 5 cm was reached. All separations were run at room temperature with a flow rate of 1.0 mL $min^{-1}$. The column was conditioned with 15 mL of 0.01 M $HNO_3$ and the flow rate was verified by timing the number of drops and determining the volume collected gravimetrically. 1000 Bq $mL^{-1}$ Am-241 and Cm-244 solutions in 0.01 M $HNO_3$ were prepared and 0.1 mL (100 Bq) of each radionuclide was loaded onto individual columns. The columns were washed with 20 mL of 0.01 M $HNO_3$ to recover Am-241 followed by 20 mL of 2 M $HNO_3$ for Cm-244 elution. The eluent was collected in 4 mL fractions and 0.1 mL aliquots were counted on a Ludlum 3030 gross alpha beta counter to determine recovery in real-time and recoveries were verified using liquid scintillation counting.

## 9.3 Behavior of Americium and Curium in Mixed $NaBiO_3$/Celite Systems

### *9.3.1 Am and Cm Adsorption on 5 wt% $NaBiO_3$/Celite*

Batch adsorption studies were performed for $^{241}Am$ and $^{244}Cm$ and are used as a baseline comparison when determining the efficiency of other filter aids mixtures (Figure 9.2).

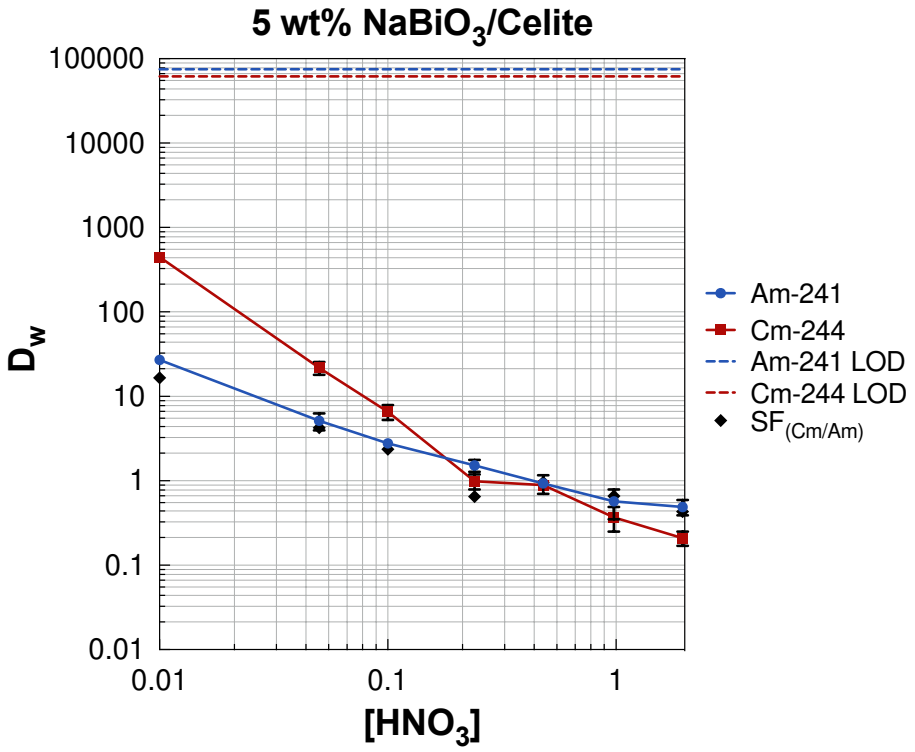


**Figure 9.2:** Adsorption of $^{241}Am$ and $^{244}Cm$ on 5 wt% $NaBiO_3$/Celite as a function of nitric acid concentration. All data points are an average of four replicates and error bars represent the uncertainty to $2\sigma$.

Similar Am/Cm adsorption behavior trends were observed and are in line with the fact that there was 95% less $NaBiO_3$ in the samples relative to the $NaBiO_3$ solid study. As in all other systems studied in this work, the greatest $SF_{Cm/Am}$ of ~17 is obtained at 0.01 M $HNO_3$. However, the Am/Cm separation performed by Richards used 0.1 M $HNO_3$ as the eluent but the $SF_{Cm/Am}$ at 0.01 M $HNO_3$ obtained in this study is only ~2. [127]

*9.3.2 Am and Cm 5 wt% $NaBiO_3$/Celite Chromatography*

Elution profiles for both radionuclides were obtained using a 5 wt% $NaBiO_3$/Celite slurry packed column with a bed height of 5 cm and a constant flow rate of 1 mL $min^{-1}$ (Figure 9.3).

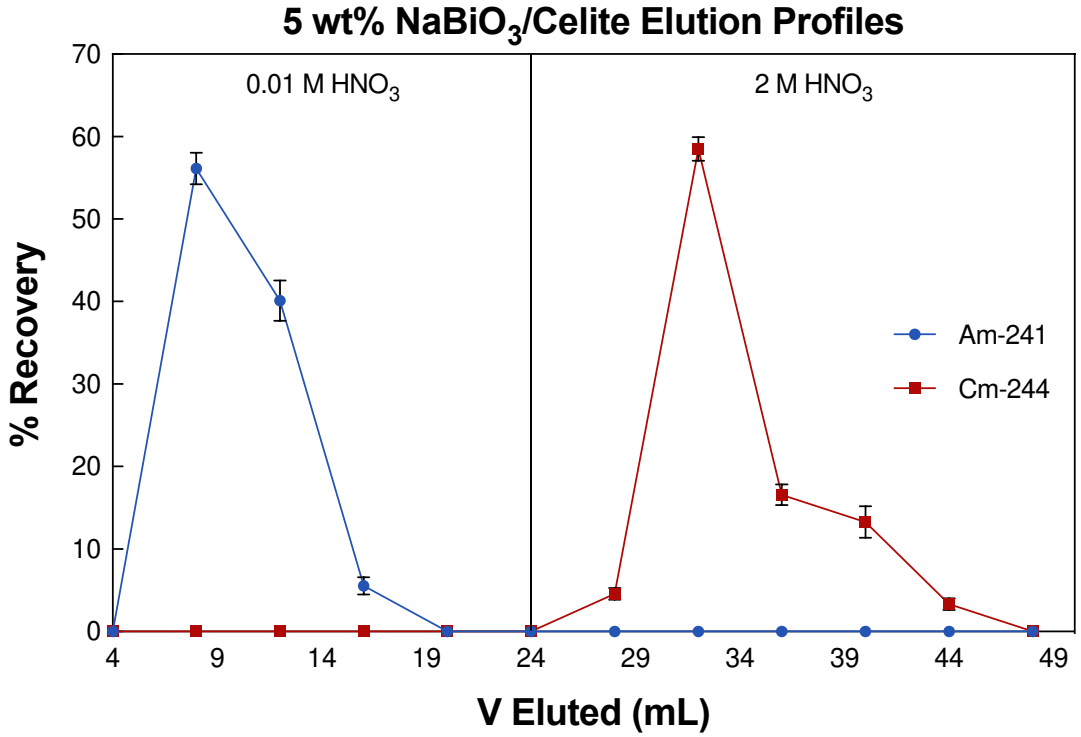


**Figure 9.3:** Elution profiles for $^{241}Am$ and $^{244}Cm$ on a 5 wt% $NaBiO_3$/Celite column with a bed height of 5 cm and flow rate of 1 mL $min^{-1}$. All data points are an average of five counting replicates of each fraction and error bars represent the uncertainty to $2\sigma$.

The elution behavior is as expected with $^{241}Am$ elution with 0.01 M $HNO_3$ and $^{244}Cm$ with 2 M $HNO_3$. An $^{241}Am$ recovery of 102% ± 8% was achieved with 12 mL of eluent with a relatively uniform peak shape. 96% ± 6% of the $^{244}Cm$ activity was recovered with 26 mL of 2 M $HNO_3$. Peak tailing as a result of band broadening was observed in the elution

profiles for both radionuclides and may be due to the nature of the mixed bed and contributions from the Celite 545.

*9.3.3 Am and Cm Adsorption on 10 wt% $NaBiO_3$/Celite*

To quantify how increasing the amount of $NaBiO_3$ in this system would improve the SFs increase the resolution between the two elution curves, the batch adsorption study was repeated by increasing the amount of $NaBiO_3$ to 10 wt% (Figure 9.4).

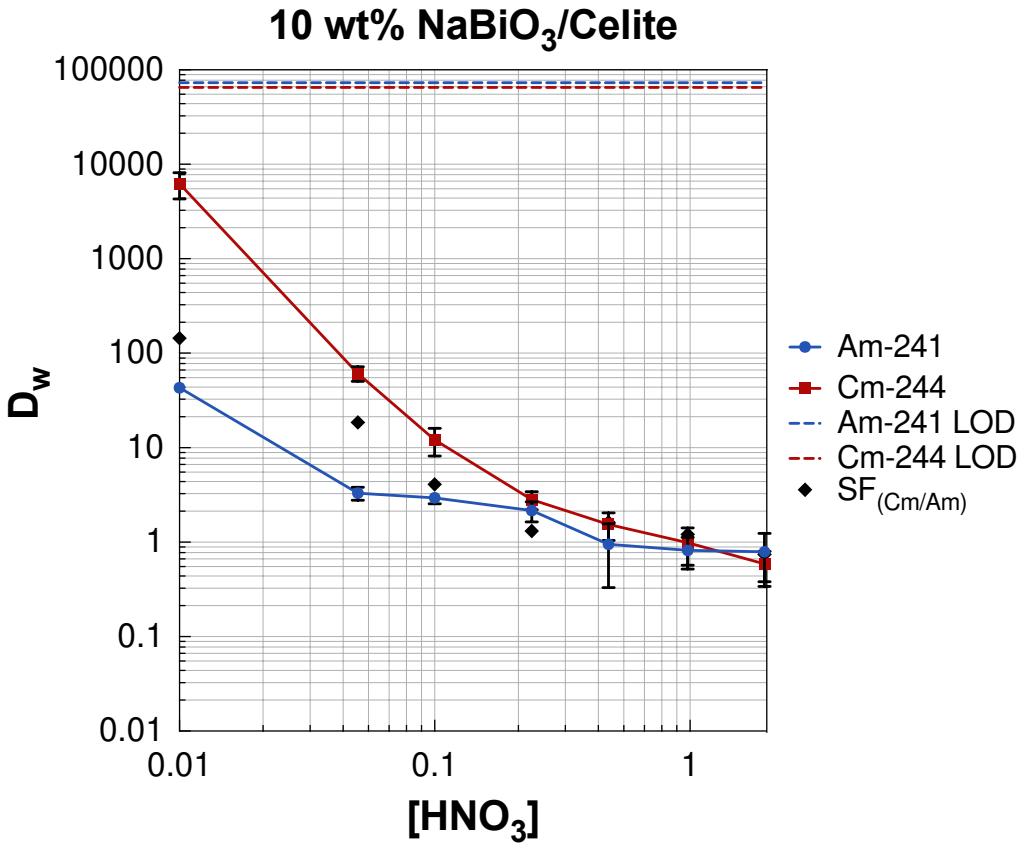


**Figure 9.4:** Adsorption of $^{241}Am$ and $^{244}Cm$ on 10 wt% $NaBiO_3$/Celite as a function of nitric acid concentration. All data points are an average of four replicates and error bars represent the uncertainty to $2\sigma$.

The adsorption curves for the 10 wt% $NaBiO_3$/Celite system follow the same trend as that for the 5 wt% mixture; however, the increase in the $NaBiO_3$ amount results in an increase

in the $D_w$ values. A slight increase in the $^{241}Am$ $D_w$ values was seen, but the $^{244}Cm$ adsorption increases to a much greater extent resulting in an increase of the SFs. At 0.01 M $HNO_3$, the $SF_{Cm/Am}$ increases by an order of magnitude from ~17 to ~145 and at 0.05 M from ~4 to ~18. However, at 0.1 M $HNO_3$ the $SF_{Cm/Am}$ doubles to ~4 making 0.01 M $HNO_3$ better for elution.

*9.3.4 Contact Time Dependency*

The influence of the physical properties of the filter aids on the kinetics system was determined through a contact time study was carried out at 0.01 M $HNO_3$ (Figure 9.5).

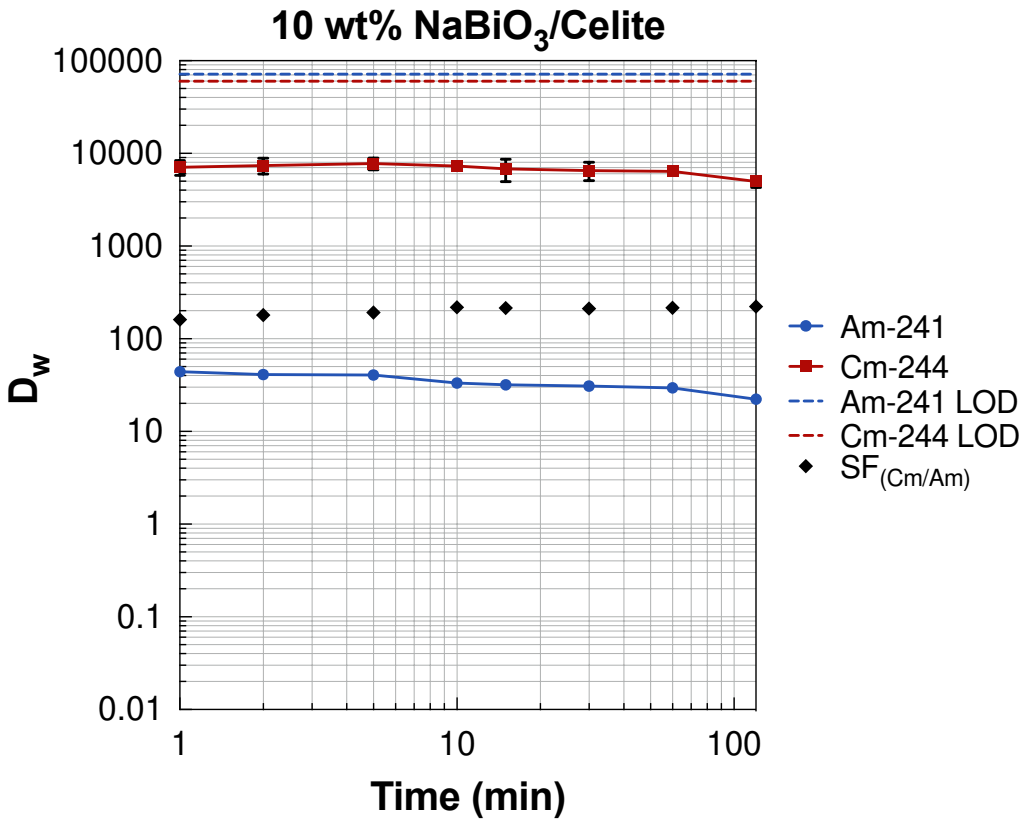


**Figure 9.5:** Adsorption of $^{241}Am$ and $^{244}Cm$ on 10 wt% $NaBiO_3$/Celite as a function of contact time at 0.01 M nitric acid. All data points are an average of four replicates and error bars represent the uncertainty to $2\sigma$.

After the first minute of contact, a $SF_{Cm/Am}$ of 160 was reached and the maximum $SF_{Cm/Am}$ of 180 obtained from the prior batch study achieved after two minutes of contact. Rapid kinetics are observed in this system, especially when compared to the kinetics of the 75 wt% $NaBiO_3$-PAN resin. The dispersion of the active $NaBiO_3$ throughout highly porous Celite 545 may allow for faster kinetics and higher capacity relative to that of $NaBiO_3$ solid alone by increasing the surface area. The $D_w$ values for both $^{241}Am$ and $^{244}Cm$ slightly decrease with increasing contact time which could be a result of properties such as particle size and surface area changing with longer contact, but the $SF_{Cm/Am}$ remains relatively constant.

*9.3.5 Adsorption Isotherm*

Separations utilizing adsorption processes are based on the interactions of the solution's components with the surface of the solid adsorbent that occur through physiosorption (electrostatics) or chemisorption (covalent bonding). Analytes are able to travel within the micropore volume of porous sorbents; thus, the porosity, pore size, pore volume, and surface area greatly influence the adsorption capabilities of the sorbent. To assess and compare the adsorption behavior of novel adsorbents, the adsorption equilibria, capacity, and kinetics must be understood.

The interactions between the analyte and the stationary phase can be described through an adsorption isotherm which measures the concentration ratio of the analyte between the two phases at equilibrium. Equilibrium is reached after sufficient contact time where the dynamic concentration of the analyte on the sorbent and in solution is achieved (rates

of adsorption and desorption are equal). These isotherms can then be modeled to determine valuable information regarding the maximum adsorption capacities, mechanisms, and thermodynamics of adsorbents to understand the influence of different adsorbent properties. The adsorption isotherm can be determined by plotting the equilibrium concentrations of the analyte on the adsorbent, $q_e$ (mg $g^{-1}$), versus in solution, $C_e$ (mg $L^{-1}$). The adsorption isotherm was obtained for $La^{3+}$ in the favorable 10 wt% $NaBiO_3$ system and is shown in Figure 9.6). $La^{3+}$ was chosen as the analyte as it has the same trivalent speciation as the $Cm^{3+}$ that is retained on $NaBiO_3$ and the ability to study this element at higher concentrations.

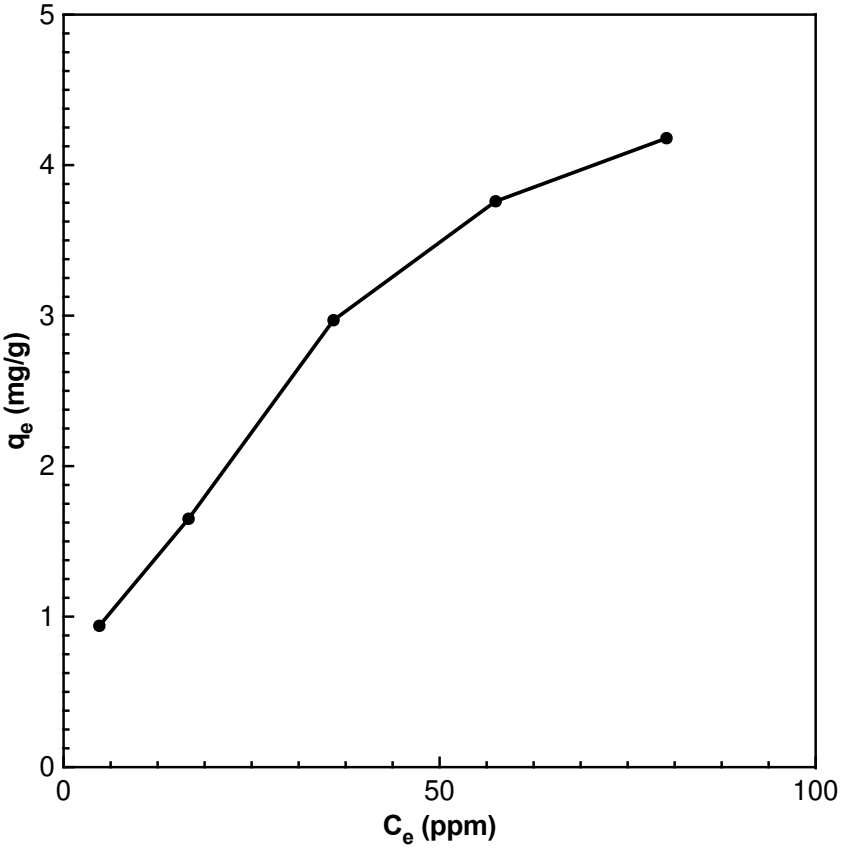


**Figure 9.6:** Mass of lanthanum adsorbed as a function of lanthanum concentration in 0.01 M nitric acid for the 10 wt% $NaBiO_3$/Celite system. All data points are an average of four replicates and error bars represent the uncertainty to $2\sigma$.

The plot of $q_e$ vs. $C_e$ for $La^{3+}$ appears to exhibit the shape of a reversible Type 1 isotherm which is characterized by a leveling out of the curve and describes adsorption for physical adsorption and/or chemisorption. The plateau shows that the degree of adsorption increases until a saturation point is reached and indicates the full occupation of all adsorption sites on the surface. Chemisorption processes display Type 1 behavior as they are limited to monolayer adsorption These isotherms also indicate that the size of the adsorbent's pores is not significantly larger than the diameter of the adsorbate; thus, higher uptakes are observed at lower concentrations due to narrow pore width. When increasing the analyte concentration, the extent of adsorption is limited by the accessible pore volume.

The Langmuir model has been applied to Type 1 isotherms to quantify and contrast the adsorption capacities of various adsorbents. This model is based on the kinetics principle that, at equilibrium, the adsorption and desorption rates are equal and was constructed around several assumptions. Following chemisorption, the model assumes monolayer adsorption, that all adsorption sites are equal so that one analyte occupies a single site, and that the analytes do not laterally interact with one another.

The Langmuir adsorption isotherm model can be applied to the adsorption isotherm using Equation 9.1.

$$q_e = \frac{Q_M K_L C_e}{1 + K_L C_e} \qquad \textbf{Equation 9.1}$$

Where $q_e$ is the amount of solute adsorbed per unit mass of solid at equilibrium (mg/g), $Q_M$ is the adsorption capacity (mg adsorbate/g adsorbent), $K_L$ is the Langmuir adsorption constant (L/mg), $C_e$ is the solute concentration in solution at equilibrium (mg/L). The monolayer adsorption capacity is also related to adsorption constant, $K_L$, useful for comparing different sorbents by correlating $K_L$ to various adsorbent porosities and surface. Thus, sorbents with greater pore volumes and larger surface areas would yield a greater adsorption capacity.

Equation 9.1 can be rearranged to a linear form (Equation 9.2) and the model can be solved through linear regression.

$$\frac{C_e}{q_e} = \frac{C_e}{Q_M} + \frac{1}{K_L Q_M} \qquad \textbf{Equation 9.2}$$

Thus, plotting the left side of the equation, $C_e/q_e$, as a function of $C_e$ produces a linear line with a slope of $1/Q_M$ which can be used to determine the adsorption capacity and Langmuir constant. In addition, a separation factor, $R_L$, can be calculated using the initial analyte concentration, $C_o$, and $K_L$ to determine the nature of adsorption (Equation 9.3). Adsorption is considered to be linear when $R_L = 1$, irreversible when equal to 0, favorable when $0 < R_L < 1$, and unfavorable when $R_L > 1$.

$$R_L = \frac{1}{1 + K_L C_o} \qquad \textbf{Equation 9.2}$$

Thus, the linear Langmuir model was applied to the adsorption isotherm by plotting $C_e/q_e$ as a function of $C_e$ yielding the linear equation of $y = 0.1715x + 5.6514$ with an $R^2$ value of 0.9581 (Figure 9.7).

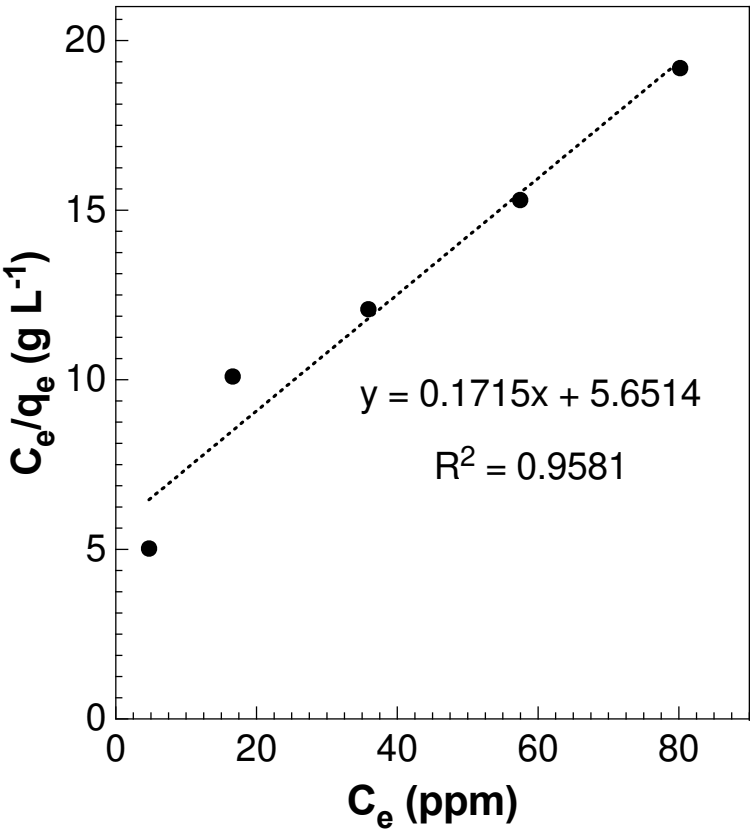


**Figure 9.7:** Langmuir adsorption isotherm for lanthanum in 0.01 M $HNO_3$ for the 10 wt% $NaBiO_3$/Celite system after a one-hour contact time. Data points represent the average of three replicates and error bars represent the standard deviation to $2\sigma$.

The slope, equal to $1/Q_m$, is 0.1715 and the adsorption capacity, $Q_m$, was determined to be 5.83 mg La per g of $NaBiO_3$. The adsorption constant, $K_L$, was calculated by dividing the slope by the y-intercept and determined to be 0.03 L $g^{-1}$ and the separation factor was $0 < R_L < 1$ which is indicative of a favorable adsorption process. Dividing $Q_m$ by the molar mass of La gives an adsorption capacity of 0.04 mmol La/g $NaBiO_3$ and multiplying by

the valance of La (+3) yields a capacity of 0.13 meq/g $NaBiO_3$. This adsorption capacity doubles the capacity of solid $NaBiO_3$ (0.066 meq/g) that was determined by Richards. Since the capacity of $NaBiO_3$ alone was determined using 20 mg of $NaBiO_3$ while this study used 5 mg of $NaBiO_3$ dispersed in 45 mg of Celite 545, the larger capacity obtained for the smaller sorbent amount indicates that the dispersion of $NaBiO_3$ allows for greater availability of the adsorption sites.[212]

### *9.3.6 Am and Cm 10 wt% $NaBiO_3$/Celite Chromatography*

A chromatographic study was carried out for the 10 wt% $NaBiO_3$/Celite system identical to that performed for the 5 wt% system (Figure 9.8).

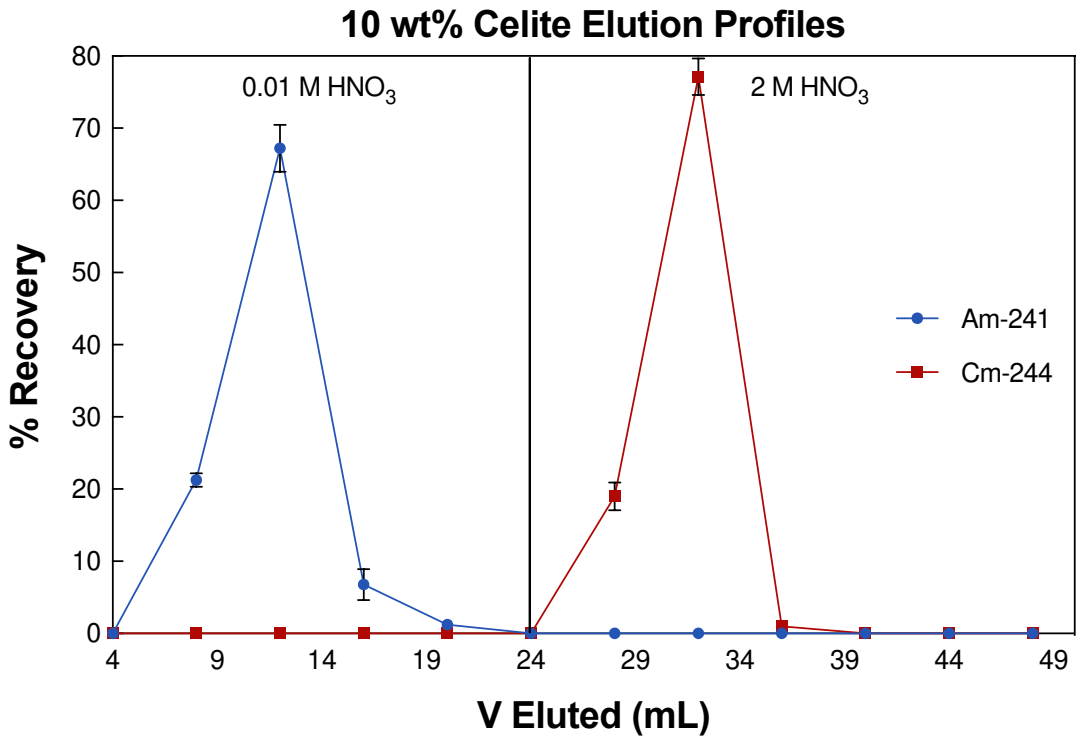


**Figure 9.8:** Elution profiles for $^{241}Am$ and $^{244}Cm$ on a 10 wt% $NaBiO_3$/Celite column with a bed height of 5 cm and flow rate of 1 mL $min^{-1}$. All data points are an average of five counting replicates of each fraction and error bars represent the uncertainty to $2\sigma$

This system resulted in 101% ± 7% $^{241}$Am recovery with 0.01 M $HNO_3$ and a 97% ± 8% $^{244}$Cm recovery with 2 M $HNO_3$. The peak tailing and peak fronting for $^{241}$Am and $^{244}$Cm, respectively, decreased the resolution of the two peaks when compared to the 5 wt% system. The peak shape of $^{241}$Am remained relatively similar, but the symmetry of the $^{244}$Cm elution peak improved and may be due to the greater amount of $NaBiO_3$ in the system relative to the 5 wt% system.

## 9.4 Behavior of Americium and Curium in Mixed $NaBiO_3$/Silica Systems

### *9.4.1 Am and Cm Adsorption on 5 wt% $NaBiO_3$/Silica*

To explore other filter aids, the batch adsorption studies were repeated for silica which showed nearly identical trends in adsorption behavior to that of the Celite 535 system (Figure 9.9). This is expected due to the similarity in the composition of celite and silica which is not expected to adsorb either radionuclide. However, differences in the particle size, shape, and porosity of the two filter aids can significantly influence the mass transfer and diffusion processes within these different materials. Therefore, the properties of the filter aid can affect the chromatographic dynamics and may change separation efficiency.

While the 5 wt% $NaBiO_3$/silica system yielded similar adsorption behavior to the Celite 545 system, it provided superior SFs across the entire lower acid concentrations making this a potentially better material than celite. This may be due to a greater porosity of the silica gel that allows for better dispersion of $NaBiO_3$ and interaction of the analyte with the material which would improve adsorption capacities. At 0.01 M $HNO_3$, the $SF_{Cm/Am}$ was ~93 and about five times greater than the $SF_{Cm/Am}$ for the 5 wt% $NaBiO_3$/celite system.

However, at 0.1 M $HNO_3$, the SF doubled to only 4 which may be a result of $NaBiO_3$ degradation as the acid concentration increases.

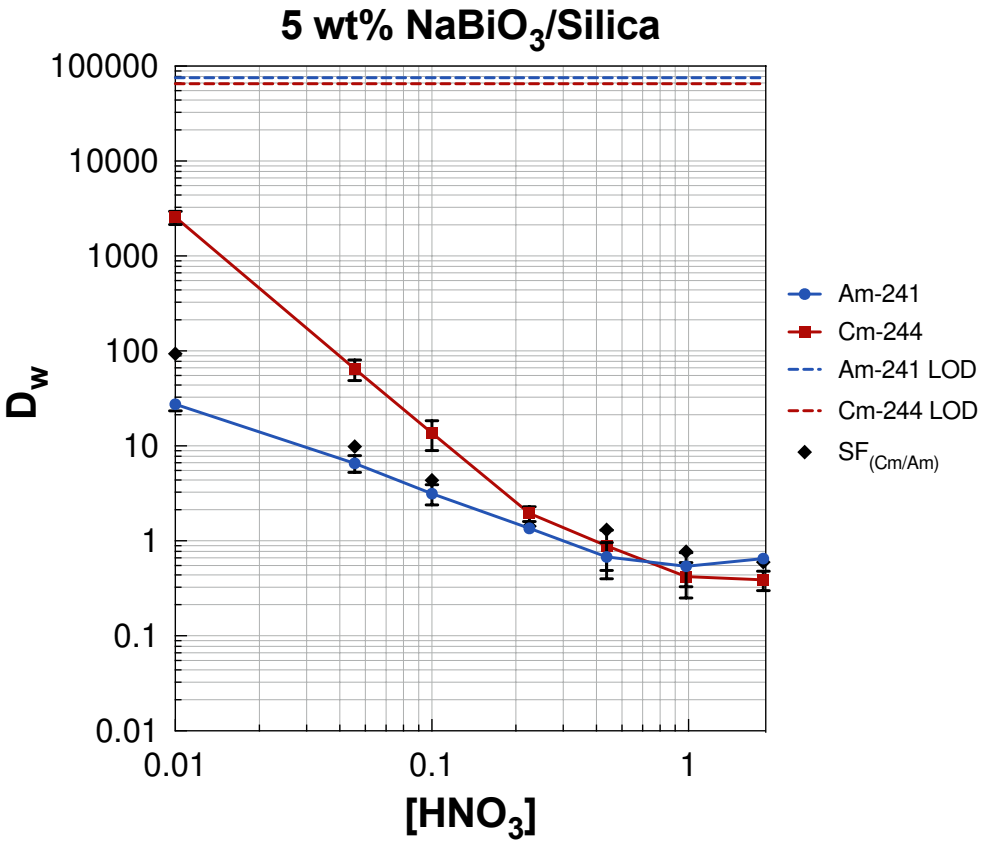


**Figure 9.9:** Adsorption of $^{241}Am$ and $^{244}Cm$ on 5 wt% $NaBiO_3$/Silica as a function of nitric acid concentration. All data points are an average of four replicates and error bars represent the uncertainty to $2\sigma$.

*9.4.2 Am and Cm 5 wt% $NaBiO_3$/Silica Chromatography*

The chromatographic performance of the 5 wt% $NaBiO_3$/Silica system was evaluated under the same separation conditions as that of the celite system (Figure 9.10). Am-241 showed rapid elution with activity recovery occurring in the load fraction and 99% ± 4% of the activity being recovered within the first three 4 mL fractions. Similarly, 98% ± 8% of the $^{244}Cm$ activity was also recovered in the same volume of the 2 M $HNO_3$ eluent with

no co-elution in the $^{241}$Am fractions. The earlier elution of $^{241}$Am gave better resolution between the two elution peaks; however, both elution curves featured slight peak tailing similar to the Celite 545 system with a lower $NaBiO_3$ amount. It is likely that with a greater amount of filter aid the dynamics of the radionuclide adsorption processes is poorer.

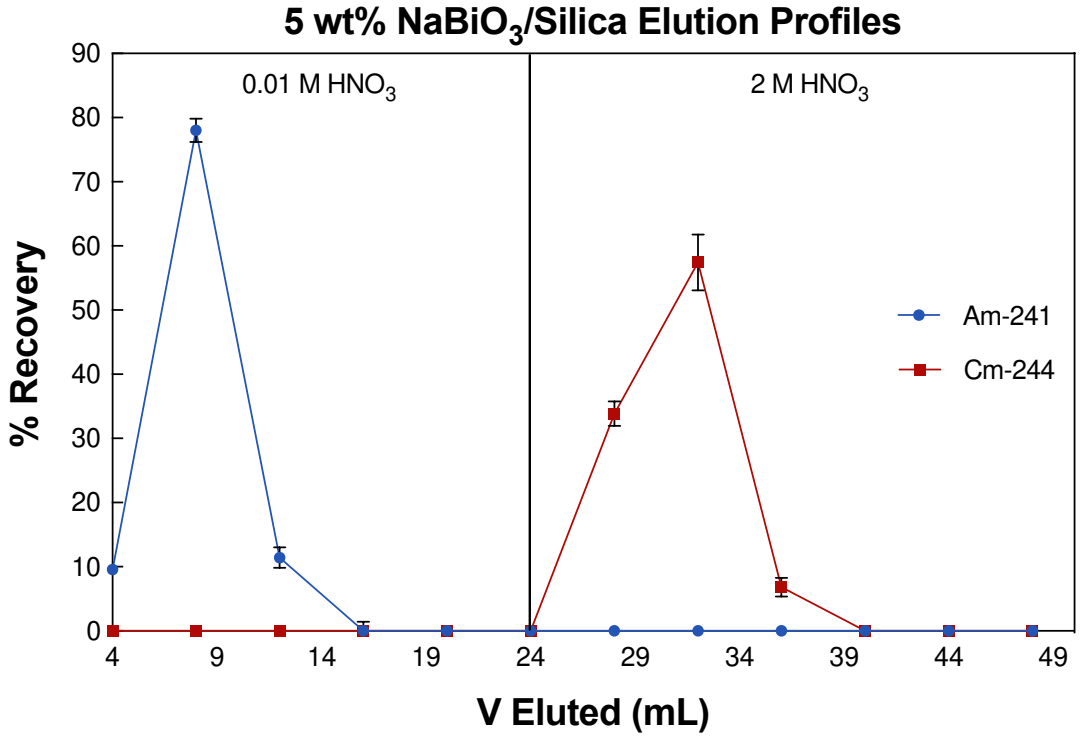


**Figure 9.10:** Elution profiles for $^{241}$Am and $^{244}$Cm on a 5 wt% $NaBiO_3$/Silica column with a bed height of 5 cm and flow rate of 1 mL min$^{-1}$. All data points are an average of five counting replicates of each fraction and error bars represent the uncertainty to 2$\sigma$.

*9.4.2 Am and Cm Adsorption on 10 wt% $NaBiO_3$/Silica*

The adsorption curves for $^{241}$Am and $^{244}$Cm on the 10 wt% $NaBiO_3$/Silica mixture showed similar trends as the 5 wt% mixture as expected with a slightly less rapid decrease in the $^{244}$Cm $D_w$ values with increasing $HNO_3$ concentration (Figure 9.11). Similar to the Celite systems, the $D_w$ values for $^{241}$Am across all acid concentrations do not increase significantly like $^{244}$Cm.

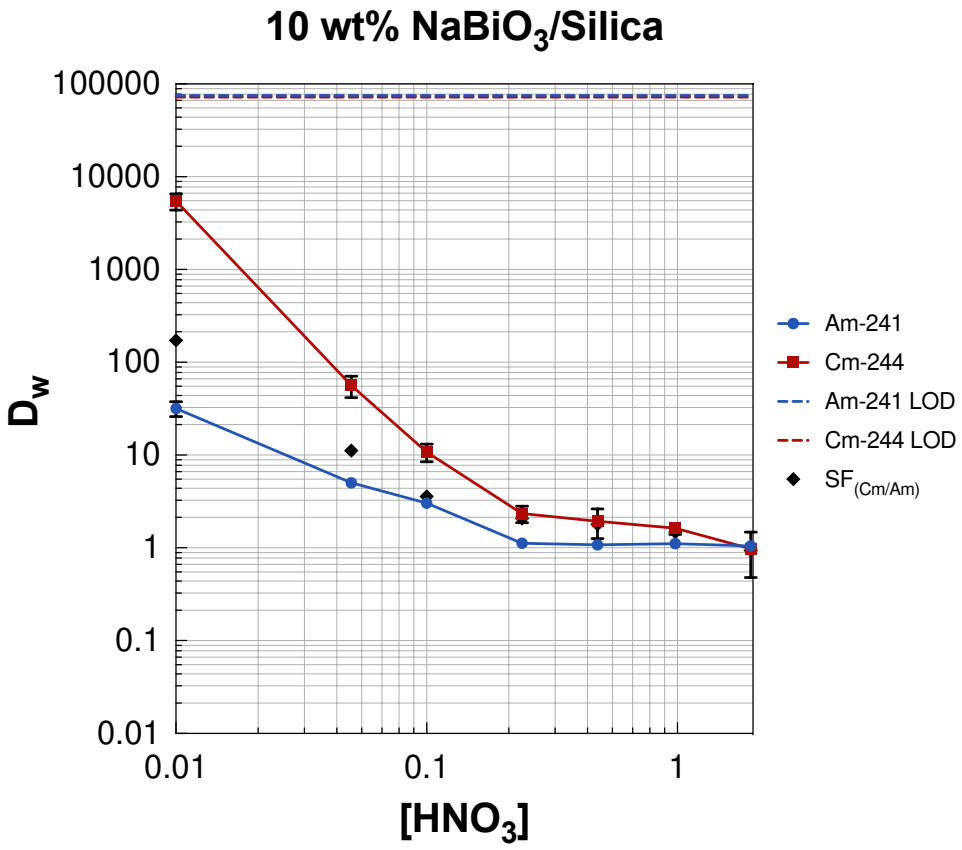


**Figure 9.11:** Adsorption of $^{241}$Am and $^{244}$Cm on 10 wt% $NaBiO_3$/Silica as a function of nitric acid concentration. All data points are an average of four replicates and error bars represent the uncertainty to 2σ.

The increase in $D_w$ values for $^{244}$Cm is also not as large for the Silica system yielding a slightly lower increase in $SF_{Cm/Am}$ values. At 0.01 M $HNO_3$, the $SF_{Cm/Am}$ increased from 93 to 172 and at 0.05 M $HNO_3$ from 10 to 11. Above 0.05 M $HNO_3$ the separation factors are nearly identical for both silica systems. Understanding the adsorption of the radionuclides onto the filter aids and how that may contribute to the adsorption seen in these studies is necessary to understand how the filter aids influence the behavior of the radionuclides in different mixed systems. Thus, fully characterizing the physical properties of the different filter aids and comparing filter aids with different porosities, pore volumes, particle sizes, and surface area would be beneficial.

*9.4.3 Contact Time Dependency*

The contact time kinetics study for the 10 wt% $NaBiO_3$/Silica system is identical to the behavior observed in the 10 wt% $NaBiO_3$/Celite system (Figure 9.12). Rapid kinetics are observed with the maximum $D_w$ values of ~31 and ~5500 for $^{241}Am$ and $^{244}Cm$ observed in the concentration dependency studies, respectively, are reached within the first minute of contact. The decrease in $D_w$ values with increasing time is less pronounced than in the Celite system and, therefore, the $SF_{Cm/Am}$ values of ~180 are more stable across all time points. The fast kinetics observed for both systems are favorable for chromatographic application.

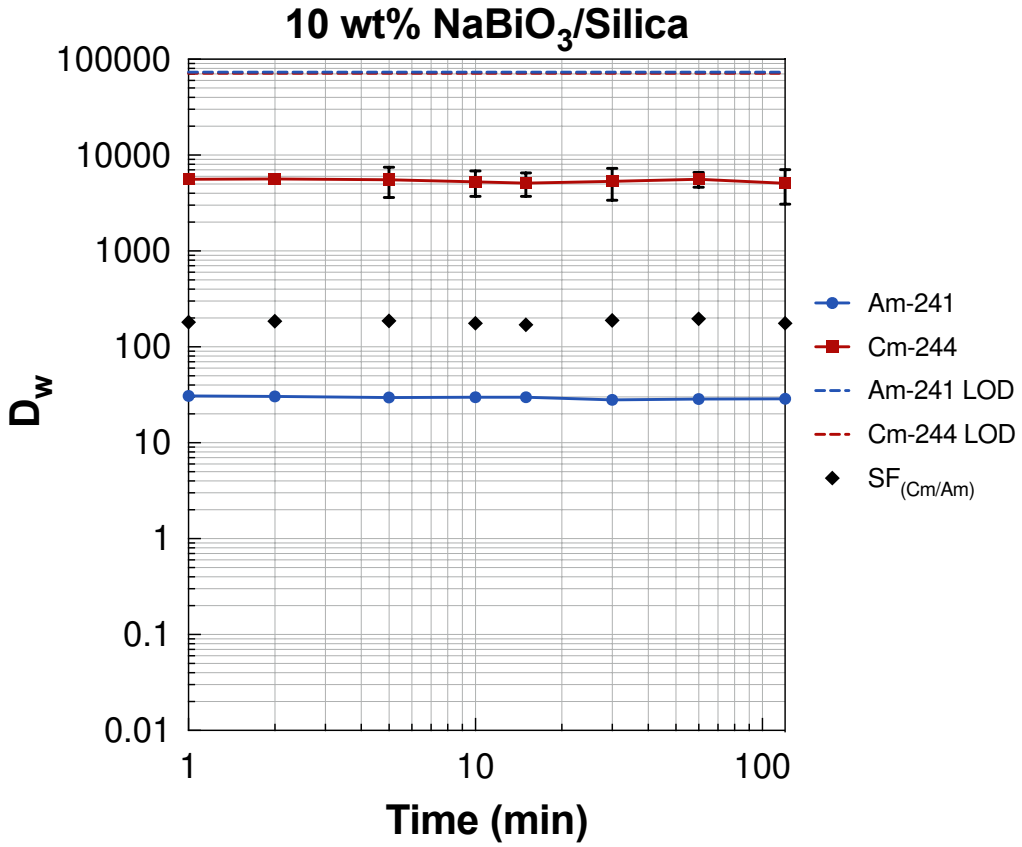


**Figure 9.12:** Adsorption of $^{241}Am$ and $^{244}Cm$ on 10 wt% $NaBiO_3$/Silica as a function of contact time at 0.01 M nitric acid. All data points are an average of four replicates and error bars represent the uncertainty to $2\sigma$.

*9.4.4 Adsorption Isotherm*

The adsorption isotherm for the 10 wt% $NaBiO_3$/silica system shows a more pronounced Type 1 adsorption curve with a distinct plateau at higher [La] concentrations which more clearly shows that dynamic equilibrium has been reached (Figure 9.13). In addition, a larger mass of La was adsorbed in the system across all [La] relative to the Celite system.

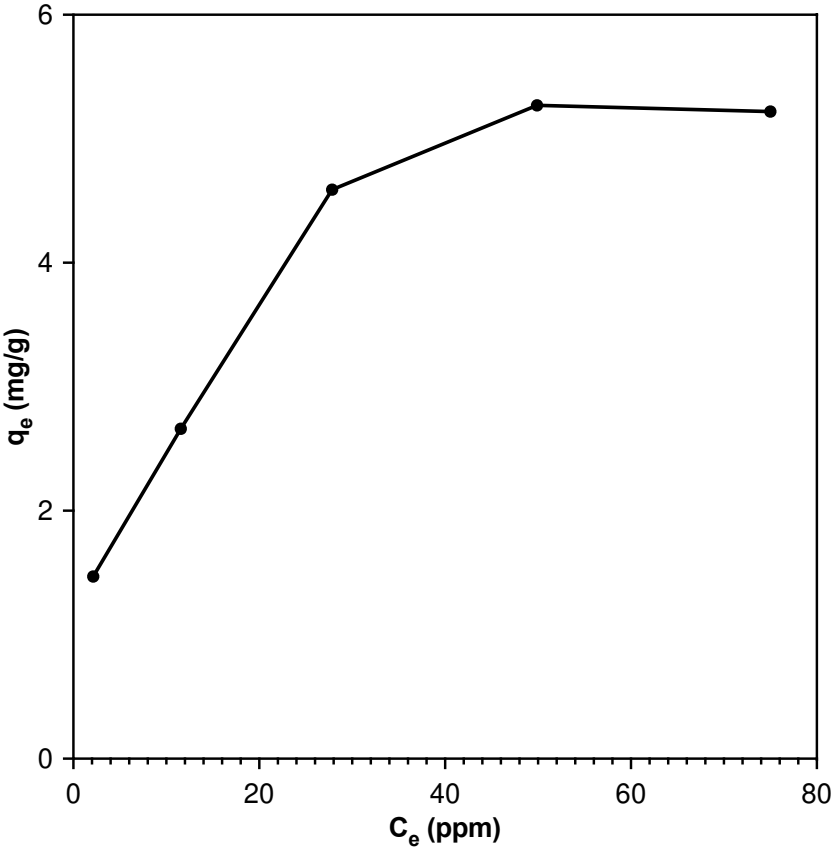


**Figure 9.13:** Mass of lanthanum adsorbed as a function of lanthanum concentration in 0.01 M nitric acid for the 10 wt% $NaBiO_3$/Silica system. All data points are an average of three replicates and error bars represent the uncertainty to $2\sigma$.

Applying the Langmuir model to adsorption isotherm via linear regression yielded a fit of $y = 0.1674x + 1.5739$ with an $R^2$ value of 0.9876 (Figure 9.14). Using the slope ($1/Q_M$) of 0.1674, the adsorption capacity was determined to be ~6 which is slightly greater than

that of the Celite 545 system. This corresponds to an adsorption capacity of 0.043 mmol La/g $NaBiO_3$ or 0.13 meq/g similar the capacity obtained for the 10 wt% $NaBiO_3$/Celite. The better fit of this system to the Langmuir model, as shown by the $R^2$ values, more clearly shows equilibrium. Similarly, the greater $K_L$ value, which indicates the ratios of the rates of adsorption and desorption implies better kinetics of the system. The larger $K_L$, which can also be related to porosity and surface area, shows that the more porous silica has improved the mass transport properties and allows for greater access of the metal ions to the ion exchange sites in this system.

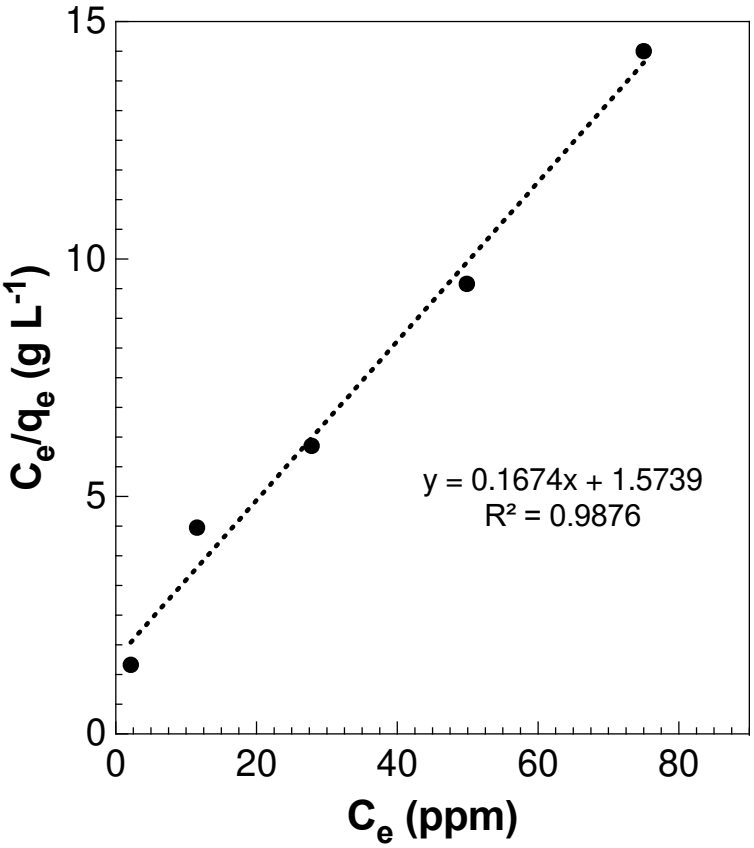


**Figure 9.14:** Langmuir adsorption isotherm for lanthanum in 0.01 M $HNO_3$ after a one-hour contact time for the 10 wt% $NaBiO_3$/Silica system.

*9.4.5 Am and Cm 10 wt% $NaBiO_3$/Silica Chromatography*

The 10 wt% $NaBiO_3$/Silica system achieved 100 ± 6% and 97 ± 5% $^{241}Am$ and $^{244}Cm$ recovery, respectively (Figure 9.15).

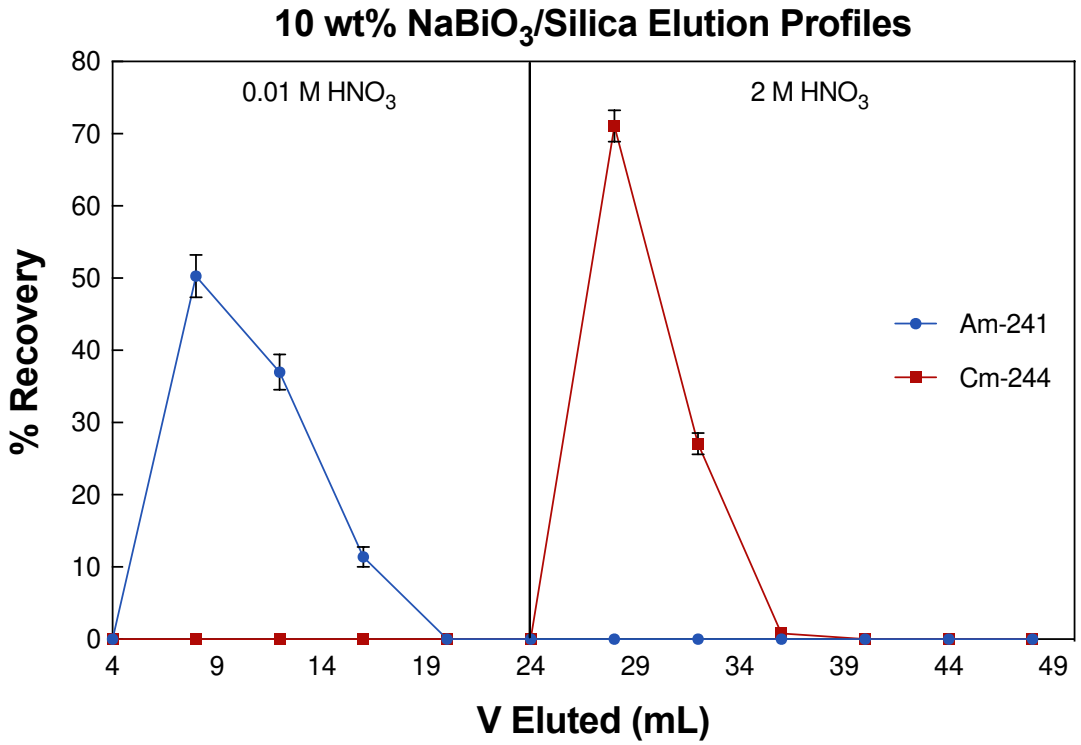


**Figure 9.15:** Elution profiles for $^{241}Am$ and $^{244}Cm$ on a 10 wt% $NaBiO_3$/Silica column with a bed height of 5 cm and flow rate of 1 mL $min^{-1}$. All data points are an average of five counting replicates of each fraction and error bars represent the uncertainty to 2σ.

The increased amount of $NaBiO_3$ resulted in the later elution of $^{241}Am$ and peak tailing which was also observed in the 10 wt% $NaBiO_3$/Celite system; thus, the 10 wt% systems decrease the resolution and therefore efficiency of the chromatographic separation. Another similar characteristic observed in both Celite and Silica systems is the improvement in the peak symmetry for $^{244}Cm$.

### 9.5 $NaBiO_3$/Alumina System

The adsorption behavior of $^{241}Am$ and $^{244}Cm$ was characterized in a 5 wt% $NaBiO_3$/Alumina system as a function of nitric acid concentration (Figure 9.16).

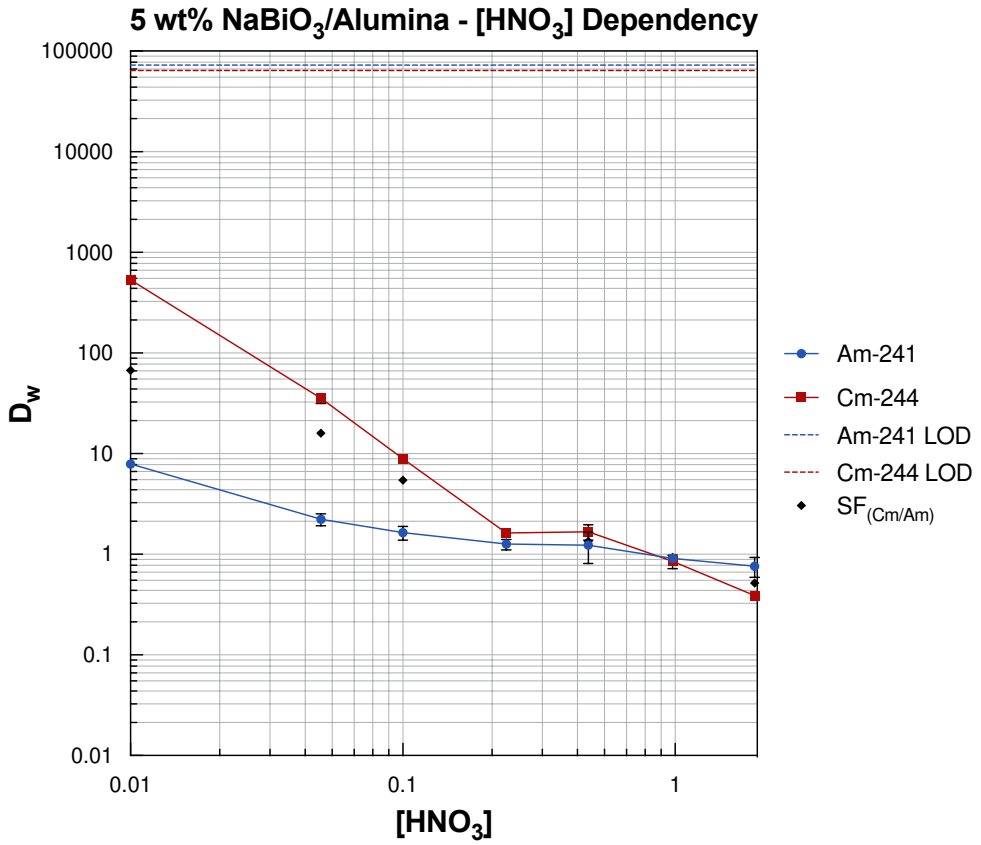


**Figure 9.16:** Adsorption of $^{241}Am$ and $^{244}Cm$ on 5 wt% $NaBiO_3$/Alumina as a function of nitric acid concentration. All data points are an average of four replicates and error bars represent the uncertainty to $2\sigma$.

Alumina is another oxide used as solid supports; however, its surface and, as a result, chemistry is more complex relative to Celite or silica. Depending on the three-dimensional structure of alumina, characteristics like hydration, number of hydroxyl groups, and defects can be altered. The adsorption curves are similar in behavior to those of the other systems, but the retention of both radionuclides decreased relative to the Silica system.

However, the alumina system is superior to the celite system with greater SFs. At 0.01 M, the $SF_{Cm/Am}$ of ~67 is in between that of the celite and silica systems, but from 0.05 to 0.5 M has greater SFs than both systems. The Am retention is also much lower than the others at 0.01 M, which may afford a faster, lower eluant volume recovery. Unfortunately, a chromatographic study could not be performed for the alumina system because the material was in a microgrit form and therefore unsuitable for chromatographic application.

### 9.6 Conclusions and Future Work

From these studies, it is clear that inorganic solid supports/filter aids are a better alternative to organic polymeric supports due to the greater separation factors and chromatographic behavior. In addition, the inorganic material is likely to be more compatible with the higher oxidation states of Am. Both Celite and silica systems were successful at achieving the complete separation of $^{241}Am$ and $^{244}Cm$ with small elution volumes, improved flow rate properties, and good peak resolution. However, further characterization is required to fully evaluate these systems.

Compared to the organic PAN systems, the inorganic filter aids maintain the favorable redox and ion exchange behavior of $NaBiO_3$ when it is dispersed throughout the mixture and provided high separation factors and complete chromatographic separations. Thus, the use of inorganic materials in a $NaBiO_3$ chromatographic system are likely to be more compatible with the higher oxidation states of Am. For the 5 wt% $NaBiO_3$ mixtures, the silica system outperformed the celite system in terms of selectivity with a $SF_{Cm/Am}$ of ~93 at 0.01 M $HNO_3$ relative to Celite's 17. When comparing the effect of $NaBiO_3$ concentration in the mixture, the SFs increased to 174 and 145 for the 10 wt% $NaBiO_3$

Celite and Silica systems, respectively. Thus, the 10 wt% mixtures were used for kinetics studies at 0.01 M $HNO_3$ where both filter aids displayed rapid kinetics with their maximum $D_w$ values reached after the first minute of contact. Both radionuclides showed a slight decrease in their $D_w$ values with longer contact times, however the SFs remained relatively constant. This same kinetic behavior was reported by Richards et. al. for $^{241}Am$ and $^{244}Cm$ on $NaBiO_3$ solid. It can be concluded that the different properties of the two filter aids do not influence the adsorption kinetics of the system.

Since it is well known that the properties of solid supports for chromatographic materials have a significant influence on parameters such as adsorption capacity, the influence of the filter aids on capacity were explored. Adsorption isotherm studies using $La^{3+}$ as a surrogate for $Cm^{3+}$ were completed for both 10 wt% systems with both isotherms corresponding to Type 1 isotherms. Thus, the Langmuir adsorption isotherm model was applied to both systems to determine the adsorption capacity of $NaBiO_3$ in these systems. Linear regression for the 10 wt% $NaBiO_3$/Celite system resulted in a slope of 0.2177 which corresponds to an adsorption capacity of ~4.6 mg La (0.033 mmol La)/g $NaBiO_3$. Taking into consideration the valance state, the capacity was determined to be 0.099 meq/g $NaBiO_3$. The silica system demonstrated a higher capacity of ~6 mg La (0.043 mmol)/g $NaBiO_3$ or 0.13 meq/g $NaBiO_3$. Both systems gave better capacities than the 0.066 meq/g $NaBiO_3$ for solid $NaBiO_3$ alone as determined by Richards et. al. which is likely a result of the dispersion of the active solid throughout the filter aid. This may be a result of differences in the available surface area, particle size, and porosity of $NaBiO_3$ in the two systems.

As UNF features a more complex system containing impurities other than Am and Cm, batch contact and chromatographic studies should be completed to understand the influence of interfering ions on the separation system. In addition, the adjustment of system parameters such as pH and ionic strength would provide a better understanding of the interactions occurring between both the metal ions and $NaBiO_3$ and $NaBiO_3$ and the solution. Since Bi(V) and Bi(III) dissolution occurs at higher (~2 M) $HNO_3$ concentrations where Cm(III) elution is expected, adsorption studies of Bi(III) should be conducted and the addition of Bi(III) in Cm(III) batch studies will illustrate whether negative interference is occurring. Additionally, since $BiO_3$ has strong oxidizing behavior in acidic solutions with the likelihood of redox reactions with $HNO_3$, the oxidizing capability may be maintained more efficiently in a different acid. Since $HNO_3$ also has a strong redox nature, performing these studies with $H_3PO_4$ or $H_2SO_4$ may prove beneficial.

While favorable chromatographic separations were demonstrated, the chromatographic efficiencies of these systems should be characterized by evaluating how the adjustment of various parameters affects the separation. The determination of the plate height as a function of column packing technique, column height and diameter, flow rate, particle size, and temperature will provide information regarding the column dynamics such as the cause of band broadening within the system. The contribution to band broadening can also be determined through the measurement of diffusion coefficients in both the stationary and mobile phases. These studies can also aid in the understanding of how

support loading or $NaBiO_3$ concentration in the filter aid mixture affects the efficiency and peak tailing characteristics.

Separations using small elution volumes with improved flow rate properties and good peak resolution were achieved for both systems. However, further characterization is required to fully evaluate their performance and potential. Breakthrough curves provide a convenient way to compare different adsorbents and should be obtained for these systems to provide information regarding mass transport and bed efficiency. The chromatographic efficiencies of these systems should be characterized by evaluating how the adjustment of various parameters affects the separation. The determination of the plate height as a function of column packing technique, column height and diameter, flow rate, particle size, and temperature will provide information regarding the column dynamics such as the cause of band broadening within the system. The contribution to band broadening can also be determined through the measurement of diffusion coefficients in both the stationary and mobile phases. These studies can also aid in the understanding of how support loading or $NaBiO_3$ concentration in the filter aid mixture affects the efficiency and peak tailing characteristics.

Beyond the use of filter aids, the immobilization of $NaBiO_3$ onto a solid support should be explored. The immobilization on silica or celite might be achieved through creating a suspension of the two solids in a volatile solvent and drying to achieve a coating. Since $NaBiO_3$ forms as a precipitate during synthesis, its coating on these supports might be carried out through its precipitation in a solution with the supports suspended.

Alternatively, $NaBiO_3$ may also be coated on $ZrO_2$ through the precipitation of $ZrO_2$ in a suspension of solid $NaBiO_3$. Other systems such as porous membranes, cation exchangers, and unconventional metal organic frameworks could also be explored.

# CHAPTER 10: CONCLUSIONS AND FUTURE WORK

## 10.1 Summary

The work presented in this dissertation provides a foundation off which to build off of when exploring the application of $NaBiO_3$ to chromatographic systems for radiochemical separations. It is clear that, while favorable Am oxidation and Cm ion exchange reactions are at play, numerous other mechanisms are occurring within this system that add several layers of complexity when considering the role $NaBiO_3$ could play in radiochemical separations.

## 10.2 Behavior of Sodium Bismuthate in Nitric Acid Systems

The quantification of the solution chemistry of $NaBiO_3$ in nitric acid suggests that redox reactions with water and excess acid facilitate its dissolution and degradation (in terms of Bi(V) reduction to Bi(III)). The increase in solution pH at lower $HNO_3$ concentrations requires the adjustment of all working solutions to ensure that the system's conditions are as intended. As the actinides are prone to hydrolysis at higher pH values, this effect is significant; however, it could not be determined with confidence that hydrolysis was the cause of high $D_w$ values at low nitric acid concentrations. Since increased material dissolution and $O_2$ gas production occurs at higher acid concentrations that limits column flow rate, performing these separations at lower acid concentrations is preferred.

Understanding both the dissolution and degradation of $NaBiO_3$ could provide insight into the loss of solid material necessary for ion exchange and any accompanying redox

reactions occurring between $NaBiO_3$ and the solution. The presence of $BiO_3^-$, whether as a solid or in solution, is essential in ensuring the oxidation and stability of Am. It is clear that at 2 M $HNO_3$, significant ingrowth of Bi(V) and Bi(III) in solution occurs. The washing off of Bi(V) reduces the longevity of the $NaBiO_3$ solid for chromatographic separations, and it is necessary to select system conditions that limit the loss of the active material.

While aqueous $BiO_3^-$ ions have the potential benefit of stabilizing $AmO_2^{2+}$ in solution, the decay kinetics must be understood. While Bi(V) reduction to Bi(III) occurs through redox reactions with species present in solution such as Am, the redox reactions with water and excess acid decrease the Bi(V) economy which subsequently affects the extent of radionuclide oxidation and overall success of a redox-based separation. Measuring the absorbance value of a post-$NaBiO_3$ contact solution at 527 nm over time will aid in the elucidation of the decay kinetics. The decay of Bi(V) is also an important consideration due to the ingrowth of Bi(III) which has the potential to act as a competing ion for Cm(III) and other trivalent lanthanides. These dissolution and decay studies should be completed across all nitric acid concentrations, temperatures, and for extended periods of time to fully characterize degradation behavior and optimize separation parameters.

The oxidation of Am(III) to Am(IV) results in the formation of the americyl, $AmO_2^{2+}$, species that has a much different charge density from that of Cm(III) ions. Degradation of $NaBiO_3$ can also be explored as a function of ionic radii and charge density by repeating the initial $[Bi]_{Total}$ and [Bi(V)] experiments in the presence of various lanthanides and actinides. This would give insight into how the diffusion of these ions into and out of the

solid structure may distort the structure and increase its dissolution. Thus, the degradation of the solid ion exchange structure would be estimated through the dissolution behavior of $NaBiO_3$ as various ions interact.

### 10.3 Adsorption and Chromatographic Behavior of Americium and Curium on Polymer Supported $NaBiO_3$ Sorbents

The incorporation of inorganic ion exchanges within polymeric supports has been successfully demonstrated making it an attractive option for the improvement of the chromatographic performance of solid $NaBiO_3$. However, the favorable adsorption behavior of $^{241}Am$ and $^{244}Cm$ observed on $NaBiO_3$ solid as a result of combined redox and ion exchange mechanisms diminished upon its incorporation into PAN and PES polymeric matrices. While the specific polymer and its physio-chemical properties have a large influence over the performance of the active ion exchanger, the method used to prepare these materials is identical to that of commercially available PAN-based resins.

The changes that occurred within both the $NaBiO_3$ structure and the polymeric supports for the resins prepared for this dissertation should be explored through standard characterization methods such as scanning electron microscopy and energy dispersive x-ray spectroscopy (SEM/EDS) for material surface and elemental analysis as well as powder x-ray diffraction (p-XRD) to identify any significant changes in the $NaBiO_3$ solid state structure. Obtaining material characterization for both $NaBiO_3$ and polymeric supports before and after resin preparation will aid in the elucidation of negative structural changes.

Although this approach did not produce the expected data, it provides the groundwork for future research to explore the incorporation of $NaBiO_3$ within a suitable support material. Following the characterization of the prepared resins, modifications to the preparation conditions may yield a material that preserves the favorable redox and ion exchange behavior of $NaBiO_3$ while improving the chromatographic properties. Alternate support materials that are also inorganic in nature may prove to be more appropriate and could be prepared through precipitation of either $NaBiO_3$ or the support material. This provides the pathway towards research related to preparation methods, structural characterization, adsorption, and chromatographic studies.

### 10.4 Adsorption and Chromatographic Behavior of Early Actinides and Europium on $NaBiO_3$ Materials

While an Am/Cm separation is the main focus of this dissertation, the application of a $NaBiO_3$-based method within used nuclear fuel reprocessing requires the characterization of other metal ions that may be present in the feed solution. In addition, finding logical points in the currently proposed reprocessing flowsheets allows for the potential simplification of the back end of the nuclear fuel cycle. Thus, the adsorption and chromatographic behavior of the earlier actinides, U and Pu, as well as a trivalent lanthanide, Eu, was characterized. Since the hexavalent oxidation state is accessible to both U and Pu with lower reduction potentials, their oxidation by $NaBiO_3$ is feasible. Therefore, a group hexavalent actinide separation from the trivalent lanthanides can significantly decrease the number of reprocessing steps for used nuclear fuel. The adsorption and chromatographic behavior of other lanthanides, specifically Ce, rare earth

elements, and fission products should be determined so that the application of a $NaBiO_3$ system within the nuclear fuel cycle can be more thoroughly understood.

While the adsorption behavior of $^{233}U$ and $^{239}Pu$ generally followed the same trends are hexavalent Am, deviations at 0.01 M $HNO_3$ were more in line with that of trivalent Cm. However, lower $D_w$ values were observed at higher acid concentrations which may be a result of difference in charge densities and the resulting interactions with $NaBiO_3$ as well as differences in $NaBiO_3$ sources and purities. More surprisingly, $^{233}U$ displayed various behavior between batch studies and materials which requires further studies to clarify the speciation in these systems. Since the redox chemistry of the early actinides is extensive, there is a great deal of understanding regarding these radionuclides in a $NaBiO_3$ system that is required if one were to consider the possibility of a group hexavalent actinide separation. Characterization of the An oxidation states through UV-Vis analysis and careful control of the speciation in the stock solutions is necessary to continue with the An(VI)/Ln(III) separation approach.

### 10.5 Adsorption and Chromatographic Behavior of Americium and Curium in Mixed Sodium Bismuthate Systems

Following the unsuccessful PAN resin studies, this project shifted back to Richards et. al. use of Celite 545 as a column filter aid that improved flow properties to achieve a near-complete separation. While this method was successful, characterization of the influence of the filter aid on the system was not completed. Thus, adsorption, kinetics, and capacity

studies were completed to determine how the different properties of various filter aids affect the adsorption and chromatographic behavior of $^{241}Am$ and $^{244}Cm$.

The dispersion of $NaBiO_3$ throughout inorganic filter aids preserved the adsorption behavior observed for $NaBiO_3$ solid and provided separation factors as high as 174 and 145 for the 10 wt% $NaBiO_3$ Celite 535 and silica systems, respectively. Both systems exhibited rapid kinetics with these SFs reached within the first minute of contact and maintained for at least two hours. In addition, the adsorption capacities of both systems were improved relative to that of solid $NaBiO_3$.

All filter aid systems produced fast and complete separations of $^{241}Am$ and $^{244}Cm$ which provides viable methods to be used on the analytical scale. Further comparison of these systems can be carried out through breakthrough curve determination to elucidate mass transport and diffusion behavior. The adjustment and evaluation of column parameters is necessary to obtain a high efficiency chromatographic system. However, more extensive characterization is required to determine the efficacy of a $NaBiO_3$ separation for UNF reprocessing. The effect of interfering ions, radiolytic damage, high radionuclide loading must be considered. This work can be further expanded to explore the immobilization of $NaBiO_3$ on the filter aid materials studied here as well as on other inert supports suitable for chromatography. Overall, $NaBiO_3$ provides an excellent route towards a rapid and efficient Am(VI)/Cm(III) separation necessary for radioanalytical chemistry.

## REFERENCES


[1] International Energy Agency. *World Energy Outlook*; IEA: Paris, FR, 2019.

[2] United Nations. *Paris Agreement*; 2015.

[3] Mickey, C. D. Nuclear Energy. *J. Chem. Educ.* **1980**, *57* (5), 360–361.

[4] U.S. Nuclear Waste Technical Review Board. *Six Overarching Recommendations for How to Move the Nation's Nuclear Waste Management Program Forward*; 2021.

[5] Environmental Protection Agency. *Public Health and Environmental Radiation Protection Standards for Yucca Mountain, Nevada*; 73 FR 61255; 2008.

[6] *Implications of Partitioning and Transmutation in Radioactive Waste Management*; International Atomic Energy Agency, Ed.; Technical report series; International Atomic Energy Agency: Vienna, 2004.

[7] *Compendium of Dose Coefficients Based on ICRP 60*; ICRP Publication 119. Ann. ICRP 41(Suppl.); International Commission on Radiological Protection, 2012.

[8] Magill, J.; Berthou, V.; Haas, D.; Galy, J.; Schenkel, R.; Wiese, H.-W.; Heusener, G.; Tommasi, J.; Youinou, G. Impact Limits of Partitioning and Transmutation Scenarios on the Radiotoxicity of Actinides in Radioactive Waste. *Nucl. Energy* **2003**, *42* (5), 263–277.

[9] Bergelson, B. R.; Gerasimov, A. S.; Tikhomirov, G. V. Radiotoxicity and Decay Heat Power of Spent Nuclear Fuel of VVER Type Reactors at Long-Term Storage. *Radiat. Prot. Dosimetry* **2005**, *115* (1–4), 445–447. https://doi.org/10.1093/rpd/nci211.

[10] *United States Nuclear Tests July 1945 through September 1992*; DOE/NV--209-REV 15; United States Department of Energy Nevada Operations Office: Las Vegas, Nevada, 2000.

[11] Limited Test Ban Treaty, 1963. https://2009-2017.state.gov/t/avc/trty/199116.htm (accessed 2023-03-07).

[12] *Comprehensive Nuclear-Test-Ban Treaty*; United Nations, 1996.

[13] *Fiscal Year 2022 Stockpile Stewardship Management Plan*; National Nuclear Security Administration, United States Department of Energy: Washington, DC, USA, 2022.

[14] Glasstone, S.; Dolan, P. J. *The Effects of Nuclear Weapons*; Department of Defense and Department of Energy: Washington, DC, USA, 1977.

[15] Hecker, S. S. The Complex World of Plutonium Science. *MRS Bull.* **2001**, *26* (9), 672–678.

[16] Hoffman, R.; Kelley, K.; Dietrich, F.; Bauer, R.; Mustafa, M. *Modeled Neutron and Charged-Particle Induced Nuclear Reaction Cross Sections for Radiochemistry in the Region of Yttrium, Zirconium, Niobium, and Molybdenum*; UCRL-TR-222275; Lawrence Livermore National Laboratory, 2006. https://doi.org/10.2172/898501.

[17] Rathkopf, J. A.; Miller, D. S.; Owen, J. M.; Stuart, L. M.; Zika, M. R.; Eltgroth, P. G.; Madsen, N. K.; McCandless, K. P.; Nowak, P. F.; Nemanic, M. K.; Gentile, N. A.; Keen, N. D.; Box, P. O.; Palmer, T. S. *KULL: LLNL'S ASCI Inertial Confinement Fusion Simulation Code*; UCRL-JC-137053; Lawrence Livermore National Laboratory, 2000.

[18] U.S. Department of Energy. *Plutonium: The First 50 Years*; Technical Report DOE/DP-0137; U.S. Department of Energy, 1996.

[19] *The United States Plutonium Balance, 1944 - 2009*; Technical Report DOE/DP-0137 UPD; USDOE National Nuclear Security Administration (NNSA), Ofice of Defense Nuclear Security (NA-70): United States, 2012.

[20] Keegan, R. P.; Gehrke, R. J. A Method to Determine the Time since Last Purification of Weapons Grade Plutonium. *Appl. Radiat. Isot.* **2003**, *59* (2–3), 137–143.

[21] Medalia, J. E. *Nuclear Weapon "Pit" Production: Options to Help Meet a Congressional Requirement*; CRS Report 7–5700; Congressional Research Service, 2015.

[22] Jandel, M.; Bredeweg, T. A.; Bond, E. M.; Chadwick, M. B.; Clement, R. R.; Couture, A.; O'Donnell, J. M.; Haight, R. C.; Kawano, T.; Reifarth, R.; Rundberg, R. S.; Ullmann, J. L.; Vieira, D. J.; Wilhelmy, J. B.; Wouters, J. M.; Agvaanluvsan, U.; Parker, W. E.; Wu, C. Y.; Becker, J. A. Neutron Capture Cross Section of Am-241. *Phys. Rev. C* **2008**, *78* (3).

[23] Wisshak, K.; Käppeler, F. The Neutron Captur and Fission Cross Section of Americium-241 in the Energy Range from 10 to 250 KeV. *Nucl. Sci. Eng.* **1980**, *76* (2), 148–162.

[24] Wisshak, K.; Wickenhauser, J.; Käppeler, F.; Reffo, G.; Fabbri, F. The Isomeric Ratio in Thermal and Fast Neutron Capture of Americium-241. *Nucl. Sci. Eng.* **1982**, *81* (3), 396–417.

[25] Hanna, G. C.; Harvey, B. G.; Moss, N. The Neutron Capture Cross Section of Am 241. *Phys. Rev.* **1951**, *81* (3), 486–487.

[26] Hulet, E. K.; Hoff, R. W.; Bowman, H. R.; Michel, M. C. Thermal-Neutron Fission Cross Sections for Isotopes of Plutonium, Americium, and Curium. *Phys. Rev.* **1957**, *107* (5), 1294–1296.

[27] Wolfsberg, K.; Ford, G. P.; Smith, H. L. Thermal Neutron-Induced Fission Cross Section of Am-242m. *J. Nucl. Energy, Parts A/B* **1966**, *20*, 588–590.

[28] Buckner, M. Q.; Wu, C. Y.; Henderson, R. A.; Bucher, B.; Wimer, N.; Chyzh, A.; Bredeweg, T. A.; Baramsai, B.; Couture, A.; Jandel, M.; Mosby, S.; Ullmann, J. L. Comprehensive Am-242m Neutron-Induced Reaction Cross Sections and Resonance Parameters. *Phys. Rev. C* **2017**, *95* (6).

[29] Buckner, M. Q.; Wu, C. Y.; Henderson, R. A.; Bucher, B.; Wimer, N.; Chyzh, A.; Bredeweg, T. A.; Baramsai, B.; Couture, A.; Jandel, M.; Mosby, S.; Ullmann, J. L.; DANCE Collaboration. Measurement of the Am 242 m Neutron-Induced Reaction Cross Sections. *Phys. Rev. C* **2017**, *95* (2).

[30] Gharibyan, N. Intragroup Separation of Trivalent Lanthanides and Actinides for Neutron Capture Experiments in Stockpile Stewardship Sciences.Pdf, University of Nevada, Las Vegas, 2011.

[31] Seaborg, G. T. Forty Years of Plutonium Chemistry: The Beginnings. In *Plutonium Chemistry*; Carnall, W. T., Choppin, G. R., Eds.; ACS Symposium Series; AMERICAN CHEMICAL SOCIETY: WASHINGTON, D.C., 1983; Vol. 216. https://doi.org/10.1021/bk-1983-0216.

[32] Seaborg, G. T.; Loveland, W. D. The Bismuth Phosphate Process. In *The Elements Beyond Uranium*; John Wiley & Sons: New York, N.Y., 1990; pp 93–94.

[33] *Oak Ridge Natl. Lab. Rev.* **1992**, *25* (3,4).

[34] Gerber, M. S. *A Brief History of the T Plant Facility at the Hanford Site*; WHC-MR-0452; Westinghouse Hanford Company, 1994.

[35] Warf, J. C. Extraction of Cerium(IV) Nitrate by Butyl Phosphate. *J. Am. Chem. Soc.* **1949**, *71*, 2187.

[36] Herbert H. Anderson; Asprey, L. B. Solvent Extraction Process for Plutonium. US2924506A, February 9, 1960.

[37] Nunez, L.; Vandegrift, G. F. *Evaluation of Hydroxamic Acid in Uranium Extraction Process: Literature Review*; ANL-00/35, 782579; 2001.

[38] Taylor, R. J.; May, I.; Wallwork, A. L.; Denniss, I. S.; Hill, N. J.; Galkin, B. Ya.; Zilberman, B. Ya.; Fedorov, Yu. S. The Applications of Formo- and Aceto-Hydroxamic Acids in Nuclear Fuel Reprocessing. *J. Alloys Compd.* **1998**, *271–273*, 534–537.

[39] Thompson, M. C.; Norato, G. F.; Kessinger, G. F.; Pierce, R. A.; Rudisill, T. S.; Johnson, J. D. *Demonstration of the UREX Solvent Extraction Process with Dresden Reactor Fuel Solution*; WSRC-TR-2002-00444; Westinghouse Savannah River Company: Aiken, SC, 2002.

[40] Kumari, I.; Kumar, B. V. R.; Khanna, A. A Review on UREX Processes for Nuclear Spent Fuel Reprocessing. *Nucl. Eng. Des.* **2020**, *358*, 110410.

[41] Senentz, G.; Drain, F.; Bagnaz, C. COEXTM Recycling Plant: A New Standard for an Integrated Plant. In *GLOBAL 2009 Congress*; Paris, FR, 2009.

[42] Baron, P.; Cornet, S. M.; Collins, E. D.; DeAngelis, G.; Del Cul, G.; Fedorov, Yu.; Glatz, J. P.; Ignatiev, V.; Inoue, T.; Khaperskaya, A.; Kim, I. T.; Kormilitsyn, M.; Koyama, T.; Law, J. D.; Lee, H. S.; Minato, K.; Morita, Y.; Uhlíř, J.; Warin, D.; Taylor,

R. J. A Review of Separation Processes Proposed for Advanced Fuel Cycles Based on Technology Readiness Level Assessments. *Prog. Nucl. Energy* **2019**, *117*, 103091.

[43] Riddle, C. L.; Baker, J. D.; Law, J. D.; McGrath, C. A.; Meinkrantz, D. H.; Mincher, B. J.; Peterman, D. R.; Todd, T. A. Fission Product Extraction (FPEX): Development of a Novel Solvent for the Simultaneous Separation of Strontium and Cesium from Acidic Solutions. *Solvent Extraction and Ion Exchange* **2004**, *23* (3), 449–461.

[44] Law, J.; Peterman, D.; Riddle, C.; Meikrantz, D.; Todd, T. Advances in Development of the Fission Product Extraction Process for the Separation of Cesium and Strontium From Spent Nuclear Fuel. In *11th International Conference on Environmental Remediation and Radioactive Waste Management, Parts A and B*; ASMEDC: Bruges, Belgium, 2007; pp 525–528.

[45] Richter, B.; Hoffman, D. C.; Mtingwa, S. K.; Omberg, R. P.; Pillon, S.; Rempe, J. L. *Report of Advanced Nuclear Transformation Technology Subcommittee of the Nuclear Energy Research Advisory Committee*; 2004.

[46] Gelis, A. V.; Vandegrift, G. F.; Bakel, A.; Bowers, D. L.; Hebden, A. S.; Pereira, C.; Regalbuto, M. C. Extraction Behavior of Actinides and Lanthanides in TALSPEAK, TRUEX, and NPEX Processes of UREX+. *Radiochimica Acta* **2009**, *97* (4–5).

[47] Horwitz, E. P.; Schulz, W. W. *Solvent Extraction and Recovery of the Transuranic Elements from Waste Solutions Using the TRUEX Process*; International Meeting on Solvent Extraction and Ion Exchange in the Nuclear Fuel Cycle; CONF-850974--2; Harwell, UK, 1985.

[48] Horwitz, E. P.; Kalina, D. C.; Diamond, H.; Vandegrift, G. F.; Schulz, W. W. The TRUEX Process - A Process for the Extraction of the Transuranic Elements from Nitric Ac in Wastes Utilizing Modified PUREX Solvent. *Solvent Extraction and Ion Exchange* **1985**, *3* (1–2), 65–109.

[49] Schulz, W. W.; Horwitz, E. P. The TRUEX Process and the Management of Liquid TRU Waste. *Separation Science and Technology* **1988**, *23* (12–13), 1191–1210.

[50] Horwitz, E. P.; Schulz, W. W.; Cecille, L.; Casarci, M.; Pietrelli, L. The TRUEX Process: A Vital Tool for Disposal of U.S. Defense Nuclear Waste. In *New Separation Chemistry for Radioactive Waste and Other Specific Applications*; Rome, Ital, 1991; pp 21–29.

[51] Law, J.; Brewer, K.; Herbst, R.; Todd, T.; Wood, D. *Waste Manage.* **1999**, *19*, 27–37.

[52] Law, J. D.; Garn, T. G.; Meinkrantz, D. H.; Warburton, J. *Separation Science and Technology* **2010**, *45*, 1769–1775.

[53] Chamberlain, D. B.; Conner, C.; Hutter, J. C.; Leonard, R. A.; Wygmans, D. G.; Vandegrift, G. F. TRUEX Processing of Plutonium Analytical Solutions at Argonne National Laboratory. *Sep. Sci. Technol.* **1997**, *32* (1–4), 303–326.

[54] Adnet, J.-M.; Miguirditchian, M.; Hill, C.; Heres, X.; Lecomte, M.; Masson, M.; Brossard, P.; Baron, P. Development of New Hydrometallurgical Processes for Actinide Recovery: GANEX Concept. In *GLOBAL 2005*; Tsukuba, Japan, 2005; p 119.

[55] Miguirditchian, M.; Sorel, C.; Camès, B.; Bisel, I.; Baron, P.; Espinoux, D.; Calor, J.-N.; Viallesoubranne, C.; Lorrain, B.; Masson, M. HA Demonstration in the Atalante

Facility of the Ganex 1st Cycle for the Selective Extraction of Uranium from HLW. **2009**.

[56] Brown, J.; McLachlan, F.; Sarsfield, M.; Taylor, R.; Modolo, G.; Wilden, A. Plutonium Loading of Prospective Grouped Actinide Extraction (GANEX) Solvent Systems Based on Diglycolamide Extractants. *Solvent Extraction and Ion Exchange* **2012**, *30* (2), 127–141.

[57] Madic, C.; Testard, F.; Hudson, M. J.; Liljenzin, J.-O.; Christiansen, B.; Ferrando, M.; Facchini, A.; Geist, A.; Modolo, G.; Gonzales-Espartero, A.; De Mendoza, J. *PARTNEW - New Solvent Extraction Processes for Minor Actinides*; CEA-R-6066; CEA, 2004.

[58] Madic, C.; Hudson, M. J.; Liljenzin, J.-O.; Glatz, J. P.; Nannicini, R.; Facchini, A.; Kolarik, Z.; Odoj, R. *New Partitioning Techniques for Minor Actinides*; European Report EUR-19149; 2000.

[59] Courson, O.; Lebrun, M.; Malmbeck, R.; Pagliosa, G.; Romer, K.; Christiansen, B.; Glatz, J. P. Partitioning of Minor Actinides from HLLW Using the DIAMEX Process. Part 1 - Demonstration of Extraction Performances and Hydraulic Behavior of the Solvent in a Continuous Process. *Radiochimica Acta* **2000**, *88* (12), 857–863.

[60] Malmeck, R.; Courson, O.; Pagliosa, G.; Romer, K.; Satmark, B.; Glatz, J. P.; Baron, P. Partitioning of Minor Actinides from HLLW Using the DIAMEX Process. Part 2 - “Hot” Continuous Counter-Current Experiment. *Radiochimica Acta* **2000**, *88* (12), 865–872.

[61] Serrano-Purroy, D.; Baron, P.; Christiansen, B.; Malmbeck, R.; Sorel, C.; Glatz, J. P. Recovery of Minor Actinides from HLLW Using the DIAMEX Process. *Radiochimica Acta* **2005**, *93* (6), 351–355.

[62] Neidig, M. L.; Clark, D. L.; Martin, R. L. Covalency in F-Element Complexes. *Coord. Chem. Rev.* **2013**, *257* (2), 394–406.

[63] Weaver, B.; Kappelmann, F. A. *TALSPEAK: A New Method of Separating Americium and Curium from the Lanthanides by Extraction from an Aqueous Solution of an Aminopolyacetic Acid Complex with a Monoacidic Organophosphate or Phosphonate*; ORNL-3559, 4028257; 1964; p ORNL-3559, 4028257. https://doi.org/10.2172/4028257.

[64] Nash, K. L. The Chemistry of TALSPEAK: A Review of the Science. *Solvent Extr. Ion Exch.* **2015**, *33* (1), 1–55.

[65] Nilsson, M.; Nash, K. L. Review Article: A Review of the Development and Operational Characteristics of the TALSPEAK Process. *Solvent Extr. Ion Exch.* **2007**, *25* (6), 665–701.

[66] Gelis, A. V.; Lumetta, G. J. Actinide Lanthanide Separation Process—ALSEP. *Ind. Eng. Chem. Res.* **2014**, *53* (4), 1624–1631.

[67] Lumetta, G. J.; Gelis, A. V.; Carter, J. C.; Niver, C. M.; Smoot, M. R. The Actinide-Lanthanide Separation Concept. *Solvent Extr. Ion Exch.* **2014**, *32* (4), 333–347.

[68] Wilden, A.; Kreft, F.; Schneider, D.; Paparigas, Z.; Modolo, G.; Lumetta, G. J.; Gelis, A. V.; Law, J. D.; Geist, A. Countercurrent Actinide Lanthanide Separation Process (ALSEP) Demonstration Test with a Simulated PUREX Raffinate in Centrifugal Contactors on the Laboratory Scale. *Appl. Sci.* **2020**, *10* (20), 7217.

[69] Cotton, S. A. *Lanthanide and Actinide Chemistry*; Inorganic chemistry; Wiley: Chichester, England ; Hoboken, NJ, 2006.

[70] Glatz, J.-P.; Souček, P.; Malmbeck, R. Key Challenges in Advanced Reprocessing of Spent Nuclear Fuels. In *Reprocessing and Recycling of Spent Nuclear Fuel*; Elsevier, 2015; pp 49–62. https://doi.org/10.1016/B978-1-78242-212-9.00003-4.

[71] *Implications of Partitioning and Transmutation in Radioactive Waste Management*; International Atomic Energy Agency, Ed.; Technical report series; International Atomic Energy Agency: Vienna, 2004.

[72] Burns, J. D.; Moyer, B. A. Group Hexavalent Actinide Separations: A New Approach to Used Nuclear Fuel Recycling. *Inorg. Chem.* **2016**, *55* (17), 8913–8919.

[73] McCann, K.; Mincher, B. J.; Schmitt, N. C.; Braley, J. C. Hexavalent Actinide Extraction Using *N* , *N* -Dialkyl Amides. *Ind. Eng. Chem. Res.* **2017**, *56* (22), 6515–6519.

[74] Dong, X.; Yan, Q.; Wang, Z.; Feng, X.; Chen, J.; Xu, C. Group Separation of Hexavalent Actinides from Lanthanides through Selective Extraction by Sterically Hindered 2-Ethylhexyl Phosphonic Acid Mono-2-Ethylhexyl Ester. *Ind. Eng. Chem. Res.* **2022**, *61* (46), 17175–17182.

[75] Kooyman, T.; Buiron, L.; Rimpault, G. A Comparison of Curium, Neptunium and Americium Transmutation Feasibility. *Ann. Nucl. Energy* **2018**, *112*, 748–758.

[76] Marsh, J. K. The Separation of the Lanthanons (Rare-Earth Elements). *Q. Rev. Chem. Soc.* **1947**, *1* (2), 126.

[77] Aspinall, H. C. *Chemistry of the F-Block Elements*; Advanced Chemistry Texts; Gordon & Breach: Amsterdam, 2001.

[78] *The Chemistry of the Actinide and Transactinide Elements*, 3rd ed.; Morss, L. R., Edelstein, N. M., Fuger, J., Katz, J. J., Eds.; 2006.

[79] Choppin, G. R.; Liljenzin, J.-O.; Rydberg, J.; Ekberg, C. *Radiochemistry and Nuclear Chemistry*, 4th edition.; Elsevier/AP, Academic Press is an imprint of Elsevier: Amsterdam ; Boston, 2013.

[80] Pyykko, P. Relativistic Effects in Structural Chemistry. *Chem. Rev.* **1988**, *88* (3), 563–594.

[81] Pepper, Melanie.; Bursten, B. E. The Electronic Structure of Actinide-Containing Molecules: A Challenge to Applied Quantum Chemistry. *Chem. Rev.* **1991**, *91* (5), 719–741.

[82] Choppin, G. R. Comparative Solution Chemistry of the 4f and 5f Elements. *J. Alloys Compd.* **95**, *223* (2), 174–179.

[83] Seaborg, G. T.; James, R. A.; Ghiorso, A. *The New Element Curium (Atomic Number 96)*; AECD-2182; United States Atomic Energy Commission, 1948.

[84] Seaborg, G. T.; James, R. A.; Morgan, L. O. *The New Element Americium (Atomic Number 95)*; AECD-2185; United States Atomic Energy Commission, 1948.

[85] Ghiorso, A.; James, R. A.; Morgan, L. O.; Seaborg, G. T. Preparation of Transplutonium Isotopes by Neutron Irradiation. *Phys. Rev.* **1950**, *78* (4), 472–472. https://doi.org/10.1103/PhysRev.78.472.

[86] Seaborg, G. T. *Transuranium Elements: A Half Century*; LBL-29445; Lawrence Livermore National Laboratory, 1990.

[87] Seaborg, G. T. The Chemical and Radioactive Properties of the Heavy Elements. *Chem. Eng. News* **1945**, *23* (23), 2190–2193.

[88] David, F. Thermodynamic Properties of Lanthanide and Actinide Ions in Aqueous Solutions. *J. -Common Met.* **1986**, *121*, 27–42.

[89] Knope, K. E.; Soderholm, L. Solution and Solid-State Structural Chemistry of Actinide Hydrates and Their Hydrolysis and Condensation Products. *Chem. Rev.* **2013**, *113* (2), 944–994.

[90] Werner, L. B.; Perlman, I. The Pentavalent State of Americium. *J. Am. Chem. Soc.* **1951**, *73* (1), 495–496.

[91] Asprey, L. B.; Stephanou, S. E.; Penneman, R. A. A New Valance State of Americium, Am(VI). *J. Am. Chem. Soc.* **1950**, *72* (3), 1426–1426.

[92] Bourges, J. Y.; Guillaume, B.; Koehly, G.; Hobart, D. E.; Peterson, J. R. Coexistence of Americium in Four Oxidation States in Sodium Carbonate-Sodium Bicarbonate Medium. *Inorg. Chem.* **1983**, *22* (8), 1179–1184.

[93] Asprey, L. B.; Penneman, R. A. Preparation and Properties of Aqueous Tetravalent Americium. *Inorg. Chem.* **1962**, *1* (1), 134–136.

[94] Street, K.; Seaborg, G. T. The Separation of Americium and Curium from the Rare Earth Elements. *J. Am. Chem. Soc.* **1950**, *72*, 2790–2792.

[95] Diamond, R. M.; Street, K.; Seaborg, G. T. An Ion-Exchange Study of Possible Hybridized 5f Bonding in the Actinides. *J. Am. Chem. Soc.* **1954**, *76*, 1461–1469.

[96] Hale, W. H.; Lowe, J. T. Rapid, Gram-Scale Separation of Curium from Americium and Lanthanides by Cation Exchange Chromatography. *Inorg. Nucl. Chem. Lett.* **1969**, *5* (5), 363–368.

[97] Chuveleva, E. A.; Peshkov, A. S.; Kharitonov, O. V.; Firsova, L. A. Separation of Curium and Americium Microquantities by Chromatographic Method with

Introduction of Separating Ions. 1. Use of Solution of Nitrilotriacetic Acid Solution as Eluent. *Radiokhimiya* **1999**, *41* (5), 439–441.

[98] Chuveleva, Eh. A.; Peshkov, A. S.; Kharitonov, O. V.; Firsova, L. A. Separation of Curium and Americium Microquantities by Chromatographic Method with Introduction of Separating Ions: 2. Effect of Cadmium Ion Quantity and Method of It Introduction in the System on Efficiency of Curium and Americium Separation. *Radiokhimiya* **1999**, *41* (5), 442–444.

[99] Chuveleva, Eh. A.; Peshkov, A. S.; Kharitonov, O. V.; Firsova, L. A. Separation of Curium and Americium Microquantities by Chromatographic Method with Introduction of Separating Ions: 3. Effect of the Type of Holding Ion on the Process of Separation of Curium and Americium during Elution by Nitrilotriacetic Acid Solution. *Radiokhimiya* **1999**, *41* (5), 445–447.

[100] Chuveleva, E. A.; Peshkov, A. S.; Kharitonov, O. V.; Firsova, L. A. Separation of curium and americium microquantities by chromatographic method with introduction of separating ions. 4. Separation with the use of eluent on the basis of diethylenetriaminepentaacetic acid. *Radiokhimiya* **1999**, *41* (5), 474–476.

[101] Kraak, W.; Van Der Heijden, W. A. Anion Exchange Separation between Americium and Curium and between Several Lanthanide Elements. *J. Inorg. Nucl. Chem.* **1966**, *28* (1), 221–224. https://doi.org/10.1016/0022-1902(66)80248-8.

[102] Lebedev, I. A.; Myasoedov, B. F.; Guseva, L. I. Use of Alcoholic Solutions for the Isolation and Purification of Americium and Curium with Anion-Exchangers. *J. Radioanal. Nucl. Chem.* **1974**, *21*, 259–266.

[103] Horwitz, E. P.; Bloomquist, C. A. A.; Sauro, L. J.; Henderson, D. J. The Liquid-Liquid Extraction of Certain Tripositive Transplutonium Ions from Salted Nitrate Solutions with a Tertiary and Quaternary Amine. *J. Inorg. Nucl. Chem.* **1966**, *28*, 2313–2324.

[104] Horwitz, E. P.; Orlandini, K. A.; Bloomqulst, C. A. A. The Separation of Americium and Curium by Extraction Chromatography Using a High Molecular Weight Quaternary Ammonium Nitrate. *Inorg. Nucl. Chem. Lett.* **1966**, *2*, 87–91.

[105] Horwitz, E. P.; Bloomquist, C. A. A.; Orlandini, K. A.; Henderson, D. J. The Separation of Milligram Quantities of Americium and Curium by Extraction Chromatography. **1967**, *8* (3), 127–132.

[106] Horwitz, E. P.; Sauro, L. J.; Bloomquist, C. A. A. The Extraction Chromatography of Californium and Einsteinium with a High Molecular Weight Quaternary Ammonium Nitrate. *J. Inorg. Nucl. Chem.* **1967**, *29* (8), 2033–2040.

[107] Pearson, R. G. Hard and Soft Acids and Bases. *J. Am. Chem. Soc.* **1963**, *85*, 3533–3539.

[108] Jensen, M. P.; Chiarizia, R.; Shkrob, I. A.; Ulicki, J. S.; Spindler, B. D.; Murphy, D. J.; Hossain, M.; Roca-Sabio, A.; Platas-Iglesias, C.; De Blas, A.; Rodríguez-Blas, T. Aqueous Complexes for Efficient Size-Based Separation of Americium from Curium. *Inorg. Chem.* **2014**, *53* (12), 6003–6012. https://doi.org/10.1021/ic500244p.

[109] Zsabka, P.; Wilden, A.; Van Hecke, K.; Modolo, G.; Verwerft, M.; Cardinaels, T. Beyond U/Pu Separation: Separation of Americium from the Highly Active PUREX Raffinate. *J. Nucl. Mater.* **2023**, *581*, 154445. https://doi.org/10.1016/j.jnucmat.2023.154445.

[110] Silva, R. J.; Bidoblio, G. R.; Rand, M. H.; Robouch; Wanner, H.; Puigdomenech, I. *Chemical Thermodynamics of Americium*; Elsevier: New York, 1995.

[111] Ohyoshi, A.; Jyo, A.; Shinohara, T. Kinetics of the Reaction of Americium(III) with Peroxydisulfate. *Bull. Chem. Soc. Jpn. 44*, 3047–3051.

[112] Hindman, F. D. Actinide Separations for Alpha Spectrometry Using Neodymium Fluoride Coprecipitation. *Anal. Chem.* **1986**, *58* (6), 1238–1241.

[113] Sill, C. W. Precipitation of Actinides as Fluorides of Hydroxides for High Resolution Alpha Spectrometry. *Nucl. Chem. Waste Manag.* **1987**, *7*.

[114] Stephanou, S. E.; Penneman, R. A. Observations on Curium Valence States; A Rapid Separation of Americium and Curium. *J. Am. Chem. Soc.* **1952**, *74* (14), 3701–3702.

[115] Holcomb, H. P. Separation of Americium from Curium with Calcium Fluoride. *Anal. Chem.* **1964**, *36* (12), 2329–2332.

[116] Mason, G. W.; Bollmeier, A. F.; Peppard, D. F. Partition of Oxidized Americium from Actinides(III) and Lanthanides(III). *J. Inorg. Nucl. Chem.* **1970**, *32* (3), 1011–1022.

[117] Burns, J. D.; Shehee, T. C.; Clearfield, A.; Hobbs, D. T. Separation of Americium from Curium by Oxidation and Ion Exchange. *Anal. Chem.* **2012**, *84* (16), 6930–6932.

[118] McCann, K.; Brigham, D. M.; Morrison, S.; Braley, J. C. Hexavalent Americium Recovery Using Copper(III) Periodate. *Inorg. Chem.* **2016**, *55* (22), 11971–11978.

[119] Hara, M.; Suzuki, S. Oxidation of Americium(III) with Sodium Bismuthate. *J. Radioanal. Chem.* **1977**, *36* (1), 95–104.

[120] Mincher, B. J.; Martin, L. R.; Schmitt, N. C. Tributylphosphate Extraction Behavior of Bismuthate-Oxidized Americium. *Inorg. Chem.* **2008**, *47* (15), 6984–6989.

[121] Mincher, B. J.; Schmitt, N. C.; Tillotson, R. D.; Elias, G.; White, B. M.; Law, J. D. Characterizing Diamylamylphosphonate (DAAP) as an Americium Ligand for Nuclear Fuel-Cycle Applications. *Solvent Extr. Ion Exch.* **2014**, *32* (2), 153–166. https://doi.org/10.1080/07366299.2013.850288.

[122] Martin, L. R.; Mincher, B. J.; Schmitt, N. C. *Understanding the Chemistry of Uncommon Americium Oxidation States for Application to Actinide/Lanthanide Separations*; INL/CON-07-12162; Idaho National Laboratory, 2007.

[123] McCann, K.; Mincher, B. J.; Schmitt, N. C.; Braley, J. C. Hexavalent Actinide Extraction Using N, N-Dialkyl Amides. *Ind. Eng. Chem. Res.* **2017**, *56* (22), 6515–6519.

[124] Law, J. D.; Mincher, B. J.; Tillotson, R. D.; Schmitt, N. C.; Grimes, T. S. Oxidation and Extraction of Am(VI) Using a Monoamidic Extractant in 3D Printed Centrifugal Contactors. *J. Radioanal. Nucl. Chem.* **2018**, *318* (1), 35–41.

[125] Kulyako, Yu. M.; Malikov, D. A.; Trofimov, T. I.; Perevalov, S. A.; Pilyushenko, K. S.; Vinokurov, S. E.; Myasoedov, B. F. Separation of Americium and Curium in Nitric Acid Solutions via Oxidation of Am(III) by Bismuthate and Perxenate Ions. *Radiochemistry* **2020**, *62* (5), 581–586.

[126] Kumada, N.; Kinomura, N.; Sleight, A. W. Ion-Exchange Reaction of Na+ in NaBiO3*nH2O with Sr2+ and Ba2+. *Solid State Ion.* **1999**, *122*, 183–189.

[127] Richards, J. M.; Sudowe, R. Separation of Americium in High Oxidation States from Curium Utilizing Sodium Bismuthate. *Anal. Chem.* **2016**, *88* (9), 4605–4608. https://doi.org/10.1021/acs.analchem.6b01026.

[128] Sklodowska-Curie, M. Rayons Émis Par Les Composés de l'uranium et Du Thorium. *Comptes Rendus des Séances de l'Academie des Sciences* **1898**, *126*, 1101–1103.

[129] Curie, P.; Curie, M.; Bémont, G. Sur Une Nouvelle Substance Fortement Radio-Active Contenue Dans La Pechblende. *Comptes Rendus des Séances de l'Academie des Sciences* **1898**, *127*, 1215–1217.

[130] Debierne, A. Sur Un Nouvel Élément Radio-Actif: L'actinium. *Comptes Rendus des Séances de l'Academie des Sciences* **1900**, *130*, 906–908.

[131] Debierne, A. Sur Une Nouvelle Matiére Radio-Active. *Comptes Rendus des Séances de l'Academie des Sciences 129*, 593–595.

[132] Crookes, W. Radio-Activity of Uranium. *Proc. Roy. Soc.* **1900**, *66* (A), 409–422.

[133] Crookes, W. The Emanations of Radium. *Proc. Roy. Soc.* **1903**, *71* (A), 405–408.

[134] Rutherford, E.; Soddy, F. The Radioactivity of Thorium Compunds. I. An Investigation of the Radioactive Emanation. *J Chem Soc Trans* **1902**, *81*, 321–350.

[135] Soddy, F. The Radioactivity of Uranium. *J Chem Soc Trans* **1902**, *81*, 860–865.

[136] Boltwood, B. B. The Production of Radium from Uranium. *Am. J. Sci.* **1905**, *4* (20), 239–244.

[137] Hahn, O. Über Ein Neues, Die Emanation Des Thoriums Gebendes Radioaktives Element. *Jahrbuch der Radioaktivität und Elektronik* **1905**, *2*, 233–266.

[138] Meitner, L.; Frisch, O. R. Products of the Fission of the Uranium Nucleus. *Nature* **1939**, *143*, 471–472.

[139] McMillan, E.; Abelson, P. H. Radioactive Element 93. *Phys. Rev.* **1940**, *57* (12), 1185–1186. https://doi.org/10.1103/PhysRev.57.1185.2.

[140] Seaborg, G. T.; Mcmillan, E. M.; Kennedy, J. W.; Wahl, A. C. Radioactive Element 94 from Deuterons on Uranium. *Phys. Rev.* **1946**, *69* (7–8), 366–367.

[141] Seaborg, G. T.; James, R. A.; Morgan, L. O. *The New Element Americium (Atomic Number 95)*; 2185; United States Atomic Energy Commission: Oak Ridge, Tennessee, 1948.

[142] Seaborg, G. T. The Transuranium Elements. *Science* **1946**, *104* (2704), 379–386.

[143] Wilm, A. Physical Metallurgical Experiments on Aluminum Alloys Containing Magnesium. *Metallurgie* **1911**, *8*, 223.

[144] Hardy, H. K.; Heal, T. J. Report on Precipitation. *Prog. Met. Phys.* **1954**, *5*, 143–278.

[145] Nielsen, A. E. Precipitation; CCA-591; 1970; Vol. 42, pp 319–333.

[146] Jarvenin, G. Precipitation and Crystallization Processes; Consortium for risk evaluation with stakeholder participation (CRESP) 16, 2008; pp 1–14.

[147] Seaborg, G. T. *Plutonium Chemistry*; ACS Symposium Series; AMERICAN CHEMICAL SOCIETY: WASHINGTON, D.C., 1983; Vol. 216. https://doi.org/10.1021/bk-1983-0216.

[148] Kolthoff, I. M. Theory of Coprecipitation. The Formation and Properties of Crystalline Precipitates. *J. Phys. Chem.* **1932**, *36* (3), 860–881.

[149] Choppin, G. R. Solvent Extraction Processes in the Nuclear Fuel Cycle; Japan, 2005; Vol. 12, pp 1–10.

[150] Freiser, H.; Morrison, G. H. Solvent Extraction in Radiochemical Separations. *Annu. Rev. Nucl. Sci.* **1959**, *9* (1), 221–244.

[151] Diamond, R. M.; Tuck, D. G. Extraction of Inorganic Compounds into Organic Solvents. In *Progress in Inorganic Chemistry*; Cotton, F. A., Ed.; John Wiley & Sons, Inc.: Hoboken, NJ, USA, 2007; pp 109–192. https://doi.org/10.1002/9780470166031.ch3.

[152] Rodden, C. J. Analytical Chemistry of Uranium; U.S. Aomic Energy Commission: New Brunswick, NJ, 1953; Vol. 2, pp 1598–1601.

[153] Marcus, Y. Solvent Extraction by Selective Ion Solvation. *Pure Appl. Chem.* **1982**, *54* (12), 2327–2334.

[154] Kraus, C. A. The Ion-Pair Concept, Its Evolution and Some Applications. *J. Phys. Chem.* **1956**, *60* (2), 129–141.

[155] Moore, F. L. New Approach to Separation of Trivalent Actinide Elements from Lanthanide Elements. Selective Liquid-Liquid Extraction with Tricaprylmethylammonium Thiocyanate. *Anal. Chem.* **1964**, *36* (11), 2158–2162.

[156] Farbu, L.; Alstad, J.; Augustson, J. H. Synergistic Solvent Extraction of Rare-Earth Metal Ions with Thenoyltrifluoroacetone Admixed with Tributylphosphate. *J. Inorg. Nucl. Chem.* **1974**, *36* (9), 2091–2095.

[157] Geier, R. G.; Browne, L. M. *Solvent Extraction Equipment Evaluation Study Part 1. Review of the Literature*; BNWL-2186 Pt 1; Pacific Northwest National Laboratory: Richland, Washington, 1977.

[158] Craig, L. C.; Post, O. Apparatus for Countercurrent Distribution. *Anal. Chem.* **1949**, *21* (4), 500–504.

[159] Badawy, M. E. I.; El-Nouby, M. A. M.; Kimani, P. K.; Lim, L. W.; Rabea, E. I. A Review of the Modern Principles and Applications of Solid-Phase Extraction Techniques in Chromatographic Analysis. *Anal. Sci.* **2022**, *38* (12), 1457–1487.

[160] Ansari, S. A.; Mohapatra, P. K. A Review on Solid Phase Extraction of Actinides and Lanthanides with Amide Based Extractants. *J. Chromatogr. A* **2017**, *1499*, 1–20.

[161] Tswett, M. On a New Category of Absorption Phenomena and Their Application to Biochemical Analysis. *Proc. Warsaw Soc. Nat. Sci., Biol. Sect.* **1903**, *14* (6).

[162] Wilson, J. N. A Theory of Chromatography. *J. Am. Chem. Soc.* **1940**, *62* (6), 1583–1591.

[163] Martin, A. J. P.; Synge, R. L. M. A New Form of Chromatogram Employing Two Liquid Phases: A Theory of Chromatography. *Briochemical Journal* **1941**, *35* (12).

[164] Giddings, J. C. The Random Downstream Migration of Molecules in Chromatography. *J. Chem. Educ.* **1958**, *35* (12), 588.

[165] Dorfner, K. Introduction to Ion Exchange and Ion Exchangers. In *Ion Exchangers*; DE GRUYTER, 1991; pp 7–188. https://doi.org/10.1515/9783110862430.7.

[166] van Deemter, J. J.; Zuiderweg, F. J.; Klinkenberg, A. Longitudinal Diffusion and Resistance to Mass Transfer as Causes of Nonideality in Chromatography. *Chem. Eng. Sci.* **1956**, *5*, 271.

[167] Moody, H. W. The Evaluation of the Parameters in the van Deemter Equation. *J. Chem. Educ.* **1982**, *59* (4), 290.

[168] Gritti, F.; Guiochon, G. The van Deemter Equation: Assumptions, Limits, and Adjustment to Modern High Performance Liquid Chromatography. *J. Chromatogr. A* **2013**, *1302*, 1–13.

[169] Thompson, H. S. *Royal Agr. Soc. Journal* **1850**, *11*, 68.

[170] Way, J. T. *Royal Agr. Soc. Journal* **1850**, *11*, 313.

[171] Boyd, G. E.; Schubert, J.; Adamson, A. W. The Exchange Adsorption of Ions from Aqueous Solutions by Organic Zeolites. I. Ion-Exchange Equilibria. *J. Am. Chem. Soc.* **1947**, *69* (11), 2818–2829.

[172] Boyd, G. E.; Adamson, A. W.; Myers, L. S. The Exchange Adsorption of Ions from Aqueous Solutions by Organic Zeolites. II. Kinetics. *J. Am. Chem. Soc.* **1947**, *69* (11), 2836–2848.

[173] Boyd, G. E.; Myers, L. S.; Adamson, A. W. The Exchange Adsorption of Ions from Aqueous Solutions by Organic Zeolites. III. Performance of Deep Adsorbent Beds under Non-Equilibrium Conditions. *J. Am. Chem. Soc.* **1947**, *69* (11), 2849–2859.

[174] Kumar, S.; Jain, S. History, Introduction, and Kinetics of Ion Exchange Materials. *J. Chem.* **2013**, *2013*, 1–13.

[175] Alexandratos, S. D. From Ion Exchange Resins to Polymer-Supported Reagents: An Evolution of Critical Variables: From Ion Exchange Resins to Polymer-Supported Reagents: An Evolution of Critical Variables. *J. Chem. Technol. Biotechnol.* **2018**, *93* (1), 20–27.

[176] Alexandratos, S. D. Ion-Exchange Resins: A Retrospective. *Ind. Eng. Chem. Res.* **2009**, *48* (1), 388–398.

[177] Staby, A.; Sand, M.-B.; Hansen, R. G.; Jacobsen, J. H.; Andersen, L. A.; Gerstenberg, M.; Bruus, U. K.; Jensen, I. H. Comparison of Chromatographic Ion-Exchange Resins. *J. Chromatogr. A* **2005**, *1069* (1), 65–77.

[178] Bourg, I. C.; Sposito, G. *Ion Exchange Phenomena*; No. LBNL-4940E; Lawrence Berkeley National Laboratory (LBNL): Berkeley, CA, 2011.

[179] Topp, N. E.; Pepper, K. W. Properties of Ion-Exchange Resins in Relation to Their Structure. Part I. Titration Curves. *J, Chem. Soc. (Resumed)* **1949**, 3299–3303.

[180] Cutler, I. B.; Cook, M. A. A Theory of Cation Exchange Reactions with Clay Minerals. *J. Am. Ceram. Soc.* **1953**, *36* (5), 165–170.

[181] Cook, M. A.; Cutler, I. B.; Hill, G. R.; Wadsworth, M. E.; Oblad, A. G. A Mechanism of Cation and Anion Exchange Capacity. *J. Phys. Chem.* **1953**, *57* (1), 1–6.

[182] Duncan, J. F. A Theoretical Treatment of Cation Exchangers - II. Equilibria between an Ion Exchanger and an Aqueous Solution with a Common Cation. *Proc. R. Soc. Lond. Ser. Math. Phys. Sci.* **1952**, *214* (1118), 344–355.

[183] Waxman, M. H.; Sundheim, B. R.; Gregor, H. P. Studies on Ion Exchange Resins. VI. Water Vapor Sorption by Polystyrenesulfonic Acid. *J. Phys. Chem.* **1953**, *57* (9), 969–973.

[184] Seidel-Morgenstern, A. Experimental Determination of Single Solute and Competitive Adsorption Isotherms. *J. Chromatogr. A* **200AD**, *1037* (1–2), 255–272.

[185] Helfferich, F.; Plesset, M. S. Ion Exchange Kinetics. A Nonlinear Diffusion Problem. *J. Chem. Phys.* **1958**, *28* (3), 418–424.

[186] Helfferich, F. Ion-Exchange Kinetics. V. Ion Exchange Accompanied by Reactions. *J. Phys. Chem.* **1965**, *69* (4), 1178–1187. https://doi.org/10.1021/j100888a015.

[187] Ayawei, N.; Ebelegi, A. N.; Wankasi, D. Modelling and Interpretation of Adsorption Isotherms. *J. Chem.* **2017**, *2017*, 1–11.

[188] Horwitz, E. P.; Bloomquist, C. A. A. Chemical Separations for Super-Heavy Element Searches in Irradiated Uranium Targets. *J. Inorg. Nucl. Chem.* **1975**, *37* (2), 425–434.

[189] Fidelis, I.; Siekierski, S. Separation of Heavy Rare Earths by Reversed-Phase Partition Chromatography. *J. Chromatogr. A* **1961**, *5*, 161–165. https://doi.org/10.1016/S0021-9673(01)92836-5.

[190] Horwitz, E. P.; Bloomquist, C. A. A. The Preparation, Performance and Factors Affecting Band Spreading of High Efficiency Extraction Chromatographic Columns for Actinide Separations. *J. Inorg. Nucl. Chem.* **1972**, *34* (12), 3851–3871.

[191] Philip Horwitz, E.; Chiarizia, R.; Dietz, M. L. A NOVEL STRONTIUM-SELECTIVE EXTRACTION CHROMATOGRAPHIC RESIN*. *Solvent Extr. Ion Exch.* **1992**, *10* (2), 313–336. https://doi.org/10.1080/07366299208918107.

[192] Chiarizia, R.; Horwitz, E. P.; Dietz, M. L. ACID DEPENDENCY OF THE EXTRACTION OF SELECTED METAL IONS BY A STRONTIUM.SELECTIVE EXTRACTION CHROMATOGRAPHIC RESIN: CALCULATEDVS.EXPERIMENTAL CURVES*. *Solvent Extr. Ion Exch.* **1992**, *10* (2), 337–361. https://doi.org/10.1080/07366299208918108.

[193] Maes, A.; Cremers, A. Charge Density Effects in Ion Exchange. Part 2.—Homovalent Exchange Equilibria. *J. Chem. Soc. Faraday Trans. 1 Phys. Chem. Condens. Phases* **1978**, *74* (0), 1234.

[194] Metzger, F. J. A RAPID AND ACCURATE VOLUMETRIC METHOD FOR THE DETERMINATION OF CERIUM IN THE PRESENCE OF OTHER RARE EARTHS. *J. Am. Chem. Soc.* **1909**, *31* (5), 523–525.

[195] Metzger, F. J.; Heidelberger, M. THE VOLUMETRIC DETERMINATION OF CERIUM IN CERITE AND MONAZITE. *J. Am. Chem. Soc.* **1910**, *32* (5), 642–644.

[196] Lundell, G. E. F. THE INTERFERENCE OF COBALT IN THE BISMUTHATE METHOD FOR MANGANESE [1]. *J. Am. Chem. Soc.* **1923**, *45* (11), 2600–2603.

[197] Cunningham, T. R.; Coltman, R. W. The Determination of Manganese - Part I - A Study of the Bismuthate Method. *Ind. Eng. Chem.* **1924**, *16* (1), 58–63.

[198] Kargosha, K.; Noroozifar, M. Solid-Phase Sodium Bismuthate as an Oxidant in Flow Injection Analysis: Determination of Manganese in Effluent Streams. *Anal. Chim. Acta* **2000**, *413* (1–2), 57–61.

[199] Moore, F. Langley. Liquid-Liquid Extraction Method for the Separation of Cerium(IV) from Berkelium(IV) and Other Elements. *Anal. Chem.* **1969**, *41* (12), 1658–1661.

[200] Mincher, B. J.; Martin, L. R.; Schmitt, N. C. Tributylphosphate Extraction Behavior of Bismuthate-Oxidized Americium. *Inorg. Chem.* **2008**, *47* (15), 6984–6989.

[201] Mincher, B. J.; Martin, L. R.; Schmitt, N. C. Diamylamylphosphonate Solvent Extraction of Am(VI) from Nuclear Fuel Raffinate Simulant Solution. *Solvent Extr. Ion Exch.* **2012**, *30* (5), 445–456.

[202] Burstein, G. T.; Wright, G. A. Bismuth (V) Aqueous Fluoride Solution. *Nature* **1969**, *221* (5176), 169–170.

[203] Ford-Smith, M. H.; Habeeb, J. J. Kinetics of Oxidation-Reduction Reactions between Elements of Groups V and VII. Part I. Bismuth(V) with Halide Ions and Other Reductants. *J. Chem. Soc. Dalton Trans.* **1973**, No. 4, 461.

[204] Chaudhuri, M. K.; Islam, N. S.; Purkayastha, S. Reaction of Sodium Bismuthate with Fluoride in an Aqueous Medium to Give Fluoro Compounds of Bismuth(III). *J. Fluorine Chem.* **1991**, *52*, 117–123.

[205] Rice, N. T.; Dalodière, E.; Adelman, S. L.; Jones, Z. R.; Kozimor, S. A.; Mocko, V.; Root, H. D.; Stein, B. W. Oxidizing Americium(III) with Sodium Bismuthate in Acidic Aqueous Solutions. *Inorg. Chem.* **2022**, *61* (33), 12948–12953.

[206] Mills, A.; Li, X. Kinetics of Reductive Dissolution of Sodium Bismuthate by Cell' and Mnll Ions. *J CHEM SOC FARADAY TRANS* **1994**, *90*, 2939–2944.

[207] Kozma, K.; Surta, T. W.; Molina, P. I.; Lyubinetsky, I.; Stoxen, W.; Byrne, N. M.; Dolgos, M.; Nyman, M. Probing the Local Structure of Crystalline NaBiO3·XH2O and Its Acidified Derivatives. *J. Solid State Chem. 263*, 216–223.

[208] Ding, Y.; Zhou, P.; Tang, H. Visible-Light Photocatalytic Degradation of Bisphenol A on NaBiO3 Nanosheets in a Wide PH Range: A Synergistic Effect between Photocatalytic Oxidation and Chemical Oxidation. *Chem. Eng. J. 291* (149–160), 2016.

[209] Ding, Y.; Xia, X.; Ruan, Y.; Tang, H. In Situ H + -Mediated Formation of Singlet Oxygen from NaBiO 3 for Oxidative Degradation of Bisphenol A without Light Irradiation: Efficiency, Kinetics, and Mechanism. *Chemosphere* **2015**, *141*, 80–86. https://doi.org/10.1016/j.chemosphere.2015.06.048.

[210] Einkauf, J. D.; Wilcox, A. J.; Burns, J. D. Solubility and Complexation of the Bismuthate Ion in Nitric Acid Systems. *Inorg. Chem.* **2018**, *57* (24), 15341–15349.

[211] Einkauf, J. D.; Burns, J. D. Interactions of the Bismuthate Anion with Alkali, Alkaline Earth, Lanthanide, and Actinide Metals in Nitric Acid Systems. *ACS Appl. Energy Mater.* **2020**, *3* (2), 1593–1601.

[212] Richards, J. M. Use of Sodium Bismuthate Chromatography for the Separation of Americium from Curium and Other Elements in Spent Nuclear Fuel, University of Nevada, Las Vegas, Las Vegas, Nevada, 2018.

[213] Saiduzzaman, M.; Yanagida, S.; Takei, T.; Kumada, N.; Ogawa, K.; Moriyoshi, C.; Kuroiwa, Y.; Kawaguchi, S. Crystal Structure, Thermal Behavior, and Photocatalytic Activity of NaBiO3·nH2O. *Inorg. Chem.* **2018**, *57* (15), 8903–8908.

[214] Saiduzzaman, M.; Takei, T.; Kumada, N. Hydrothermal Magic for the Synthesis of New Bismuth Oxides. *Inorg. Chem. Front.* **2021**, *8* (11), 2918–2938.

[215] Šebesta, F. Composite Sorbents of Inorganic Ion-Exchangers and Polyacrylonitrile Binding Matrix: I. Methods of Modification of Properties of Inorganic Ion-Exchangers for Application in Column Packed Beds. *J. Radioanal. Nucl. Chem.* **1997**, *220* (1), 77–88.

[216] Marsh, S. F.; Svitra, Z. V.; Bowen, S. M. *Distributions of 15 Elements on 58 Absorbers from Simulated Hanford Double-Shell Slurry Feed (DSSF)*; LA-12863; Los Alamos National Laboratory, 1994; p LA--12863, 10113481. https://doi.org/10.2172/10113481.

[217] Sebesta, F.; John, J.; Motl, A.; Stamberg, K. *Evaluation of Polyacrylonitrile (PAN) as a Binding Polymer for Absorbers Used to Treat Liquid Radioactive Wastes*; SAND95-2729; Sandia National Laboratories, 1995. https://doi.org/10.2172/168591.

# APPENDIX

**Table 6.1:** Raw Data for Figure 6.3

| Am-241/Cm-244 Adsorption on $NaBiO_3$ Solid | | | | | |
|---|---|---|---|---|---|
| **$[HNO_3]$** | **Am $D_w$** | **STD Am-241** | **Cm-244 $D_w$** | **STD Cm-244** | **$SF_{(Cm/Am)}$** |
| 0.01 | 1368.11 | 39.79 | 28588.38 | LOD | 20.90 |
| 0.05 | 47.18 | 5.20 | 2495.69 | 435.34 | 52.90 |
| 0.10 | 15.79 | 0.77 | 261.46 | 31.40 | 16.55 |
| 0.24 | 3.77 | 0.87 | 15.17 | 1.50 | 4.03 |
| 0.48 | 4.41 | 0.39 | 4.05 | 1.21 | 0.92 |
| 0.98 | 2.93 | 0.73 | 1.46 | 0.85 | 0.50 |
| 1.96 | 2.00 | 0.44 | 0.86 | 0.21 | 0.43 |

**Table 6.2:** Raw Data for Figure 6.4

| Volume of $HNO_3$ Sorbed on $NaBiO_3$ Solid | | |
|---|---|---|
| **$[HNO_3]$** | **AVG V Lost (mL/50 mg resin)** | **STD V Lost (mg/50 mg resin)** |
| 0.01 | 0.0681 | 0.0009 |
| 0.05 | 0.072 | 0.006 |
| 0.1 | 0.070 | 0.008 |
| 0.25 | 0.07 | 0.01 |
| 0.5 | 0.076 | 0.009 |
| 1 | 0.083 | 0.007 |
| 2 | 0.095 | 0.007 |

**Table 6.3:** Raw Data for Figure 6.5

| Pre- and Post-$NaBiO_3$ Contact $HNO_3$ Concentrations | | | | |
|---|---|---|---|---|
| **Desired $[HNO_3]$** | **Pre-Contact $[HNO_3]$** | **STD $[HNO_3]$** | **Post-Contact $[HNO_3]$** | **STD $[HNO_3]$** |
| 0.01 | 0.0095 | 0.0003 | 0.0002 | 2.1E-06 |
| 0.05 | 0.050 | 0.001 | 0.0003 | 1.7E-06 |
| 0.1 | 0.097 | 0.001 | 0.0243 | 0.0004 |
| 0.25 | 0.239 | 0.008 | 0.155 | 0.002 |
| 0.5 | 0.483 | 0.006 | 0.398 | 0.054 |

| | | | | |
|---|---|---|---|---|
| 1 | 0.959 | 0.016 | 0.845 | 0.040 |
| 2 | 1.954 | 0.011 | 1.624 | 0.023 |

**Table 6.4:** Raw Data for Figure 6.6

| % Change in $[HNO_3]$ Post-$NaBiO_3$ Contact | | |
|---|---|---|
| **Desired $[HNO_3]$** | **% Change** | **STD (%)** |
| 0.01 | 97.33 | 0.02 |
| 0.05 | 99.30 | 0.07 |
| 0.1 | 74.95 | 0.04 |
| 0.25 | 35.04 | 0.24 |
| 0.5 | 17.61 | 5.39 |
| 1 | 11.90 | 3.99 |
| 2 | 16.90 | 2.35 |

**Table 6.5:** Raw Data for Figure 6.7

| % Activity Lost | | | | | | | | |
|---|---|---|---|---|---|---|---|---|
| **$[HNO_3]$** | **Am-241** | | **Cm-244** | | **U-233** | | **Pu-239** | |
| | **% Lost** | **% STD** | **% Lost** | **% STD** | **% Lost** | **% STD** | **% Lost** | **% STD** |
| 0.01 | 0.5 | 0.3 | 34.0 | 8.0 | 5.0 | 2.0 | 20.0 | 11.0 |
| 0.05 | 1.6 | 0.6 | 10.0 | 6.0 | 4.0 | 1.0 | 0.5 | 0.2 |

**Table 6.5:** Raw Data for Figure 6.8

| $BiO_3^-$ Absorption at 527 nm | | | |
|---|---|---|---|
| **Time (min)** | **$[HNO_3]$ (M)** | **Wavelength (nm)** | **A (a.u.)** |
| 15 | 2 | 527 | 0.015 |
| 30 | 2 | 527 | 0.019 |
| 60 | 2 | 527 | 0.029 |
| 120 | 2 | 527 | 0.047 |
| 180 | 2 | 527 | 0.051 |

**Table 6.6:** Raw Data for Figure 6.9

| $[BiO_3^-]$ Dissolution | | |
|---|---|---|
| **Time (min)** | **$[HNO_3]$** | **$[BiO_3^-]$ (mM)** |
| 15 | 2 | 1.34 |
| 30 | 2 | 1.73 |
| 60 | 2 | 2.61 |
| 120 | 2 | 4.19 |
| 180 | 2 | 4.61 |

**Table 6.7:** Raw Data for Figure 6.10

| $[BiO_3^-]$ Dissolution Kinetics | | |
|---|---|---|
| **Time (min)** | **$[HNO_3]$** | **$(1-[BiO_3^-]_t/[BiO_3^-]^{eq})^{1/3}$** |
| 15 | 2 | 0.891 |
| 30 | 2 | 0.855 |
| 60 | 2 | 0.757 |
| 120 | 2 | 0.450 |

**Table 6.8:** Raw Data for Figure 6.11

| $[Bi]_{Total}$ Dissolution | | |
|---|---|---|
| **Time (min)** | **$[HNO_3]$** | **[Bi] (mM)** |
| 15 | 2 | 1.420 |
| 30 | 2 | 3.175 |
| 60 | 2 | 14.746 |
| 120 | 2 | 35.904 |
| 180 | 2 | 64.669 |

**Table 7.1:** Raw Data for Figure 7.1

| Am-241/Cm-244 Adsorption on 75 wt% $NaBiO_3$-PAN (Lot 1) | | | | | |
|---|---|---|---|---|---|
| **$[HNO_3]$** | **Am-241 $D_w$** | **Am-241 STD** | **Cm-244 $D_w$** | **Cm-244 STD** | **$SF_{(Cm/Am)}$** |
| 0.01 | 1461.37 | 38.65 | LOD | LOD | 11.07 |
| 0.05 | 4.80 | 2.11 | 4.15 | 0.99 | 0.86 |
| 0.10 | 4.93 | 0.93 | 3.55 | 1.3 | 0.72 |
| 0.24 | 4.46 | 0.51 | 3.26 | 0.33 | 0.73 |
| 0.48 | 4.78 | 1.02 | 3.13 | 0.75 | 0.65 |

| | | | | | |
|---|---|---|---|---|---|
| 0.98 | 4.95 | 1.22 | 3.84 | 2.14 | 0.78 |
| 1.96 | 6.40 | 3.23 | 3.47 | 0.54 | 0.54 |

**Table 7.2:** Raw Data for Figure 7.2

**Am-241/Cm-244 75 wt% $NaBiO_3$-PAN Precondition Time Dependency**

| Time (min) | Am-241 $D_w$ | Am-241 STD | Cm-244 $D_w$ | Cm-244 STD | $SF_{(Cm/Am)}$ |
|---|---|---|---|---|---|
| 1 | 1321.83 | 154.38 | LOD | LOD | 11.55 |
| 2 | 1356.70 | 145.8 | LOD | LOD | 11.25 |
| 5 | 1343.57 | 17.3 | LOD | LOD | 11.36 |
| 10 | 1392.87 | 143.98 | LOD | LOD | 10.96 |
| 15 | 1327.65 | 128.62 | LOD | LOD | 11.50 |
| 30 | 1285.01 | 51.92 | LOD | LOD | 11.88 |
| 60 | 1187.30 | 8.93 | LOD | LOD | 12.85 |
| 120 | 1184.66 | 147.51 | LOD | LOD | 12.88 |

**Table 7.3:** Raw Data for Figure 7.3

**Am-241/Cm-244 75 wt% $NaBiO_3$-PAN Contact Time Dependency**

| Time (min) | Am-241 $D_w$ | Am-241 STD | Cm-244 $D_w$ | Cm-244 STD | $SF_{(Cm/Am)}$ |
|---|---|---|---|---|---|
| 1 | 34.37 | 22.63 | 31.71 | 2.68 | 0.92 |
| 2 | 86 | 25.03 | 80.76 | 4.88 | 0.94 |
| 5 | 376.92 | 28.73 | 467.67 | 86.56 | 1.24 |
| 10 | 902.72 | 71.61 | 1768.12 | 155.86 | 1.96 |
| 15 | 1066.81 | 6.71 | LOD | LOD | 15.49 |
| 30 | 1322.18 | 17.43 | LOD | LOD | 12.50 |
| 60 | 1359.4 | 156.55 | LOD | LOD | 12.15 |
| 120 | 1259.53 | 16.89 | LOD | LOD | 13.12 |
| 180 | 1499.03 | 202.95 | LOD | LOD | 11.02 |
| 240 | 1351.07 | 83.86 | LOD | LOD | 12.23 |
| 300 | 1424.23 | 230.98 | LOD | LOD | 11.60 |

**Table 7.4:** Raw Data for Figure 7.4

**Am-241/Cm-244 75 wt% $NaBiO_3$-PAN Temperature Dependency**

| Temp (C) | $D_w$ Am-241 | Am-241 STD | $D_w$ Cm-244 | Cm-244 STD | $SF_{(Cm/Am)}$ |
|---|---|---|---|---|---|
| 20 | 921.56 | 125.34 | LOD | LOD | 16.73 |
| 30 | 584.74 | 63.18 | LOD | LOD | 26.36 |

| | | | | | |
|---|---|---|---|---|---|
| 40 | 245.65 | 22.43 | LOD | LOD | 62.75 |
| 50 | 153.65 | 28.93 | LOD | LOD | 100.33 |
| 60 | 198.16 | 32.63 | LOD | LOD | 77.79 |

**Table 7.5:** Raw Data for Figure 7.6

**Am-241/Cm-244 Recovery – 75 wt% $NaBiO_3$-PAN**

| Fraction | V Eluted (mL) | Am-241 | | Cm-244 | |
|---|---|---|---|---|---|
| | | % Recovery | STD % Recovery | % Recovery | STD % Recovery |
| Load | 2 | 0.0 | 0.06 | 0.0 | 0.00 |
| F1 - 0.01 M | 12 | 2.4 | 0.51 | 0.4 | 0.71 |
| F2 - 0.01 M | 22 | 1.5 | 0.44 | 0.0 | 0.00 |
| F3 - 0.01 M | 32 | 1.6 | 0.51 | 0.0 | 0.00 |
| F4 - 0.01 M | 42 | 1.7 | 0.44 | 0.0 | 0.00 |
| F5 - 0.01 M | 52 | 1.6 | 0.57 | 0.0 | 0.00 |
| F6 - 0.01 M | 62 | 1.5 | 0.36 | 0.0 | 0.00 |
| F7 - 0.01 M | 72 | 2.2 | 0.51 | 0.0 | 0.00 |
| F8 - 0.05 M | 82 | 46.0 | 3.92 | 25.5 | 1.42 |
| F9 - 0.05 M | 92 | 27.3 | 1.71 | 51.4 | 1.89 |
| F10 - 0.05 M | 102 | 15.2 | 0.65 | 25.1 | 0.71 |
| F11 - 0.05 M | 112 | 3.0 | 0.86 | 0.8 | 0.71 |
| F12 - 0.05 M | 117 | 1.0 | 0.19 | 0.0 | 0.00 |
| F13 - 0.05 M | 127 | 0.0 | 0.0 | 0.0 | 0.0 |
| F14 - 0.05 M | 137 | 0.0 | 0.0 | 0.0 | 0.0 |
| F15 - 0.05 M | 147 | 0.0 | 0.0 | 0.0 | 0.0 |
| **Total** | | **105.14** | **10.74** | **103.25** | **5.45** |

**Table 7.6:** Raw Data for Figure 7.7

**Am-241/Cm-244 Recovery – 5 wt% $NaBiO_3$-PAN/PAN Bead**

| Fraction | V Eluted (mL) | Am-241 | | Cm-244 | |
|---|---|---|---|---|---|
| | | % Recovery | STD % Recovery | % Recovery | STD % Recovery |
| Load | 0.1 | 0.0 | 0.00 | 0.0 | 0.00 |
| F1 - 0.01 M | 15.1 | 68.1 | 8.13 | 82.6 | 5.50 |
| F2 - 0.01 M | 30.1 | 23.5 | 4.07 | 19.1 | 9.53 |

| | | | | | |
|---|---|---|---|---|---|
| F3 - 2.0 M | 45.1 | 7.0 | 7.04 | 0.0 | 0.00 |
| F4 - 2.0 M | 50.1 | 0.0 | 0.00 | 0.0 | 0.00 |
| **Total** | | **98.64** | **19.27** | **101.69** | **15.04** |

**Table 7.7:** Raw Data for Figure 7.8

| **Am-241/Cm-244 Recovery – 10 wt% $NaBiO_3$-PAN/PAN Bead** | | | | | |
|---|---|---|---|---|---|
| **Fraction** | **V Eluted (mL)** | **Am-241** | | **Cm-244** | |
| | | **% Recovery** | **STD % Recovery** | **% Recovery** | **STD % Recovery** |
| Load | 0.1 | 0.0 | 0.00 | 0.0 | 0.00 |
| F1 - 0.01 M | 15.1 | 60.1 | 4.73 | 0.0 | 0.00 |
| F2 - 0.01 M | 30.1 | 27.3 | 4.91 | 0.0 | 0.00 |
| F3 - 2.0 M | 45.1 | 8.2 | 0.00 | 0.0 | 0.00 |
| F4 - 2.0 M | 50.1 | 0.0 | 0.00 | 77.8 | 5.18 |
| F5 - 2.0 M | 60.1 | 0.0 | 0.0 | 0.0 | 0.0 |
| **Total** | | **95.58** | **9.46** | **77.83** | **5.18** |

**Table 7.8:** Raw Data for Figure 7.9a

| **Am-241/Cm-244 Adsorption on 75 wt% $NaBiO_3$-PAN (Lot 2)** | | | | | |
|---|---|---|---|---|---|
| **[$HNO_3$]** | **Am-241 $D_w$** | **Am-241 STD** | **Cm-244 $D_w$** | **Cm-244 STD** | **$SF_{(Cm/Am)}$** |
| 0.01 | 1105.48 | 7.78 | 63968.21 | 0 | 57.86 |
| 0.05 | 34.81 | 3.75 | 41.95 | 5.77 | 1.20 |
| 0.10 | 4.51 | 0.53 | 3.70 | 0.49 | 0.82 |
| 0.24 | 1.59 | 0.17 | 1.49 | 0.28 | 0.93 |
| 0.48 | 1.61 | 0.46 | 1.57 | 0.43 | 0.98 |
| 0.98 | 1.59 | 0.62 | 1.59 | 0.59 | 1.00 |
| 1.96 | 1.51 | 0.52 | 1.42 | 0.1 | 0.94 |

**Table 7.9:** Raw Data for Figure 7.9b

| **Am-241/Cm-244 Adsorption on 50 wt% $NaBiO_3$-PAN** | | | | | |
|---|---|---|---|---|---|
| **[$HNO_3$]** | **Am-241 $D_w$** | **Am-241 STD** | **Cm-244 $D_w$** | **Cm-244 STD** | **$SF_{(Cm/Am)}$** |
| 0.01 | 49.80 | 12.7 | 64.64 | 6.02 | 1.30 |
| 0.05 | 1.86 | 0.21 | 2.13 | 1.09 | 1.14 |
| 0.10 | 1.51 | 0.16 | 1.15 | 0.27 | 0.76 |
| 0.24 | 1.58 | 0.04 | 1.20 | 0.41 | 0.76 |
| 0.48 | 1.55 | 0.07 | 1.42 | 0.33 | 0.92 |

| | | | | | |
|---|---|---|---|---|---|
| 0.98 | 1.49 | 0.27 | 2.01 | 0.77 | 1.35 |
| 1.96 | 1.50 | 0.41 | 2.53 | 0.87 | 1.69 |

**Table 7.10:** Raw Data for Figure 7.9c

**Am-241/Cm-244 Adsorption on 25 wt% $NaBiO_3$-PAN**

| $[HNO_3]$ | Am-241 $D_w$ | Am-241 STD | Cm-244 $D_w$ | Cm-244 STD | $SF_{(Cm/Am)}$ |
|---|---|---|---|---|---|
| 0.01 | 7.52 | 0.25 | 4.71 | 0.6 | 0.63 |
| 0.05 | 1.76 | 0.33 | 1.76 | 0.19 | 1.00 |
| 0.10 | 1.45 | 0.54 | 1.54 | 0.2 | 1.06 |
| 0.24 | 1.41 | 0.26 | 1.53 | 0.14 | 1.09 |
| 0.48 | 1.39 | 0.09 | 1.82 | 0.29 | 1.32 |
| 0.98 | 1.75 | 0.81 | 1.59 | 0.29 | 0.90 |
| 1.96 | 1.85 | 1.06 | 2.07 | 0.79 | 1.12 |

**Table 7.11:** Raw Data for Figure 7.9d

**Am-241/Cm-244 Adsorption on 10 wt% $NaBiO_3$-PAN**

| $[HNO_3]$ | Am-241 $D_w$ | Am-241 STD | Cm-244 $D_w$ | Cm-244 STD | $SF_{(Cm/Am)}$ |
|---|---|---|---|---|---|
| 0.01 | 4.75 | 0.82 | 5.26 | 1.41 | 1.11 |
| 0.05 | 1.78 | 0.24 | 1.82 | 0.32 | 1.02 |
| 0.10 | 1.63 | 0.2 | 1.88 | 1.01 | 1.15 |
| 0.24 | 1.46 | 0.45 | 1.58 | 0.16 | 1.08 |
| 0.48 | 1.56 | 0.39 | 1.64 | 0.36 | 1.05 |
| 0.98 | 1.45 | 0.08 | 1.68 | 0.27 | 1.16 |
| 1.96 | 2.98 | 0.58 | 1.63 | 0.34 | 0.55 |

**Table 7.12:** Raw Data for Figure 7.10

**Am-241/Cm-244 Adsorption on Polyacrylonitrile**

| $[HNO_3]$ | Am-241 $D_w$ | Am-241 STD | Cm-244 $D_w$ | Cm-244 STD | $SF_{(Am/Cm)}$ |
|---|---|---|---|---|---|
| 0.01 | 15.19 | 1.26 | 13.11 | 1.1 | 1.16 |
| 0.05 | 1.19 | 0.23 | 0.7 | 0.26 | 1.71 |
| 0.10 | 1.32 | 0.13 | 1.00 | 0.11 | 1.32 |
| 0.24 | 2.52 | 0.12 | 1.34 | 0.53 | 1.87 |
| 0.48 | 2.88 | 0.12 | 1.86 | 0.34 | 1.55 |
| 0.98 | 2.09 | 0.73 | 2.37 | 0.49 | 0.88 |
| 1.96 | 7.45 | 1.7 | 7.2 | 2.53 | 1.03 |

**Table 7.13:** Raw Data for Figure 7.11

**Am-241/Cm-244 Adsorption on 10 wt% $NaBiO_3$-PES**

| [$HNO_3$] | Am-241 $D_w$ | Am-241 STD | Cm-244 $D_w$ | Cm-244 STD | $SF_{(Am/Cm)}$ |
|---|---|---|---|---|---|
| 0.01 | 7.79 | 0.51 | 1.71 | 0.15 | 4.55 |
| 0.05 | 3.68 | 0.08 | 0.80 | 0.11 | 4.61 |
| 0.10 | 1.69 | 0.51 | 0.68 | 0.22 | 2.46 |
| 0.24 | 3.25 | 0.61 | 0.72 | 0.32 | 4.48 |
| 0.48 | 1.35 | 0.62 | 0.48 | 0.20 | 2.82 |
| 0.98 | 2.43 | 0.26 | 0.89 | 0.12 | 2.74 |
| 1.96 | 2.83 | 0.01 | 0.29 | 0.07 | 9.91 |

**Table 8.1:** Raw Data for Figure 8.1

**U-233/Pu-239/Eu-152 Adsorption on $NaBiO_3$ Solid**

| [$HNO_3$] | U-233 $D_w$ | U-233 STD | Pu-239 $D_w$ | Pu-239 STD | Eu-152 $D_w$ | Eu-152 STD |
|---|---|---|---|---|---|---|
| 0.01 | 2381.65 | 1017.97 | 857.49 | 76.32 | 4645.78 | 0.00 |
| 0.05 | 84.61 | 14.15 | 39.06 | 19.06 | 1780.58 | 931.32 |
| 0.10 | 19.07 | 2.06 | 6.04 | 2.09 | 92.69 | 6.70 |
| 0.24 | 19.59 | 2.80 | 2.93 | 1.03 | 7.28 | 0.68 |
| 0.48 | 26.89 | 2.27 | 1.27 | 0.22 | 4.50 | 0.34 |
| 0.98 | 54.40 | 4.85 | 1.98 | 1.89 | 1.85 | 0.87 |
| 1.96 | 378.71 | 50.78 | 1.77 | 1.45 | 0.33 | 0.04 |

**Table 8.2:** Raw Data for Figure 8.2

**U-233/Pu-239/Eu-152 Recovery – 5 wt% $NaBiO_3$/Celite**

| Fraction | V Eluted (mL) | U-233 | | Pu-239 | | Eu-152 | |
|---|---|---|---|---|---|---|---|
| | | % Recovery | STD % Recovery | % Recovery | STD % Recovery | % Recovery | STD % Recovery |
| Load | 0.1 | 0 | 0 | 0 | 0 | 0 | 0 |
| F1 - 0.1 | 15.1 | 83.31 | 4.23 | 80.46 | 8.87 | 0 | 0 |
| F2 - 2.0 | 30.1 | 11.69 | 9.52 | 16.34 | 5.62 | 100.07 | 9.15 |
| F3 - 2.0 | 45.1 | 1.67 | 2.29 | 4.4 | 3.58 | 0 | 0 |
| F4 - 2.0 | 60.1 | 0.84 | 1.87 | 0 | 0 | 0 | 0 |
| **Total** | | **97.51** | **17.19** | **101.2** | **18.07** | **100.07** | **9.15** |

**Table 8.3:** Raw Data for Figure 8.3

| U-233/Pu-239 Adsorption on 75 wt% $NaBiO_3$-PAN (Lot 2) | | | | | |
|---|---|---|---|---|---|
| **[$HNO_3$]** | **U-233 $D_w$** | **U-233 STD** | **Pu-239 $D_w$** | **Pu-239 STD** | **$SF_{(U/Pu)}$** |
| 0.01 | LOD | LOD | LOD | LOD | 0.78 |
| 0.05 | 4.88 | 1.21 | 0.96 | 0.06 | 5.11 |
| 0.10 | 4.20 | 1.02 | 1.64 | 1.71 | 2.56 |
| 0.24 | 10.13 | 1.17 | 2.33 | 1.35 | 4.34 |
| 0.48 | 15.11 | 1.40 | 0.59 | 0.39 | 25.72 |
| 0.98 | 46.51 | 2.87 | 1.09 | 0.98 | 42.75 |
| 1.96 | 338.79 | 36.29 | 1.11 | 0.30 | 304.02 |

**Table 8.4:** Raw Data for Figure 8.4

| U-233/Pu-239 Adsorption on Polyacrylonitrile | | | | | |
|---|---|---|---|---|---|
| **[$HNO_3$]** | **U-233 $D_w$** | **U-233 STD** | **Pu-239 $D_w$** | **Pu-239 STD** | **$SF_{(U/Pu)}$** |
| 0.01 | 0.62 | 0 | 7.15 | 0.66 | 0.09 |
| 0.05 | 2.66 | 0.02 | 2.09 | 1.3e-001 | 1.27 |
| 0.10 | 6.04 | 2.91 | 1.33 | 0.59 | 4.54 |
| 0.24 | 7.82 | 2.42 | 2.35 | 0.85 | 3.33 |
| 0.48 | 18.78 | 8.77 | 6.03 | 1.47 | 3.11 |
| 0.98 | 21.69 | 3.15 | 7.63 | 2.12 | 2.84 |
| 1.96 | 113.34 | 23.42 | 20.38 | 1 | 5.56 |

**Table 8.5:** Raw Data for Figure 8.5

| U-233/Pu-239 75 wt% $NaBiO_3$-PAN (Lot 2) Contact Time Dependency | | | | | |
|---|---|---|---|---|---|
| **Time (min)** | **U-233 $D_w$** | **U-233 STD** | **Pu-239 $D_w$** | **Pu-239 STD** | **$SF_{(Pu/U)}$** |
| 1 | 16.07 | 11.3 | 16.22 | 12.61 | 1.13 |
| 2 | 29.62 | 22.81 | 32.06 | 25.16 | 1.00 |
| 5 | 165.08 | 49.96 | 239.26 | 22.09 | 1.26 |
| 10 | 16650.95 | LOD | 1003.34 | 369.22 | 1.29 |
| 15 | 16650.95 | LOD | 2035.24 | 412.48 | 0.12 |
| 30 | 16650.95 | LOD | 22471.89 | LOD | 1.15 |
| 60 | 16650.95 | LOD | 22471.89 | LOD | 1.15 |
| 120 | 16650.95 | LOD | 22471.89 | LOD | 1.15 |

**Table 8.6:** Raw Data for Figure 8.6

| U-233/Pu-239 Recovery – 10 wt% $NaBiO_3$-PAN/PAN Bead | | | | | |
|---|---|---|---|---|---|
| **Fraction** | **V Eluted (mL)** | **U-233** | | **Pu-239** | |
| | | **% Recovery** | **STD % Recovery** | **% Recovery** | **STD % Recovery** |
| Load | 1 | 22.6 | 2.17 | 7.5 | 1.74 |
| F1 - 2.0 M | 2 | 48.8 | 1.64 | 18 | 0.68 |
| F2 - 2.0 M | 3 | 17.2 | 2.84 | 11.5 | 0.85 |
| F3 - 2.0 M | 4 | 3.6 | 1.39 | 6 | 1.02 |
| F4 - 2.0 M | 5 | 1.6 | 0.66 | 3.9 | 1.53 |
| F5 - 2.0 M | 6 | 0.3 | 0.75 | 2.4 | 1.19 |
| F6 - 2.0 M | 7 | 0.3 | 0.75 | 0 | 0.0 |
| F6 - 2.0 M | 8 | 0.0 | 0.0 | 0 | 0.0 |
| **Total** | | **94.4** | **10.2** | **49.3** | **7.01** |

**Table 8.7:** Raw Data for Figure 8.7

| U-233/Pu-239/Eu-152 Adsorption on 75 wt% $NaBiO_3$-PAN (Lot 1) | | | | | | |
|---|---|---|---|---|---|---|
| **$[HNO_3]$** | **U-233 $D_w$** | **U-233 STD** | **Pu-239 $D_w$** | **Pu-239 STD** | **Eu-152 $D_w$** | **Eu-152 STD** |
| 0.01 | 4.03 | 0.23 | 1.62 | 0.2 | 24.11 | 1.77 |
| 0.05 | 2.04 | 0.06 | 0.99 | 0.23 | 2.52 | 0.52 |
| 0.10 | 1.14 | 0.07 | 0.61 | 0.06 | 1.81 | 0.18 |
| 0.24 | 1.69 | 0.39 | 1.03 | 0.4 | 2.02 | 0.1 |
| 0.48 | 1.66 | 0.52 | 0.72 | 0.01 | 2.08 | 0.28 |
| 0.98 | 1.16 | 0.46 | 0.71 | 0.01 | 1.35 | 0.24 |
| 1.96 | 4.03 | 0.23 | 1.62 | 0.2 | 24.11 | 1.77 |

**Table 9.1:** Raw Data for Figure 9.1

| [La] Calibration Curve | | |
|---|---|---|
| **$[HNO_3]$** | **[As] (ppm)** | **[La] (ppm)** |
| 0.01 | 0.02167 | 0 |
| 0.01 | 0.03132 | 1 |
| 0.01 | 0.09377 | 5 |
| 0.01 | 0.18591 | 10 |
| 0.01 | 0.81865 | 50 |
| 0.01 | 1.62746 | 100 |

**Table 9.2:** Raw Data for Figure 9.2

| Am-241/Cm-244 Adsorption on 5 wt% $NaBiO_3$/Celite 535 | | | | | |
|---|---|---|---|---|---|
| **[$HNO_3$]** | **Am-241 $D_w$** | **Am-241 STD** | **Cm-244 $D_w$** | **Cm-244 STD** | **$SF_{(Cm/Am)}$** |
| 0.01 | 27.04 | 1.96 | 447.59 | 33.83 | 16.55 |
| 0.05 | 5.13 | 1.17 | 21.75 | 3.78 | 4.24 |
| 0.10 | 2.77 | 0.24 | 6.56 | 1.31 | 2.37 |
| 0.24 | 1.52 | 0.24 | 0.99 | 0.20 | 0.65 |
| 0.48 | 0.93 | 0.23 | 0.89 | 0.09 | 0.96 |
| 0.98 | 0.57 | 0.22 | 0.37 | 0.12 | 0.66 |
| 1.96 | 0.49 | 0.10 | 0.21 | 0.04 | 0.43 |

**Table 9.3:** Raw Data for Figure 9.3

| Am-242/Cm-244 Recovery – 5 wt% $NaBiO_3$/Celite 535 | | | | | |
|---|---|---|---|---|---|
| **Fraction** | **V Eluted (mL)** | **Am-241** | | **Cm-244** | |
| | | **% Recovery** | **STD % Recovery** | **% Recovery** | **STD % Recovery** |
| Load | 4 | 0.00 | 0.53 | 0.00 | 0.00 |
| F1 - 0.1 M | 8 | 56.15 | 1.93 | 0.00 | 0.00 |
| F2 - 0.1 M | 12 | 40.10 | 2.45 | 0.00 | 0.00 |
| F3 - 0.1 M | 16 | 5.55 | 1.07 | 0.00 | 0.00 |
| F4 - 0.1 M | 20 | 0.00 | 0.53 | 0.00 | 0.00 |
| F5 - 0.1 M | 24 | 0.00 | 0.53 | 0.00 | 0.00 |
| F6 - 2 M | 28 | 0.00 | 0.53 | 4.56 | 0.72 |
| F7 - 2 M | 32 | 0.00 | 0.53 | 58.51 | 1.44 |
| F8 - 2 M | 36 | 0.00 | 0.00 | 16.60 | 1.24 |
| F9 - 2 M | 40 | 0.00 | 0.00 | 13.28 | 1.90 |
| F10 - 2 M | 44 | 0.00 | 0.00 | 3.32 | 0.72 |
| F11 - 2 M | 48 | 0.00 | 0.00 | 0.00 | 0.00 |
| **Total** | | **101.80** | **8.12** | **96.27** | **6.02** |

**Table 9.4:** Raw Data for Figure 9.4

| Am-241/Cm-244 Adsorption on 10 wt% $NaBiO_3$/Celite 535 | | | | | |
|---|---|---|---|---|---|
| **[$HNO_3$]** | **Am-241 $D_w$** | **Am-241 STD** | **Cm-244 $D_w$** | **Cm-244 STD** | **$SF_{(Cm/Am)}$** |
| 0.01 | 43.08 | 4.16 | 6225.15 | 1930.48 | 144.50 |
| 0.05 | 3.30 | 0.51 | 61.01 | 10.77 | 18.48 |
| 0.10 | 2.95 | 0.40 | 12.08 | 3.95 | 4.10 |

| | | | | | |
|---|---|---|---|---|---|
| 0.24 | 2.16 | 0.52 | 2.82 | 0.61 | 1.31 |
| 0.48 | 0.95 | 0.62 | 1.54 | 0.50 | 1.62 |
| 0.98 | 0.82 | 0.30 | 0.99 | 0.42 | 1.21 |
| 1.96 | 0.79 | 0.45 | 0.59 | 0.21 | 0.74 |

**Table 9.5:** Raw Data for Figure 9.5

| Am-241/Cm-244 10 wt% $NaBiO_3$/Celite 535 Contact Time Dependency | | | | | |
|---|---|---|---|---|---|
| **Time (min)** | **Am-241 $D_w$** | **Am-241 STD** | **Cm-244 $D_w$** | **Cm-244 STD** | **$SF_{(Cm/Am)}$** |
| 1 | 44.03 | 0.92 | 7077.92 | 1293.06 | 160.75 |
| 2 | 41.06 | 2.57 | 7410.26 | 1441.94 | 180.48 |
| 5 | 40.68 | 3.59 | 7776.83 | 1135.40 | 191.15 |
| 10 | 33.26 | 1.99 | 7278.60 | 286.49 | 218.81 |
| 15 | 31.76 | 1.97 | 6796.41 | 1828.95 | 214.00 |
| 30 | 30.89 | 2.55 | 6533.36 | 1468.71 | 211.49 |
| 60 | 29.55 | 1.86 | 6388.64 | 765.64 | 216.17 |
| 120 | 22.30 | 1.51 | 4975.59 | 694.04 | 223.07 |

**Table 9.6:** Raw Data for Figure 9.6

| 10 wt% $NaBiO_3$/Celite 535 Adsorption Isotherm | |
|---|---|
| **$C_e$ (ppm)** | **$q_e$ (mg/g)** |
| 4.75 | 0.94 |
| 16.63 | 1.65 |
| 35.91 | 2.97 |
| 57.46 | 3.76 |
| 80.19 | 4.18 |

**Table 9.7:** Raw Data for Figure 9.7

| 10 wt% $NaBiO_3$/Celite 535 Langmuir Adsorption | |
|---|---|
| **$C_e$ (ppm)** | **$C_e/q_e$ (g $L^{-1}$)** |
| 4.75 | 5.03 |
| 16.63 | 10.1 |
| 35.91 | 12.08 |
| 57.46 | 15.3 |
| 80.19 | 19.19 |

**Table 9.8:** Raw Data for Figure 9.8

| Am-241/Cm-244 Recovery – 10 wt% $NaBiO_3$/Celite 535 | | | | | |
|---|---|---|---|---|---|
| **Fraction** | **V Eluted (mL)** | **Am-241** | | **Cm-244** | |
| | | **% Recovery** | **STD % Recovery** | **% Recovery** | **STD % Recovery** |
| Load | 4 | 0.00 | 0.00 | 0.00 | 0.00 |
| F1-0.1 | 8 | 21.28 | 0.93 | 0.00 | 0.00 |
| F2-0.1 | 12 | 67.23 | 3.25 | 0.00 | 0.00 |
| F3-0.1 | 16 | 6.78 | 2.14 | 0.00 | 0.00 |
| F4-0.1 | 20 | 1.23 | 0.53 | 0.00 | 0.00 |
| F5-0.1 | 24 | 0.00 | 0.00 | 0.00 | 0.00 |
| F6-2 | 28 | 0.00 | 0.00 | 18.98 | 1.94 |
| F7-2 | 32 | 0.00 | 0.00 | 77.13 | 2.54 |
| F8-2 | 36 | 0.00 | 0.00 | 0.98 | 0.73 |
| F9-2 | 40 | 0.00 | 0.00 | 0.00 | 0.00 |
| F10-2 | 44 | 0.00 | 0.00 | 0.00 | 0.00 |
| F11-2 | 48 | 0.00 | 0.00 | 0.00 | 0.00 |
| **Total** | | **100.53** | **6.84** | **97.09** | **5.22** |

**Table 9.9:** Raw Data for Figure 9.9

| Am-241/Cm-244 Adsorption on 5 wt% $NaBiO_3$/Silica | | | | | |
|---|---|---|---|---|---|
| **$[HNO_3]$** | **Am-241 $D_w$** | **Am-241 STD** | **Cm-244 $D_w$** | **Cm-244 STD** | **$SF_{(Cm/Am)}$** |
| 0.01 | 27.41 | 4.08 | 2559.85 | 409.70 | 93.40 |
| 0.05 | 6.57 | 1.32 | 64.80 | 15.93 | 9.87 |
| 0.10 | 3.15 | 0.76 | 13.68 | 4.74 | 4.35 |
| 0.24 | 1.36 | 0.08 | 1.95 | 0.35 | 1.43 |
| 0.48 | 0.68 | 0.28 | 0.89 | 0.40 | 1.31 |
| 0.98 | 0.54 | 0.21 | 0.42 | 0.17 | 0.77 |
| 1.96 | 0.65 | 0.07 | 0.39 | 0.09 | 0.60 |

**Table 9.10:** Raw Data for Figure 9.10

| Am-241/Cm-244 Recovery – 5 wt% $NaBiO_3$/Silica | | | | | |
|---|---|---|---|---|---|
| **Fraction** | **V Eluted (mL)** | **Am-241** | | **Cm-244** | |
| | | **% Recovery** | **STD % Recovery** | **% Recovery** | **STD % Recovery** |
| Load | 4 | 9.56 | 0.00 | 0.00 | 0.00 |

| | | | | | |
|---|---|---|---|---|---|
| F1 - 0.1 | 8 | 78.05 | 1.85 | 0.00 | 0.00 |
| F2 - 0.1 | 12 | 11.41 | 1.60 | 0.00 | 0.00 |
| F3 - 0.1 | 16 | 0.00 | 1.41 | 0.00 | 0.72 |
| F4 - 0.1 | 20 | 0.00 | 0.00 | 0.00 | 0.00 |
| F5 - 0.1 | 24 | 0.00 | 0.00 | 0.00 | 0.00 |
| F6 – 2.0 | 28 | 0.00 | 0.00 | 33.88 | 1.90 |
| F7 – 2.0 | 32 | 0.00 | 0.00 | 57.44 | 4.37 |
| F8 – 2.0 | 36 | 0.00 | 0.00 | 6.83 | 1.44 |
| F9 – 2.0 | 40 | 0.00 | 0.00 | 0.00 | 0.00 |
| F10 – 2.0 | 44 | 0.00 | 0.00 | 0.00 | 0.00 |
| F11 – 2.0 | 48 | 0.00 | 0.00 | 0.00 | 0.00 |
| **Total** | | **99.03** | **4.87** | **98.15** | **8.43** |

**Table 9.11:** Raw Data for Figure 9.11

**Am-241/Cm-244 Adsorption on 10 wt% $NaBiO_3$/Silica**

| **[$HNO_3$]** | **Am-241 $D_w$** | **Am-241 STD** | **Cm-244 $D_w$** | **Cm-244 STD** | **$SF_{(Cm/Am)}$** |
|---|---|---|---|---|---|
| 0.01 | 31.79 | 5.74 | 5463.32 | 1090.06 | 171.85 |
| 0.05 | 5.02 | 0.61 | 56.13 | 14.57 | 11.17 |
| 0.10 | 3.03 | 0.23 | 10.82 | 2.32 | 3.58 |
| 0.24 | 1.12 | 0.05 | 2.34 | 0.47 | 2.08 |
| 0.48 | 1.08 | 0.04 | 1.94 | 0.68 | 1.80 |
| 0.98 | 1.11 | 0.04 | 1.63 | 0.23 | 1.48 |
| 1.96 | 1.05 | 0.01 | 0.98 | 0.50 | 0.94 |

**Table 9.12:** Raw Data for Figure 9.12

**Am-241/Cm-244 10 wt% $NaBiO_3$/Silica Contact Time Dependency**

| **Time (min)** | **Am-241 $D_w$** | **Am-241 STD** | **Cm-244 $D_w$** | **Cm-244 STD** | **$SF_{(Cm/Am)}$** |
|---|---|---|---|---|---|
| 1.00 | 30.93 | 2.51 | 5595.51 | 586.87 | 180.91 |
| 2.00 | 30.54 | 2.03 | 5660.74 | 393.46 | 185.37 |
| 5.00 | 29.75 | 2.66 | 5559.52 | 1936.66 | 186.88 |
| 10.00 | 29.93 | 3.57 | 5286.18 | 1570.91 | 176.64 |
| 15.00 | 29.93 | 1.02 | 5104.45 | 1401.76 | 170.55 |
| 30.00 | 28.16 | 0.70 | 5327.63 | 1950.47 | 189.20 |
| 60.00 | 28.53 | 0.98 | 5612.65 | 982.38 | 196.72 |
| 120.00 | 28.75 | 2.31 | 5084.58 | 2000.77 | 176.86 |

**Table 9.13:** Raw Data for Figure 9.13

| 10 wt% $NaBiO_3$/Silica Adsorption Isotherm | |
|---|---|
| $C_e$ (ppm) | $q_e$ (mg/g) |
| 2.14 | 1.47 |
| 11.57 | 2.66 |
| 27.85 | 4.59 |
| 49.91 | 5.27 |
| 75 | 5.22 |

**Table 9.14:** Raw Data for Figure 9.14

| 10 wt% $NaBiO_3$/Silica Langmuir Adsorption | |
|---|---|
| $C_e$ (ppm) | $C_e/q_e$ |
| 2.14 | 1.46 |
| 11.57 | 4.35 |
| 27.85 | 6.07 |
| 49.91 | 9.48 |
| 75 | 14.38 |

**Table 9.15:** Raw Data for Figure 9.15

| Am-241/Cm-244 Recovery – 10 wt% $NaBiO_3$/Silica | | | | | |
|---|---|---|---|---|---|
| Fraction | V Eluted (mL) | Am-241 | | Cm-244 | |
| | | % Recovery | STD % Recovery | % Recovery | STD % Recovery |
| Load | 4 | 0.00 | 0.00 | 0.00 | 0.00 |
| F1-0.1 | 8 | 50.27 | 2.97 | 0.00 | 0.00 |
| F2-0.1 | 12 | 37.01 | 2.45 | 0.00 | 0.00 |
| F3-0.1 | 16 | 11.41 | 1.41 | 0.00 | 0.00 |
| F4-0.1 | 20 | 0.00 | 0.00 | 0.00 | 0.00 |
| F5-0.1 | 24 | 0.00 | 0.00 | 0.00 | 0.00 |
| F6-2 | 28 | 0.00 | 0.00 | 71.10 | 2.20 |
| F7-2 | 32 | 0.00 | 0.00 | 27.09 | 1.47 |
| F8-2 | 36 | 0.00 | 0.00 | 0.80 | 0.73 |
| F9-2 | 40 | 0.00 | 0.00 | 0.00 | 0.00 |
| F10-2 | 44 | 0.00 | 0.00 | 0.00 | 0.00 |
| F11-2 | 48 | 0.00 | 0.00 | 0.00 | 0.00 |
| **Total** | | **98.68** | **6.83** | **98.99** | **4.41** |

**Table 9.16:** Raw Data for Figure 9.16

| Am-241/Cm-244 Adsorption on 5 wt% $NaBiO_3$/Alumina | | | | | |
|---|---|---|---|---|---|
| **[$HNO_3$]** | **Am-241 $D_w$** | **Am-241 STD** | **Cm-244 $D_w$** | **Cm-244 STD** | **$SF_{(Cm/Am)}$** |
| 0.01 | 7.91 | 0.63 | 533.46 | 21.14 | 67.42 |
| 0.05 | 2.22 | 0.30 | 35.44 | 3.96 | 15.96 |
| 0.10 | 1.64 | 0.26 | 8.92 | 0.59 | 5.45 |
| 0.24 | 1.26 | 0.15 | 1.63 | 0.13 | 1.29 |
| 0.48 | 1.23 | 0.42 | 1.67 | 0.29 | 1.35 |
| 0.98 | 0.91 | 0.04 | 0.85 | 0.13 | 0.93 |
| 1.96 | 0.76 | 0.17 | 0.39 | 0.02 | 0.52 |

## LIST OF ABBREVIATIONS AND ACRONYMS

| | |
|---|---|
| AHA | Acetohydroxamic acid |
| ALSEP | Actinide Lanthanide SEParation |
| An | Actinide |
| CMPO | Carbamoylmethylphosphine oxide |
| COEX | Combined EXtraction |
| CTBT | Comprehensive Nuclear Test Ban Treaty |
| DGA | Diglycolamide |
| DIAMEX | DIAMide EXtraction |
| $D_w$ | Weight Distribution Ratio |
| FPEX | Fission Product EXtraction |
| FPs | Fission Products |
| GANEX | Group ActiNide EXtraction |
| GHG | Greenhouse Gas |
| ICP-OES | Inductively Coupled Plasma Optical Emission Spectroscopy |
| ICRP | International Commission on Radiological Protection |
| Ln | Lanthanide |
| LSC | Liquid Scintillation Counting |
| LTBT | Limited Test Ban Treaty |
| LWR | Light Water Reactor |
| MAs | Minor Actinides |
| MOX | Mixed Oxide |

| | |
|---|---|
| $NaBiO_3$ | Sodium Bismuthate |
| NFC | Nuclear Fuel Cycle |
| NPEX | Neptunium Plutonium EXtraction |
| P&T | Partitioning and Transmutation |
| PAN | Polyacrylonitrile |
| PES | Polyethersulfone |
| PUREX | Plutonium, Uranium, Reduction, EXtraction (PUREX) |
| REEs | Rare Earth Elements |
| SF | Separation Factor |
| SSMP | Stockpile Stewardship and Management Program |
| TALSPEAK | Trivalent Actinide Separations by Phosphorous Reagent Extraction from Aqueous Komplexes |
| TBP | Tributylphosphate |
| tHM | Tons of Heavy Metal |
| TODGA | *N,N,N',N'*-tetraoctyl diglycolamide |
| TRU | Transuranic |
| TRUEX | TRansUranium EXtraction |
| U | Uranium |
| UNF | Used Nuclear Fuel |
| UREX | URanium EXtraction |
| WGPu | Weapons Grade Plutonium |